Nature and Mechanisms of Abiotic and Biotic Stress Responses and Signaling in the *Pinus nigra- Diplodia* spp. Pathosystem

DISSERTATION

Presented in Partial Fulfillment of the Requirements for the Degree Doctor of Philosophy in the Graduate School of The Ohio State University

By

SOUMYA KANTI GHOSH

MS, MSc.

Graduate Program in Plant Pathology

The Ohio State University

2023

Dissertation Committee:

Dr. Pierluigi Bonello

Dr. Guo-Liang Wang

Dr. David Mackey

Dr. Jason C. Slot

Dr. Tea Meulia

ABSTRACT

Plants continually confront a multitude of environmental challenges that can impede their growth, development, and survival, and thereby have evolved a remarkable array of responses to environmental stresses to ensure their persistence on the landscape and optimize growth. These stress responses are remarkably plastic and adaptable to a changing environment and have been the subject of intense research interest. The study of plant stress responses provides critical insights into fundamental physiological processes and has practical implications for agriculture, conservation, and ecosystem management. Understanding the intricate signaling cascades and molecular components that underlie plant stress responses is essential for developing strategies to enhance stress tolerance in crops, mitigate the impact of climate change on ecosystems, and conserve plant biodiversity.

In recurring encounters of tree species with both abiotic stress and pathogenic invasions, delimiting stress responses will be instrumental for conservation and management practices. Building on current understanding of induced resistance in the *Pinus nigra* - *Diplodia* spp. pathosystem, we hypothesized that, (1) predisposition of Austrian pine to abiotic stress such as climate change (CC) leads to increased susceptibility to pathogenic infections by *Diplodia*

spp. and this heightened susceptibility is explainable by a detailed analysis of the transcriptional regulation of both the host and pathogen, (2) attack of Austrian pine by *D. pinea* results in a systemic induced resistance (SIR) phenotype that intensifies over time, and (3) this phenotype is mediated by the accumulation of terpenoids and is explainable by a detailed analysis of signaling pathways involving phytohormones in specific patterns.

The test of the first hypothesis is described in Chapter 2. We subjected Austrian pine trees to simulated CC conditions of high temperatures and prolonged water scarcity, followed by infection with either *D. pinea*, or the less aggressive sister pathogen, *D. scrobiculata*, followed by incubation for two weeks. We found that CC impacted trees had similar disease severity, regardless of pathogen aggression, while *D. pinea* remained the more aggressive pathogen compared to *D. scrobiculata* under normal conditions. This was supported by evidence of suppressed primary metabolism and defense in pines infected by *D. pinea*, while infection by *D. scrobiculata* results in elevated levels of defense response, amidst an unaltered primary metabolism compared to *D. pinea* infected trees under control temperature and water availability. Under CC conditions, suppressed primary and secondary metabolism along with phytohormone signaling and defense responses in the host coupled with enhanced primary metabolism in *D. scrobiculata* leads to increased aggressiveness of the pathogen and enhanced host susceptibility.

In Chapter 3, we used a factorial design to test hypothesis 2. SIR potency was measured at 0.5 days, 3 days, and 10 days post-induction by *D. pinea* infection. This was accompanied by a detailed characterization of the accumulation patterns of individual and co-regulated terpenoids and other volatile compounds at the different time points. We found that some individual compounds, as well as clusters of coordinated compounds, were strongly correlated

with the strength of SIR. The role of several of these compounds in SIR was supported by their fungistatic activity, demonstrated at *in vivo* relevant concentrations.

To test the third hypothesis (Chapter 4), we used the same experimental approach used in Chapter 3, to investigate the effects of induction by pathogen attack or wounding alone on systemic elicitation of defense related gene expression, as well as triggering of stress hormones and their associated signal transduction pathways after 0.5, 1, 1.5, 2, 3, and 7 days. We found evidence of systemic induction of pathogen recognition within 0.5 days post-induction, along with significantly higher levels of abscisic acid (ABA) and activity of ROS-detoxifying enzyme genes, followed by significant and progressively stronger jasmonic acid (JA) pathway-mediated responses within a day and up to a week of induction.

Taken together, the dissertation highlights key mechanisms of conifer tree resistance/susceptibility against aggressive pathogens of worldwide concern like *D. pinea*, and the deleterious effects that CC can have on these relationships. It also confirms that SIR is expressed during early stages of induction and demonstrates that terpenoids play an important role in the early expression of SIR. Finally, this research demonstrates that SIR is largely mediated by the JA pathway, in concert with an early involvement of ABA. Therefore, the foundation of this model pathosystem is further cemented for future work in this area of science in conifers, which will help inform better breeding efforts and management practices in the future.

ACKNOWLEDGEMENTS

In the labyrinthine corridors of academia, I found guiding lights, kindred spirits, and intellectual sustenance to navigate this scholarly odyssey. Embarking on the journey towards a doctoral degree as a first-generation college student has been a profound and transformative experience, one that has been shaped by the support and sacrifices of countless individuals and the resilience instilled in me by my family's legacy. This dissertation represents not only my academic pursuits but also a testament to the dreams of generations before me and the opportunities they bestowed upon my journey.

First and foremost, I extend my heartfelt appreciation to my academic advisor, Pierluigi (Enrico) Bonello, whose wisdom, guidance, and unwavering support have been the guiding star of this academic voyage. Your mentorship and belief in my potential have shaped not just this dissertation but have been instrumental to the growth of my intellect and philosophies.

I am also incredibly grateful to the members of my advisory committee, Dr. Guo-Liang Wang, Dr. David Mackey, Dr. Jason Slot, and Dr. Tea Meulia. Your continued counsel, support, and diverse perspectives in aspects of course work, publications, research grants, public speaking, instrumentation, have honed my abilities as a student, scholar, lecturer, mentor, public speaker, and have guided my inquisition for better understanding of the world, that are often amiss the common eye.

I extend my heartfelt appreciation to the faculty and staff at The Ohio State University who provided a nurturing and intellectually stimulating environment for my growth as a scholar. Your dedication to fostering academic excellence is commendable. I am immensely fortunate to be a Buckeye for life.

To my mother, Ratna Ghosh and my father, Tushar Kanti Ghosh whose dreams and sacrifices made it possible for me to stand on the precipice of this achievement. Your unwavering faith through the journey from humble beginnings to raising a doctoral student is a testament to the enduring power of education and has sustained my spirit through every challenge in life.

To my friends and peers who walked this academic path with me, thank you for your camaraderie, encouragement, and understanding during the challenges we faced together. Our shared experiences have made this journey not only possible but also memorable.

This dissertation is not just an academic accomplishment but also a tribute to the generations of my family who dreamt of this moment. It is a symbol of the possibilities that emerge when determination meets opportunity. To all those who have played a part in this journey, your contributions are imprinted on every page of this dissertation, and I am deeply grateful for your unwavering support. As I conclude this chapter, I look forward to a future where I can pay forward the support and knowledge I have received. Together, we continue to explore the boundless frontiers of human understanding.

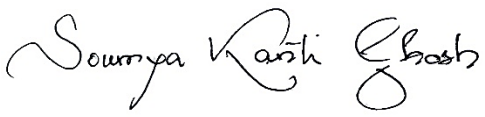

VITA

Education

M.S. Plant Pathology, The Ohio State University, Columbus, OH ……. 2020

M.Sc. Forestry (Forest Pathology), Forest Research Institute (Deemed) University, Dehradun, India ……. 2014

B.Sc. (Honors) in Botany, University of Calcutta, Kolkata, India ……..... 2012

Work

Junior Research Associate, ITC Life Sciences & Technology Center (ITC Ltd.), Bengaluru, India ……... 2017-2018

Faculty of Chemistry and Biology, St. Michael's School, Durgapur, India 2015-2017

Publications

Gossner, M. M., Perret-Gentil, A., Britt, E., Queloz, V., Glauser, G., Ladd, T., Roe, A. D., Cleary, M., Liziniewicz, M., Nielsen, L. R., **Ghosh, S. K**., Bonello, P., & Eisenring, M. (2023). A glimmer of hope – ash genotypes with increased resistance to ash dieback pathogen show cross-resistance to emerald ash borer. *New Phytologist*,. https://doi.org/https://doi.org/10.1111/nph.19068

Ghosh, S. K., Slot, J. C., Visser E. A., Naidoo, S. N., Sovic, M. G., Conrad, A. O., Kyre, B., Vijayakumar, V., Bonello, P. (2022). Mechanisms of Pine Disease Susceptibility Under Experimental Climate Change. *Frontiers in Forests and Global Change*, 1–21. https://doi.org/10.3389/ffgc.2022.872584

Ghosh, S.K. (2014) *Water centric cities of the future- Macro scale assessment of the impacts of the Bindal River on the Dehradun city*. Asia Pacific Workshop on Forest Hydrology- Water and Forests- Beyond Traditional Forest Hydrology. Proceedings of Novel Research Approaches. 1: 221-226

Ghosh, S. K., Pandey, A., Arora, S., & Dwivedi, V. D. (2013). Comparative modeling and docking studies of β-galactosidase from Aspergillus niger. *Network Modeling and Analysis in Health Informatics and Bioinformatics*, *2*(4), 297–302. https://doi.org/10.1007/s13721-013-0046-6

Fields of study

Major Field:	Graduate Program in Plant Pathology
Specialization:	Biochemistry and Molecular Biology

TABLE OF CONTENTS

LIST OF FIGURES

LIST OF TABLES

CHAPTER 1
LITERATURE REVIEW

1.1 Stress responses in plants

Any deviation in optimal conditions that are required to sustain plant structural integrity and physiological homeostasis can be referred to as plant stress (Lichtenthaler 1996; Kranner et al, 2010). The term 'stress' has been used in the context of physics as an external force applied over a unit area, while in medical lexicon, the term "stress was first incorporated by Hans Selye as "nonspecific response of the body to any demand" (Tan and Yip, 2018). However, the term plant stress was formalized by plant ecophysiologist Larcher (1987) using earlier propositions by the botanist Stocker (1932 and 1947) about drought resistance in plants, and subsequently the causal agents were addressed as the stressors (Lichtenthaler 1996).

The tolerance plasticity of plants to stress, akin to the elasticity modulus of solid matter in physics, can be influenced by the intensity and duration of the stress that can be detrimental to plant health and its resources. Higher intensity and longer duration of stress can cause distress by depleting resources and thus compromising plant defenses. On the other hand, prolonged exposure to lower stress intensities, or transient high-intensity stress events can enhance tolerance to future stress effects by amplifying metabolic pathways associated with growth and reinforcement, also referred to as the eustress effect (Kranner et al, 2010). Moreover, the nature

of the stressor has also helped dichotomize plant stress into abiotic stress, induced upon abnormal conditions of light, water scarcity or drought, extreme temperatures, and high salinity, and biotic stress that encompass threats due to predation by herbivores and pests, or competition and parasitism due to pathogenic invasions by organisms such as bacteria, viruses, nematodes, phytoplasmas, and fungi.

Abiotic and biotic stressors can generate either a eustress effect or distress effect based on the intensity and exposure duration of the stressor, as well as the outcome and magnitude of response generated in plants for remediating the crisis. For instance, distress occurs in vegetative tissues of vascular plants with prolonged water deficit conditions, or drought, with water potential below the permanent wilting point, however, shorter periods of water deficit conditions with water potential that is lower than permanent wilting point may induce long-term tolerance (Kranner et al, 2010). In this context, prolonged low water potential in the tissues under drought conditions is called dehydration avoidance, while the stress tolerance that determines plant predisposition to sustain metabolism under water deficit conditions is referred to as drought resistance (Vadez et al., 2011; Lipiec et al., 2013). For biotic stresses imposed by herbivores, insects, parasites, and pathogens, tolerance and induction of resistance can be the result of the plant genotype governing constitutive levels of reinforcement and defense, along with instances of resistance priming or induction through prior and pre-existing biotic interactions (Jung et al., 2012; Krokene, 2015; Wilkinson et al., 2019). For instance, acquired resistance to pests and pathogenic invasions is a result of sequential success during prior biotic interactions of the plant that results in sustained induction of structural and physiological defense, while an overwhelming invasion for the constitutive and induced levels of defense can induce decline and depletion of primary resources resulting in reduced fitness and plant mortality (Wilkinson et al., 2019). The demand

for plant resources may also impact the likelihood of stress occurring in different plant organs. For instance, changes in moisture content creates a progressive water potential difference, mediating transpiration, capillary transport water up the xylem, and water absorption into the roots from soil, forming the soil-plant-atmosphere continuum of water (Taiz and Zeiger, 2002). The effects of stress can also vary between systemic tissues of the plant depending on their anatomical composition and physiological characteristics, which includes an array of abiotic tolerance and biotic defense responses.

1.2 Plant defense strategies against pathogens: structure and metabolism

Essential plant resources like photosynthates, amino acids, and other plant nutrients are always at risk of being lost to enemies, like pathogens, that rely on plants as the primary producers and are therefore guarded using an assortment of defense strategies that have evolved over the course of plant and pathogen co-evolution. While select defenses pre-exist constitutively, recognition of specific pathogens can also induce reinforcements of constitutive defenses, as well as *de novo* induction of specific forms of biochemical defense, such as pathogenesis-related proteins, resistance proteins, and specialized metabolites (Gautam et al., 2020). In unchallenged plants, these compounds may be constitutively stored in vacuoles and plastids, or in specialized cells like polyphenolic parenchyma cells and resin canals in conifers and their biosynthesis in plants may or may not be induced if constitutive phenolic resources remain undisturbed in unchallenged plants or are sufficient to repel the biotic stress/es. Therefore, the inducibility of defense responses may vary depending on the attack strategy of the invading insect pests, or biotrophic and necrotrophic fungal pathogens (Gautam et al., 2020).

Plant specialized metabolites have been shown to be particularly important in defense (Pichersky and Lewinsohn, 2011; Li et al., 2020). They are a diverse group of compounds (> 200,000 across

the kingdom Plantae so far documented ((Pichersky and Lewinsohn, 2011; Rieseberg et al., 2023) and they vary between species, between different ontogenetic stages of the same plant, or between different tissues or organs on the same plant. Their biosynthesis imposes heavy costs in carbon and other nutrients at the expense of plant growth and development (Neilson et al., 2013). In trees such as conifers, like all other plants, constitutive tree defenses impose lower allocation costs and support an inherently generalized response against all biotic stresses, while induced defenses are costlier and incur longer time periods for deployment but are efficient in mediating pathogen-specific responses (Cipollini & Heil, 2010, Wilkinson et al., 2019). The tradeoffs in allocation of resources between defense and growth/differentiation has been considered in plant defense theory through various hypotheses such as the growth-differentiation balance hypothesis, the optimal defense hypothesis, the growth-rate hypothesis, and the carbon-nutrient balance hypothesis (Stamp 2003; Walters 2010).

Pre-formed defenses: Plants have evolved various strategies of defense against invading pests and pathogens, that are pre-formed or pre-exist as structural or anatomical, and biochemical forms of defense. The epidermis forms the outermost layer of the plant and is often the interface for plant- biotic/ abiotic interactions. The epidermis in the shoot and non-woody stems and branches are usually reinforced with different hydrophobic layers such as epicuticular wax films and crystals that prevents excess loss of water from the plant, and they have also been known to limit direct access by pathogens (Walters 2010; Belete 2018). Suberized periderm in plants and conifers are composed of the bark and cork, abscission layer formation, formation of tyloses in xylem vessels, and resin canals (Franceschi et.al. 2005; Agrios, 2005). The root epidermis is usually suberized for added protection against invasion underneath the soil level (Walters 2010). Specialized tissue types like stone cells, polyphenolic parenchyma (PP) cells, resin cells,

sclerenchyma and calcium-oxalate containing cells are some of the various constitutive defenses reported in conifers (Franceschi et.al. 2005). Epidermal cell walls are composed of cellulose chains crosslinked to each other via glycans and pectin, and with polyphenolic polymers of lignin that confer rigidity to the cell wall and protects it against microbial degradation (Walters 2010). In woody species like conifers, resin ducts and PP cells are incorporated in root and stem cortical layers and release toxic metabolites upon cell disruption (Franceschi et.al. 2005; Wilkinson et al., 2019).

Induced defenses: Defense responses are also induced upon invasion by pests and pathogens, that can range from periderm formation and formation of abscission layer, to programmed cell death and hypersensitive response. Also, antimicrobial compounds are called phytoanticipins if they are present constitutively in unchallenged plants, or phytoalexins if they are induced by attack. Phytoalexins include a variety of antimicrobial proteins, small peptides, enzymes, small RNAs, reactive oxygen species (ROS), and specialized metabolites. Phenolics, terpenoids, and nitrogen-containing organic compounds like defense proteins, alkaloids, and cyanogenic glycosides constitute the three major groups of specialized phytochemicals that are critical for mediating plant defense against biotic stresses from pests and pathogens (Walters 2010), and can act as both phytoanticipins and phytoalexins, depending on the compounds and the specific circumstances. Other important defense metabolites include saponins, glucosinolates, and anthocyanins (Marchiosi et al., 2020). All these metabolites are derived from the carbon precursors glucose and sucrose in the chloroplast (Fig. 1.1).

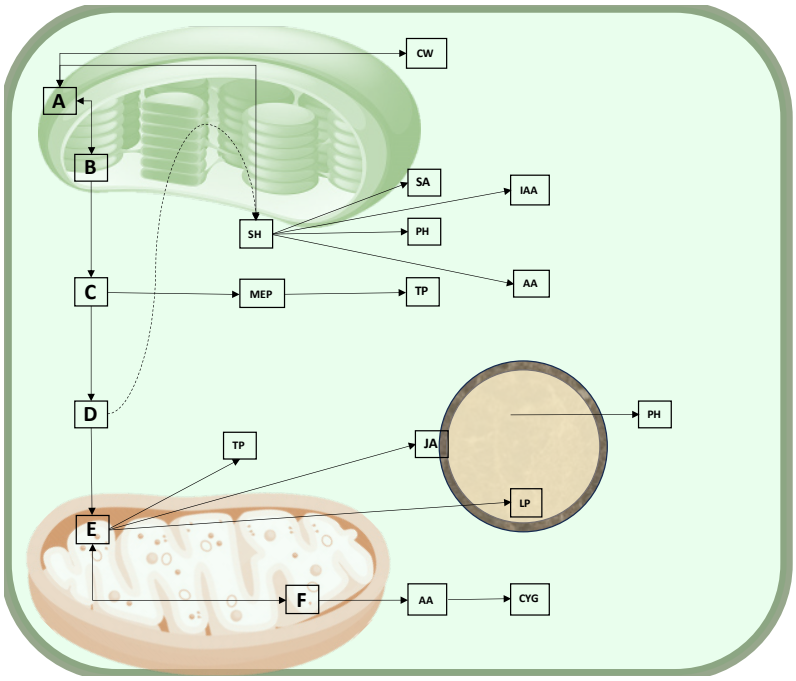

Figure 1.1. Fixation of carbon resources such as glucose and sucrose via different plastidial, peroxisomal (brown circle), and cytosolic intermediates into the Krebs cycle as acetyl co-enzyme A, also gives rise to various specialized metabolites involved in plant stress responses.

The primary photosynthates glucose and fructose are synthesized in plant chloroplasts and transported to the mitochondria for Krebs cycle, through a series of carbon intermediates produced in both organelles as well as the cytosol. These carbon intermediates serve as precursors for specialized metabolic pathways for the downstream biosynthesis of terpenoids, phenolics, alkaloids, and various amino acids for defense protein synthesis (Fig. 1.1).

Terpenoids are a diverse group of low molecular weight compounds, with a backbone of isoprene monomers (C_5 building block). They are synthesized in plants through the methylerythritol phosphate pathway in the cytosol and the mevalonic acid pathway in the plastids from three-carbon (C_3) precursors, 3-phosphoglyceric acid and pyruvic acid, respectively (Fig. 1.1). Under the mevalonate pathway, the biosynthesis of sesquiterpenoids, triterpenoids,

polyprenols, phytosterols, and brassinosteroids occurs in the cytosol, while the biosynthesis of ubiquinones and polyprenols occur in the mitochondria. Similarly, the methylerythritol pathway in plants is used for the biosynthesis of hemiterpenoids (e.g., isoprene), monoterpenoids, diterpenoids, chlorophyll, carotenoids, cytokinins, gibberellins, tocopherols, and plastoquinones in plant plastids (Tholl 2015). More subtle variations in terpenoids are produced by a variety of modifications, including oxygenation mediated by large families of cytochrome P450s, followed by conjugation into a great variety of motifs and functional groups (War et al., 2011; Castells, 2015). These compounds are involved in growth, photosynthesis, energy synthesis (ATP), but more importantly, they are involved in response to biotic and abiotic stress. Accumulation of volatile terpenoids in the photosynthetic membranes has been hypothesized to enhance membrane functionality, with implications for thermal stress responses (Behnke et al., 2007; Behnke et al., 2009). They may become involved in direct interactions with both cytosolic and apoplastic oxidants and can also alter reactive oxygen species (ROS) signaling. Other membrane-bound terpenoids such as tocopherol and carotenoids have been associated with ROS scavenging (Goh et al., 2012; Boncan et al., 2020). Various terpenoids are also part of herbivore-induced plant volatiles (HIPV) complexes, which may exert direct toxicity towards insects but attracting insect enemies like parasitoids and predators in what is known as indirect defense (Eyles et al., 2009; War et al., 2011; Plata-Rueda et al., 2018; Chiu & Bohlmann, 2022). In conifers terpenoids accumulate in resin canals, which may be present constitutively or induced upon pest or pathogenic invasion throughout the stem and roots and get released by cell disruption caused by attack (Chiu & Bohlmann, 2022; Castells, 2015). Additionally, various monoterpenes and sesquiterpenes have also been associated with generating phytoalexin

responses against bacterial and fungal pathogens (He et al., 2023; Tholl 2015), with implicated involvement in defense priming (Riedlmeier et al., 2017).

The four-carbon (C_4) intermediates, erythrose-4-phosphate and phosphoenolpyruvate are precursors in the shikimate biosynthetic pathway (Fig. 1.1). Shikimic acid is the precursor of chorismic and isochorismic acids (which can be further derived into aromatic amino acids such as tyrosine, tryptophan, phenylalanine), and the plant hormones indole acetic acid and salicylic acid, tetrahydrofolic acid (vitamin B9), as well as other plant pigments and quinones. The enzyme phenylalanine ammonia lyase (*PAL*) catalyzes the conversion of phenylalanine into the phenolic acid, *trans*-cinnamic acid, while tyrosine can be converted into *p*-coumaric acid by *PAL* activity as well. Other phenolic acids like caffeic acid, ferulic acid, 5-hydroxyferulic acid, and sinapic acid, as well as chalcones, flavones, isoflavones and anthocyanins, are also synthesized from *trans*-cinnamate and *p*-coumarate. Phenolic acids are also derived into corresponding phenolic aldehydes, and ultimately into various polyphenolic lignin compounds such as coniferin, hydroxyconiferin, hydroxyphenyl lignin, guaiacyl lignin, syringyl lignin, as well as flavonoids, coumarins, eugenol, methyleugenol and anethole. Procyanidins and proanthocyanidins are flavonol derivatives that constitute the condensed tannins groups of defense polyphenolics. This diversity of compounds and their intermediates is aided by the fact that they are synthesized in plastids, mitochondria, peroxisome, and the cytosol, However, lignin biosynthesis occurs exclusively in the cytosol (Liu et al., 2018; Marchiosi et al., 2020). Phenolic compounds play important roles in plant growth, development, and pigmentation of plant organs, as well as in abiotic stress tolerance and defense against pests and pathogens (Lattanzio et al., 2006; Naikoo et al., 2019). Besides cellulose and hemicellulose, the secondary cell wall of plants is also fortified with lignin, mostly composed of monolignol compounds such as sinapoyl alcohol

S-unit, coniferyl alcohol G-unit, and *p*-coumaroyl alcohol H-unit (Liu et al., 2018), which serve as constitutive defense in plant cells. Other phenolics and polyphenols may also be stored in vacuoles as glycosidic derivatives. Phenolics and polyphenols are also recognized as potent antioxidants, with one or more proton donor sites in their carboxyl and hydroxyl functional groups that target free radicals like superoxides (O_2^-) in the cytosol and apoplastic space (Rene et al., 2016). This important feature aids in phenolics mediated abiotic stress tolerance to drought, salt stress, oxidative stress, heavy metal toxicity, heat, and cold stress. An increased accumulation of phenolic compounds has also been shown in response to water deficit and chilling conditions (Chung et al., 2006**;** Naikoo et al., 2019). Interestingly, excess metal ions like cadmium, lead, nickel, zinc, iron, copper, in the cytosol and apoplast can also be efficiently chelated by various phenolic compounds like flavonoids and anthocyanins, due to the chelating effects of their resonance-stabilized hydroxyl and carboxyl functional groups (Kisa et al., 2016; Noor et al., 2023). Flavonoids and anthocyanins have been shown to protect against UV-B radiation (280-320 nm) due to higher wavelength absorption ranges that prevent UV-mediated photosynthetic damage (Falcone Ferreya et al., 2012). Accumulation of phenolic compounds such as cinnamic acid, *p*-coumaric acid, gallic acid, and salicylic acid, and phenolic glycosides in trees such as verbascoside, picein, piceol, pungenin, pungeol have been shown to be inducible by insect pest attack (Delvas et al., 2011; Whitehill et al., 2014; Dixit et al., 2017; Gossner et al., 2023). Volatile phenolic acids such as coumaric, cinnamic, syringic, and vanillic acids can also reportedly attract natural enemies and parasitoids of insect pests by enhancing kairomone levels in arthropod gut, besides direct toxicity and reduced fecundity post infestation and feeding (Boege 2004; Eleftherianos et al., 2006; Rani and Pratyusha, 2014). At the same time, a variety of phenolic compounds, including phenolic acids, phenolic glycosides, flavanols,

dihydrochalcones and lignin have been shown to have antifungal activity, and therefore may aid in localized and systemic defense against pathogenic invasion (Sherwood & Bonello, 2013; Shalaby and Horwitz, 2015; Gautam et al., 2020).

In plant cells, one of the major mechanisms for biosynthesis of amino acids involves various carbon precursors that also act as intermediates in the conversion of fructose-6-phosphate to pyruvate, and then oxaloacetate (Fig. 1.1). Amino acids may exist in the cytosol or apoplast, and they can be polymerized, or translated into various homomeric or heteromeric defense proteins and enzymes, such as defensins, thionins, lectins, arcelins, cyclotides, ureases, α-amylase and protease inhibitors, cell perforation peptides, transcription factors, receptor-like kinases, and ribosome activating proteins (RIP), and they can be converted into nitrogen-containing specialized metabolites like alkaloids, glucosinolates, and cyanogenic glycosides (Singh, 2018; Jain et al., 2022).

Pathogenesis-related (*PR*) proteins are usually monomeric proteins that are synthesized in response to pathogenesis and salicylate and jasmonate signaling. Currently, seventeen different PR protein families have been described in plants, while the identity of two additional PR protein families remains putative. Defense proteins like defensins, thionins, thaumatin-like proteins, β-1,3-glucanases, chitinase types I-VII proteins, proteinase inhibitors, endoproteinases, ribonuclease-like proteins, lipid transfer proteins, germins (oxalate oxidase), germin-like proteins and other antifungal and antiviral proteins have been identified as plant *PR* proteins that are synthesized in response to biotic stress due to fungal, bacterial, and viral pathogens (van Loon, 1985; Agrios, 2005; Joshi et al., 2021). Pattern recognition receptors (PRR) like receptor-like kinases (*RLK*) and receptor-like proteins (*RLP*) are located in the cell membrane and possess an extracellular domain and a transmembrane domain, with an occasional cytoplasmic tail. The

apoplastic domain can be composed of leucine-rich repeats (*LRR*), cysteine-rich repeats (*CRR*), serine/threonine domains, chitinase, thaumatin protein domains that recognize a variety of microbial cell wall components, nucleic acids, and metabolic compounds, while the transmembrane domain influences plant growth and differentiation. Similar proteins in the cytosol known as receptor-like cytoplasmic kinases (*RLCK*) are involved in intracellular pathogen-triggered immunity (PTI) signaling, calcium signaling, and mitogen-activated protein kinase (*MAPK*) signaling (Wang and Fiers, 2009; Sun and Zhang, 2020; Dievart et al., 2020).

Alkaloids may be derived from aromatic amino acids, with or without conjugal steroid chains, that have been shown to inhibit the spread of insect pests and pathogenic infection in plants (Liu et al., 2023). Glucosinolates and cyanogenic glycosides are stored in vacuoles and are converted into toxic derivatives such as aglycones, thiocyanates, hydrogen cyanide, and thioglucosides upon membrane rupture and have been shown to be involved in defense against insect damage as well as fungal pathogen activity (Zagrobelny et al., 2004; Singh et al., 2015; Vanhook, 2015).

Specialized metabolites like auxin, cytokinins, gibberellins, ethylene, salicylic acid (SA), jasmonic acid (JA), abscisic acid (ABA), azelaic acid (AZA), pipecolic acid (PA), ethylene (ET) and brassinosteroids are established plant hormones that regulate plant growth and development, as well as the importance of SA, JA, ET, ABA, AZA, PA, and brassinosteroids in stress responses due to drought, high salinity, herbivore damage, and pathogenic attacks. These compounds arise out of various biosynthetic pathways such as the shikimate pathway (SA synthesis), oxylipin cycle (JA synthesis), methyl erythritol pathway (ABA synthesis), or from amino acids such as pipecolic acid (lysine derived), or fatty acids and steroids such as azelaic acid and brassinosteroids. These compounds are selectively induced upon stress stimulus

perception, and mediate local and systemic signaling of either defense responses during pest or pathogenic attacks, or tolerance responses due to abiotic stresses.

1.3 How plants recognize and respond to stress

In the real world, plants seldom experience single stress events, and the nature of stress responses may overlap between stressors (Huber and Bauerle, 2016). Evidence of phenotypic effects of stress may mainfest the defense responses mentioned earlier, or symptom development, if the defenses have failed and the plant is running out of resources. At the cellular level, stress perception and responses occur in an integrated cascade of biochemical activities.

One mechanism through which plant cells perceive stress stimuli is by detecting molecular and cellular fragments that can be unique to microorganisms as microbial-associated molecular patterns (MAMPS), while recognition of relocated endogenous plant molecules and damaged plant cellular fragments can be perceived as damage-associated molecular patterns (DAMPS). The major DAMPS identified in plants include cuticle fragments and monomers; damaged cell wall fragments like oligogalacturonides (*Ogs*) and xyloglucan oligosaccharides; apoplastic peptides and polypeptides like systemin, inceptin, (*Zip1*), plant elicitor peptides (*Peps*), (*CAPE*), (*RALF*), (*HypSys*), and certain high mobility group box (*HMGB*) proteins; extracellular nucleotides like extracellular ATP and DNA (*e*ATP and *e*DNA), as well as apoplastic sugars and glutathione and (Choi and Klessig, 2016; Hou et al., 2019). On the other hand, non-self-recognition at the cell surface is critical for mediating defense responses against pathogenic invasions and are efficiently handled by MAMPS depending on the type of pathogen. For instance, bacterial presence can be recognized by specific MAMPS associated with bacterial cells such as flagellin, peptidoglycan, lipopolysaccharides, prokaryotic elongation factors (*EF*) like *EF* thermo-unstable proteins (*EF-Tu*), cold shock proteins, harpins, rhamnolipids, bacterial

superoxide dismutase, or even bacterial DNA, while fungal PAMPS recognized in plants include chitin, chito-oligosaccharides, β-glucan, ergosterol, ethylene-inducing xylanase (*EIX*), sphingolipids like cerebrosides, necrosis and ethylene-inducing protein (*Nep1*), *Nep*-like proteins (*NLP*), and cellulose-binding elicitor lectin (*CBEL*) (Nicaise et al., 2009; Vidhyasekaran 2014).

The highly selective nature of PAMPS and DAMPS are efficiently recognized by specific pattern recognition receptors (PRR) embedded throughout the cell membrane, that constantly monitor clues of pathogenic presence in the apoplast, or DAMPS resulting out of plant-pathogen interactions, such as peptides and oligosaccharides. Plant PRRs can either be receptor-like kinases (*RLK*) composed of an extracellular domain, a transmembrane domain, and a cytoplasmic domain, or receptor-like proteins (*RLP*) that lack a cytoplasmic domain. The reported extracellular domains of plant PRRs comprise of leucine rich repeats (*LRR*), lysin motifs (*LysM*), lectin-like motifs and epidermal growth factor (*EGF*)-like domains, that cater to the recognition of an array of PAMPS and DAMPS (Saijo et al., 2018). In recognition of DAMPS, for instance, systemin cell-wall receptors (*SR160*) perceive systemin proteins, *Peps* Receptors (*PEPR*) perceive plant elicitor peptides (*Peps*), wall associated kinases (*WAK1*) recognize oligogalacturonides (*Ogs*) from damaged cell wall fragments and Does Not Respond to Nucleotides 1 (*DORN1*) receptors recognize extracellular ATP (*e*ATP) (Choi and Klessig, 2016). Similarly, various PRR for PAMPS include *RLKs* like flagellin sensing receptors *FLS2* and *FLS3* for recognition of *flg22* and *flgll28* epitopes of bacterial flagella, the *EF* receptor proteins (*EFR*) that recognize prokaryotic *EF-Tu*, *XPS1* for xanthine/uracil permease (*xup25*) recognition, chitin elicitor receptor kinase (*CERK1*) for recognition of chitin and related compounds (Nicaise et al., 2009; Mott et al., 2016; Saijo et al., 2018). Similarly, *LysM-RLPs* like

the chitin elicitor binding protein (*CEBiP*) can also recognize apoplastic chitin and induce subsequent defense response (Shimizu et al., 2010).

On recognition of MAMPS and DAMPS by the extracellular domains of various PRRs, cytoplasmic co-receptors are recruited for dimerization or polymerization of PRRs and subsequent activation of cytoplasmic kinases, which results in calcium (Ca^{2+}) influx and activation of calcium-dependent protein kinases (*CDPKs*), mitogen-activated protein kinase (*MAPK*), and phytohormone signaling and transcriptional reprogramming. This also results in rapid generation of ROS, nitric oxide, release of phenolics and terpenoids, alteration of the cell wall, and biosynthesis of *PR* and other defense proteins. Successful outcome of these cascades during the initial stages of infection results in pathogen triggered immunity (PTI) (Newman et al., 2013; Rathore and Ghosh, 2018; Ramírez-Zavaleta et al., 2022). PTI can result in activation of several signaling pathways, including rapid influx of extracellular calcium (Ca^{2+}), activation of *MAPK*, besides other signaling pathways like ROS, salicylic acid (SA), jasmonic acid (JA), ethylene, n-hydroxy pipecolic acid, cytokinin, and lipids (Nyugen et al., 2021; Ramírez-Zavaleta et al., 2022). However, pathogens may evade detection by PRRs by releasing various effector molecules that can suppress PRR activity and prevent synthesis of ROS and defense proteins. Plants possess diverse resistance (R) proteins identified with two conserved features, nucleotide-binding (*NB*) and leucine rich repeats (*LRR*) -containing receptors, combinedly referred to as *NLR* proteins that can selectively recognize pathogenic effectors, either directly, or indirectly, and subsequently trigger cellular events associated with effector triggered immunity (ETI). One of such responses triggered by NLRs may lead to programmed cell death and the hypersensitive response (HR). PRR and NLR-mediated defense responses are similar and overlapping, although

ETI mediated defense responses reportedly are of larger magnitude and longer duration PTI (Tsuda and Katagiri, 2010; Nyugen et al., 2021).

Limiting the spread of pathogens through HR response and cell death is beneficial, but only against parasitic pathogens that are biotrophic, and not against necrotrophs. Specific pathogen recognition and response strategies are therefore required. Such specificity is mediated by distinct hormonal signaling. For instance, SA, its derivatives, and associated *PR* proteins have been associated with PTI, ETI and HR mediated response against biotrophic pathogens, while JA, its derivatives and its consortium of *PR* and defense proteins combat necrotrophic pathogens, while an HR response has not been described in association with JA signaling. SA, JA, and ethylene are key players in defense against biotic stress, while JA, ABA, ET have been reported in response to abiotic stress. Besides prominent role of these phytohormones in stress responses, their interactions or crosstalk with growth hormones such as auxin, cytokinins, and GA, also imply their importance in plant growth and development as well as long-distance signaling in plants (Huber and Bauerle, 2016; Pieterse et al., 2012). Signaling to neighboring cells and tissues over short distances may be conveyed via the apoplast, and involve extracellular ATP, nicotinamide adenine phosphate (NAD/ NADP), pipecolic acid, plant elicitor peptides (*Peps*), ROS, and phytocytokines such as rapid alkalinization factors (*RALF*) (Vlot et al., 2021; Sun and Zhang, 2020). Plant volatile compounds such as methyl salicylate, methyl jasmonate and monoterpenes have also been associated with systemic induction of defense responses upon pathogenic attack, over short distances (Huber and Bauerle, 2016). Knowledge of systemic signaling of plant defense over long distances, e.g., in trees, is still in its infancy, with three main types of long-distance stress signals have been proposed in plants so far: hydraulic, chemical, and electric.

Hydraulic signals are arguably the initial carriers of stress stimuli for systemic responses, and they are generated by positive or negative changes in cell wall pressure caused by the expansion of the xylem sap (+), or a decrease in the water potential gradient within the xylem column (-) due to a wounding or damage event. During cell events leading to HR response, changes in apoplastic water potential have been linked with reduced bacterial pathogen load (Wright and Beattie, 2004). Besides, aquaporin channels in the cell membrane that regulate the systemic hydraulic continuum between bundle sheath and mesophyll (Sade et al., 2014), can also contribute to PAMP-triggered defense responses such as callose deposition, enhanced *MAPK* signaling, and *NPR/PR* activation and enhanced H_2O_2 transport (Li et al., 2020). Additionally, prolonged low water potential in the apoplast may also trigger reduction or complete obstruction in xylem conductivity related to defense-associated vascular restriction of some bacterial pathogens (Beattie, 2011). Eventually, a gradient of xylem tension potential may also result in stomatal closure and reduction in stomatal conductance, net photosynthesis, and transpiration, and also trigger ABA signaling (Kim et al., 2004; Bauer et al., 2013). However, direct evidence of systemic induction of tolerance or defense responses by long-distance hydraulic signals has yet to be collected.

Chemical signals have been discussed with respect to polyatomic molecules and plant metabolites that are likely involved in systemic responses of various defense metabolites and plant hormones. Various plant metabolites, proteins, and transcription factors, like the defective in induced resistance (*DIR1*) protein, the diterpenoid aldehyde dehydroabietinal (DA), legume lectin-like proteins (*LLP*), glycerol-3-phosphate, azelaic acid-induced (*AZI1*) proteins, master regulator of cell cycle entry and proliferative metabolism (*MYC2*), jasmonate associated ZIM domain (*JAZ*), coronatine insensitive (*COI-1*), have been discussed in context of recognition of

biotic stresses in distal plant tissues. Volatile monoterpenes have also been associated with defense signaling, via systemic interaction with *LLPs* and subsequent activation of SA, pipecolic acid, and azelaic acid-mediated defense responses (Vlot et al., 2021). The involvement of plant hormones such as SA and JA in long-distance biotic stress signaling remains debatable, owing to slower propagation speeds than hydraulic and electric signals (Huber and Bauerle, 2016). However, volatile derivatives of SA and JA such as methyl salicylate and methyl jasmonate, as well as the JA conjugate jasmonoyl isoleucine have been reported as potential long-distance signals in plants (Chen et al., 2019; Liu et al., 2011).

Electrical signals are often discussed in context ion gradients resulting out of imbalances in calcium (Ca^{2+}), chloride (Cl^{-}), potassium (K^{+}), and (H^{+}) ions across the plasma membrane or between cells through plasmodesmata, leading to a transient voltage potential depending on the stimulus type and the resulting ion/anion fluxes. The propagation signal can be of four types, action potential (AP), and cold shock slow wave potential (SWP), wound potential (WP), and system potential (SP) (Choi et al., 2016; Huber and Bauerle, 2016). APs are elicited by non-invasive stimuli including electrical stimuli, acid rain, and irradiation, whereas SWPs are mainly elicited by abiotic and biotic stressors such as mechanical wounding, tissue burning, or herbivore attack; finally, WPs and SPs are elicited upon wounding (Huber and Bauerle, 2016; Gallé et al., 2015). Localized ABA accumulation may also induce an auto-propagating ROS/ Ca^{2+} wave that functions as long-distance systemic signal. Similarly, damage induced accumulation of glutamate and subsequent activation of glutamate receptor-like (*GLR*) proteins may trigger rapid auto-propagating calcium (Ca^{2+}) waves that induce systemic JA-mediated defense signaling (Toyota et al., 2018; Takahashi and Shinozaki, 2019). Also, while localized efflux of H^{+}, K^{+}, and ROS is part of PCD, the resultant intercellular gradient of these ions also generates an auto-propagating

signal caused by rapid depolarization and re-polarization of adjacent plant cells or tissues (Shabala and Pottosin, 2014; Huber and Bauerle, 2016). At the same time, the rapid propagation of ionic fluxes between cells movement of these signals may also trigger systemic activity of SA, JA, ROS, and *PR* proteins mediated defense (Choi et al., 2016; Toyota et al., 2018). Therefore, the nature of long distance signaling in response to biotic and abiotic plant stress are variegated and their transmission are interconnected and simultaneously regulated, which complicates their segregation into biotic and abiotic long signals, as often attempted for localized stress responses.

However, signaling must be involved in acquired resistance (Wilkinson et al., 2019). Acquired, or induced, resistance, can be defined, at its core, as an alerted state by which the plant responds more rapidly and forcefully to a pathogen if the host was exposed to the same or a different pathogen/microbe in the recent past, akin in outcome to vaccination in animals. Plants exhibit various forms of acquired resistance that are expressed over time, and in systemic tissues, such as systemic acquired resistance (SAR), induced systemic resistance (ISR), and systemic induced resistance (SIR) which also imply the existence of long-distance stress signals in plants. SAR is defined as a plant response specifically against biotrophic and hemibiotrophic pathogens, and certain insect pests. that results in priming of defenses to produce quicker and heightened resistance against successive attacks. Several mechanisms of SAR have been proposed to date, involving PTI/ETI-mediated SA accumulation, and subsequent activation of defense responses, localized HR, suppression of non-expressor of *PR* genes (*NPR1*) and *NPR3/ NPR4* proteins for enhanced *PR1* synthesis, as well as defense signaling involved in systemic induction of pipecolic acid, nitric oxide, ROS, glycerol-3-phosphate, azelaic acid, azelaic-induced (*AZI1*) proteins, and defective in induced resistance (*DIR1*) proteins. All these compounds, except nitric oxide, have been associated with SAR signaling through both xylem and phloem transmission routes (Vlot et

al., 2021; Chandra and Sharma, 2023). ISR is defined as a plant response induced by beneficial plant-microbe interactions, specifically by plant growth-promoting rhizobacteria (PGPR), mediated by the JA pathway and expressed against hemi-biotrophic pathogens; however, the defense response is like PTI and ETI response observed in SAR induction (Pieterse et al., 2014). The *MYC2* and myeloblastosis viral oncogene homolog (*MYB*) transcription factors are critical ISR components and also belong to the JA signal transduction pathway. The *MYB* transcription factors are involved in defense against hemi-biotrophic and necrotrophic pathogens, while they can also induce the synthesis of rhizospheric compounds like scopoletin to foster root colonization. Other components of ISR include systemic activity by ethylene, azelaic acid, and *AZI1* and *LLP* transcription factors. Thus, mechanisms of defense responses may overlap between SAR and ISR induction, although an SA-independent *NPR1* induction may also occur systemically during ISR responses (Vlot et al., 2021; Yu et al., 2021).

Unlike SAR and ISR, systemic induced resistance (SIR) is recognized in plant-pathogen interactions, such as those in trees, where signaling systems and induction of defense responses have not been well characterized, are non-specific and not exclusive to any specific pathogen type or lifestyle, i.e., it simply refers to the outcome phenotype (see Bonello et al., 2001, who based this definition on Kuc et al., 1983). In forest trees, SIR was unequivocally initially reported in Monterey pine against hemi-biotrophic pathogens like *Fusarium circinatum*, which causes pitch canker (Bonello et al., 2001; Gordon et al., 2010; Swett et al., 2015). Subsequently, SIR (and systemic induced susceptibility, or SIS) has also been demonstrated in Austrian pine against *Diplodia pinea* that causes shoot and tip blight and canker (Blodgett et al. 2007). SIR has also been demonstrated in Norway spruce (*Picea abies* (L.) Karst.) against sublethal doses of the blue stain fungi, *Ceratocystis polonica* (C. Moreau) between a week and up to a year post

induction, whereas a higher attack density may be detrimental to plant health and turn fatal (Krokene et al., 2003). Other forms of SIR have also been reported, often addressed with varying nomenclature such as mycorrhizae induced resistance (MIR). Further, root colonization of solanaceous plants by AM fungi, *Rhizophagus* spp., *Glomus* spp., induces systemic resistance against root rot pathogen, *Phytopthora infestans* (Gallou et al., 2011), as well as the chewing pest, *Trichoplusia ni* (Hübner) (Schoenherr et al., 2019), and against the root-knot causing nematode, *Meloidogyne incognita* (Vos et al, 2013). The colonization of barley roots by the endophytic fungi, *Piriformospora indica* generates confers systemic resistance against the biotrophic foliar pathogen, *Blumeria graminis* f. sp. *hordei* (Molitor et al., 2011). Also, SIR has also been reported in tomato plants against the root-knot nematode, *Meloidogyne javanica* upon induction with β-amino butyric acid (Oka et al., 2007). In the aforementioned pathosystems, the form of acquired or induced resistance may or may not adhere to reported defense mechanism and underlying signaling, as described in SAR or ISR.

Interestingly, the evidence of SIR in Monterey pine has been invoked as a long-term mechanism of ecosystem recovery in California from invasion by *F. circinatum*, a non-native pathogen (Gordon et al. 2020). Under ideal conditions, initial stress events can be resisted by the combination of the plant's constitutive and induced defenses, conferring broad-spectrum resistance against subsequent attacks by similar or different pests and pathogens. However, an overwhelming initial invasion or attack by pathogens and pests can result in depletion of plant resources and consequent failure of SIR, resulting instead in systemic induced susceptibility (SIS) (Bonello et al., 2006; Blodgett et al., 2007).

1.4 The Austrian pine- *Diplodia pinea* pathosystem

The existing line of knowledge about plant defense and the mechanisms of their selective deployment in response to an abiotic or biotic stress is based on robust and replicated studies on various pathosystems. A pathosystem represents one or more host species and a parasite (or pathogens and whole microbiome) species that can influence host-pathogen population dynamics, genetics, and evolution at the community level. Furthermore, pathosystems are also influenced by environmental factors alone, as in wild pathosystems, or they may be influenced by both environmental and anthropogenic factors, as in cultivated pathosystems (Lebeda & Burdon, 2023). Among tree pathosystems, the Austrian pine (*Pinus nigra* Arnold)- *Diplodia pinea* (Desm.) J. Kickx (formerly *Sphaeropsis sapinea* (Fr.) Dyko & B. Sutton) pathosystem has become a model for studying not only defense responses in trees, but also the expression of SIR in perennial host- pathogen interactions (Sherwood & Bonello, 2016; Sherwood et al, 2015; Blodgett et al, 2007; Luchi et al, 2005).

Austrian pine is an evergreen, two-needle pine species that can be found across southern Europe, Asia Minor, and northern Africa. It is considered a drought, high salinity, and industrial pollution-tolerant species. Consequently, it is used for industrial shelterbelts or roadside plantations, or in urban landscapes in the midwestern, eastern, and southern parts of the U.S (United States). (CABI, 2023; Kunert et al., 2021; Hutnik et al., 2014). Austrian pine wood is also commercially used in housing construction and furniture, while pulpwood may be desirable for the paper industry (CABI, 2023). Austrian pine is also one of many hosts for the necrotrophic fungus, *D. pinea,* which causes tip and shoot blight and canker in a variety of hosts in the families Pinaceae, Cupressaceae, Rosaceae, Visaceae, and Betulaceae. *D. pinea* is a cosmopolitan and opportunistic pathogen, reported in the Americas, Africa, and Southern

Europe, with reports of progression into Northern Europe, South and South-East Asia, and Oceania (CABI, 2023).

The fungus, *D. pinea* can exist asymptomatically in hosts, causing latent infections that become activated by abiotic host stress conditions. Like all canker-like pathogens, it usually requires a wound or natural opening (e.g., stomata) to enter the host, but it can also infect though direct penetration of expanding shoot tips and needles. Infection causes necrotic symptoms that may vary depending on pre-existing stresses, especially water stress (Blumenstein et al., 2022). Visible yellowing of tips followed by progressive browning or necrosis may lead to shoot blight. Infected twigs, branches, and stems develop cankerous lesions that spread longitudinally and can lead to stunting and gradual deformity of branches. Underlying wood in mature branches may be stained from green to brown to blue-black, and old cankers are bound by callus. Progressive infection in stressed trees may lead to shoot dieback, forking of branches, and crooked leaders. Infected cones are darkish in color, deformed, and shrunken. The pathogen can also overwinter externally as pycnidia on dead cones, branches, and needles that can be retained on trees for extended periods and whose conidia can be dispersed by wind, rain splash, and insect vectors to newer hosts (Cornell Plant Disease Diagnostic Clinic, 2015; The Ohio State University Extension, 2016).

D. pinea is phylogenetically placed in the Botryosphaeriaceae and associated anamorphic fungi and identified as morphotype A and C, while morphotype B has been identified as a sister species, *D. scrobiculata* (J. de Wet, B. Slippers & M. J. Wingfield, sp. nov.; *sensu* De Wet et al., 2003; Smith and Stanosz, 2006). The latter sister species was first reported in North America as a shoot blight pathogen (Burgess et al., 2004), along with recent reports in Northern Spain on *P. radiata* (Manzanos et al., 2017), and further as a canker pathogen of *Tetraclinis articulata*

(juniper gum) in Tunisia (Hlaiem et al., 2022). *D. scrobiculata* is usually associated with low levels of pathogenicity than *D. pinea* (Blodgett and Bonello, 2003), however, it is reported to have similar pathogenicity as *D. pinea* on *P. patula* plantations in South Africa (Bihon et al., 2011). This property has allowed us to test hypotheses about the nature of virulence in this pathosystem under changing climatic scenarios (Ghosh et al., 2022). Importantly, in this pathosystem, the virulence of the pathogen (or, conversely, the level of susceptibility of a host individual) can be assessed by measuring the length of lesions (shoot tip dieback; cankers) produced in response to mechanical inoculations, including verifying the SIR phenotype (Sherwood & Bonello, 2016; Blodgett et al, 2007).

1.5 Research questions

Our laboratory has published several papers describing the nature of defense responses expressed locally and systemically in this system (Blodgett and Bonello, 2003; Bonello and Blodgett, 2004; Luchi et al., 2005; Wang et al., 2006; Blodgett et al., 2007; Wallis et al., 2007; Sherwood et al., 2015; Sherwood and Bonello, 2016). Cross-induction of SIR between *D. pinea* and the European pine sawfly has also been demonstrated (Eyles et al., 2007). Systemic elicitation of defense responses has been demonstrated upon prior induction of Austrian pine stem with both live and killed mycelia of *D. pinea*, as well as protein extracts from the pathogen (Bonello and Blodgett, 2004). Phenotypically, the size of the canker or lesions produced by *D. pinea* infection has also been demonstrated as an indicator of disease severity (Sherwood and Bonello, 2016). Further, an SIR response has been demonstrated at least, after 2 weeks post an induction infection by *D. pinea* (Wallis et al., 2011). In terms of defense response, traumatic resin duct induction has been observed in the APDP system at 4 days post-induction by *D. pinea*, and 12 days (about 1 week 5 days) post wounding or mock induction (Luchi et al., 2005). SIR responses have also been

associated with the induction of phenolic compounds such as lignin, stilbenes, and phenolic glycosides (Wallis et al., 2007; Wallis et al., 2011), as well as their growth fungistatic properties against *D. pinea in vitro* (Sherwood et al., 2013). However, significant induction of phenolics in unchallenged plant tissues has only been noted after two weeks post-induction by *D. pinea* and depends on nutrient availability (Wallis et al., 2011). Further, the SIR/SIS expression in the pathosystem has been demonstrated as plastic and can dissipate in the absence of challenge infection after two weeks post-induction, as well as its expression is organ-specific (Blodgett et al, 2007). The dissertation addressesthe following gaps in knowledge with respect to the established literature in the pathosystem.

(1) In Chapter 2, we investigated the combined effects of simulated climate change (CC) scenarios of elevated temperatures and water scarcity along with pathogenic infections with *D. pinea,* or *D. scorbiculata* on Austrian pine. We measured lesion lengths after two weeks to assess degree of infection and followed up with a dual-transcriptomics approach to investigate possible gene expression changes post infection in the Austrian pine- *Diplodia* spp. pathosystem, under normal and CC conditions. While we found higher pathogenicity due to *D. pinea* infection than *D. scrobiculata* under normal conditions, both species were similarly pathogenic under CC conditions. We also found that suppressed primary metabolism associated with carbon and nitrogen along with suppressed defenses results in increased pathogenesis during *D. pinea* invasion, while unaltered primary metabolism and heightened defenses confer lower pathogenicity observed in *D. scrobiculata* infected trees. Under CC conditions, host pines experience suppressed primary metabolism and defenses, leading to enhanced aggressiveness in *D. scrobiculata* infection.

(2) In Chapter 3, we investigated early evidence of SIR expression against pathogenic attack, in continuation with reports of SIR expression in the APDP pathosystem starting at 10 days after induction (Sherwood and Bonello, 2016). We conducted an experiment in 2020, where we induced Austrian pine stems by either infection with *D. pinea*, or by wounding (mock), followed by incubation for either 12 hours (0.5 days), 72 hours (3 days), or 10 days (about 1 and a half weeks), and followed up with a systemic challenge infection. We measured lesion lengths after two weeks to assess the degree of infection, and later compared them across treatments to investigate evidence of SIR due to the nature induction, and across different incubation times. We found that SIR is exhibited within 0.5 days of induction by *D. pinea*, and also to a lesser degree due to wounding, and this response increases over time, up to 10 days of incubation post induction.

(3) Following the evidence of SIR in the experiment conducted in 2020, we also describe our investigations of the role of various monoterpenes, sesquiterpenes, and other plant volatile compounds in early induction of SIR in Chapter 3. We subsequently extracted, quantified, and classified levels of terpenoids, using gas chromatography mass spectrometry (GC-MS), in Austrian pine phloem sampled at pre- induction and pre- challenge, as well as their levels at two weeks after challenge inoculations. We found sixteen compounds belonging to monoterpenes, sesquiterpenes, and other plant volatile compounds with significant responses in our treatment groups, including first report of involvement of dodecanol and n-dodecyl acrylate in induced defenses in pines. We also found a nuanced role of various co-regulated terpenoids in SIR expression, along with fungistatic activity of the co-regulated compounds in measured SIR concentrations.

(4) In Chapter 4, we describe our study conducted in 2021, where we induced Austrian pine trees using a similar study model as described in Chapter 3, except without the challenge inoculation, and sampled the unchallenged phloem from a systemic location similar to Chapter 3 after an incubation of either 0.5 days, 1 day, 1.5 days, 2 days, 3 days, or 7 days. We sampled the phloem from a systemic location, like the Chapter 2 model, and examined changes in gene expression, and used liquid chromatography-tandem mass spectrometry to characterize phytohormone changes. We found significant responses by jasmonic acid, and its precursor and derivative compounds associated with the SIR response exhibited by Austrian pine in response to pathogenic induction, along with nuanced responses of abscisic acid, auxin, along with differential expression of their associated signaling pathways.

CHAPTER 2
MECHANISMS OF PINE DISEASE SUSCEPTIBILITY UNDER EXPERIMENTAL CLIMATE CHANGE

2.1 Introduction

The elevated temperatures predicted under climate change scenarios can directly impact plant physiology. The effects are expressed mostly through exacerbation of water limitation due to elevated vapor pressure deficits, which impose extra demands on the water relation capabilities of trees (Adams et al., 2009; Williams et al., 2013). Under sub-lethal drought conditions, physiological processes other than carbon starvation or interruption of water conduction can render droughted plants more susceptible to mortality from pathogen attack. For example, plants often respond by reducing photosynthesis and growth, accumulating compatible solutes (osmoprotectants) such as the amino acid proline (Pro), producing reactive oxygen species (ROS), and altering specialized metabolism, among other processes (Chaves et al., 2003; Bhargava and Sawant, 2013).

One system-level question emerges from this conceptual framework: "How does climate change-associated stress affect the internal environment of a tree to predispose it to fungal infection?" This is currently one of the top 10 unanswered questions in plant-pathogen interactions (Harris et al., 2020).

Tree pathosystems, such as those involving *Diplodia* spp. and other Botryosphaeriaceae, represent a large class of emerging diseases caused by opportunistic fungi that mostly 'sit-and-wait' as asymptomatic endophytes, becoming highly destructive necrotrophs only under certain environmental conditions (Herre et al., 2007; Slippers and Wingfield, 2007), such as low water availability (Blodgett et al., 1997a; b). However, the molecular and metabolic mechanisms underlying stress-induced tree susceptibility to pathogens remain poorly understood. This hampers predictions of how tree pathosystems will behave and evolve under projected climate change scenarios. System-level studies of the main players will address this deficiency (Bostock et al., 2014). Our work to date using the Austrian pine (*Pinus nigra*) - *D. pinea* pathosystem has addressed basic mechanisms underlying host susceptibility under normal growth (Blodgett and Bonello, 2003; Luchi et al., 2005; Wang et al., 2006; Eyles et al., 2007; Barto et al., 2008; Wallis et al., 2008; Wallis et al., 2011; Sherwood and Bonello, 2013; Sherwood and Bonello, 2016) as well as under drought conditions. Under relatively severe drought, we have observed alterations in (1) levels of some free phenolics, lignin, and terpenoids; (2) Pro metabolism; (3) ROS homeostasis; and (4) possible alteration in programmed cell death (PCD), and fungal capacity to neutralize/take advantage of host responses (Sherwood et al., 2015).

Our aim in this study was to investigate how climate change affects the interactions between host and opportunistic pathogens like *Diplodia* spp. Our main objectives were to simulate a climate change scenario and test the outcomes of pathogenic infections of contrasting aggressiveness under different scenarios of climate conditions. To do so, we subjected 3-year-old Austrian pine saplings to simulated climate change conditions of combined reduced water availability and elevated temperatures. After a period of exposure to the climate conditions, we inoculated the saplings and monitored infection processes using two closely related species of contrasting

aggressiveness: *D. pinea* (aggressive) and *D. scrobiculata* (non-aggressive) (Blodgett and Bonello, 2003; de Wet et al., 2003). To gain insight into system-level processes, we conducted transcriptomic analyses of simultaneous host and pathogen responses. We hypothesized that any shifts in aggressiveness (or, conversely, host susceptibility) due to climate change conditions would be more evident with *D. scrobiculata* and results in differential dual (host and pathogen) gene expression in the preliminary stages of infection.

2.2 Materials and methods

2.2.1 Plant material

Open pollinated, 3-year-old potted Austrian pine saplings were received from Willoway Nurseries (Madison, OH). Trees were maintained in an ornamental nursery yard in the Dept. of Horticulture and Crop Sciences at The Ohio State University (Columbus, OH). After repotting trees into a potting mix consisting of Com-Til compost (provided by Department of Public Utilities, city of Columbus, OH), pine bark, and organic matter (1:1:1 = v:v:v) comprised primarily of composted yard waste, trees were transferred to the greenhouse for several months of growth.

2.2.2 Growth chamber conditions

Three weeks before inoculation, trees were transferred to two growth chambers for acclimation. We imposed the following conditions (more details in Appendix A1.):

Control treatment (CT): daily minimum of 15 ºC and maximum of 28 ºC (corresponding to a 16/8 h light/dark cycle), and RH of 60% throughout, to generate a VPD of 0.7 and 1.5 kPa (http://cronklab.wikidot.com/calculation-of-vapour-pressure-deficit) during dark and light, respectively.

CC treatment (CCT): daily minimum of 20 ºC and maximum of 33 ºC (corresponding to a 16/8 h light/dark cycle), and RH of 60% throughout, to generate a VPD of 0.9 and 2.0 kPa during dark and light, respectively. Pre-dawn needle water potentials were measured with a Scholander pressure bomb (PMS Instrument Co., Corvallis, OR).

2.2.3 Inoculation treatments

Our experimental design was constrained by logistical limitations imposed by the availability of growth chambers: one for the CT and one for the CCT. To account for variation between growth compartments (Potvin, 2000), we used a split-plot design with combined heat/drought treatment, simulated by less watering along with higher temperatures (the CCT) as the main plot factor (represented by individual growth chambers) and inoculation state (i.e., mock-inoculated and plants inoculated with *D. pinea* or *D. scrobiculata*) and sampling time (i.e., 12 and 72 h, and three weeks post-inoculation) as the subplot factors (Potvin, 2000). Each inoculation treatment was replicated six times, for a total of 18 trees in each chamber.

On February 17, 2017, trees were inoculated with *D. pinea* or *D. scrobiculata*, or mock inoculated. Isolates of *D. pinea* (Sherwood and Bonello, 2013) and *D. scrobiculata* (Santamaria et al., 2011) were obtained from Dr. Glenn Stanosz of University of Wisconsin Madison and grown and maintained on PDA (Potato Dextrose Agar) in the dark at room temperature. Each treated shoot was lightly wounded by removing a small (< 5 x 5 mm) area of epidermis, using a razor blade, 3-4 cm distal to the transition point between previous and current year growth. Inoculum (or just PDA growth medium in the case of mocks) was placed on the wound, mycelium side down, and the inoculation court was then wrapped with parafilm. Each tree was randomly assigned to a single inoculation treatment (mock, *D. pinea* or *D. scrobiculata*) and randomly treated on six different branches (two branches per time point). The whole inoculation

process was conducted over the course of five hours. No uninoculated controls were used due to growth chamber space availability imposing limitations on numbers of usable plants.

Shoots were sampled at 12 h, 72 h (three days), and three weeks for transcriptomics and dissected at three weeks for determination of relative susceptibility (phenotype) based on lesion lengths. All mock inoculations resulted in no lesions and were excluded from determination of relative susceptibility. Lesions from *D. pinea* and *D. scrobiculata*-infected branches on each tree were averaged and the means used as single data point for that tree. Differences in lesion length between *D. pinea* and *D. scrobiculata* were analyzed separately for CT and CCT trees using two-tailed t-tests assuming unequal variances, as the number of available biological replicates was n = 3-6.

We did not have the resources to conduct RNA-seq analysis at all time points, so we decided to analyze host and fungal responses at 72 h, which we deemed the best compromise to uncover significant genes in the interactions. Based on all our work for the past 18 years on this system, we did not expect any detectable systemic effects of multiple, concurrent inoculations on different shoots of the same tree over the local host responses expressed in each shoot.

2.2.4 Tissue sampling

At sampling time, shoots were removed with pruners, placed individually into paper coin envelopes, and immediately flash frozen in liquid N before transfer to -80 ºC until processing. Subsequently, tissues were harvested to contain either the whole lesion on CT saplings, or the margin of the much longer lesions on CCT saplings, by collecting shavings obtained with a liquid N-chilled razor blade and liquid N-chilled tweezers. Shavings were first dropped into a 50 ml Falcon tube containing liquid N, and then transferred to pre-weighed 2-ml screw-capped

Eppendorf tubes, which were then dropped into liquid N. The tubes were transferred to cardboard freezer boxes and stored at -80 ºC.

2.2.5 RNA extraction and gene expression analysis

Tissue collected 72 h post-inoculation was ground in liquid nitrogen using a mortar and pestle that were pre-chilled in liquid N. Ground tissue was returned to the sampling tube and weight determined before storage at -80 ºC. RNA extraction was carried out following a standard protocol (Chang et al., 1993) modified for pine samples (500 ul extraction buffer preheated at 65˚C, sample in buffer incubated at 65˚C for an hour), from approximately three biological replicates of each treatment combination. RNA extracts were then treated with DNaseI, amplification grade per the manufacturer's instructions (Invitrogen, ThermoFisher Scientific, Waltham, MA, USA) and cleaned-up with the RNeasy Plant Mini Kit per manufacturer's instructions (Qiagen, Germantown, MD, USA). Samples were quantified spectrophotometrically using a NanoDrop (Thermo Scientific, Wilmington, Delaware, USA) and quality and concentration were assessed using TapeStation (Agilent Technologies, Inc., Santa Clara, CA, USA). Samples with 260/280 nm and 260/230 nm ratios between 1.8–2.2 and 1.6–2.2, respectively, were considered of sufficient purity. Stranded illumina RNAseq library were prepared (Molecular and Cellular Imaging Center, The Ohio State University, Wooster, Ohio, USA) and 150 bp paired-end obtained on Illumina NextSeq500 platform (Nationwide Children's Hospital Genome Center, Ohio, USA).

2.2.6 Sequence quality control, assembly, and annotation

Transcriptom assembly was done at xxxx by xxxxx in South Africa and Fig. A1.2 (Appendix A1.) depicts the workflow. Sequenced reads quality was assessed using FastQC (http://www.bioinformatics.babraham.ac.uk/projects/fastqc/) and reads were trimmed for

adaptors and low-quality bases with Trimmomatic v0.36 (Bolger et al., 2014). Reads > 40bases were retained. Reads were mapped to the *Pinus tecunumanii* transcriptome (Visser et al., 2018) using kallisto v0.44.0 (Bray et al., 2016) and expression data were clustered. To generate a *P. nigra* reference transcriptome, reads from all lanes were pooled, and a series of preliminary transcriptomes was assembled using transABYSS v2.0.1 (Robertson et al., 2010), with a *k*-mer range of 21 to 51 with a step of 2 and 55 to 75 with a step of 4, and Trinity v2.4.0 (Grabherr et al., 2011), with a *k*-mer range of 21 to 31 with a step of 2 using trimmed data as well as *in silico* normalized trimmed reads both *de novo* and genome guided against the *P. taeda* v2.01 genome assembly (https://treegenesdb.org/). The preliminary assemblies were combined, and the resulting superset of transcripts was run through the Evidential genes pipeline (Gilbert, 2016) to reduce redundancy and select for optimally assembled transcripts, producing a set of putative host unigenes.

As an unannotated *D. pinea* reference genome was available, pathogen unigenes were predicted using AUGUSTUS v3.3.3 (Stanke et al., 2008) on the *Diplodia pinea* genome (Van Der Nest et al., 2014) using the *Aspergillus fumigatus* training annotation as well as *Diplodia corticola* cDNA (ENA accession PRJNA325745) to improve the prediction. Both pine and fungal unigenes were annotated using EnTAP v0.8.2 (Hart et al., 2020) with GeneMarkS-T v5.1 (Tang et al., 2015), diamond v0.8.31 (Buchfink et al., 2014) and eggnog v0.12.7 (Huerta-Cepas et al., 2016). Annotation parameters used were minimum query coverage = 80, minimum target coverage = 60, and minimum e-value = $1.0e^{-05}$. BLASTp similarity search alignments were performed against the RefSeq complete protein (release 87), UniProt/SwissProt-KB (2018-04) and NCBI non-redundant (nr, 2018-04) databases for both species, as well as the TAIR10 proteome for pine. For the host, the final reference unigenes were produced by removing

sequences with best BLASTp hits from the following taxa as contaminants: Fungi, Bacteria, Insecta, Opisthokonta, Archaea, Viruses and Alveolata. The pine and *Diplodia* proteomes were further annotated using GhostKOALA (Kanehisa et al., 2016) to add KEGG orthology (KO) numbers and Mercator (Lohse et al., 2014) was used to annotate the Austrian pine proteome for analysis with MapMan (Thimm et al., 2004).

2.2.7 Analysis of differentially expressed genes (DEGs)

Read mapping and expression quantification: Host (from the final reference transcriptome assembly) and pathogen (predicted from the *D. pinea* reference genome) unigenes were concatenated to produce a combined reference transcriptome. Kallisto v0.44.0 (Bray et al., 2016) was used to map the concatenated sequenced reads and quantify expression against the combined reference for each sample. Kallisto output was imported into R v4.0.4 (R Core Team 2021) using tximport v1.22.0 (Soneson et al., 2015) to separate host and pathogen mapped read sets and perform expression analysis. Transcripts that were only represented in mock samples were removed and only those transcripts were retained, which had at least 20 reads in 3 or more samples in each dataset.

For the host: Host expression was analyzed using DESeq2 v1.34.0 (Love et al., 2014). Filtered count data were read into a differential expression (DE) object and library sizes were estimated by treatment type. A Poisson distance matrix was generated for the normalized host reads to determine possible clustering of samples by treatment type. A multi-dimensional scaling (MDS) plot was generated to investigate possible correlation by treatment or condition. Analyses of DEGs were then performed for the following pairwise comparisons of interest: (1) host responses to *D. pinea* vs. mock inoculation under CT, (2) host responses to *D. scrobiculata* vs. mock inoculation under CT, (3) dual responses of host and pathogen following *D. pinea* attack

vs. *D. scrobiculata* attack under CT, (4) dual responses of host and pathogen following *D. scrobiculata* attack under CCT vs. CT (Fig. 2.1).

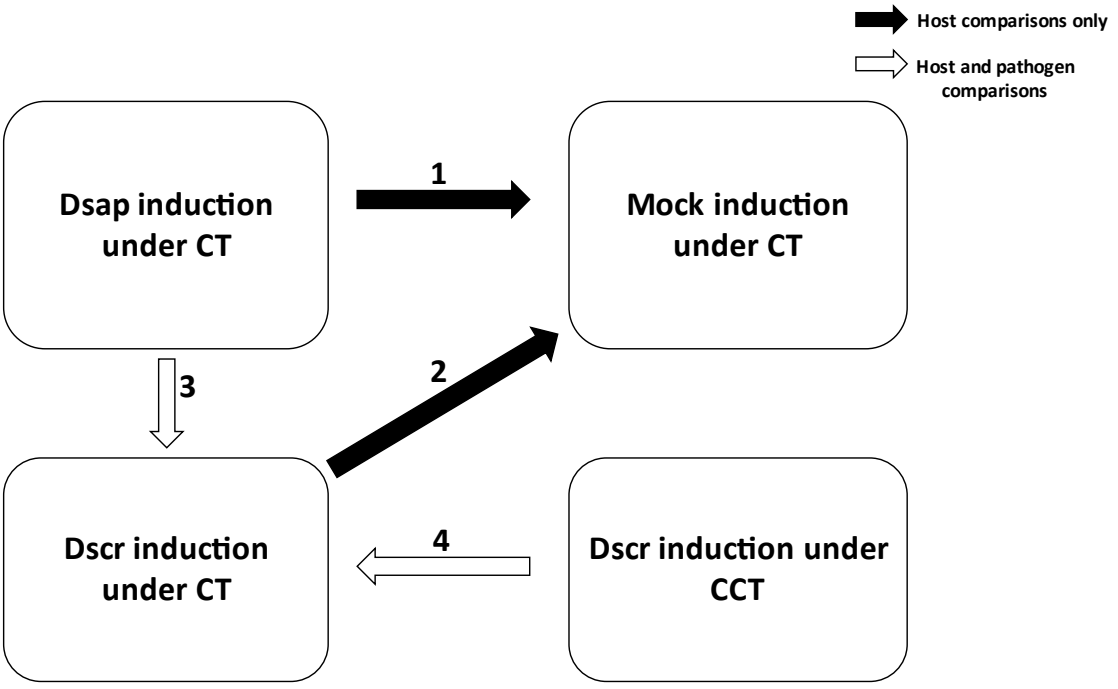

Figure 2.1. Pairwise comparisons carried out in this study for estimating differential gene expression. Black arrows indicate comparisons for host only; white arrows indicate both host and pathogen comparisons. CT: control treatment; CCT: climate change treatment; Dsap: inoculated with *Diplodia pinea*; Dscr: inoculated with *D. scrobiculata*; Mock: inoculated with PDA only.

For the pathogen: Both DESeq2 v1.34.0 (Love et al., 2014) and edgeR v3.36.0 (Robinson et al., 2010) were used to identify differentially expressed genes for the pathogen comparisons. Filtered counts were read into a DE object and effective library sizes were estimated for each treatment type. An MDS plot was generated to visualize the profile differences between different treatment types (climate conditions and inoculation type) and a mean-variance plot was generated to

determine the overall fitness of the model. Pairwise comparisons for DEGs were established as follows: (3) *D. pinea* vs. *D. scrobiculata* during infection of pines under CT, (4) *D. scrobiculata* during infection of CCT pines vs. CT pines (Fig. 2.1).

To perform GO functional enrichment analysis of gene functions, we tested our pre-defined lists of DEGs as per respective host and pathogenic comparisons against a global list of biological gene ontologies assigned for all the annotated genes of our study. We used a false discovery rate (FDR) $p < 0.05$ and a threshold of $\log_2$ fold change ratio of ± 0.5 (~ 1X fold change in expression). These filtered DEGs were sorted by EGGNOG annotations and KEGG pathways reconstructed to visualize what genes were affected in global metabolic pathways. However, to investigate biological relevance of the most significant and highly expressed genes for a given comparison we applied a more stringent threshold of $\log_2$ fold change ratio of ± 2.3 (~ 5X fold change in expression).

2.3 Results

2.3.1 Abiotic stress

On February 14, March 1, March 3, and March 8, 2017, needle water potentials averaged -0.1 kPa and -1.3 kPa, -0.3 kPa and -2.0 kPa, -0.3 kPa and -2.0 kPa, and -0.1 kPa and -2.4 kPa, (N = 6 for each mean), for the pines in the CT and CCT chambers. Differences in water potential were reflected in needle appearance (Fig. 2.2A).

A

B

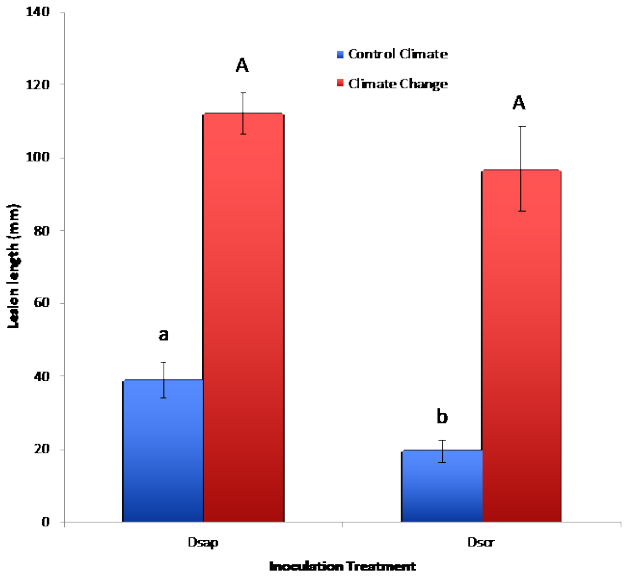

Figure 2.2. (A) Chlorotic and partly desiccated appearance of mock-induced pine needles subjected to climate change treatment (left) vs. deep green and turgid needles in the control treatment (right). **(B)** Lesion lengths (mm) measured three weeks post inoculation. X-axis: Dsap: inoculation with *D. pinea*; Dscr: inoculation with *D. scrobiculata*; mock: inoculation with PDA only. Blue bars represent the control climate treatment (CT), red bars the climate change treatment (CCT). Error bars: standard error of the mean. Different letters represent significant differences within climate treatment at $p < 0.05$.

2.4 Diplodia scrobiculata *is as aggressive as* D. pinea *under CC conditions*

Three weeks post-inoculation, all pines in the CT chamber were alive and had developed lesions in all pathogen inoculated pines. On the other hand, trees in the CCT chamber appeared close to dying with at least half (greater than 50%) of them having at least 1/3 of the crown still green but

chlorotic (Fig. 2.2A). In all cases, lesions on CCT saplings were significantly longer than those on CT plants (Fig. 2.2B). Notably, lesions produced by *D. scrobiculata* in the CCT chamber (Fig. A1.1 in Appendix A1.) were as long as those produced by *D. pinea*, i.e., *D. scrobiculata* became as aggressive as *D. pinea* or, conversely, the host became equally susceptible to both pathogens (Fig. 2.2B).

2.4.1 Metatranscriptome assemblies

Illumina RNAseq sequencing generated 857,867,066 raw reads. After quality trimming 539,379,336 (~ 63%), ranging from 40 to 150 nucleotides, were retained for the assembly. Preliminary k-mer assemblies were produced *de novo* (n = 33) and genome guided against the *P. taeda* v2.01 genome (n = 6), followed by concatenation to produce a superset containing 5,246,838 transcripts (Table 2.1). This superset was further reduced, using the Evidential genes pipeline, to 315,357 transcripts for 30,632 Austrian pine unigenes, while 13,863 *D. pinea* unigenes were extracted from the *D. pinea* genome using the Augustus gene prediction pipeline (Table 2.1).

Table 2.1. Summary of assembly statistics of RNA reads for Austrian pine and *Diplodia* spp. reads.

Parameters[1]	**Concatenated assemblies**	**Evigene (*P. nigra*)**	**Pini_v1.0[2]**	**Non-pine**	**Unannotated**	**Augustus Evigene (*D. sapinea*)**
N	5,246,838	30,632	19,882	3,677	7,073	13,863
N50	1,210	1,762	2,022	801	718	5,670
Smallest	350	351	351	351	351	297

Largest	10,917	10,561	10,561	6,147	5,321	22,668
						(**continued**)
N bases	4,870,308,207	40,263,498	32,680,629	2,704,062	4,878,807	61,522,400
Mean length	948.91	1314.43	1643.73	735.4	689.78	4437.00
N > 1 k	1,406,126	15,207	13,633	641	933	9,347
N > 10 k	14	2	2	0	0	3
N with ORF	2,254,456	23,281	18,122	2,458	2,701	8,381
Mean ORF %	63.21	78.25	78.91	82.52	71.45	60.46

2.4.2 Functional annotation of host and pathogen transcriptome

The Austrian pine and *D. pinea* unigenes were annotated using EnTAP (Hart et al., 2020). Non-pine sequences as well as unannotated sequences were discarded (Table 2.1). Annotation resulted in *P. nigra* v1.0 assembly (Pini_v1.0) containing 19,882 unigenes (8,196 with KEGG Orthology – KO – numbers) and 10,612 *D. pinea* unigenes (4,021 with KO numbers). [All raw sequence reads are publicly available in NCBI, and accession information is provided in Table A1.1 (Appendix 1).

2.4.3 DEG (Differentially expressed genes) analyses

Mapping and filtering produced a subset of 17,443 expressed genes for Austrian pine and 2,303 expressed genes for *Diplodia* spp. The similarity of the host reads was assessed using a Poisson matrix (Fig. A1.3, Appendix A1.); identical treatment types generally showed the closest relationships. Reads obtained after mapping to respective host and pathogen transcriptomes constituted a library size of 15-20 million reads per sample for the host and 0.004 - 0.3 million

reads per sample for the pathogen datasets, respectively (Fig. 2.3). The mean-variance plot indicated that the Poisson model was likely inappropriate for the fungi due to higher-than-expected dispersion over the mean (Fig. A1.4, Appendix A1.). Therefore, we generated respective MDS plots for host RNA-seq data and filtered pathogen RNA-seq data, to evaluate clustering based on treatment / species types (Fig. A1.5, Appendix A1.).

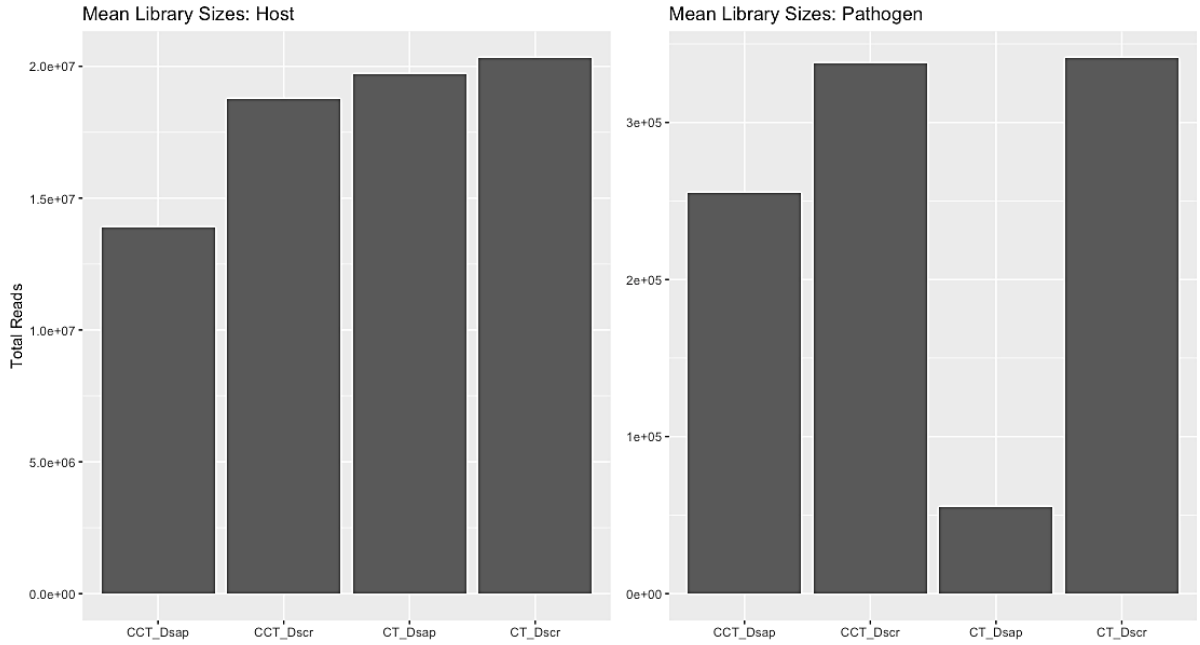

Figure 2.3. Average library sizes retrieved for host and pathogen for all treatment types after mapping of reads to respective host and pathogen transcriptome. Host average library size range: 15-20 million reads; pathogen average library size range: 0.004-0.3 million reads. CT: control treatment; CCT: climate change treatment; Dsap: inoculated with *Diplodia pinea*; Dscr: inoculated with *D. scrobiculata*.

A series of comparisons enabled us to dissect the changes in gene expression patterns associated with key metabolic responses in the host and pathogens under the two climate conditions (Fig. 2.1, Table A1.2, Appendix A1). Specifically, comparisons 1 and 2 in Fig. 2.1 focus on host gene expression resulting from pathogen inoculation under CT, comparison 3 focuses on dual

responses of host and pathogen following *D. pinea* vs. *D. scrobiculata* inoculation under CT, while comparison 4 centers on dual responses of host and pathogen following *D. scrobiculata* inoculation under CCT vs. CT. The volcano plots in Fig. 2.4 provide an overview of the numbers of highly significant DEGs for the four comparisons, which were then investigated by their EGGNOG annotations (Huerta-Cepas et al., 2016), followed by mapping to KEGG (Kanehisa and Sato, 2020) pathways and biological processes through Gene Ontology (GO).

We also looked at gene expression overlaps between different host and pathogen comparisons, respectively. We found 2,526 (31%) overlapping DEGs between comparisons 1 and 2, while 405 (5%) DEGs were exclusive to CTDsap vs. CTMock and 2,910 (35%) DEGs were exclusive to CTDscr vs. CTMock (Fig. 2.4). At the same time, 437 (5%) DEGs overlapped between comparisons 2 and 4, with 1,099 (13%) DEGs exclusive to CCTDscr vs. CTDscr (Fig. 2.5). Similarly for pathogen comparisons, we found 12 (6%) DEGs overlapping between comparisons 3 and 4. Comparison 3 produced 40 (21%) DEGs and 135 (72%) DEGs were mapped to CCTDscr vs. CTDscr, respectively (Fig. 2.5). The complete sets of DEGs and their corresponding GO: Biological processes, for individual comparisons of host and pathogen were tested for enrichment using the TopGO package (Alexa and Rahnenfuhrer, 2021). The classic Fisher method was selected for running the enrichment analysis based on quality comparisons with the elimKS method (Fig. A1.6, Appendix A1.). Enriched GO terms are listed in Table A1.2, Appendix A1.

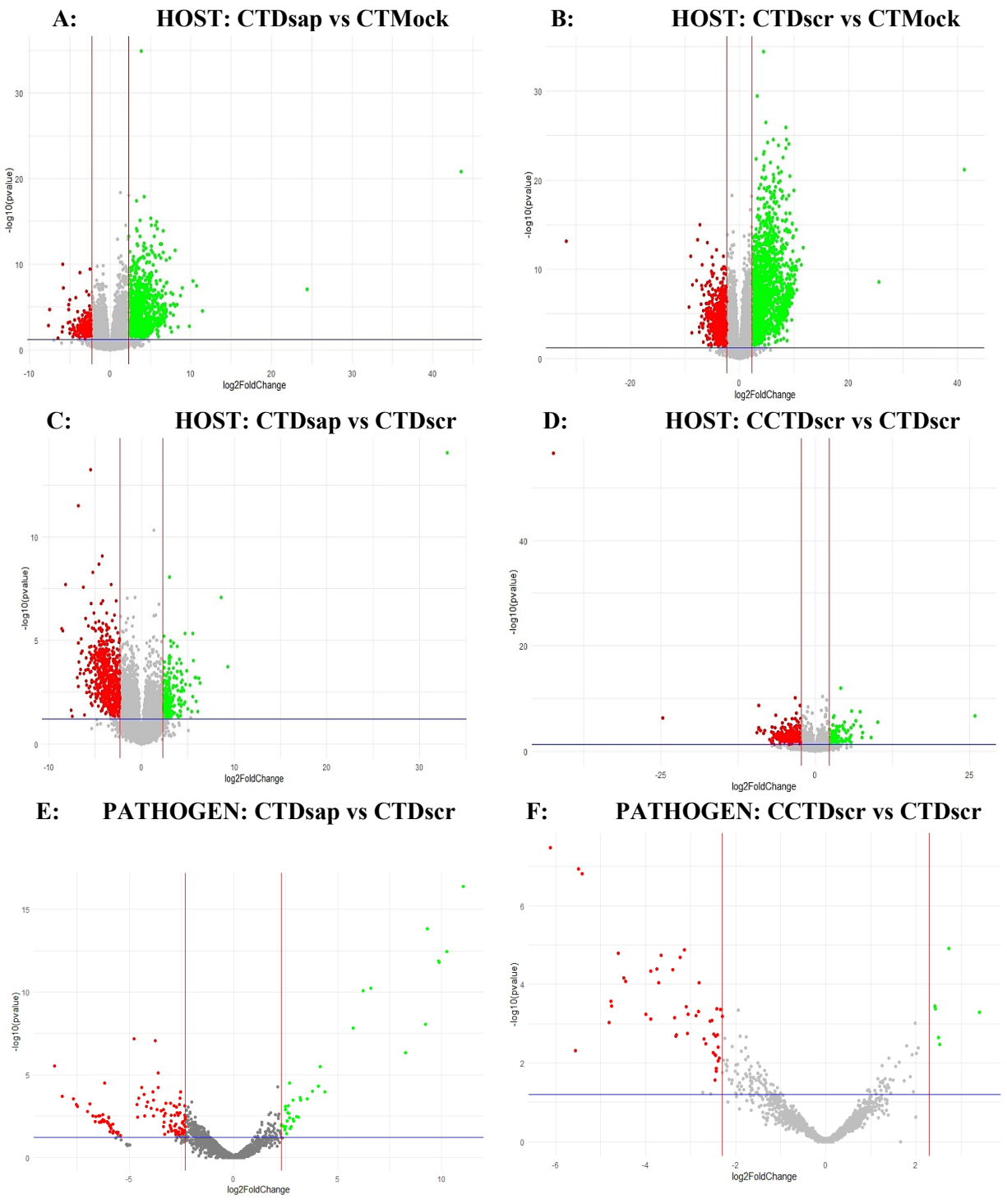

Figure 2.4. Volcano plots of DE genes for individual host and pathogen comparisons. Upregulated and downregulated genes marked in green and red, respectively, based on actual fold-change > 5 (upregulated) or < -5 (downregulated) [i.e., log2 (fold-change) > 2.3 (up) or < -2.3 (down)] and $p < 0.05$. Labels: A - host comparison 1, B - host comparison 2, C - host comparison 3, D - host comparison 4, E - pathogen comparison 3, F - pathogen comparison 4 (Fig. 2.1). CT: control treatment; CCT: climate change treatment; Dsap: *Diplodia pinea*; Dscr: *D. scrobiculata*; Mock: mock inoculated.

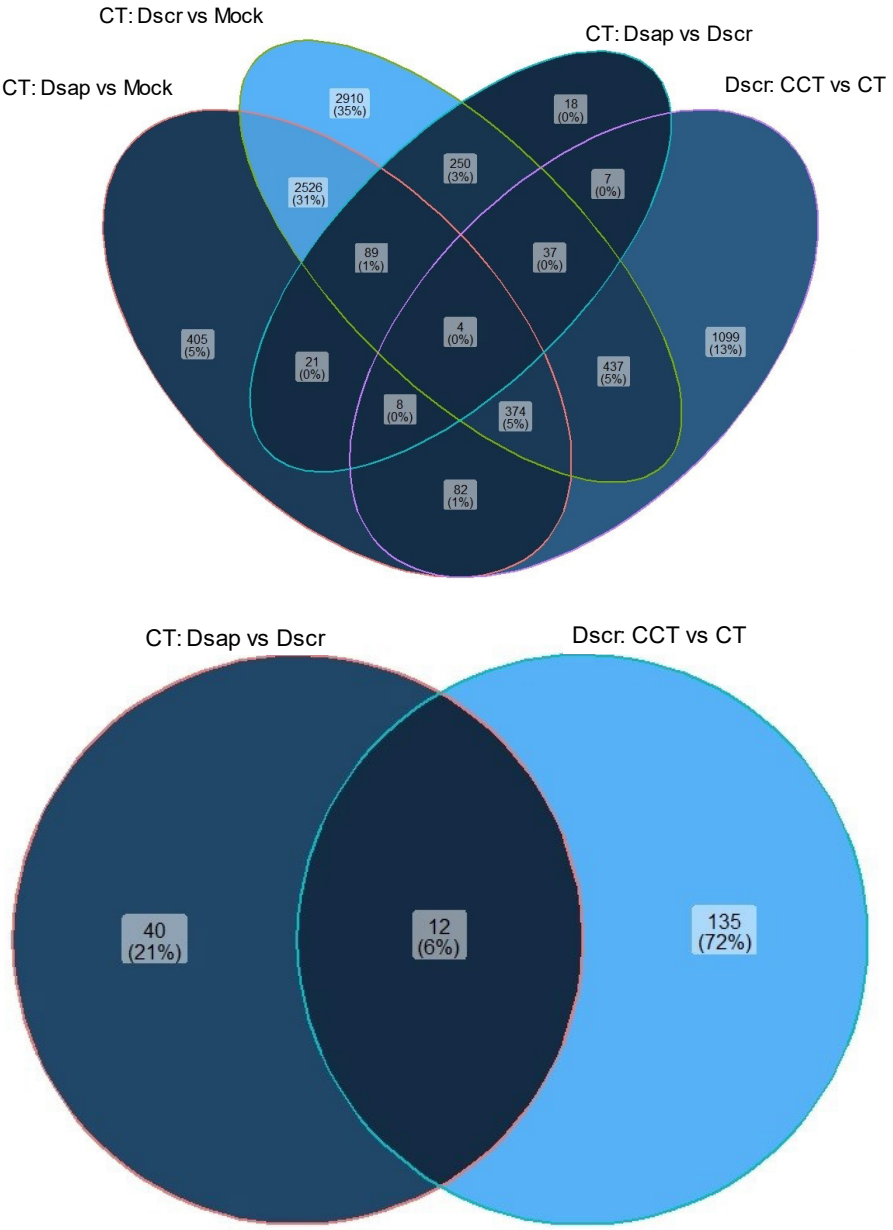

Figure 2.5. Venn diagram showing unique and overlapping sets of DE genes for host (top) and pathogen (bottom). CT: control treatment; CCT: climate change treatment; Dsap: *Diplodia pinea*; Dscr: *D. scrobiculata*; Mock: mock inoculated.

2.4.4 Host responses

2.4.5 Comparison 1: D. pinea infection vs. mock under CT

In this comparison, a total of 3,509 genes were differentially expressed (adj. p-value < 0.05). 2,661 of these were assigned KEGG orthologs and were mapped to various general pathways, while 1,221 were annotated to various GO terms. Out of all 3,509 DEGs, 781 were annotated *via* all three platforms (i.e., EGGNOG, KEGG, and GO) and were assigned to various metabolic functions/pathways. DEGs were annotated to 32 different GO terms, including response to stimulus (646 DEGs), response to stress (381 DEGs), response to oxygen containing compounds (425 DEGs), response to endogenous stimulus (236 DEGs), response to biotic stimulus (292 DEGs), and defense response (298 DEGs), among other responses (Fig. 2.6A). Our stringent filtering threshold (actual fold-change ± 5) produced a list of 512 DEGs, with 308 upregulated genes and 204 downregulated genes that had KEGG and GO annotations (Host-comparison1 in Table A1.2, Appendix A1).

Primary metabolic responses: Among 28 DEGs with photosynthetic GO terms, only two were assigned to both KEGG and GO (Fig. 2.7A). Six different transcripts were mapped to fatty acid biosynthesis on KEGG and assigned to fatty acid or lipid metabolism GO terms (Fig. 2.7A).

Defense associated responses: GO terms associated with defense responses, such as oxygen containing compounds (646 DEGs), defense response to fungus (73 DEGs), response to chitin (40 DEGs), cell wall thickening (4 DEGs), and callose deposition (8 DEGs) were identified (Fig. 2.6A). 12 DEGs were mapped to the KEGG pathway for plant-pathogen interactions. Two calcium binding (CML - calmodulin like) proteins associated with cell morphogenesis involved

in differentiation and 18 DEGs assigned to GO: calcium-mediated signaling were identified (Fig. 2.6A). Three transcripts were annotated to pathogenesis-related protein 1 (PR1) on KEGG and EGGNOG and assigned GO: defense response, along with a WRKY transcription factor and another transcript annotated to disease resistance (RPS2) (Fig. 2.7B) (Host-comparison1 in Table A1.2, Appendix A1).

Phytohormone responses: 15 transcripts were mapped to the plant hormone transduction pathway on KEGG, including significant responses for jasmonate ZIM domain-containing (JAZ) proteins, gibberellin receptor (GID1), and auxin responsive GH3 gene (Fig. 2.7B).

Specialized metabolic responses: The biosynthesis and metabolism of terpenoids were represented in various GO terms such as terpenoid metabolic process (17 DEGs), tetraterpenoid biosynthetic process (5 DEGs), sesquiterpenoid metabolic process (6 DEGs), and diterpenoid metabolic process (9 DEGs) (Fig. 2.6A). We found 7 DEGs mapped to terpenoid backbone biosynthesis on KEGG, 29 DEGs associated with GO: phenylpropanoid metabolic process (Fig. 2.6A), and 11 DEGs mapped to phenylpropanoid biosynthesis pathway on KEGG. These included beta-glucosidase, cinnamyl alcohol dehydrogenase, peroxidase, 4-coumarate-CoA ligase, cinnamoyl-CoA reductase, chalcone synthase, and flavonoid 3'-monooxygenase (Fig. 2.7B) (Host-comparison1 in Table A1.2, Appendix A1).

The enrichment analysis produced a list of 10 most significant GO terms with respect to both classic Fisher and Kolmogorov-Smirnov elimination tests. The most enriched terms included obsolete oxidation-reduction process, carbohydrate metabolic process, cellular amino acid metabolic process, fatty acid metabolic process, and response to chitin in hosts infected with *D. pinea* compared to mock under control climate conditions.

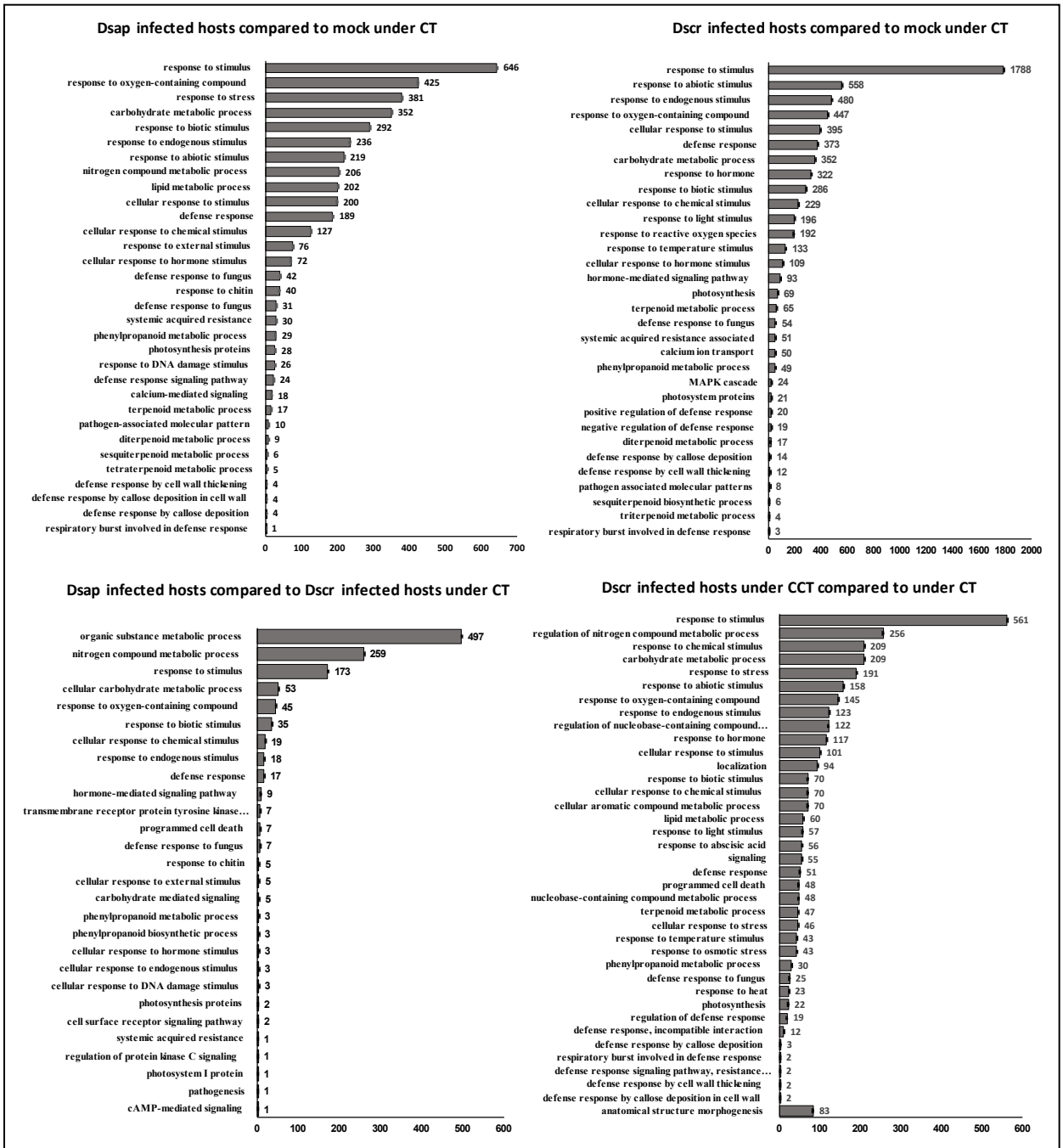

Figure 2.6. A. Significant host gene functions annotated using Blast2GO. X-axis: number of differentially expressed genes; y-axis: ontology associated functions. Left: comparison 1; right: comparison 2 (Fig. 2.1). **B.** Significant host gene functions annotated using Blast2GO. X-axis: number of differentially expressed genes; y-axis: ontology associated functions. Left: comparison 3; right: comparison 4 (Fig. 2.1).

(continued)

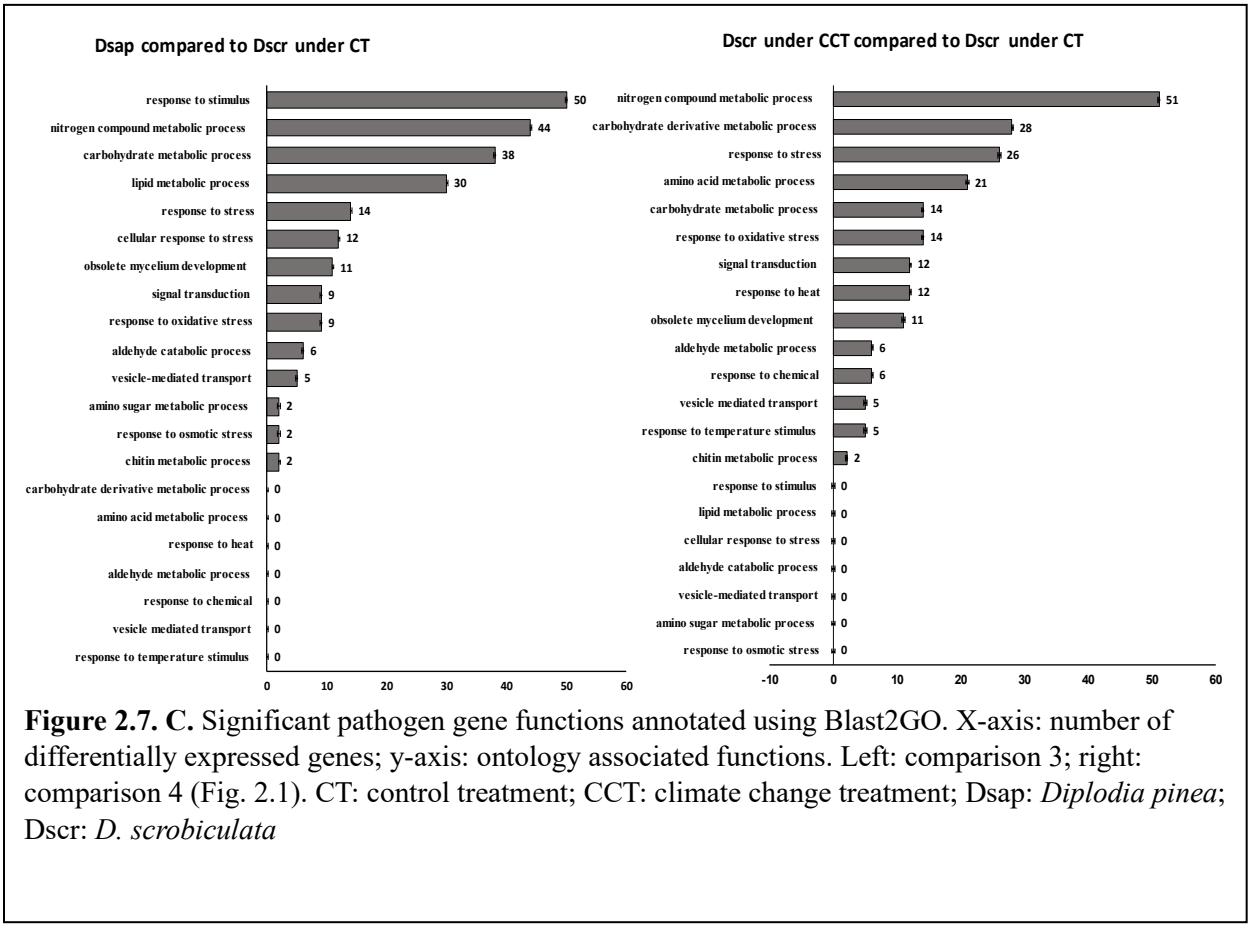

Figure 2.7. C. Significant pathogen gene functions annotated using Blast2GO. X-axis: number of differentially expressed genes; y-axis: ontology associated functions. Left: comparison 3; right: comparison 4 (Fig. 2.1). CT: control treatment; CCT: climate change treatment; Dsap: *Diplodia pinea*; Dscr: *D. scrobiculata*

2.4.6 Comparison 2: D. scrobiculata infection vs. mock under CT

In this comparison, a total of 6,628 genes were differentially expressed. 2,935 of these were assigned KEGG orthologs and were mapped to various general pathways, while 2,384 were annotated to various GO terms. Out of all 6,628 DEGs, 1,576 were filtered *via* annotation on all three platforms and mapped to 32 different GO terms including response to stimulus (1,788 DEGs), response to biotic stimulus (286 DEGs), defense response (373 DEGs), carbohydrate metabolic process (352 DEGs), among others (Fig. 2.6A). Our 5-fold threshold produced a

filtered list of 2,434 DEGs, with 1,537 upregulated genes and 897 downregulated genes (Host-comparison2 in Table A1.2, Appendix A1).

Primary metabolic responses: 90 DEGs were represented by photosynthesis through GO annotation (Fig. 2.6A), and further identified on KEGG, including ATP synthase (ATPF1D), photosystem II (psb27) protein, and a chlorophyll a-b binding (LHCB7) protein (Host-comparison2 in Table A1.2, Appendix A1) (Fig. 2.7A). 21 DEGs were mapped to fatty acid biosynthesis process on KEGG, including fatty acid synthase genes, short-chain type dehydrogenase (fabG), and acyl-CoA-synthetase (Host-comparison2 in Table A1.2, Appendix A1). Under nitrogen metabolism, carbonic anhydrase (CAH) protein and another glutamate dehydrogenase (gdhA) transcript were higher in *D. scrobiculata* infected pines as compared to mock infected pines (Fig. 2.7A).

Defense associated responses: A total of 495 DEGs were mapped to various GO terms associated with defense responses by the host, including defense response (373 DEGs), defense response to fungus (54 DEGs), defense response by cell wall thickening (12 DEGs), and callose deposition (14 DEGs) (Fig. 2.6A). 25 DEGs were assigned to the plant-pathogen interaction pathway (Fig. 2.6A), including calcium binding (CML) protein, calmodulin (CALM) protein, elongation factor Tu, heat shock (HSP90A) protein, and WRKY proteins (Fig. 2.7B).

Phytohormone and associated responses: A total of 415 DEGs were assigned to hormone related GO terms, including GO: response to hormone (322 DEGs) and hormone mediated signaling pathway (93 DEGs) and 43 DEGs were mapped to the plant hormone signal transduction pathway (Fig. 2.6A). Most significant DEGs included JAZ proteins, auxin responsive GH3 gene, xyloglucan endotransglucosylase hydrolase (TCH4) protein, gibberellin receptor (GID1) protein,

coronatine-insensitive (COI-1) protein, ubiquitin dependent protein catabolic process, two-component response regulator (ARR-A) protein, protein phosphatase 2C, cyclin D3 (CYCD3) protein (Fig. 2.7B).

Specialized metabolic responses: 32 DEGs were mapped to terpenoid backbone biosynthesis pathway on KEGG (Fig. 2.6A). Most significant DEGs included acetyl-CoA acetyltransferase and farnesyl pyrophosphate synthetase (FPPS) protein (Fig. 2.7B). We also found 22 transcripts mapped to the phenylpropanoid biosynthesis pathway on KEGG, including cinnamyl alcohol dehydrogenase, peroxidase, reductase, and 4-coumarate-CoA ligase (4CL) (Fig. 2.7B). Further, there were 11 transcripts mapped to flavonoid biosynthesis pathway on KEGG, including chalcone synthase (CHS), flavonoid 3'-monooxygenase (CYP75B1) (Fig. 2.7B).

The enrichment analysis produced a list of 19 most significant GO terms with respect to both classic Fisher and Kolmogorov-Smirnov elimination tests.. The most enriched terms included ribosome biogenesis, rRNA metabolic process, response to chitin, and cytosolic transport.

Dsap infected hosts compared to mock under CT	**Dscr infected hosts compared to mock under CT**
Photosynthesis	
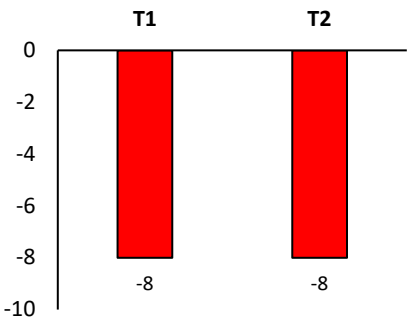	**No significant change**

(**continued**)

Fatty acid biosynthesis	
No significant change	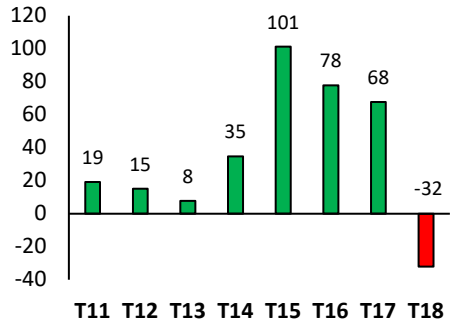
Nitrogen metabolism	
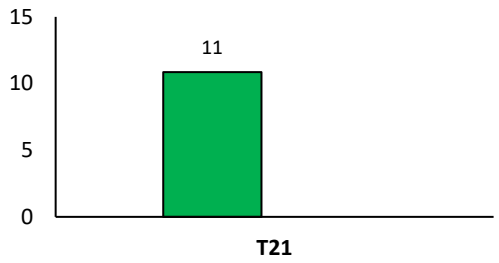	

Figure 2.7. A. Most significant DE genes by actual fold-change (Y-axis) > 5 (up) or < -5 (down) and $p < 0.05$, in host metabolic pathways (T = transcript): T1 – ATP synthase delta chain, T2 – photosystem II, T11-T14 – fabG, T15 – FAS1, T16 – FAS2, T17-T18 – FAB2, T21 – carbonic anhydrase, T24 – gdhA (Table A1.2, Appendix A1). Numeric bar labels indicate actual fold-change of respective transcripts.

Dsap infected hosts compared to mock under CT	Dscr infected hosts compared to mock under CT
Defense responses	
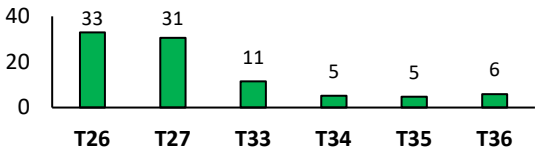	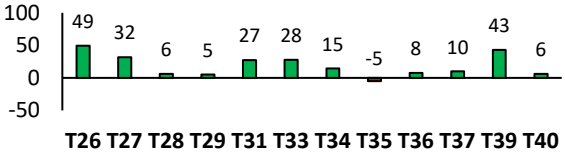

(continued)

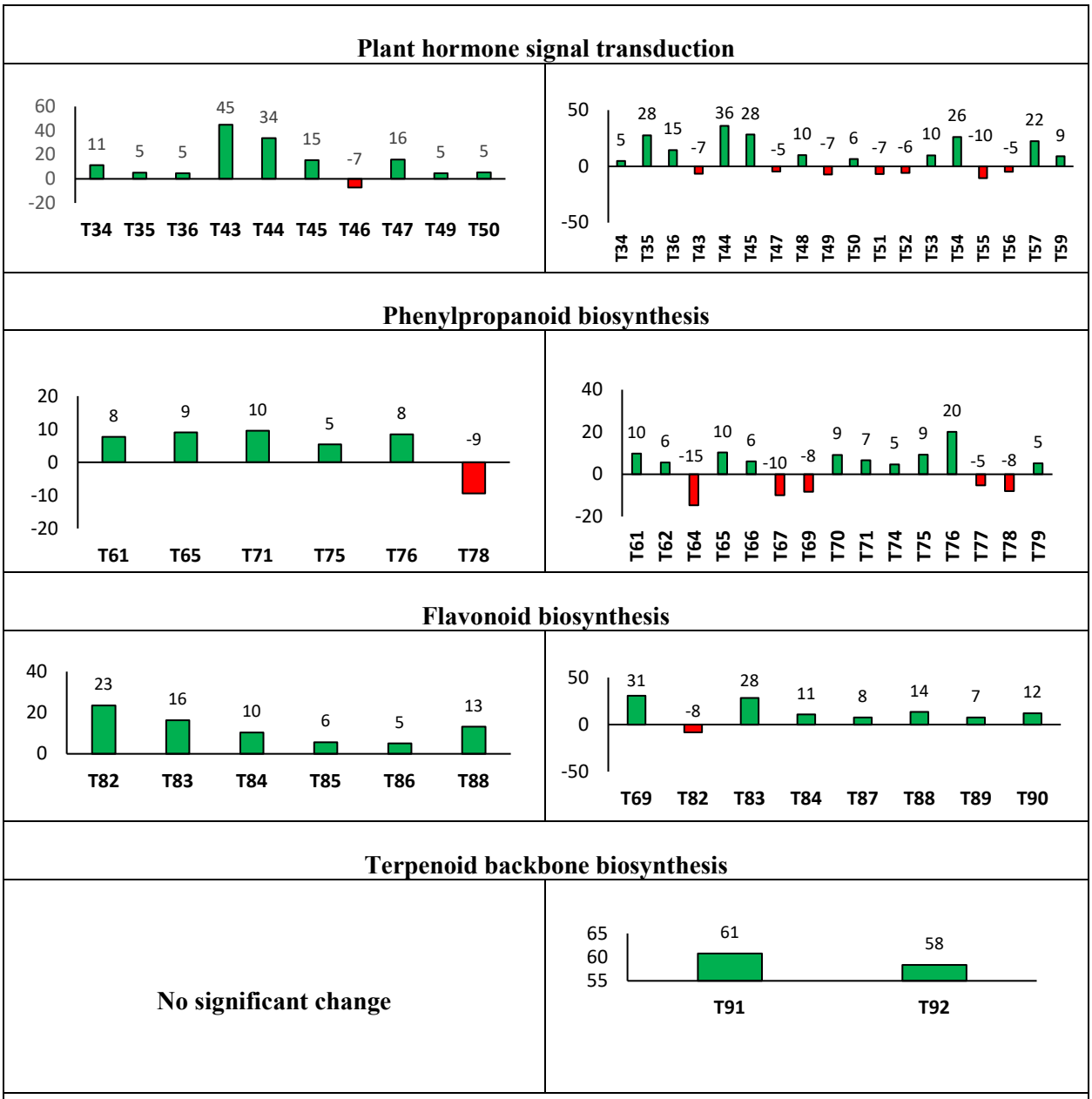

Figure 2.7. B. Most significant DE genes by actual fold-change (Y-axis) > 5 (up) or < -5 (down) and $p < 0.05$, in host metabolic pathways (T = transcript): T26-T29- CML, T31-CALM, T33-T35- PR1, T36- WRKY, T37-39- enhanced disease susceptibility, T40- efTu, T43-T45- JAZ, T46-T47- auxin responsive protein, T49- GID1, T50-T52 PP2C, T53- COI1, T54- ARR-A, T55- serine threonine protein kinase, T56-T57- TCH4, T59- cyclin D3, T61-T62- cinnamoyl alcohol dehydrogenase, T64-T67- peroxidase, T69- caffeoyl CoA o-methyltransferase, T70-T71- beta glucosidase, T74-T77- 4-coumarate CoA ligase, T78-cinnamoyl CoA reductase, T79- putative lysophospholipase, T82-T87- chalcone synthase, T88-T89- flavonoid 3'-monoxygenase, T90- anthocyanidin reductase, T91- acetyl CoA-acetyltransferase, T92- farnesyl pyrophosphate synthetase (Table A1.2, Appendix A1). Numeric bar labels indicate actual fold-change of respective transcripts.

Dsap infected hosts compared to Dscr infected hosts under CT	Dscr infected hosts under CCT compared to under CT
Photosynthesis	
No significant change	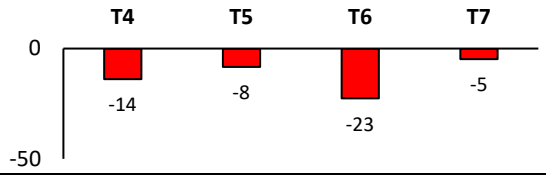
Carbon fixation	
No significant change	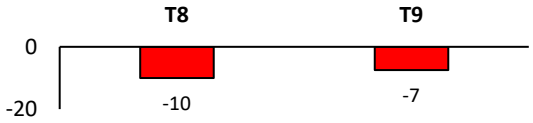
Carbohydrate metabolic process	
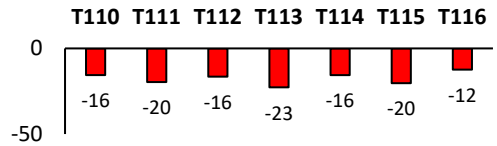	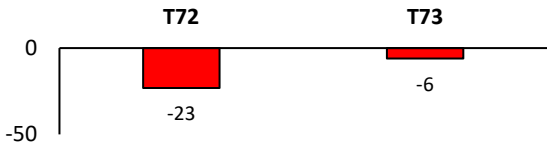
Fatty acid biosynthesis	
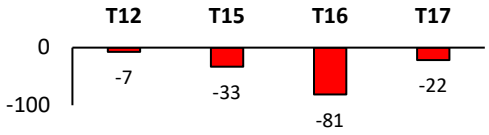	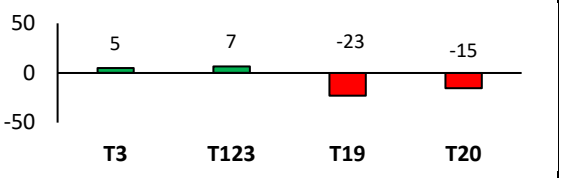
Nitrogen metabolic process	

(continued)

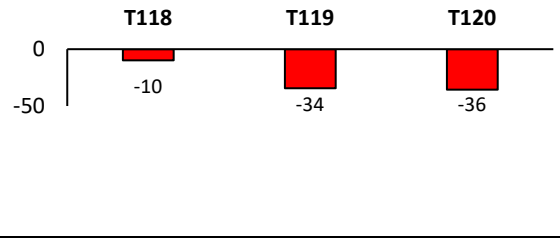

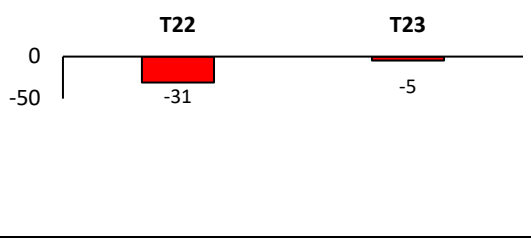

Plant defense responses

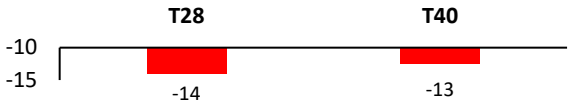

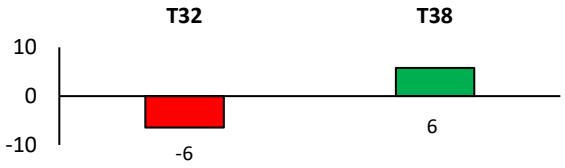

Figure 2.7. C. Most significant DE genes by actual fold-change (Y-axis) > 5 (up) or < -5 (down) and $p < 0.05$, in host metabolic pathways (T = transcript): T3- a/bccP, T4- ferredoxin, T5-T7- chlorophyll a-b binding protein, T8- fructose-1,6-bisphosphatase, T9- GAPD, T12- fabG, T15- FAS1, T16- FAS2, T17- fadD, T22, T23- carbonic anhydrase, T28, T32- CML, T38- WRKY, T40- efTu, T72, T73- beta-glucosidase, T110, T111- isocitrate dehydrogenase, T112- dihydrolipoyl dehydrogenase, T113- citrate synthase, T114- ATP-citrate synthase subunit, T115- fumarate hydratase, T116- aconitase hydratase, T118- gdhA, T119- alanine aminotransferase, T120- PyrABCN, T123- alcohol dehydrogenase. (Table A1.2, Appendix A1). Numeric bar labels indicate actual fold-change of respective transcripts.

Dsap infected hosts compared to Dscr infected hosts under CT	**Dscr infected hosts under CCT compared to under CT**
Plant hormone signal transduction	
No significant change	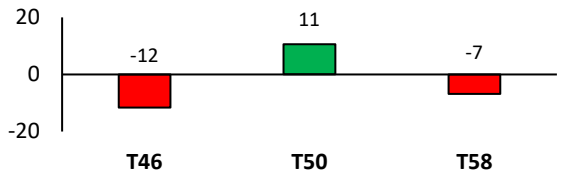
Phenylpropanoid biosynthesis	

(continued)

No significant change	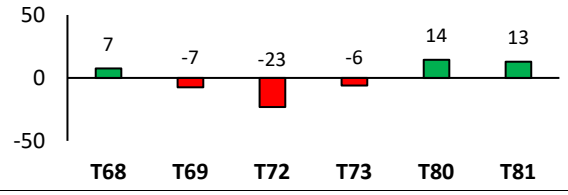
Flavonoid biosynthesis	
No significant change	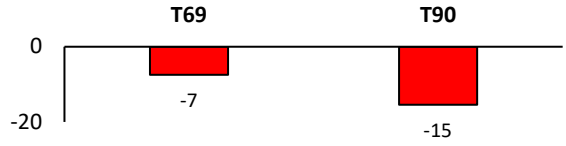
Terpenoid backbone biosynthesis	
No significant change	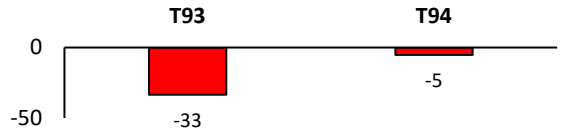
MAPK signaling pathway	
No significant change	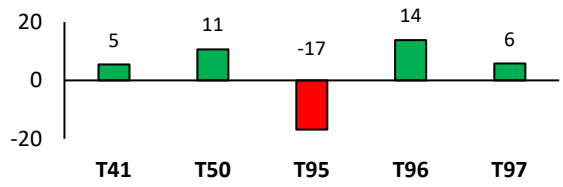
Glutathione metabolism	
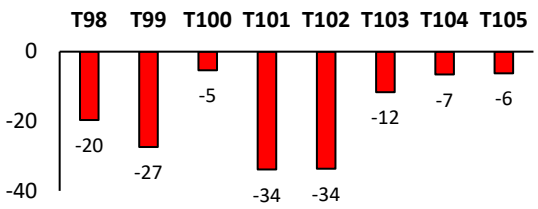	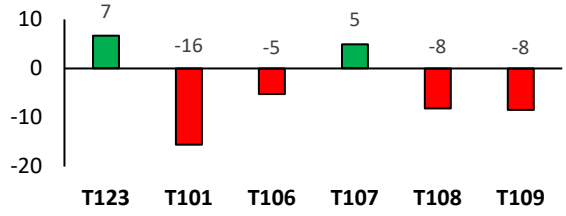

Figure 2.7. D. Most significant DE genes by actual fold-change (Y-axis) > 5 (up) or < -5 (down) and $p < 0.05$, in host metabolic pathways (T = transcript): T41- ROS burst protein, T46- auxin responsive protein, T50- PP2C, T58- TCH4, T68- peroxidase, T69- caffeoyl-CoA o-methyl transferase, T72, T73- beta glucosidase, T80, T81- reductase, T90- anthocyanidin reductase, T93, T94- GGPPS, T95- Cu transporting ATPase, T96- chitinase, T97- 1-aminocyclopropane-1-carboxylate synthase, T98- isocitrate dehydrogenase, T99- T106- glutathione reductase, T107- glutathione peroxidase, T108- RRM1, T109- RNDP

reductase, T123-alcohol dehydrogenase (Table A1.2, Appendix A1). Numeric bar labels indicate actual fold-change of respective transcripts.

2.4.7 Comparison 3: Effects of D. pinea vs. D. scrobiculata infections under CT

In this comparison, a total of 434 genes were differentially expressed. All 434 DEGs were assigned to KEGG orthologs and were mapped to various general pathways, but only 172 were annotated to various GO terms. 130 host DEGs were annotated to different metabolic pathways on all three platforms, with higher number of annotations for pathways like response to stimulus (50 DEGs), lipid metabolic process (30 DEGs), nitrogen compound metabolic process (44 DEGs), and carbohydrate metabolic process (38 DEGs) (Fig. 2.6B). Our 5-fold threshold produced a filtered list of 233 genes that were expressed less in hosts infected by *D. pinea* relative to *D. scrobiculata* infected hosts (Host-comparison3 in Table A1.2, Appendix A1).

Primary metabolic responses: Under the citric acid cycle pathway on KEGG and assigned GO: carbohydrate metabolic process, significant DEGs were reported for isocitrate dehydrogenase genes, citrate synthase genes, dihydrolipoyl dehydrogenase, fumarate hydratase, aconitate hydratase (Fig. 2.7C). Under nitrogen metabolism, significant DEGs were annotated as alanine aminotransferase and glutamate dehydrogenase (Fig. 2.7C). Four transcripts mapped to fatty acid biosynthesis pathway on KEGG were also downregulated, including fatty acid synthase, acyl-CoA-synthase, and short chain dehydrogenase (Fig. 2.7C).

Defense associated responses: Three genes mapped to the plant-pathogen interactions and MAPK signaling pathway on KEGG and assigned GO: receptor mediated endocytosis, nucleotide metabolic process, mitochondrial translation, were downregulated. Of them,

calmodulin, serine-threonine protein kinase, elongation factor efTu protein were the most significant DEGs (Fig. 2.7D).

Phytohormone and associated responses: Under plant hormone signal transduction pathway on KEGG, significant DE included xyloglucan endotransglucosylase hydrolase protein (TCH4) and assigned GO: response to external stimulus, plant-type cell wall organization (Fig. 2.7D). Additionally, 9 DEGs were mapped to the glutathione metabolism pathway on KEGG and assigned GO: response to oxidative stress, glutamate metabolic process, NADP metabolic process, including glutathione S-transferase and glutathione reductase (Fig. 2.7D). Others cAMP signaling pathway associated genes such as cell division control protein RAC1, RAS homolog gene family protein RHOA, and a serine threonine protein phosphatase were lower (Fig. 2.7D).

The cinnamoyl alcohol dehydrogenase, mapped to phenylpropanoid and lignin biosynthesis pathways was also lower in *D. pinea* infected hosts relative to *D. scrobiculata* infected hosts (Fig. 2.7D).

The enrichment analysis produced a list of 10 most significant GO terms with respect to both classic Fisher and Kolmogorov-Smirnov elimination tests. The most enriched terms included DNA metabolic process, DNA methylation, DNA duplex unwinding, leaf vascular tissue pattern formation, and phloem or xylem histogenesis.

Comparison 4: Host response to D. scrobiculata *infection under CCT*

In this comparison, a total of 2,048 genes were differentially expressed. 732 of these were mapped to various KEGG pathways and 679 DEGs assigned to various GO terms and the most represented GO functions included response to stress (561 DEGs), response to nitrogen

metabolic process (256 DEGs), carbohydrate metabolic process (209 DEGs), response to oxygen-containing compound (145 DEGs), response to abiotic stimulus (158 DEGs), and defense response (51 DEGs) (Fig. 2.6B). Our 5-fold threshold produced a filtered list of 936 DEGs, with 162 upregulated genes and 674 downregulated genes (Host-comparison4 in Table A1.2, Appendix A1).

Primary metabolic responses: We found that 7 transcripts mapped to KEGG pathways associated with photosynthesis and carbon fixation, including chlorophyll A-B binding protein, ferredoxin protein, phosphoenolpyruvate carboxykinase, fructose-1,6-bisphosphatase, and glyceraldehyde-3-dehydrogenase (Fig. 2.7C). We also found two beta-glucosidase genes downregulated 23-fold and 6-fold, respectively in pines infected with *D. scrobiculata* under CCT as compared to CT (Fig. 2.7C). We also found 60 genes mapped to GO terms associated with lipid metabolic process, including myristoyl-acyl carrier protein thioesterase, and fatty acyl-CoA reductase (Fig. 2.7C). An alcohol dehydrogenase gene assigned to GO: response to hypoxia, response to abiotic stimulus, was also upregulated (Fig. 2.7C).

Defense associated responses: Among the key GO terms related to defense, 51 DEGs were assigned to defense response, 101 DEGs assigned to cellular response to stimulus, 158 DEGs for response to abiotic stress, 25 DEGs for defense response to fungus, 70 DEGs for response to biotic stress (Fig. 2.6B). Other important defense associated GO functions included respiratory burst involved in defense, resistance gene-related defense response signaling pathway, defense response by cell wall thickening, and defense response by callose deposition (Fig. 2.6B). We further found 9 DEGs mapped to the plant-pathogen interactions pathway on KEGG. Significant DEGs included 3-ketoacyl-coa synthase, respiratory burst oxidase, calcium binding protein, and WRKY transcription factor (Fig. 2.7C and 2.7D).

Phytohormone responses: We also found 117 DEGs assigned GO: response to hormone, 56 DEGs assigned GO: response to abscisic acid (Fig. 2.6B), and 9 DEGs mapped to the plant hormone signal transduction process on KEGG. Significant DEGs included auxin-responsive protein, phosphatase 2C, xyloglucan endotransglucosylase hydrolase, and copper-transporting ATPase protein (Fig. 2.7D). Other DEGs mapped under the host mitogen associated protein kinase (MAPK) signaling included respiratory burst oxidase, chitinase and 1-aminocyclopropane -1-carboxylate synthase (ACS6) (Fig. 2.7D). Interestingly, we also found 14 DEGs mapped to the glutathione metabolism pathway, besides 145 DEGs assigned GO: response to oxygen-containing compound and 2 DEGs assigned GO: respiratory burst involved in defense (Fig. 2.6B). Significant DEGs included glutathione S-transferase, and glutathione peroxidase (Fig. 2.7D) (Host-comparison4 in Table A1.2, Appendix A1).

Specialized metabolic responses: We also observed 47 DEGs assigned to GO: terpenoid metabolic process (Fig. 2.6B), and 7 transcripts that were mapped to the terpenoid backbone biosynthesis pathway, including geranylgeranyl pyrophosphate synthase (Fig. 2.7C). 30 DEGs were assigned to phenylpropanoid metabolic process (Fig. 2.6B), and 7 DEGs were mapped to the phenylpropanoid and flavonoid biosynthesis pathway on KEGG, including reductase, caffeoyl-CoA o-methyltransferase, peroxidase, and flavonoid 3'-monooxygenase (Fig. 2.7D) (Host-comparison4 in Table A1.2, Appendix A1).

The enrichment analysis produced a list of 13 most significant GO terms with respect to both classic Fisher and Kolmogorov-Smirnov elimination tests (Host-comparison4 in Table A1.2, Appendix A1.). The most enriched terms included cotyledon vascular tissue pattern formation, alpha-amino acid biosynthetic process, mRNA metabolic process, fatty acid beta-oxidation, and establishment of localization in cell.

2.4.8 Pathogen responses

2.4.9 Comparison 3: D. pinea vs. D. scrobiculata infections under CT

In this comparison, a total of 211 genes were differentially expressed. Out of these, 156 DEGs were assigned KEGG orthologs and were mapped to various general pathways, and 172 DEGs were annotated to various GO terms. Our 5-fold threshold produced a filtered list of 58 DEGs, with 27 genes more highly expressed, and 21 genes expressed lower in *D. pinea* relative to *D. scrobiculata* (Pathogen-comparison3 in Table A1.2, Appendix A1). We also found 30 DEGs that were assigned to various GO terms and the most represented GO functions included response to stimulus (50 DEGs), response to nitrogen metabolic process (44 DEGs), carbohydrate metabolic process (38 DEGs), and lipid metabolic process (30 DEGs) (Fig. 6C).

Primary metabolic responses: We found two transcripts mapped to KEGG pathways for carbon metabolism and biosynthesis of amino acids. Significant DEGs included glyceraldehde-3-phosphate dehydrogenase, and triose phosphate isomerase under various carbon-associated pathways (Table 2.2). Additionally, a thiamine biosynthesis protein (NMT1) that was assigned GO: nitrogen metabolic process, aromatic compound metabolic process, was also higher (Table 2.2). Under various lipid associated pathways, a sterol 24-c-methyltransferase transcript, and RING finger transcript were also reported (Table 2.2).

Specialized metabolism and signaling: We also found a gamma-glutamyl transpeptidase transcript annotated to glutathione metabolism pathway on KEGG and assigned GO: response to nitrogen starvation, and elongation factor 2 transcript to be lower in *D. pinea* as compared to *D. scrobiculata* under CT (Table 2.2).

The enrichment analysis produced a list of 8 most significant GO terms with respect to both classic Fisher and Kolmogorov-Smirnov elimination tests (Table A1.2, Appendix A1.). The most enriched terms included nuclear chromosome segregation, ascospore-type prospore assembly, protein deubiquitination, polyol metabolic process, and response to stress.

Table 2.2. Significant DE genes under various metabolic pathways for pathogen comparison 3 (Fig. 2.1): CTDsap vs CTDscr.

Transcript ID	**EGGNOG**	**logFC**	**Actual FC**	**Adj. p-value**	**KEGG Orthology**
Carbon metabolic process					
tig00000024.g11826.t1	glyceraldehyde-3-phosphate dehydrogenase	6.3	39.7	3.09E-11	K00134
tig00000027.g13503.t1	Triose-phosphate isomerase	3.2	10.2	0.002	K01803
AMPK signaling pathway					
tig00000005.g4874.t1	elongation factor 2	2.9	8.2	0.002	K03234
Necroptosis					
tig00000005.g4528.t1	Heat shock protein	2.7	7.3	7.83E-06	K04079
tig00000002.g2373.t1	Histone H2A	9.9	97.6	4.54E-11	K11251
Plant-pathogen interaction					
tig00000005.g4528.t1	Heat shock protein	2.7	7.3	4.54E-11	K04079
Steroid biosynthesis					
tig00000010.g9170.t1	Sterol 24-c-methyltransferase	-2.6	- 6.7	0.00088	K00559
Thiamine metabolism					

(continued)

tig00000021.g11454.t1	Thiamine biosynthesis protein (Nmt1)	2.6	6.9	0.01510	K18278
tig00000003.g3794.t1	RING finger	-5.4	-29.3	0.00180	K01061
Glutathione metabolism					
tig00000006.g5533.t1	gamma-glutamyl transpeptidase	-4.5	-20.7	5.47E-05	K00681

2.4.10 Comparison 4: D. scrobiculata under CCT vs CT

We documented a total of 147 DEGs significantly affected by climate treatment. Out of these 147 DEGs, 56 were assigned KEGG orthologs and were mapped to various general pathways, and all were annotated with GO terms. Thereafter, our 5-fold threshold produced a filtered list of 30 DEGs, with 6 upregulated and 24 downregulated by climate change conditions (Table A1.2, Appendix A1). The same 56 DEGs that had KEGG orthologs were also assigned various GO terms, including nitrogen compound metabolic process (51 DEGs), carbohydrate and its derivative metabolic process (42 DEGs), response to stress (26 DEGs), response to heat (12 DEGs) (Fig. 2.6C).

Table 2.3. Significant DE genes under various metabolic pathways for pathogen comparison 4 (Fig. 2.1): CCTDscr vs CTDscr.

Transcript ID	**EGGNOG**	**logFC**	**Actual FC**	**Adj. p-value**	**KEGG Orthology**
Sucrose and starch metabolism					
tig00000002.g1573.t1	beta-glucosidase	-2.8	-8	0.048378	K05349
tig00000001.g1035.t1	L-iditol 2-dehydrogeanse	2.5	6.4	0.003366	K00008

(continued)

Biosynthesis of amino acids					
tig00000027.g13503.t1	Triose-phosphate isomerase	3.8	14.1	0.022454	K01803
tig00000001.g1232.t1	glutamine synthetase	-2.4	-5.5	0.038446	K01915
Nitrogen metabolic process					
tig00000006.g5807.t1	cyanide hydratase	3.4	11.9	0.009250	K10675
tig00000021.g11454.t1	Thiamine biosynthesis protein (Nmt1)	2.4	5.9	0.000427	K18278
Plant-pathogen interactions					
tig00000003.g3121.t1	cardiolipin synthase	-2.3	-5.1	0.042621	K08744
tig00000007.g6441.t1	heat shock HSP1	-2.9	-8.3	0.000627	K03283
Necroptosis					
tig00000001.g1232.t1	glutamine synthetase	-2.4	-5.5	0.038446	K01915
Translation					
tig00000007.g6659.t1	large subunit ribosomal protein L7Ae	-4.8	-23.2	0.000942	K02936
tig00000011.g9633.t1	small subunit of the ribosomal protein S15e	-4.8	-22.6	0.000356	K02958
tig00000011.g9947.t1	Aspartyl-tRNA synthetase	2.3	5.1	0.000431	K01876

Primary metabolic responses: Various carbon metabolizing enzyme genes such as triose phosphate isomerase, beta-glucosidase, L-iditol 2-dehydrogenase, and cardiolipin synthase were among the most significant (Table 1.2). We also found 21 DEGs assigned GO: amino acid

metabolic process (Fig. 2.6C), including thiamine biosynthesis protein (NMT1), cyanide hydratase, aspartyl-tRNA-synthetase, heat shock protein (HSPA1), large subunit of ribosomal protein L7Ae and small subunit of the ribosomal protein (Table 2.3). The large subunit was assigned GO: cytoplasmic translation, obsolete mycelium development and the small subunit was assigned GO: RNA export from nucleus, cytoplasmic translation (Table 2.3), although both subunits are constituents of the EF-Tu protein domain.

The enrichment analysis produced a list of 11 most significant GO terms with respect to both classic Fisher and Kolmogorov-Smirnov elimination tests (Table A1.2, Appendix A1.). The most enriched terms included ATP metabolic process, cellular amino acid catabolic process, alpha-amino acid catabolic process, electron transport chain, and respiratory electron transport chain.

2.5 Discussion

Climate change poses major physiological challenges that can shift the dynamics of tree-pathogen interactions (Desprez-Loustau, 2006). The CCT used in this study mimicked possible climate change scenarios that allowed the investigation of how host and pathogens may be impacted by such adverse conditions. While we found clear indications of abiotic stress responses in both host and pathogen, we acknowledge that the responses we documented are on a noticeably short time scale, one that does not consider longer term adaptive responses, both physiological/ecological (habituation) and evolutionary. Even so, we found that a simulated CCT shifted the outcome of the interactions between Austrian pine and the normally non-aggressive fungus *D. scrobiculata*, resulting in lesions on par with *D. pinea*. We speculate either enhanced

aggressiveness of the pathogen, increased susceptibility of the host, or both, support the phenotypic findings of past studies (reviewed in Desprez-Loustau, 2006).

We dissected the underlying molecular features of this phenomenon via a dual transcriptomics approach. One challenge with this approach is that read recovery rates vary widely between host and pathogen due to substantially lower absolute amounts of pathogen RNA relative to host RNA in infected tissues (Naidoo et al., 2018). We mitigated this challenge in our recovery method for host and pathogen reads by filtering out transcripts that were only represented in mock samples but had no reads in infected samples. We further only retained transcripts that were represented at least 20 times in at least three sample types irrespective of treatment combination (Visser et al., 2019; Hernandez-Escribano et al., 2020).

Within these limits we asked several key questions through different comparisons, considering the host response to the two pathogens separately, the host response under climate change conditions and the pathogen responses under both climate change and control climate. The most significant DEGs were then analyzed under two major categories, primary and specialized metabolism, the latter associated with defense. This eventually resulted in the cellular models presented in Fig. 2.8, one for the host and one for the pathogens. We infer the following conclusions from the main comparisons in the study.

2.5.1 Reduced host photosynthetic rate contributes to D. pinea pathogenesis

Host photosynthetic pathways were suppressed, specifically in *D. pinea* infection vs. mock inoculation under CT (comparison 1). The ATP synthase delta chain protein and photosystem II proteins are localized in the chloroplast and are involved in ATP proton pump assembly and PSII (photosystem II) light harvesting complex, respectively. Meanwhile, carbonic anhydrase (CAH)

is involved in important cellular functions such as mesophyll carbon dioxide conductance, oxidative stress protection, lipid biosynthesis, and phytohormone mediated signaling (Polishchuk, 2021) but, perhaps more importantly, with ABA-independent stomatal closure (Kolbe et al., 2018). Taken together, this evidence suggests that attack by *D. pinea* suppresses photosynthesis, leading to host carbon starvation.

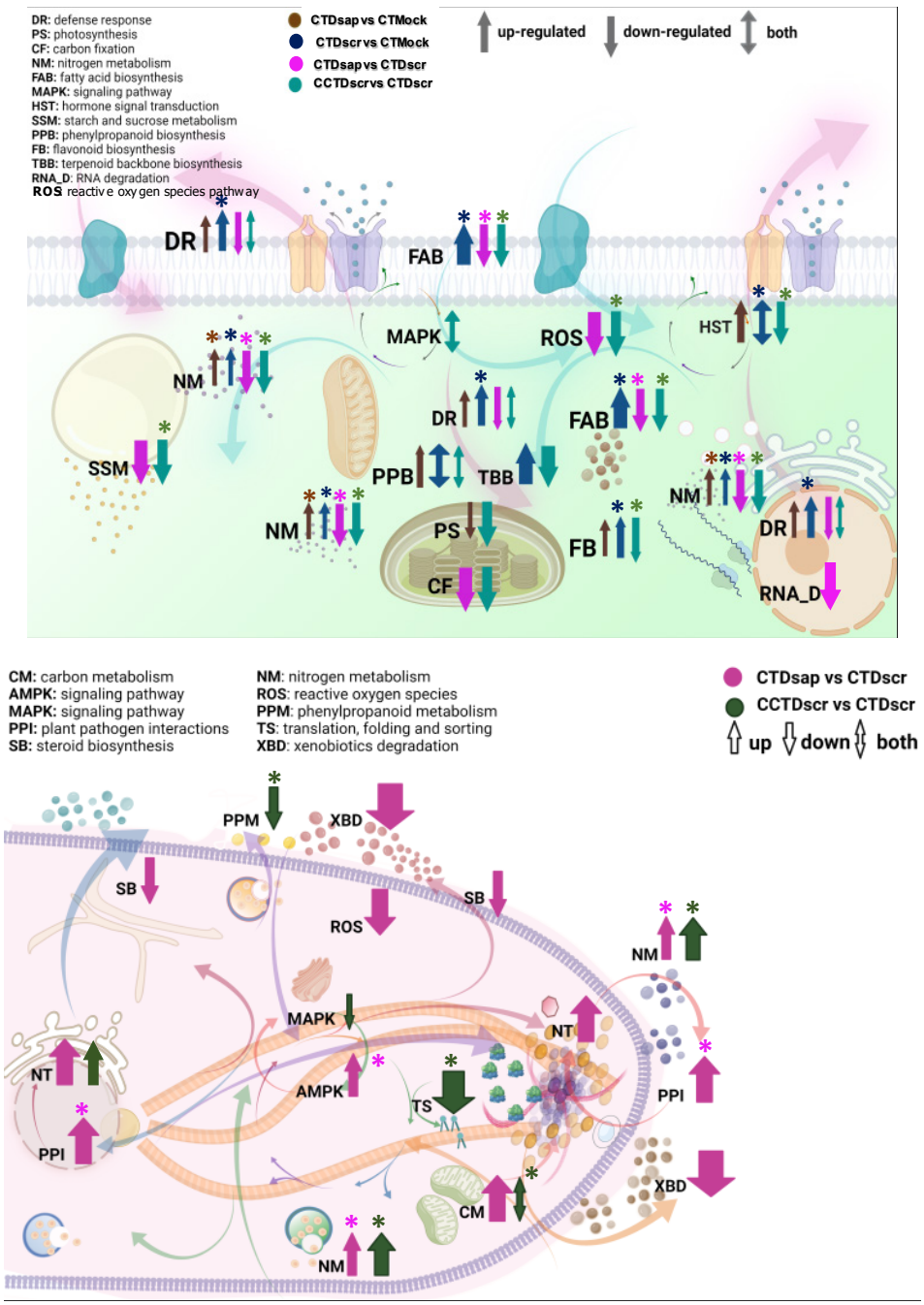

Figure 2.8. Working models of host (top) and pathogen (bottom) cellular networks of various primary and specialized metabolic pathways. Abbreviations represent GO function and colored arrows indicate respective host and pathogen comparisons. Arrow widths represent arbitrary relative magnitude of changes in significantly expressed DE genes mapped under each pathway for a given host/pathogen comparison. Enriched pathways are marked with asterisks.

2.5.2 Suppressed host defense responses contribute to D. pinea pathogenesis

Under CT, and compared directly to *D. scrobiculata* infection, critical defense responses were suppressed by *D. pinea* infection, including calmodulin-like (CML) protein genes that have been associated with HR expression (Chiasson et al., 2005), enhanced resistance to insect pests (Ma et al., 2008), and biotrophic and hemi-biotrophic lifestyles (Leba et al., 2012). Similarly, PR proteins, an inducible and diverse group that accumulate in response to stress and have been demonstrated to be significantly associated with necrotrophic pathogens (Boccardo et al., 2019), were suppressed, as were WRKY transcription factors, which reportedly mediate the cross-talk between salicylic acid and jasmonic mediated defense signaling (Li et al., 2004; Zheng et al., 2006). Finally, pathways associated with biosynthesis of specialized metabolites like phenolics and flavonoids, which have been associated with resistance in this system (Sherwood and Bonello, 2013), were also suppressed. Thus, compared to *D. scrobiculata* infection, the elicitation of host defense responses by *D. pinea* is severely impaired under CT, which explains, at least in part, the baseline difference in aggressiveness between the two pathogens.

2.5.3 Necrotrophic host interactions with D. pinea trigger phytohormone crosstalk

Plant defense responses are regulated by the crosstalk between phytohormone pathways. Under CT and upon *D. pinea* infection, Austrian pine responded by ramping up crosstalk of various phytohormones, leading primarily to jasmonate-mediated defense signaling, consistent with the basic necrotrophic aspects of this association. Such response was concomitant with a downregulation of auxin and gibberellic acid-responsive genes and an upregulation of PP2C type proteins. Jasmonate ZIM-domain (JAZ) containing proteins have been associated with regulation of jasmonate accumulation via suppression of MYC2 proteins (Chini et al. 2007), while auxin responsive genes are linked to reductions of host defense by suppression of the salicylic acid

pathway (Djami-Tchatchou et al., 2020). Gibberellin receptors such as GID1 are crucial for GA signal transduction and have been associated with enhanced susceptibility in host plants via antagonistic crosstalk with jasmonate pathways (Song et al. 2014). Finally, PP2C type proteins have been linked to modulation of defense responses by possible suppression of various target PR proteins and ROS-scavenging enzymes (Zhu et al., 2018).

2.5.4 D. scrobiculata-induced host nitrogen and fatty acid metabolism contributes to host defense

Our data suggest that *D. scrobiculata* infection increases metabolism and transport of amino acids and lipids but does not affect photosynthesis, unlike *D. pinea* under CT. However, one glutamate dehydrogenase (GDH) transcript was upregulated, suggesting that infection results in enhanced reversible transamination of 2-oxoglutarate to form glutamate (Labboun et al., 2009), which contributes to leaf glutamate homeostasis along with the NADH-GOGAT cycle. The fatty acid biosynthesis pathway was also overall highly induced. Among induced fatty acid enzymes, acyl-CoA dehydrogenase and various short chain fatty acid dehydrogenases catalyze the initial step in respective cycles of fatty acid beta oxidation. Similarly, fatty acid synthases (FAS) catalyze the biosynthesis of various long chain fatty acids from respective precursor acyl-CoAs. Furthermore, xyloglucan endotransglucosylase hydrolase (XTH) activity was enhanced. XTH induces cell growth and extension (Miedes et al., 2014) *via* increased short chain xyloglucan synthesis (Niraula et al., 2021). Taken together, this evidence suggests that Austrian pine enhances homeostasis and growth processes in response to *D. scrobiculata* infection under CT, contributing to a positive outcome for the host against this less aggressive pathogen.

2.5.5 D. scrobiculata elicits a stronger defense response

Under CT, *D. scrobiculata* infection elicited a much stronger host defense response compared to *D. pinea* infection and the mock treatment *via* enhancement of PR protein biosynthesis, as well as calcium and jasmonate-mediated defense signaling. This was especially evident by enhanced biosynthesis of coronatine insensitive1 (COI1) proteins, which are critical in almost every step of jasmonate signaling (Katsir et al., 2008). There are further indications of phytohormone cross-talk from enhanced ARR-A proteins that are involved in age-related defense response in coordination with phytohormones such as salicylates, jasmonates, and ethylene (Shah and Zeier, 2013). At the same time, enhanced CALM proteins, along with CMLs, a calcium dependent protein kinase, and calcineurin B-like proteins suggests active regulation of the calcium-calmodulin signaling pathway (Cheval et al., 2013), which has been associated with responses to both biotic and abiotic stress.

D. scrobiculata also induced host defense-associated phenylpropanoid pathways, demonstrated by several significant DEGs. Cinnamoyl alcohol dehydrogenases (CAD) are involved in lignin biosynthesis and have been associated with defense-induced phenylpropanoid metabolism (Logemann et al., 1997; Tronchet et al., 2010). Furthermore, the peroxidase-generated apoplastic oxidative burst contributes to damage associated molecular pattern (DAMP)-elicited immunity (Survila et al., 2016). We also documented an induction in flavonoid and terpenoid biosynthesis. Strong induction of host defenses is likely a key contributor to the less aggressive baseline phenotype exhibited by *D. scrobiculata* infection under CT.

6. Impaired host primary metabolism and defense responses further aid D. pinea pathogenesis

D. pinea had more profound effects than *D. scrobiculata* on host primary metabolism. What appears to be a rapid depletion of carbon, nitrogen, and lipid resources might explain why the host is less able to counter a *D. pinea* infection than a *D. scrobiculata* infection under CT. We observed some overlap in DEGs between biological comparisons 1 and 2, where we investigated host responses to *D. pinea* vs. mock and host responses to *D. scrobiculata* vs. mock inoculation, respectively, under CT. We then used comparison 3 to further dissect differences in dual host and pathogen responses following *D. pinea* and *D. scrobiculata* attacks under CT. While we observed no significant differences in host photosynthetic and carbon fixation pathways, the carbohydrate metabolic process was heavily suppressed in *D. pinea* infected hosts compared to *D. scrobiculata* infected hosts. Specifically, key genes of the Krebs cycle, such as citrate synthase, aconitase hydratase (which catalyzes isomerization of citrate to isocitrate), isocitrate dehydrogenase (which catalyzes conversion of isocitrate to alpha-ketoglutarate and release of carbon dioxide), and fumarate hydratase (which catalyzes conversion of fumarate into malate) were significantly suppressed. Dihydrolipoyl dehydrogenase, which is part of the pyruvate dehydrogenase multienzyme complex that connects cytosolic glycolysis with mitochondrial citrate cycle and acts as an ROS neutralizer (Babady et al., 2007), was also suppressed.

Fatty acid biosynthesis and nitrogen metabolism were also inhibited in Austrian pine inoculated with *D. pinea,* compared to *D. scrobiculata*. Suppressed activity of critical enzymes such as gdhA, alanine aminotransferase, and glutamine aminotransferase (pyrABCN) indicate reduced nitrogen assimilation, possibly as a result of cellular hypoxia (Diab and Limami, 2016). Such processes may be the consequence of stomatal closure induced by *D. pinea* and subsequent reduction in photosynthesis and nitrogen assimilation, which ultimately leads to depletion of carbon and nitrogen, and respiratory oxygen.

Finally, we documented reduced host defense responses, as indicated by suppression of CML, efTu, and glutathione reductase. Thus, it appears that reduced assimilation/metabolism of carbon, nitrogen, and fatty acids in Austrian pine, coupled with various suppressed defense responses, contribute to the accelerated baseline pathogenesis observed with *D. pinea* vs. *D. scrobiculata* under CT.

2.5.6 Carbon metabolism and nitrogen assimilation are crucial for D. pinea information processing and pathogenesis

In line with suppression of host carbon and nitrogen assimilation, fungal nitrogen assimilation and carbon metabolism were higher in *D. pinea* compared to *D. scrobiculata* under CT. Specifically, glycolytic enzyme genes such as glyceraldehyde 3-phosphate dehydrogenase (GAPD) and another triose phosphate isomerase were enhanced in *D. pinea* compared to *D. scrobiculata* under CT. At the same time, enhanced nitrogen metabolism (Nmt1 and elongation factor 2) is also indicative of higher activity of *D. pinea* compared to *D. scrobiculata* under CT. In addition, we documented enhanced environmental information processing in *D. pinea,* as indicated by signaling pathways involved in necrotopsis, AMPK, and plant-pathogen interactions. For instance, gamma-glutamyltranspeptidase (GGT) is involved in glutathione metabolism and is associated with enhanced transport of amino acids and detoxification of free oxygen radicals (Mehdi et al., 2001). Heat shock proteins also aid in fungal morphogenesis and environmental processing, including hyphal formation and pathogenicity (Tiwari et al. 2015).

8. Climate change induces host starvation via suppression of primary metabolism

Host trees subjected to CCT and further challenged with *D. scrobiculata* displayed depletion of carbon resources, an outcome (if not a process) similar to the situation with *D. pinea* under CT. This was evident from suppression of pigments involved in photoexcitation of chlorophyll, to

enzymatic genes involved in the Calvin cycle, as well as starch and sucrose metabolism. Additionally, we also documented suppressed carbonic anhydrase activity, similar to *D. pinea* infected hosts in comparison 3. Furthermore, enhanced upstream enzymes of host fatty acid metabolism, such as biotin carboxyl carrier protein (a/bccp) and an alcohol dehydrogenase, indicated synthesis of short chain fatty acids; however, fatty acid elongation and branching was affected as indicated by suppressed myristoyl-acyl carrier protein thioesterases. Suppressed fatty acid biosynthesis suggests impairment of membrane integrity and lipid transport, which contribute to stress responses (Michaud and Jouhet, 2019). Thus, climate change conditions, as implemented here, cause suppression of carbon fixation and metabolism leading to carbon starvation, compounding the effects of *D. scrobiculata* infection and resulting in enhanced pathogenesis.

9. Climate change weakens the host by suppressing defense associated metabolic pathways

In *D. scrobiculata* infected hosts under CCT, reduced defense responses were indicated by suppression of CML and WRKY, in addition to enzymes in the phenylpropanoid biosynthesis pathway, such as caffeoyl-CoA-o-methyl transferase and beta glucosidases, and geranyl geranyl pyrophosphate synthases (GGPS) in the terpenoid biosynthesis pathway. Additionally, we documented enhanced MAPK signaling and oxidative burst, as implied by reduced glutathione metabolism, all indicative of host responses to abiotic stress. Similar to *D. pinea* infected hosts under CT, the PP2C family proteins were also induced in *D. scrobiculata* infected hosts under CCT, indicating direct host defense suppression. Reduced glutathione metabolism, by means of suppressed glutathione and ribonucleotide diphosphate reductase (RNDP) activities, further indicates reduced ROS detoxification and lowered nitrogen transport in Austrian pine under

CCT. Thus, climate change conditions, as implemented here, result in suppression of host defense responses.

10. Carbon and nitrogen assimilation are crucial for D. scrobiculata survival under climate change

Comparison 4, in which we investigated dual responses of host and pathogen following *D. scrobiculata* attack under CCT vs. CT, also revealed important patterns in gene expression in *D. scrobiculata* itself. For example, we found evidence of enhanced carbon metabolism by way of triose phosphate isomerase and enolase gene upregulation. Amino acid metabolism was enhanced as indicated by upregulation of a glutamine synthetase gene, in addition to the triose phosphate isomerase gene. Interestingly, the glutamine synthetase transcript was also mapped to the necroptosis pathway and has been reported to induce susceptibility via nitrogen competition between host and pathogen Huang et al., 2017). We also documented enhanced protein processing and stress responses, as indicated by upregulation of heat shock (HSP) proteins and an aminoacyl-tRNA synthase gene. Taken together, this evidence suggests that the focus of pathogen metabolism is to acquire carbon and nitrogen, while lowered lipid metabolism could be a response to the climate change conditions as implemented in this study.

11. Integrated model

All in all, our work highlights some major themes that facilitate a deeper understanding of pine-pathogen interactions under variable climate. We synthesize our results in two cellular models, one for the host and one for the two pathogens (Fig. 2.8). The comparisons arranged in panels of Figs. 2.6A to 2.7D highlight host responses to the two pathogens vs. the mock and, more importantly, two different scenarios of host susceptibility, one including the baseline response to

D. pinea infection under CT, the other host responses to *D. scrobiculata* infection under CCT. The first observation is that maintaining primary metabolism homeostasis is key for survival of both the host and the pathogens. Infection by *D. pinea* induces suppression of host carbon fixation and metabolism, fatty acid biosynthesis, and nitrogen metabolism, thereby leading to primary nutrient starvation (Fig. 2.8). This is further supported by enhanced carbon and nitrogen metabolism in *D. pinea* itself (Fig. 2.8), which likely further contributes to host starvation. Moreover, suppressed host fatty acid metabolic pathways likely affect membrane integrity and vesicular trafficking, thereby influencing host response to stress (Michaud and Jouhet, 2019). On the other hand, suppressed lipid metabolism and steroid biosynthesis in *D. pinea* perhaps suggests reduced activity of lipid transporters as well as reduced membrane trafficking (Rizzo et al., 2019). In contrast, infection by the less aggressive *D. scrobiculata* did not alter host carbon fixation, while nitrogen metabolism and fatty acid biosynthesis were enhanced (Fig. 2.8) along with indications of active growth and homeostasis in hosts. Thus, the impaired state of host carbon fixation and metabolism is one of the primary explanations for the higher aggressiveness of *D. pinea*, while primary metabolism of carbon, nitrogen, and fatty acids either remain unaffected or are enhanced.

Suppressed primary metabolism in *P. nigra* also likely contributes to the limitation of carbon-based defenses (phenolics, terpenoids), as well as ROS signaling. Indeed, host defense activation against *D. pinea* was on a much lesser scale, relative to *D. scrobiculata,* under the baseline conditions of CT (Fig. 2.8). For example, phenylpropanoid biosynthesis, which is at the core of defense-associated phenolics and flavonoids (Sherwood and Bonello, 2013), was much more pronounced in hosts under attack by *D. scrobiculata* than *D. pinea* (Fig. 2.8). Furthermore, terpenoid biosynthesis in *D. scrobiculata*-infected hosts was enhanced, whereas *D. pinea*

infection did not induce any changes (Fig. 2.8). Interestingly, on the pathogen side, the plant pathogen interactions pathway was more enhanced and GO enriched in *D. pinea* than in *D. scrobiculata* (Fig. 2.8). Thus, the state of specialized metabolism on both sides of the interaction supports a view in which *D. pinea* elicits global impairment of host metabolism affecting assimilation, growth and defense response *via* carbon and nitrogen starvation, explaining the occurrence of longer lesions under CT.

The picture changed dramatically under the climate change regimen for *D. scrobiculata*-infected hosts, which clearly experienced suppression of carbon fixation, starch and sucrose metabolism, nitrogen metabolism, and fatty acid biosynthesis, in a manner similar to that of hosts attacked by *D. pinea* under control climate. These pathways were also GO enriched, further highlighting how CCT led to depletion of host resources and increased *D. scrobiculata* aggressiveness (Fig. 8). Likewise, CCT induced suppression of phenylpropanoid biosynthesis, terpenoid biosynthesis, and defense response pathways in the host (Fig. 2.8). This was accompanied by suppression of ROS and hormone signaling pathways. On the pathogen side, while carbon metabolism and nitrogen metabolism were both GO enriched and enhanced, activity of phenylpropanoid metabolism was lower under CCT (Fig. 2.8), possibly due to feedback from low production of phenylpropanoids in the starving host. Concurrently, we recorded a glutamine synthetase transcript mapped to the necroptosis pathway in *D. scrobiculata* under CCT, like *D. pinea* infected hosts under CT. Also, CCT appears to affect *D. scrobiculata via* reduced MAPK signaling and post-translational protein processing, suggesting some impairment of host immune signaling (Fig. 2.8). This suggests that CCT causes genome-wide suppression of various critical host secondary metabolic pathways either directly or via suppression of primary metabolism, thereby predisposing hosts to pathogenic infections.

Taken together, our evidence shows how critical carbon and nitrogen are for sustenance of cellular integrity and operation in plant pathogen interactions, no matter what the environmental conditions. Nitrogen and carbon mobilization and transport are highly responsive to both biotic and abiotic stress, and the cumulative stress from the climate change regime and pathogenic infection further aggravates host resource depletion and thus the ability to fight off infection. This appears to ultimately explain the altered lesion phenotypes under CCT. While informative, a study like ours points to metabolic pathways being affected; however, direct measurements of metabolites are necessary to determine how CC-associated stress affects the internal environment of the tree host at a system level to predispose trees to fungal infection.

CHAPTER 3
TERPENOIDS ARE INVOLVED IN EXPRESSION OF SYSTEMIC INDUCED RESISTANCE IN AUSTRIAN PINE

3.1 Introduction

Successful tree resistance against recurring pests and pathogenic attacks depends on the combined effects of constitutive and inducible defenses. Attacking pests/pathogens are initially confronted with constitutive defenses that may include both anatomical and biochemical barriers, such as the epidermis or outer bark, and constitutive antimicrobial compounds, such as terpenoids (the major constituents of resin) and soluble and cell wall bound phenolics and their derivatives (Franceschi et al., 2005). This local response is further accompanied with an inducible defense response, which may involve physiological or anatomical changes, such as stomatal closure (Du et al., 2014), necrophylactic periderm formation (Morris et al., 2020), traumatic resin duct formation (López-Villamor et al., 2021; Luchi et al., 2005), and phytoalexin-type responses involving specialized metabolites like phenolics, lignin, and terpenoids (Van Bel & Gaupels, 2004; Franceschi et al., 2005). The inducible defense responses can then be expressed both locally and systemically, over time with recurring attacks.

Systemic induced resistance (SIR) can enhance plant immunity against subsequent pests or pathogenic attacks after successful containment of an initial attack (Bonello et al., 2006). The SIR phenomenon has been repeatedly demonstrated in the Austrian pine (*Pinus nigra*) / *Diplodia pinea* pathosystem (e.g., Sherwood & Bonello, 2016). A critical role for specialized metabolites like phenolics in Austrian pine SIR has been proposed, while the role of terpenoids remains unclear in this system (Sherwood & Bonello, 2016; Eyles et al., 2007). For instance, phenolics have only been studied in relatively late stages of SIR expression, e.g., after 16 days of incubation, at which time they are also clearly involved in negative trade-offs with terpenoids (Wallis et al., 2008).

Terpenoids are a group of specialized metabolites that appear central in direct defense response, particularly in conifers, against biotic and abiotic stresses, or in indirect defense as attractants of natural enemies of pests (Castells, 2015; Eyles et al., 2010). Terpenoids are derived from the isoprene backbone and are often oxygenated by cytochrome P450s to generate a great variety of motifs and functional groups (Moss et al., 1995; Castells, 2015). Terpenoids are the constituents of the oleoresin produced in conifers, which is composed of the volatile turpentine fraction (monoterpenoids and sesquiterpenoids), and the rosin that solidifies in contact with air (diterpenoids) (Castells, 2015). The hardening of rosin aids in covering and sealing wounds, e.g., after insect attack, and often traps insect pests, such as bark beetles, thereby stopping them in their tracks before they can penetrate the bark (Celedon & Bohlmann, 2019). Certain sesquiterpenes like β-caryophyllene can also aid directly in defense against herbivory (Huang et al., 2013; Wang et al., 2015). Similarly, many monoterpenes have been shown to have fungicidal and insecticidal properties (Prates et al., 1998; Zhang et al., 2016; Ullah et al., 2017). Certain monoterpenes, such as α-pinene, β-pinene, limonene, and myrcene have also been reported in phytoalexin responses against insect or pathogenic attacks in several plant species (Reidlmeier et al., 2017; Li et al., 2015, Xu et al., 2016; Erbilgin 2019). Furthermore, the monoterpenes myrcene, linalool, and ocimene can reportedly aid in defense priming (Riedlmeier et al., 2017). In our study system, the suppression of terpenoid biosynthetic pathways has been associated with enhanced susceptibility of Austrian pine to *D. pinea* infection under abiotic stress (Ghosh et al., 2022), highlighting a significant role of terpenes in resistance in this pathosystem. Whereas systemic accumulation of monoterpenes like α-pinene, β-pinene, and limonene have been reported based on *D. pinea* induction, or wounding (Wallis et al., 2008), the time-course of such inducible responses remains to be elucidated.

The objective of this study was to test the hypothesis that terpenoids are part for SIR in the Austrian pine / *D. pinea* pathosystem. In order to do so, we investigated evidence of SIR/ SIS in response to infection by *D. pinea*, after trees have been induced earlier by either the pathogen or wounding at a systemic, downstream location. Our results provide evidence that terpenoids are likely an important component of SIR in in this system, but this evidence is nuanced, depending on the identity of the specific terpenoids as well as other volatile organic compounds identified in the course of the study.

3.2 Materials and Methods

3.2.1 Plant and fungal material

Four-year-old, open pollinated Austrian pine trees growing in 3-gallon plastic pots (from Willoway Nursery Madison, OH) were maintained with regular fertigation and drip irrigation twice daily and moved to a greenhouse six weeks prior to experimentation, to allow for acclimation. *Diplodia pinea* strain IS-411, which was used in this study, is the same used in previous published work (Ghosh et al., 2022) and was kindly provided by Dr. Glenn Stanosz (University of Wisconsin, Madison.) The fungus was cultured on PDA for a week on the benchtop, at room temperature and with exposure to ambient light, before being used in the experiments described below.

3.2.2 Experimental model

The first goal of our study was to confirm that SIR occurs in this pathosystem (Blodgett & Bonello, 2003), and that the degree of infection can be quantified by canker or lesion lengths upon stem inoculation (Sherwood & Bonello, 2016). To do so, we *induced* opposite sides of the main stems 5 cm above the soil line (red triangles in Fig. 3.1), by extracting a 5 mm diameter plug comprising outer bark and phloem, down to the cambium, using a sterile increment borer. This tissue plug was then replaced with either a 5 mm agar plug taken from the margin of an active culture of *D. pinea* growing on PDA, or a 5 mm agar plug of PDA alone, which constituted the mock. Control trees were left uninduced (untreated/unwounded). These three "induction types" constituted the main factor in a fully factorial design. To investigate temporal patterns of SIR, we used different incubation times (subfactor) i.e., either 12 h, 72 h, or 10 d post induction, after which, all trees were *challenged* on a single side of the stem 15 cm above the induction point (red circle in Fig. 1), with the same strain of *D. pinea* and using the same inoculation technique used for the induction. This design resulted in nine treatment combinations that were applied to six trees each, for a total of 54 Austrian pine trees in the experiment (Fig. 1).

The plugs of outer bark and phloem taken from each induction and challenge site in order to perform the inoculations were then processed by separating the outer bark from the phloem, and the remaining phloem, along with residual cambial layer (i.e., the phloem cores) were stored in

falcon tubes at -80°C. Since they were excised before induction or challenge, the phloem cores thus collected constituted the pre-induction and the pre-challenge samples.

Two weeks post-challenge, lesions at both induction and challenge points were exposed by scraping off the bark with a sterile scalpel and their lengths were measured to the nearest mm. The stems of the infected trees were then harvested, and phloem tissue was sampled along the lesion margins, using a sterile 5 mm diameter increment borer. The bark was removed, and these phloem cores were stored as the post-induction and post-challenge samples, i.e., tissues that represented host responses to the pathogen at the induction and challenge sites, respectively.

3.2.3 Terpenoid analysis

Phloem cores were homogenized in liquid nitrogen and 100 mg of ground tissue from each sample was used for extraction of monoterpenes according to modified protocol based on

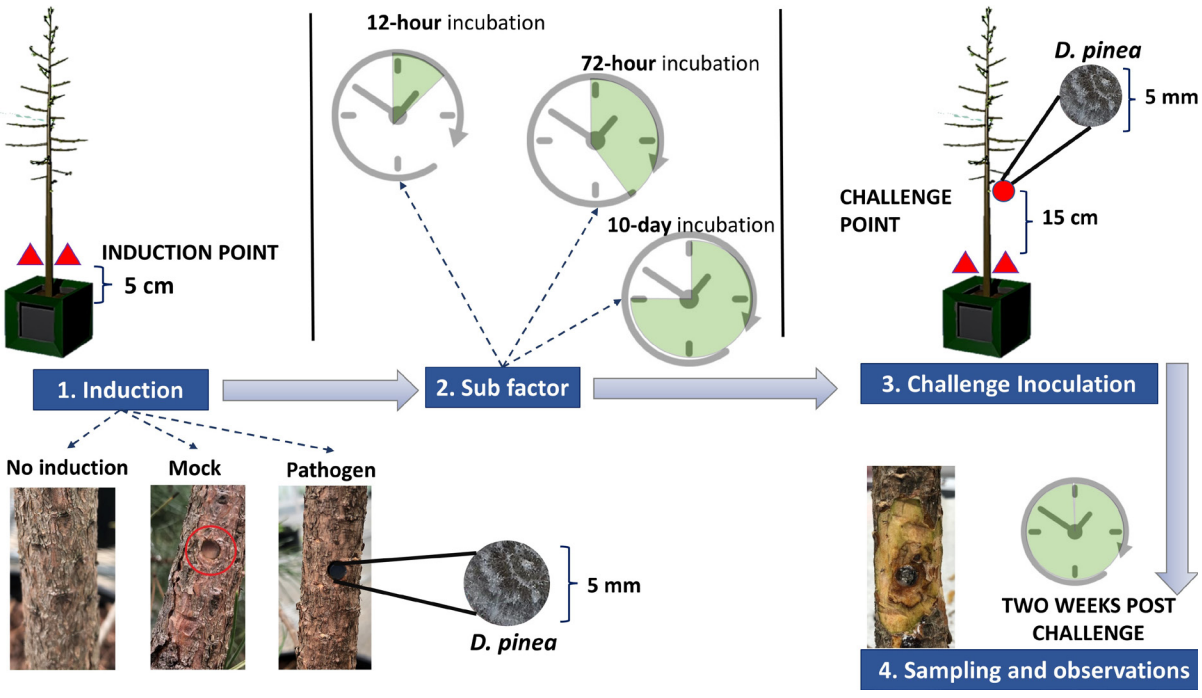

Figure 3.1. Schematic of treatment application and sampling strategy. Austrian pine stems were induced 5 cm above soil line by either inoculating them with D. pinea, wounding (mock), or leaving them untreated (red triangles). Stems were then challenged 15 cm above the induction location with D. pinea after 12 h, 72 h, and 10 days incubations (red circle). Tissues were sampled for chemical analyses pre-induction and pre-challenge, as well as post-induction and post-challenge.

Klutsch et al., 2016. Monoterpenes were extracted from the ground samples in 500 µl of solvent, containing Gas Chromatography (GC)-grade hexane and 0.004% (v/v) of pentadecane (internal standard), followed by sonication for 10 min and centrifugation at 16,500 rcf at 4°C for 15 min. The supernatant extracts were transferred into glass vials containing inserts using a plunger, without disturbing the solid residue. Sample extracts were separated on a HP-INNOWAX column (30 m x 0.25 mm ID x 0.5 um film, catalog number: 19091N-233; Agilent Tech, Santa Clara, CA, USA). Volatile fractions were subjected to electron impact (EI) ionization, with helium as a carrier gas applied at the flow rate of 1.1 mL/min. A 1 µL injection volume per sample was used with 260 °C inlet temperature along with split mode. The hard ionization of volatile fractions was carried out along a temperature gradient, with the initial temperature of the program set at 40 °C, followed by increase to 55 °C (held for 1 min), then 30 °C used to increase to 55 °C (held for 0.5 min), followed by 8 °C to increase to 122 °C (held for 2 min), then 10 °C to bring temperature to 200 °C, and finally 20 °C rate was used to bring the column temperature to 260 °C (held for 1 min). Corresponding intensities of ion fractions were captured using a GC-MS (GC:7890A, Mass Spectrometry: 5975C, Agilent Tech.). We followed an untargeted approach to identify chemicals; significant peaks were identified based on relative ion intensities in total ion chromatograms across sample treatment types. The result mass to charge ($^{m}/_{e}$) spectrum were used to assign and verify compound identities using the NIST 2017 Mass Spectral library version 2.3 (NIST, 2017).

Monoterpenes, sesquiterpenes and other compounds were quantified based on the following available standards (purity): limonene, β-pinene, (-)-borneol, and benzaldehyde-2,5 (>99%); α-pinene, 1-dodecanol, and n-dodecyl acrylate (98%); camphene, β-myrcene, α-terpineol, and terpinolene (90%); 3-carene (98.5%); bornyl acetate (97%); β-phellandrene (96%); and β-caryophyllene (80%). All standards were obtained from Sigma-Aldrich Co, MO, USA, except β-phellandrene, which was obtained from Toronto Research Chemicals Inc, ON, CAN.

3.2.4 Statistical analyses

First, we analyzed the differences in SIR phenotype by comparing lesion lengths developed 15 cm above induction, in response to the three induction treatments and three incubation times, and their interactions, using two-way fully factorial ANOVA in R (R core team, 2021). Second, we analyzed effects of induction treatment and incubation time on terpenoids using the logic flow

shown in Fig. 3.2. We began with the normalized, pre- and post-induction and pre- and post-challenge concentrations of various terpenoids, i.e., at both 5 cm and 15 cm above soil line, using a two-way fully factorial MANOVA in the *stats* package (R core team, 2021), followed by pairwise comparisons between treatment combinations. Significantly variable concentrations of response compounds were then subjected to individual ANOVAs, with significance threshold set at $\alpha < 0.05$.

3.2.5 Exploratory statistics

To further explore hidden relationships and based in part on the dimensional reduction strategy suggested by Chakraborty et al. (2013), the raw data were further subjected to unsupervised and supervised classifications following the logic flowchart, with conditioned checkpoints, shown in Fig. 2. The rationale for the tools used in the pipeline is reported in Appendix A2. The raw data were thus organized into two major multivariate matrices of the order $X \in Q^{p \times q}$ (Haddad et al., 2009), where p represents the number of measured terpenoids and q represents the number of

sampled trees, for both pre-inoculation and post-inoculations samples at both 5 cm and 15 cm above the soil line. The data matrices were then subjected to scaling across samples, either by their respective z-scores, or by quartile classification and subsequent ranking.

First, we conducted an unsupervised non-metric dimensional scaling analysis (NMDS) to

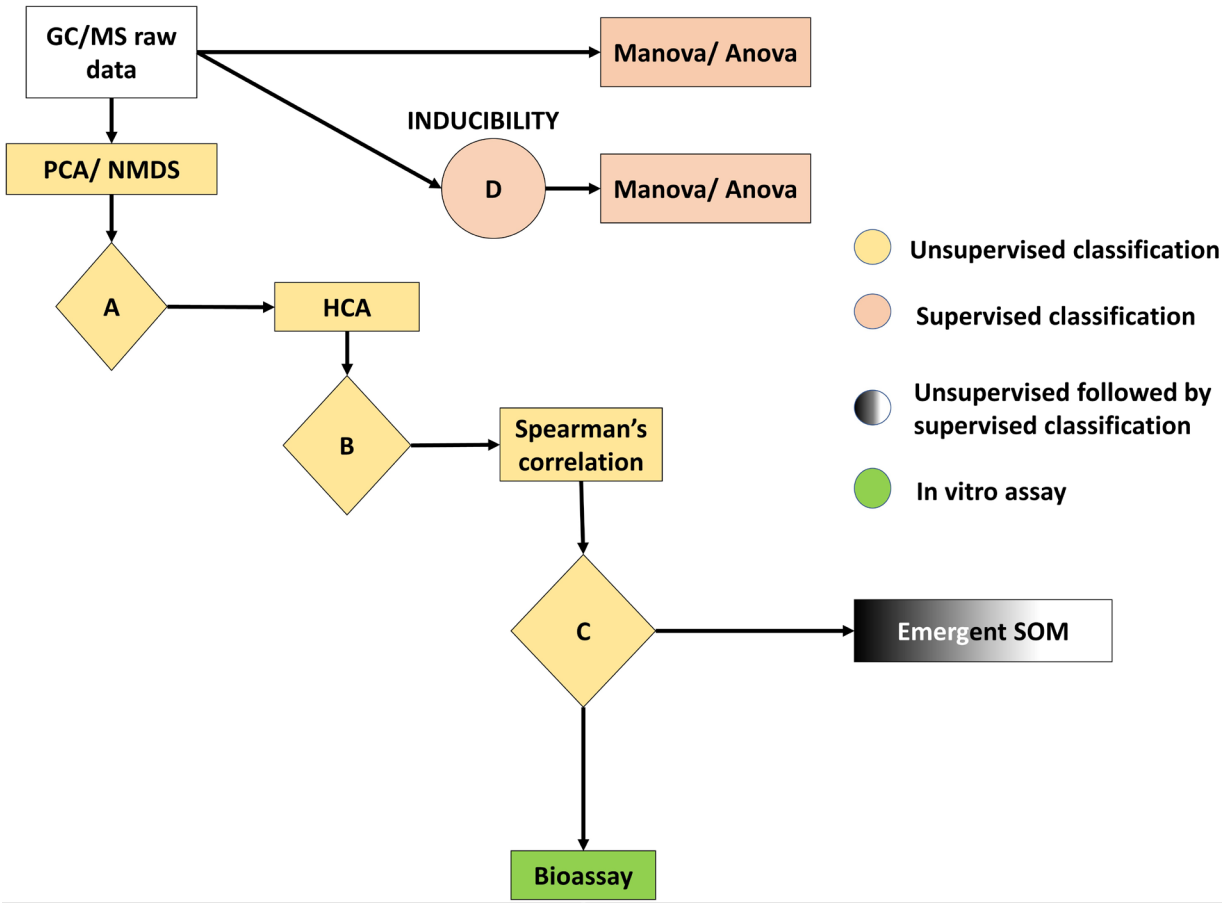

Figure 3.2. Flowchart for classification of raw concentrations of terpenoids and non-terpenoids in Austrian pine.

investigate if the accumulation of specific groups of terpenoids is significantly different in phloem cores collected at the time of induction and challenge, versus levels measured from the respective inoculation points at two weeks post challenge. We used the vegan package (Oksanen et al., 2020) in R (R core team, 2021). The optimal stress for the given matrix was graphed using the Shepherd's diagram that displays linear fit based on the squared correlation between goodness of fit of values and ordination distances. We used the Bray-Curtis distance as a measure of dissimilarity and projected global data for all sampled trees, irrespective of treatment type, into two dimensions.

To investigate whether accumulation of specific terpenoids is co-regulated, we conducted a supervised hierarchical clustering analysis (HCA) of the quartile-scaled data using furthest-neighbor joining based on squared Euclidean distance for each of the separate induction treatments (Wallis et al., 2008), using the inbuilt *stats* package and *factoextra* package (Kassambara & Mundt, 2020) in R (R core team, 2021). Thereafter, we conducted a Spearman's rank correlation analysis to ascertain if clusters of co-regulated compounds are associated with lesion length in response to any of the induction treatment/incubation time combinations, using the *stats* package (R core team, 2021).

Thereby, to further explore if/how any treatment combinations were significantly different, we conducted unsupervised training of data in each sample group and assessed the relative significance of induction type and time of incubation, followed by supervised testing and confirmation of emergent self-organizing maps (SOM), using the *kohonen* package (Wehrens & Kruisselbrink, 2018) in R (R core team, 2021).

Further, we also asked questions with respect to detected terpenoids and non-terpenoids in our study: Does the proportional (percent) change of a given compound (i.e., 66its inducibility) vary along the stem and after different incubation times? And between pre- and post-inoculation at each stem location?

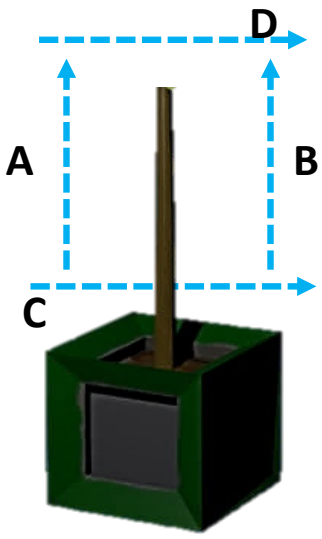

Vector A: Percent change in compound levels measured in the *pre-challenge* tissues at 12 h, 72 h, 10 d with respect to the levels at the induction site measured *before the induction* treatment was applied.

Vector B: Percent change in compound levels measured two weeks *post-challenge* at the challenge site with respect to the levels at the induction site measured at the same time.

Vector C: Percent change in compound levels measured two weeks *post-challenge* with respect to the levels measured at the induction site *before the induction* treatment was applied.

Vector D: Percent change in compound levels measured two weeks *post-challenge* with respect to the levels measured *pre-challenge* at the challenge site.

Figure 3.3. Schematic of directions (vectors) along which inducibility (percent change) of various terpenoids and other volatile organic compounds was quantified within each tree (experimental unit).

To answer these questions, the inducibility of individual compounds was categorized along different temporal and spatial vectors: (1) pre-challenge, at the challenge site, to investigate basal systemic induction, i.e., in response to the induction treatment alone (vector A in Fig. 3.3); (2) two weeks post challenge, at the challenge site, to investigate host responses to the challenge inoculation as they are affected by the induction treatment (vector B in Fig. 3.3); (3) at the induction site to investigate local changes (vector C in Fig. 3.3); and (4) at the challenge site to investigate local changes between pre- and post-challenge (vector D in Fig. 3.3). Inducibility (ΔI) was calculated as the percentage change with respect to basal levels (i.e., before any inoculation) at the time of induction/challenge inoculation.

$$\Delta I = \frac{W_{induced} - W_{basal}}{W_{basal}} \times 100\%$$

where $W_{induced}$ is the final quantity measured either upstream (vectors A and B in Fig. 3.3), or after two weeks of challenge incubation (vectors C and D in Fig. 3.3), and W_{basal} is the base

over which inducibility is estimated, i.e., basal levels at either the inoculation or challenge points. The resultant inducibility dataset was then subjected to two-way MANOVA followed by individual two-way ANOVAs to investigate significant interactions of induction treatment (i.e., *D. pinea*, mock induction and untreated control) and incubation time (i.e., 12 h, 72 h, and 10 d).

3.2.6 Bioassays

Finally, we investigated if clusters of co-regulated compounds had any fungitoxic/fungistatic against *D. pinea* (Sherwood and Bonello, 2016) or, conversely, whether any of the compounds could serve as sole carbon sources for the fungus. To answer the first question, PDA was amended with, in turn: α-pinene alone (cluster 1); β-pinene + limonene + benzaldehyde + n-dodecyl acrylate (cluster 2); and camphene + 3-carene + myrcene + terpinolene + bornyl acetate + α-terpineol + borneol + caryophyllene (cluster 3). We were not able to procure dodecanol (cluster 2), β-phellandrene and germacrene-D (cluster 3), and these compounds were therefore not included. Stocks of compound mixtures corresponding to each cluster were prepared in 100% DMSO at concentrations that, once diluted in PDA, would represent 2.0 X, 1.5 X, 1.0 X, 0.5 X, and 0.25 X concentrations, where 1.0 X is the concentration found *in planta* at two weeks post challenge, using the equivalency of 1 ml medium = 1 g phloem fresh weight (FW) (Ockels et al., 2007). To prepare the amended media, 2 ml of each compound mixture was pipetted into flasks containing 100 ml autoclaved PDA that was cooled down in a water bath to approx. 35°C. Compound addition was performed in a laminar flow hood, the flasks were gently swirled, and the medium was immediately poured into 5 cm diameter Petri dishes, while maintaining minimum airflow in a laminar flow hood. Mocks consisted of 100% DMSO alone, while unamended PDA served as negative control. We used six replicate dishes for each compound cluster/dilution combination. Plates were then inoculated with 5 mm plugs of mycelium taken from the margins of actively growing *D. pinea* cultures on PDA, sealed with a double layer of parafilm and incubated in a plastic crisper at 25°C under light. The colony radius was measured three days after plating. A two-way ANOVA was conducted to test the effects of compound concentration on fungal growth. Finally, in cases where no fungal growth was observed, the fungistatic or fungitoxic properties of the various compounds were tested by subculturing fungi from each bioassay plate into fresh, unamended PDA for 7 d (Sherwood & Bonello, 2016).

3.3 Results

Lesion length response

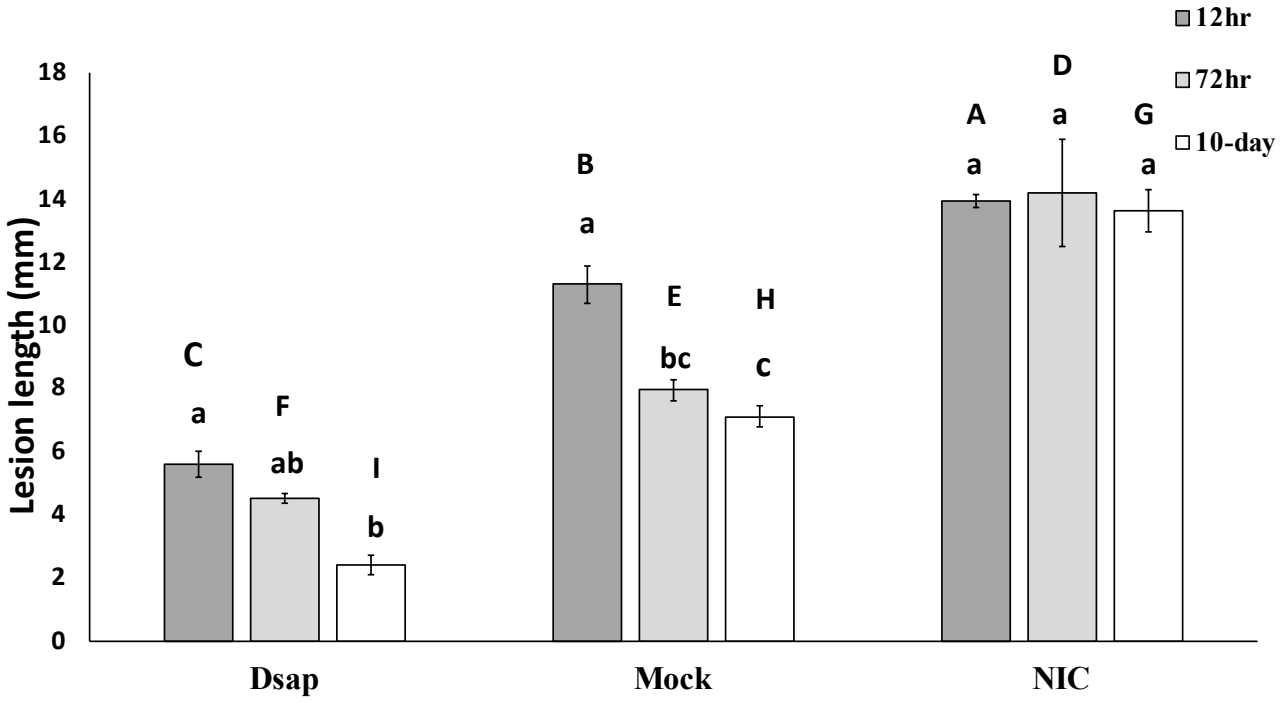

Figure 3.4. Lesion lengths measured two weeks post challenge inoculation of Austrian pine stems with D. pinea. Prior to challenge, trees had been subjected to three induction treatments and three incubation periods within each induction treatment. Dsap: *D. pinea*, mock: mock or wounding, NIC: non-induced controls. Different letters show significant differences (Tukey's HSD, $p < 0.05$); lowercase letters: comparisons of incubation periods within induction treatments; uppercase letters: comparisons of incubation periods between induction treatments. Smaller lesions in response to pathogen induction, overall and across induction treatments at the same induction period, demonstrate the SIR phenotype, while diminishing lesions over time within induction treatment show that the SIR response becomes stronger with increasing incubation time. Error bars are SE.

Challenge lesion lengths were progressively shorter with increasing time of incubation in trees that had been induced by wounding, compared to the non-induced controls, and even shorter in trees that were induced with *D. pinea* (Fig. 3.4). The shortest lesions were produced after a 10-day incubation, when they were approximately 1/3 the challenge lesions of mocks, and about 1/6 the challenge lesions on non-induced controls (Fig. 4). Induction type and induction period had a significant interaction on challenge lesion length ($F = 4.332$, $df = 2$, $p = 0.0186$). Furthermore, within the mock and pathogenic induction treatments, lesions were progressively shorter with

increasing incubation time. This was also accompanied by anecdotal observation of profuse resin exudation from all pathogen infection courts within minutes of inoculation, compared to the mock, which increased with progressing time of incubation.

Table 3.1. MANOVA and ANOVA tables of total concentrations (µg mg-1 FW) of various terpenoids and other volatile organic compounds showing significant main effects and interactions of induction type and duration of induction incubation. (* for $p < 0.05$, ** for $p < 0.01$, *** for $p < 0.001$). Subscripts to F-values are degrees of freedom.

	MANOVA					
Global	**PRE-CHALLENGE**			**POST-CHALLENGE**		
	Induction	**Incubation time**	**Induction X Incubation time**	**Induction**	**Incubation time**	**Induction X Incubation time**
	$F_{2,45}$	$F_{2,45}$	$F_{4,45}$	$F_{2,45}$	$F_{2,45}$	$F_{4,45}$
	2.74 ***	2.62 ***	1.77 **	1.4 *	3.71 ***	1.42 *
	INDIVIDUAL ANOVA					
Compounds	**Induction**	**Incubation time**	**Induction X Incubation time**	**Induction**	**Incubation time**	**Induction X Incubation time**
	$F_{2,45}$	$F_{2,45}$	$F_{4,45}$	$F_{2,45}$	$F_{2,45}$	$F_{4,45}$
α-pinene	3.2 *	4.85 *	1.31	5.86 **	1.6	1.11 *
camphene	3.94 *	4.52 *	1.18	1.9	1.83	0.79
β-pinene	2.01	3.09	1.25	2.82 **	1.78	2.42 *
3-carene	0.1	1.03	0.74	1.31	0.05	2.05
myrcene	13.18 ***	7.93 **	3.33 *	4.03 *	1.42	0.16
limonene	6.31 **	4.72 *	2.53	3.96 *	2.12	3.25 *
terpinolene	2.29	4.19	2.37	1.84	0.52	0.34

(continued)

bornyl acetate	3.05	1.87	1.4	3.49 *	1.3	0.17
α-terpineol	0.82	1.6	0.68	0.97	2.67	1.32
borneol	0.87	1.5	0.73	5.54 **	3.17	2.8 *
β-phellandrene	2.25	1.99	1.77	3.2	0.76	0.93
caryophyllene	2.55	1.63	1.08	2.26	0.02	0.53
germacrene D	3.55 *	3.03	0.8	1.83	0.52	0.15
benzaldehyde	10.98 ***	0.74	7.96 ***	0.69	26.85 ***	2.72 *
dodecanol	5.51 **	7.36 **	2.38	1.18	21.49 ***	8.85 *
n-dodecyl acrylate	26.31 ***	11.55 ***	5.84 ***	7.37 **	24.41 ***	2.11 *

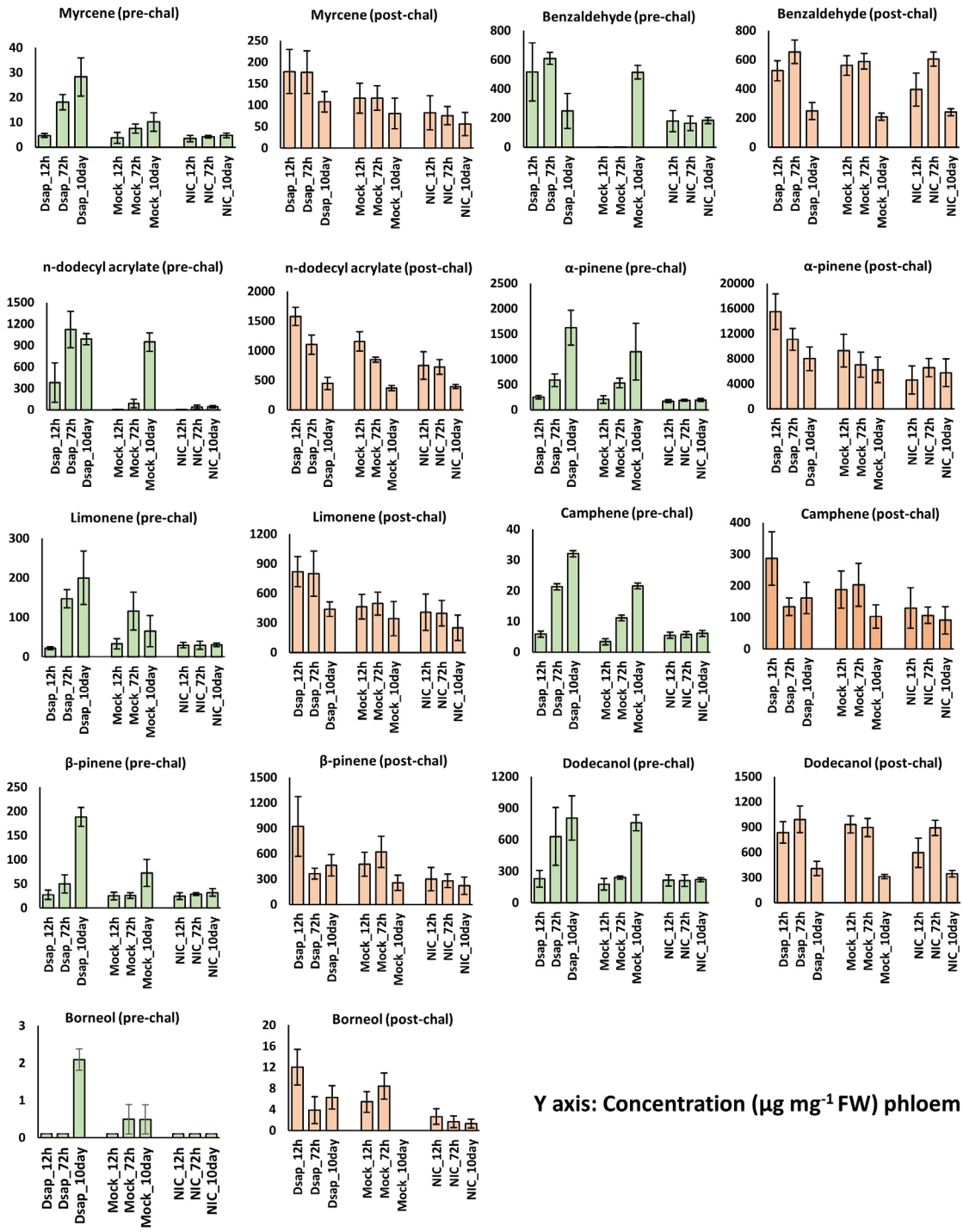

Figure 3.5. Bar plots showing total accumulation of individual terpenoids and non-terpenoids in Austrian pine stems that changed significantly at the challenge site in response to induction treatment or time of induction incubation (Tukey's HSD, $p < 0.05$). Dsap: *D. pinea* induction; mock: wound induction; NIC: non-induced control. Error bars are SE.

3.3.1 Biochemical responses

The initial MANOVA showed significant interaction effects between induction type and incubation period on terpenoids and non-terpenoids, both pre-challenge (F_4= 1.77, $p < 0.01$) and post-challenge (F_4= 1.42$p < 0.05$) (Table 3.1).

Pre-challenge: levels of myrcene, α-pinene, and camphene increased with incubation time in hosts induced with both *D. pinea* and wounding (Table 3.1; Fig. 3.5). Levels of benzaldehyde were consistently higher in pathogen induced hosts, irrespective of incubation time (Table 3.1; Fig. 3.5), while limonene, dodecanol, and n-dodecyl acrylate levels were higher only at 72-hour and 10-days (Fig. 3.5). Levels of borneol and β-pinene were highest in pathogen induced hosts at 10 days (Fig. 3.5).

Post-challenge: at 12 hours, levels of α-pinene, β-pinene, limonene, borneol, camphene, myrcene, and n-dodecyl acrylate were highest after both pathogenic and mock induction (Table 3.1; Fig. 3.5), whereas benzaldehyde and dodecanol were unaffected by either factor (Fig. 3.5). All other compounds were unaffected by interactions of treatment and time.

Having found significant effects of induction treatment and incubation period, we explored the data for other relationships of interest using various classification approaches (Fig. 3.2), beginning with an NMDS analysis. Pre-challenge, two distinct compound clusters were found; the first cluster was comprised of various monoterpenes, including α-pinene, β-pinene, camphene, myrcene, limonene, β-phellandrene, terpinolene, and borneol, while the second cluster included non-terpenoid compounds such as benzaldehyde, dodecanol, and n-dodecyl acrylate (Fig. 3.6A). Post-challenge, we did not uncover any distinct groupings (Fig. 3.6B). Iterations of random scaling in both sample sets were concluded after 100 attempts with the resultant ordination stress value of 0.058 for pre-challenge tissues and 0.055 for post-challenge tissues, indicating significant fit of our data within the two-dimensional classification. Higher dimensional configuration for the post-challenge tissues yielded similar results.

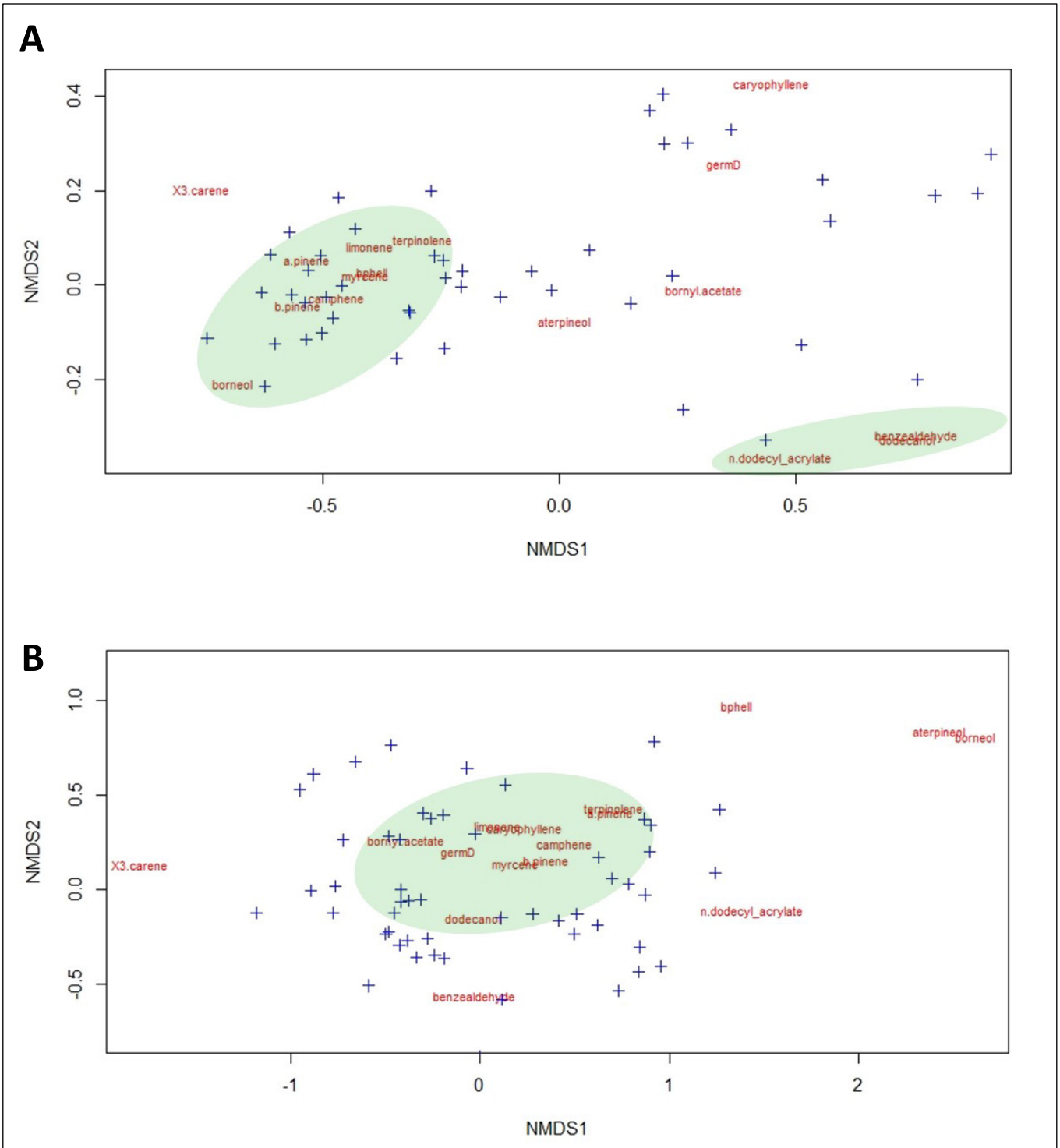

Figure 3.6. NMDS biplots of terpenoids and non-terpenoids detected at challenge location in Austrian pine **(A)** pre-challenge and **(B)** post-challenge. Blue crosses represent global orientation of concentration means from various samples based on pairwise dissimilarity matrices. Shaded ellipses group monoterpenes and other VOCs at 95% CI.

We further confirmed the ordination fitness using a Shepherd's plot that indicated significant fitting of our data against both linear and non-metric scaling, with linear regression fit R^2 values of 0.99 for pre- and post-challenge, respectively.

3.3.2 Relationships between measured compounds

Following the NMDS analysis, HCA uncovered five distinct pre-challenge clusters and three distinct post-challenge clusters for pathogen-induced trees, respectively, at 95% CI. Here, for ease of interpretation, individual compound branches are also referred to as clusters.

Pre-challenge: in response to *D. pinea* induction, α-pinene and dodecanol fell into cluster 1, whereas benzaldehyde and dodecanol branched out separately as clusters 2 and 3, respectively (Fig. 3.7A). Cluster 4 included camphene, 3-carene, myrcene, terpinolene, bornyl acetate, α-terpineol, borneol, β-phellandrene, caryophyllene, germacrene D, while cluster 5 was comprised of β-pinene, and limonene (Fig. 3.7A).

Post-challenge: α-pinene segregated into cluster 1, cluster 2 was comprised of β-pinene, limonene, benzaldehyde, dodecanol, and n-dodecyl acrylate, while cluster 3 included camphene, myrcene, terpinolene, α-terpineol, β-phellandrene, borneol, bornyl acetate, caryophyllene, and germacrene D (Fig. 3.7A).

Interestingly, mock-induced and non-induced hosts produced similar clusters, at both pre- and post-challenge (Fig. 3.7B, C), with α-pinene separating as its own cluster 1 in both pre- and post-challenge hierarchical clusters (Fig. 3.7B, C).

Pre-challenge: benzaldehyde and dodecanol constituted cluster 2, with n-dodecyl acrylate as the closest neighbor in cluster 3 for both wound-induced (Fig. 3.7B) and non-induced hosts (Fig. 3.7C). Cluster 4 was composed of β-pinene, camphene, myrcene, terpinolene, α-terpineol, β-phellandrene, borneol, bornyl acetate, caryophyllene, and germacrene D in both non-induced (Fig. 3.7C) and wound-induced hosts, although, limonene segregated as cluster 5 in the wound-induced hosts (Fig. 3.7B).

3.3.3 Relationships between measured compounds and lesion lengths

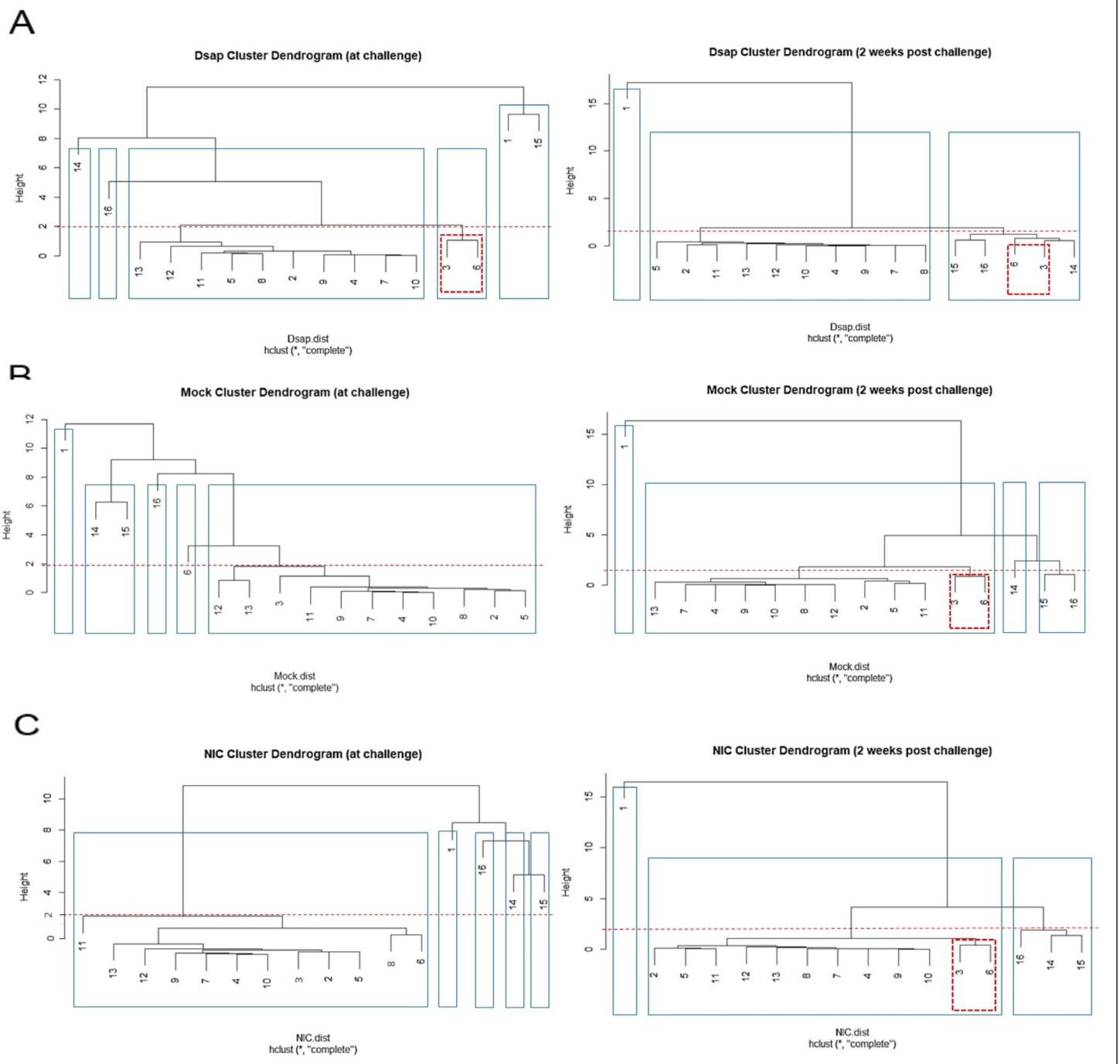

Figure 3.7. Hierarchical clustering of terpenoids and other non-terpenoids measured at the challenge sites, pre- and post-challenge, in Austrian pine stems that were earlier induced with (A) *D. pinea* (Dsap), (B) wounding (mock), or (C) non-induced (NIC). Clusters were assigned over a threshold height of 2 distance units (dotted red line), branch labels: (1) α-pinene, (2) camphene, (3) β-pinene, (4) 3-carene, (5) myrcene, (6) limonene, (7) terpinolene, (8) bornyl acetate, (9) α-terpineol, (10) borneol, (11) β-phellandrene, (12) caryophyllene, (13) germacrene D, (14) benzaldehyde, (15) dodecanol, (16) n-dodecyl acrylate. Blue boxes show cluster delimitation; red dotted box shows consistent co-regulation of (3) β-pinene and (6) limonene in all post-challenge samples as well as pre-challenge, but only in the presence of a D. pinea induction.

Post challenge: the major cluster 3 that did not qualify our threshold in both wound-induced and non-induced hosts included camphene, myrcene, terpinolene, α-terpineol, β-phellandrene, borneol, bornyl acetate, caryophyllene, and germacrene D, and a sub-cluster of β-pinene, limonene (Fig. 3.7B, C). Cluster 2 comprised of benzaldehyde, dodecanol, and n-dodecyl acrylate in non-induced hosts, while wound-induced hosts were further split into cluster 3 with benzaldehyde, and its neighboring cluster 4 consisting dodecanol and n-dodecyl acrylate (Fig. 3.7B, C).

The quartile-scaled data were reorganized into two functionally distinct clusters that represented separate biosynthetic networks, i.e., terpenoids (monoterpenes, sesquiterpenes, and terpene derivatives), and non-terpenoid plant volatile compounds. This was conducted only for pathogen-induced trees because those trees expressed the strongest SIR phenotype. In aggregate (Fig. 3.8A), terpenoids, both pre- and post-challenge, were negatively correlated with challenge lesion lengths. Interestingly, while non-terpenoids, in aggregate, were positively correlated with terpenoids both pre- and post-challenge (Fig. 3.8A), they had no correlation with challenge lesion lengths.

Correlations with challenge lesion lengths were also analyzed for clusters obtained from the HCA pipeline, to investigate relationships between co-regulated compounds reflected via significant hierarchical clusters formed due to pathogenic induction and resistance.

Pre-challenge: significant, negative correlations were observed between lesion lengths and cluster 1(α-pinene, $r_s = -0.77, \text{with } p = 0.0142$), cluster 2 (benzaldehyde, $r_s = -0.54, \text{with } p = 0.0091$), cluster 3 (n-dodecyl acrylate, $r_s = -0.85, \text{with } p = 0.0037$), and cluster 5 (β-pinene and limonene, $r_s = -0.78, \text{with } p = 0.0128$) (Fig. 3.8B).

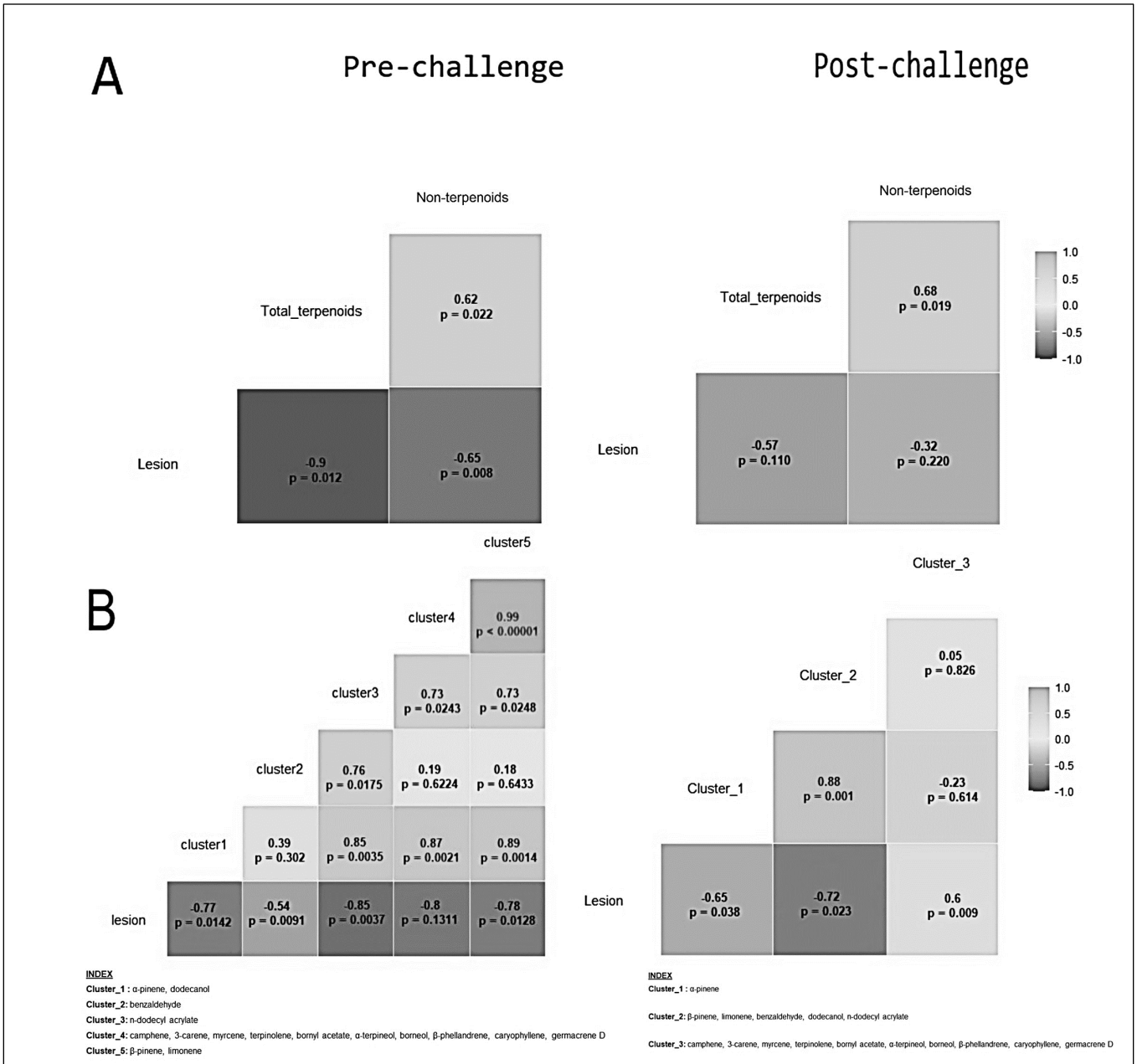

Figure 3.8. (A) Correlation indices between lesion sizes measured at two weeks post challenge of Austrian pine, and global terpenoids and non-terpenoids measured at, pre-challenge (left) and post-challenge (right). **(B)** Correlation indices between lesion sizes measured at two weeks post challenge of Austrian pine and significant hierarchical clusters of terpenoids and non-terpenoids reported in *D. pinea* induced hosts (Fig. 6a) and measured at pre-challenge (left) and post-challenge (right). Strength of correlation represented as per color index.

Post-challenge: we observed moderate, but significant, negative correlations between lesion lengths and clusters 1 (α-pinene alone, $r_s = -0.65, \text{with } p = 0.038$) and cluster 2 (β-pinene, limonene, benzaldehyde, dodecanol, and n-dodecyl acrylate, $r_s = -0.72, \text{with } p = 0.023$),

whereas the correlation was positive with cluster 3 (camphene, 3-carene, myrcene, terpinolene, bornyl acetate, α-terpineol, borneol, β-phellandrene, caryophyllene, and germacrene D, $r_s = 0.6, \text{with } p = 0.0087$) (Fig. 3.8B). Notably, we also found a strong positive correlation between clusters 1 and 2 ($r_s = 0.88, \text{with } p = 0.009$) (Fig. 3.8B).

We further conducted correlation analysis between *Z* score-scaled data for individual compounds and lesion lengths and deemed significant any correlations with coefficients > 0.5 or < - 0.5 ($p < 0.05$).

Pre-challenge: we found significant negative correlations between lesion lengths and α-pinene, camphene, β-pinene, limonene, β-phellandrene, benzaldehyde, dodecanol, and n-dodecyl acrylate, for pathogen-induced trees ($p < 0.05$) (Table A2.1, Appendix 2.). Further, significant positive correlations were found between α-pinene and camphene, β-pinene, myrcene, limonene, terpinolene, and bornyl acetate ($p < 0.05$) (Table A2.1, Appendix 2.)). In wound-induced hosts, pre-challenge, significant negative correlations were observed between lesion lengths and α-pinene, camphene, β-phellandrene, dodecanol, and n-dodecyl acrylate, while significant positive correlations were observed between α-pinene and camphene, β-pinene, myrcene, limonene, terpinolene, and β-phellandrene ($p < 0.05$) (Table A2.1, Appendix 2.).

Also, at pre-challenge, no significant correlations were found between lesion lengths and terpenoids and non-terpenoids in non-induced hosts (Table A2.1, Appendix 2.). For 12 h induction incubation, significant negative correlations were established between average lesion sizes and α-pinene, caryophyllene, and n-dodecyl acrylate ($p < 0.05$) (Table A2.1, Appendix 2.). Negative correlations occurred between average lesion sizes and α-pinene, camphene, β-pinene, myrcene, limonene, bornyl acetate, β-phellandrene, caryophyllene, germacrene D, benzaldehyde, and n-dodecyl acrylate, for 72 h induction incubation ($p < 0.05$) (Table A2.1, Appendix 2.), while similar profile of negative correlation with average lesion size was also observed during 10 d induction incubation, sparing camphene, myrcene, bornyl acetate, caryophyllene, and germacrene D ($p < 0.05$) (Table A2.1, Appendix 2.).

Post-challenge: we found significant negative correlations between lesion length and α-pinene, β-pinene, limonene, α-terpineol, benzaldehyde, dodecanol, and n-dodecyl acrylate (at $p < 0.05$) in pathogen-induced trees (Table A2.1, Appendix 2.), consistent with the findings from HCA

cluster correlations. However, for mocks and unwounded trees, we found no direct correlation with lesion length, except a negative correlation between lesion length and α-pinene (Table A2.1, Appendix 2.). Notably, for all induction treatments there were strong positive correlations between various monoterpenes, and likewise between other volatile compounds. Similarly at two weeks post challenge, α-pinene, borneol, and n-dodecyl acrylate had negative correlations with lesion lengths for 12 h induction incubation (at $p < 0.05$) (Table A2.1, Appendix 2.), while α-pinene., myrcene, caryophyllene, n-dodecyl acrylate was found to be negatively correlated with lesions for 72 h induction incubation (at $p < 0.05$) (Table A2.1, Appendix 2.). Interestingly, germacrene D and n-dodecyl acrylate were the only correlated compounds (negative) for 10 d interval between induction and challenge inoculations (at $p < 0.05$) (Table A2.1, Appendix 2.).

Then, we proceeded to generating emergent SOMs using a Gaussian function with an optimum learning rate adjusted below 300 iterations for best prediction of neuron weights, based on the recommended optimization in other studies (Natita et al., 2016, Haddad et al., 2009). The resultant U-matrix or self-organized map produced a rectangular plane of mapped data comprising 25 unique nodes that were color-coded based on one of three induction and one of three incubation time treatments based on neuron weight, where each neuron corresponded to the sum of all data recorded for any given compound.

Pre-challenge: linear learning rate was optimized at 0.1455 after 294 iterations, with the mean distance to the closest unit fixed at 0.023 units (Fig. 3.9A). The emergent pre-challenge self-organized map produced 9 fanning nodes for 72 h induction, 7 fanning nodes for 12 h induction, 5 fanning nodes for 10 d induction, while 4 fanning nodes remained inconclusive due to similar neuron weights from all treatment types (Fig. 3.9B). The emergent SOM for induction type

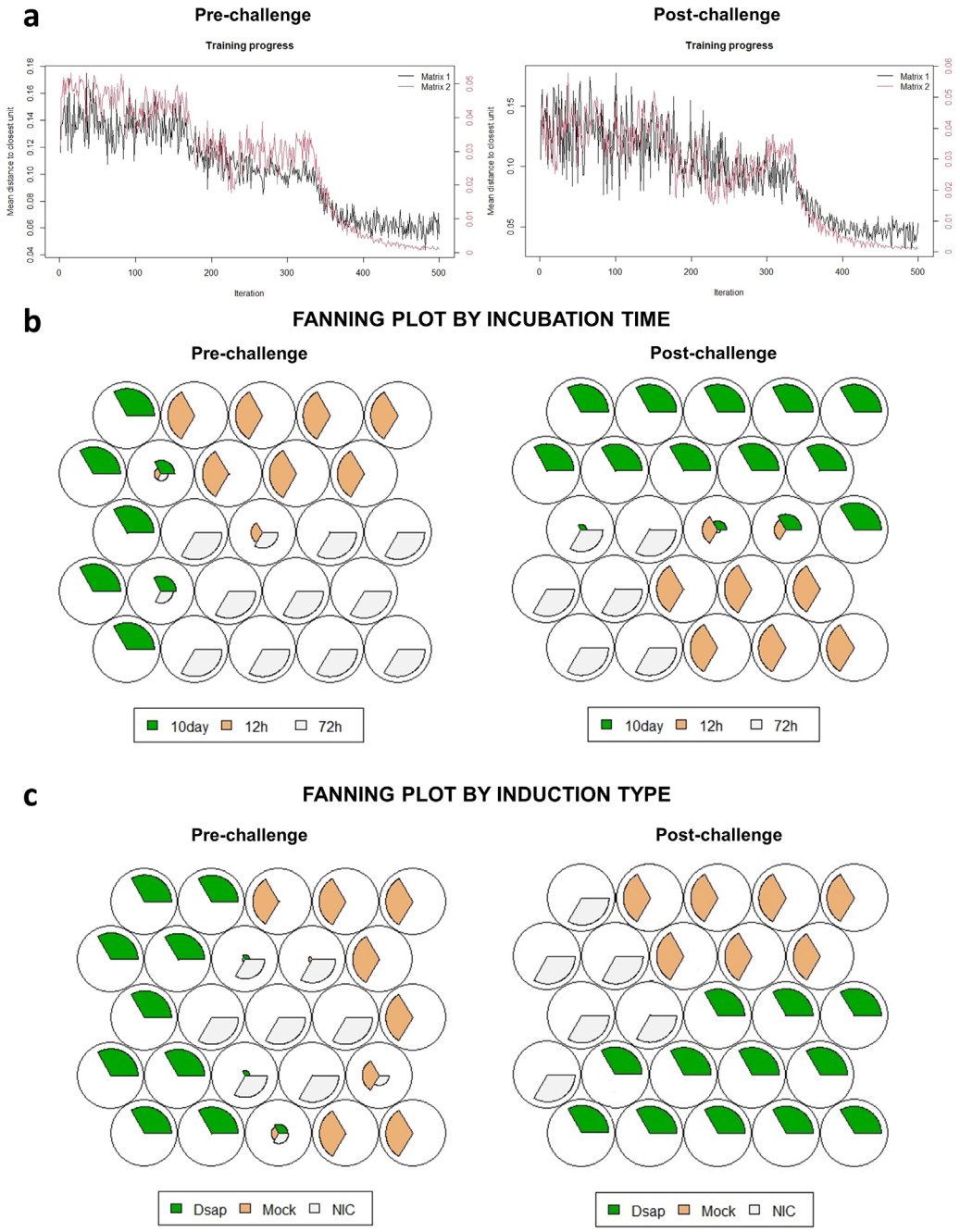

Figure 3.9. (A) Training plots for self-organizing maps based on the distance matrices of pre-challenge (left) and post-challenge (right) data. Color legend labels indicate; Dsap: *D. pinea*, mock: mock or wounding, NIC: non-induced controls. Matrix 1 and matrix 2 represent two sets of randomly selected data that are tested against the model until the mean distance between matrices is minimized. For our modeling we selected 400 iterations. (**B and C**) Emergent fanning plots represented in 5 x 5 grids of relatively clustered nodes, where greater than 40% occupancy in each node is denoted by colored fans, which represent the proportion of variation being explained by the treatment type. **(B)** Fanning plot representing clustering by incubation time, with 72-h incubation (gray nodes) occupying the highest number of nodes in pre-challenge (left) and 10-day incubation (green nodes) occupying the highest number of nodes in post-challenge (right). **(C)** Fanning plot representing clustering by induction type, with D. pinea occupying the highest number of nodes for both pre- (left) and post-challenge (right).

wound-induction, 5 fanning nodes occupied by the non-induced controls, while 4 nodes remained inconclusive due to proportions of all treatment types (Fig. 3.9C).

Post-challenge: linear learning rate was optimized at 0.1232 after 255 iterations, with the mean distance to the closest unit fixed at 0.025 units (Fig. 3.9A). The post-challenge emergent SOM produced 11 fanning nodes for 10 d induction incubation, while 12 h and 72 h induction incubation occupied 6 fanning nodes, each and 2 nodes remained inconclusive (Fig. 3.9B). In the emergent SOM for induction type, 12 fanning nodes mapped to pathogen induction, while wound induction and no induction types were mapped to 7 fanning nodes and 6 fanning nodes, respectively (Fig. 3.9C).

3.3.4 Analysis of inducibility (inducible variation)

Vector A

The interaction between induction type and incubation time on systemic inducibility of compounds before challenge was significant ($F_4 = 1.62$, $p = 0.003$) (Table 3.2). At 12 h, systemic inducibility of α-pinene, β-pinene, and benzaldehyde was significantly higher than in mock and non-induced trees (Fig. 3.10A). At 72 h, pathogen-induced trees showed higher inducibility of α-pinene and bornyl acetate, and at 10 d, higher inducibility of α-pinene and β-pinene (Fig. 3.10A).

Vector B

Post-challenge, the interaction between induction type and incubation time was significant for systemic inducibility ($F_4 = 1.8$, $p = 0.003$) (Table 3.2). The systemic inducibility of α-pinene,

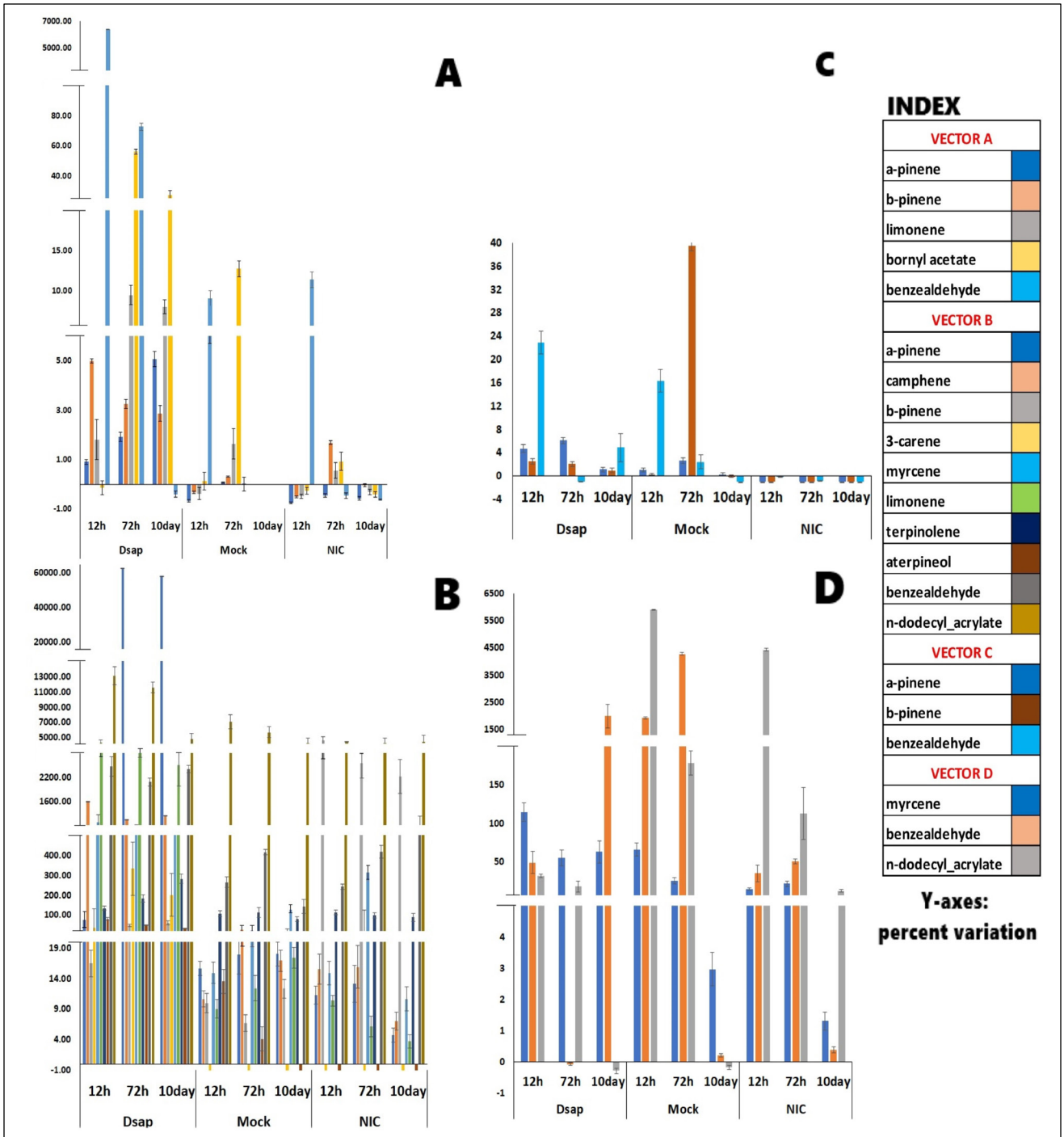

Figure 3.10. Inducibility of changing individual terpenoids and other volatile organic compounds along vectors **A, B, C, D** (see Fig. 3.2) at different incubation time points, separated by induction treatment. X-axis labels indicate induction treatments; Dsap: *D. pinea*, mock: mock or wounding, NIC: non-induced controls, for 12-hour (12h), 72-hour (72h), and 10-day incubation. Only significantly changing compounds are reported. The overall significance of individual and total compound inducibility can be found in Table 3.1. Error bars are SE.

camphene, benzaldehyde, α-terpineol, myrcene, limonene, β-phellandrene, and germacrene D was significantly higher in pathogen-induced trees after 12 h induction incubation (post-hoc

contrasts, $p < 0.05$), whereas the inducibility of β-pinene and n-dodecyl acrylate were significantly higher in both pathogen-induced and wound-induced trees after 12 h induction incubation (post-hoc contrasts, $p < 0.05$) (Fig. 3.10B). In trees that were challenged after 72 h induction incubation, systemic inducibility of α-pinene, camphene, benzaldehyde, α-terpineol, and 3-carene was significantly higher in pathogen-induced trees (post-hoc contrasts, $p < 0.05$), while n-dodecyl acrylate inducibility was higher in both pathogen-induced and wound-induced trees (post-hoc contrasts, $p < 0.05$) (Fig. 3.10B). In trees challenged after 10 d induction incubation, systemic inducibility of α-pinene, camphene, benzaldehyde, α-terpineol, 3-carene, and terpinolene was significantly higher in pathogen-induced trees (post-hoc contrasts, $p < 0.05$) (Fig. 3.10B).

Vector C

The interaction of induction type and induction incubation time on local, lower stem (induction site) inducibility over time was also significant along vector C ($F_4 = 1.91$, $p < 0.001$) (Table 3.2). The local inducibility of α-pinene and β-pinene was significantly higher (post-hoc contrasts, $p < 0.05$) in pathogen-induced trees that were also challenged after 12 h induction incubation, whereas the inducibility of benzaldehyde was significantly higher (post-hoc contrasts, $p < 0.05$) in both pathogen-induced and wound-induced trees (Fig. 3.10C). Inducibility of α-pinene and β-pinene was also significant (post-hoc contrasts, $p < 0.05$) for pathogen-induced trees that were also challenged after 72 h induction incubation (Fig. 3.10C).

Vector D

The interaction at the challenge location between induction type and incubation time was also significant ($F_4 = 1.55$, $p = 0.018$) (Table 3.2). The local inducibility of myrcene was higher in pathogen-induced trees at all induction incubation time points compared to wound-induced and non-induced hosts (Fig. 3.10D). In contrast, the local inducibility of benzaldehyde and n-dodecyl acrylate was higher (post-hoc contrasts, $p < 0.05$) in wound-induced and non-induced hosts relative to pathogen-induced hosts, especially for trees that were also challenged after 12 h and 72 h induction incubation, respectively (Fig. 3.10D).

Table 3.2. MANOVA and ANOVA tables of percent inducibility of various terpenoids and other volatile organic compounds along the four vectors/directions of the study (Fig. 3.2), showing significant main effects and interactions of induction type and duration of induction incubation (* for $p < 0.05$, ** for $p < 0.01$, *** for $p < 0.001$). Subscripts to F-values are degrees of freedom.

	MANOVA											
Global	**VECTOR A**			**VECTOR B**			**VECTOR C**			**VECTOR D**		
	Induction	**Incubation time**	**Induction X Incubation**	**Induction**	**Incubation time**	**Induction X Incubation**	**Induction**	**Incubation time**	**Induction X Incubation**	**Induction**	**Incubation time**	**Induction X Incubation**
	$F_{2,44}$	$F_{2,44}$	$F_{4,44}$	$F_{2,44}$	$F_{2,44}$	$F_{4,44}$	$F_{2,45}$	$F_{2,45}$	$F_{4,45}$	$F_{2,45}$	$F_{2,45}$	$F_{4,45}$
	5.31 ***	2.82 **	1.62 **	7.31 ***	2.52 **	1.78 **	4.13 ***	6.15 ***	1.91 ***	2.24 **	2.21 **	1.55 *
	INDIVIDUAL ANOVA											
Compounds	**Induction**	**Incubation time**	**Induction X Incubation**	**Induction**	**Incubation time**	**Induction X Incubation**	**Induction**	**Incubation time**	**Induction X Incubation**	**Induction**	**Incubation time**	**Induction X Incubation**
	$F_{2,44}$	$F_{2,44}$	$F_{4,44}$	$F_{2,44}$	$F_{2,44}$	$F_{4,44}$	$F_{2,45}$	$F_{2,45}$	$F_{4,45}$	$F_{2,45}$	$F_{2,45}$	$F_{4,45}$
α-pinene	180.12 ***	40.86 ***	27.01 ***	30.93 ***	0.33	0.33	66.18 ***	3.9 *	1.34	4.9 *	3.26 *	0.39
camphene	0.69	2.17	0.6	32.6 ***	0.35	0.35	2.3	1.22	0.87	6.64 **	2.75	0.87
β-pinene	36.52 ***	1.44	3.27 *	24.29 ***	1.39	1.46	31.58 ***	0.63	0.97	0.94	1.43	0.82
3-carene	0.63	1.2	0.44	38.51 ***	8.06 **	7.73 ***	1.39	1.23	1.41	1	0.6	0.75
myrcene	1.51	1.41	1.18	17 ***	0.33	0.7	5.6 **	2.11	1.67	6.79 **	2.97	0.73
limonene	5.55 **	1.38	0.58	19.64 ***	0.5	0.5	1.12	1.27	1.08	1.01	1.1	1.01
terpinolene	2.09	1.21	2.43	5.85 **	0.43	1.55	6.33 **	0.77	0.46	0.23	1.15	0.82

(continued)

bornyl acetate	8.28 ***	5.15 **	2.66 *	2.6	1.76	3.53 *	0.93	1.73	0.48	0.22	3.26 *	0.15
α-terpineol	1.47	1.55	2.61 *	55.69 ***	7.26 **	3.46 *	5.17 **	0.24	0.59	1.63	1.07	1.15
borneol	1.89	1.9	2.46	8.52 ***	3.8 *	1.78	1.18	0.79	1.11	3.58 *	6.13 **	1.85
β-phellandrene	0.99	0.72	1.06	23.61 ***	2.07	2.38	4.13 *	1.42	1.35	2.91	2.58	0.84
caryophyllene	4.23 *	4.67 *	1.08	4.92 *	1.14	0.27	1.57	1.72	1.53	0.93	3.94 *	0.91
germacrene D	2.53	2.41	0.7	9.74 ***	2.05	3.67 *	1.31	0.93	0.83	0.72	0.69	1.09
benzaldehyde	13.97 ***	13.64 ***	13.51 ***	29.72 ***	0.25	0.57	7.5 **	15.96 ***	4.33 **	6.46 **	1.65	5.57 ***
dodecanol	0.75	1.35	1.31	0.34	1.05	0.59	2	2.3	1.55	0.38	1.21	0.65
n-dodecyl acrylate	0.55	2.26	0.97	9.1 ***	3.89 *	1.67	2.7	2.87	2.32	3.56 *	12.54 ***	3.28 *

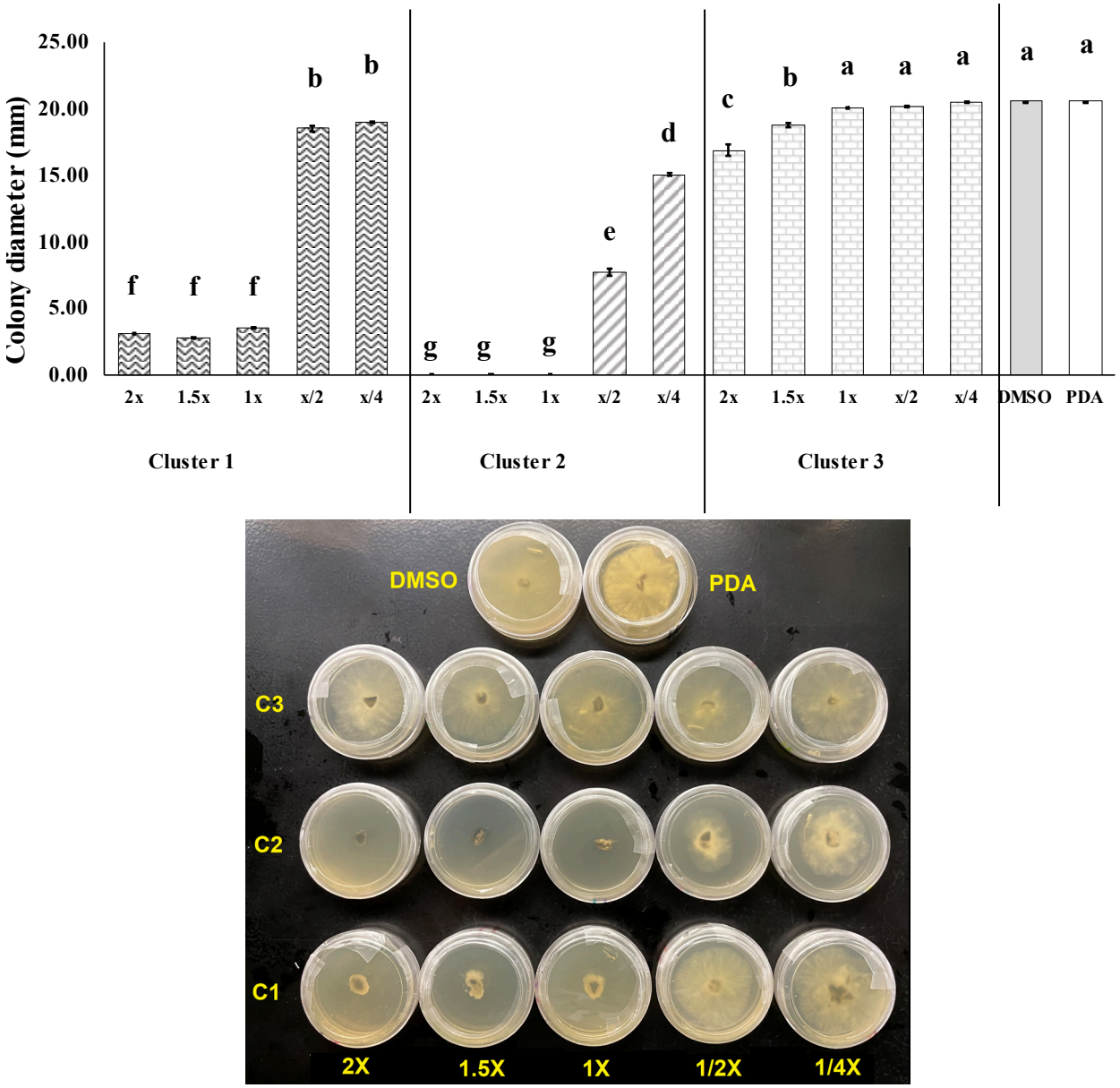

Figure 3.11. (A) Colony diameters of *D. pinea* on PDA amended with combinations of various terpenoids and other non-terpenoid compounds derived from hierarchical cluster analysis of post-challenge concentrations (Figs. 7 and 8b): Cluster (C) 1: α-pinene; C2: β-pinene, limonene, benzaldehyde, dodecanol, n-dodecyl acrylate; C3: camphene, 3-carene, myrcene, terpinolene, bornyl acetate, α-terpineol, borneol, caryophyllene. X-axis labels indicate the relative concentrations of compound mixtures by cluster, where 1X represents the mean concentration of each compound in planta applied using the equivalency of 1 ml medium = 1 g FW phloem. 2X, 1.5X, X/2, and X/4 represent concentration bracketing around the mean concentration to assess dose response patterns. Cluster 1 shows ~ 86% growth inhibition starting at 1X, with no further effects above 1X; cluster 2 shows complete inhibition at 1X concentration and above; whereas cluster 3 shows minor inhibition (up to ~ 11%) starting at 1.5X. In subculturing experiments, inhibitory compounds were shown to be fungistatic but not fungitoxic. PDA: unamended medium control; DMSO: PDA amended with DMSO; the solvent used to dissolve the compounds. **(B)** Representative culture plates showing growth patterns of D. pinea at 3 days after plating on PDA, PDA amended with DMSO, and PDA amended with the various clusters represented in panel **(A)**. Error bars are SE.

Significant effects on fungal growth were documented for various compounds and compound clusters, including significant interactions with concentration, three days after plating. Colony radii in cluster 1- and cluster 2-amended plates were significantly smaller at all concentrations compared to mock and unamended control, with smaller colonies at 2X, 1.5X, and 1X concentrations than X/2 and X/4 levels. Colony radii in cluster 3-amended plates were significantly larger compared to the corresponding concentration levels of cluster 1 and cluster 2. Further, the colony radii of cluster 3 plates were slightly smaller only at 2X and 1.5X than corresponding mock and unamended controls after 3 d, while no significant differences were observed in colony radii of 1X, X/2, and X/4 levels of cluster 3 compared to the mock and unamended control (Fig. 3.11).

3.4 Discussion

Our study confirms expression of SIR in Austrian pine stems and shows that the induction of terpenes, their derivatives and other volatile non-terpenoids is an important component of this phenotype. Also, this is the first report of dodecanol and n-dodecyl acrylate in induced defense responses in conifers, which were identified considering their spectrometric responses in our untargeted analyses were significantly higher in the analytes compared to blanks, indicating no matrix effects from column or the gradient system. SIR expression and/or systemic effects on specialized metabolism have been repeatedly demonstrated in this pathosystem, with *D. pinea* and various induction incubations ranging from 4-28 days (e.g., Sherwood et al., 2016; Wallis et al., 2008; Bonello and Blodgett, 2003; Blodgett et al., 2007). Our study shows that an SIR response can be generated in the stem in as little as 12 h post-induction, and this response gets stronger with time, in this case for a period of up to 10 d post induction, i.e., the temporal limit of the experiment. Among pines, SIR was originally demonstrated in the Monterey pine (*P. radiata*) – *Fusarium circinatum* pathosystem (pitch canker) (Bonello et al. 2001). Furthermore, cross induction of SIR between agents belonging to different Kingdoms has also been documented, for example between *D. pinea* and the European pine sawfly in Austrian pine (Eyles et al., 2007), and between the parasitic mistletoe plant *Arceuthobium americanum* and the bark beetle-vectored *Grosmannia clavigera* in jack pine (Klutsch et al., 2017). In this study, pathogenic induction with *D. pinea* produced smaller challenge lesions than the challenge lesions of wounded mocks, followed by non-induced controls. Taken together with prior work, our

confirmation of SIR reaffirms that this is likely both a universal and general defense response in trees.

Our study shows that the SIR response occurs quickly and is pronounced and is preceded by earlier accumulation of terpenoids and non-terpenoids at the induction location, as evidenced by the almost immediate anecdotal observation of profuse resin exudation from pathogen induction courts, compared to the mocks, indicating that induction of terpenoids was part of an immediate defense response that was unique to the pathogen, rather than to simple wounding and exposure to agar medium. Our study also demonstrated that terpenoids are induced systemically, as reflected in both pre- and post-challenge accumulation of various monoterpenes, sesquiterpenes, terpene derivatives and other non-terpenoids that were negatively correlated with lesion lengths formed in response to challenge inoculations (Fig. 3.8), suggesting involvement in resistance. However, compounds were co-regulated differently in the pathogen, mock, and untreated treatments, and different clusters of co-regulated compounds were either negatively or positively correlated with SIR.

In prior work focusing on phenolics, the relationship between compound accumulation and systemic effects was always measured starting several days post induction, so it is not possible to say whether phenolics are involved in SIR very early on in the interaction. We speculate that, since pines possess a constitutive resin system, a terpenoid response can occur very quickly, as documented in this study (Fig. 3.11), whereas phenolics accumulation may take longer. So, we envision a combined and overlapping response of terpenoids first and phenolics second, one that can sustain SIR for at least a few weeks, if not longer, consistent with the SIR hypothesis (Bonello et al. 2006).

While the accumulation of terpenoids and phenolics in systemic tissues upon pathogenic

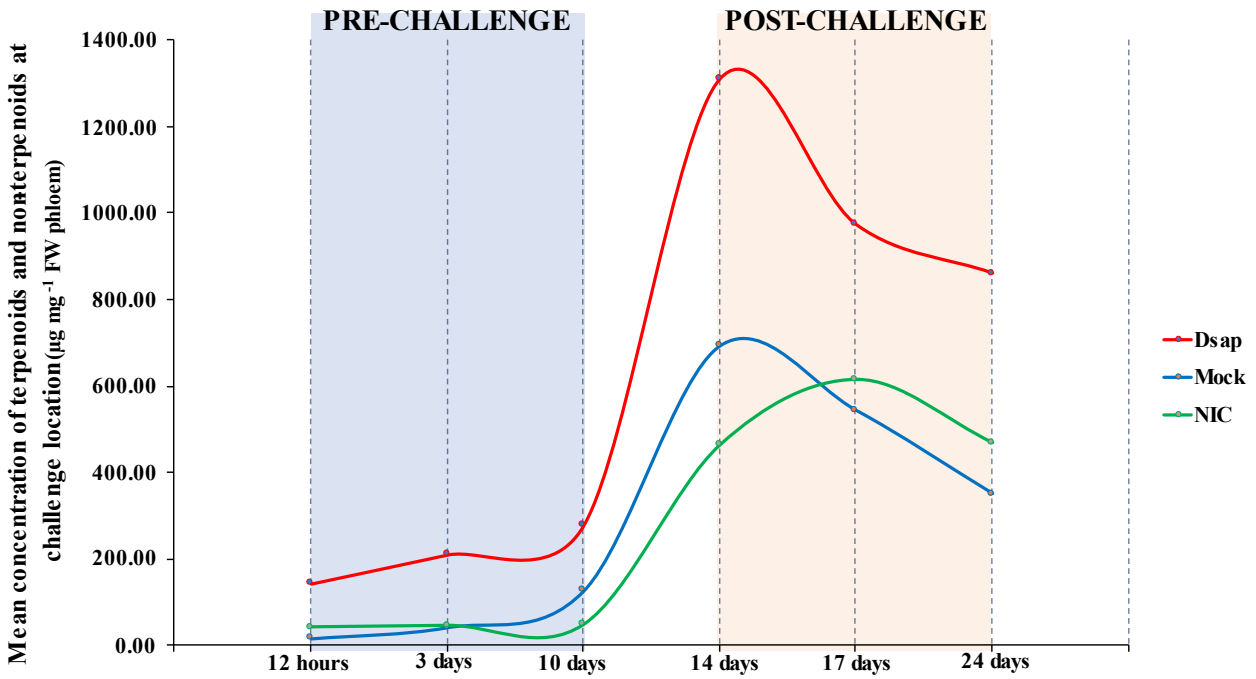

Figure 3.12. Patterns of accumulation of terpenoids and selected non-terpenoids in phloem of Austrian pine over time, by induction treatment (Dsap, mock, non-induced control – NIC) and induction time. *D. pinea* induction clearly causes a much stronger, sustained systemic response much earlier than mock induction and no-induction, both pre- and post-challenge, although compound concentrations tend to decrease after 17 days of incubation. These chemotypes clearly correlate with the SIR phenotype observed in Fig. 3.3. Error bars omitted for clarity.

invasion or pest feeding has been described in prior work (Miller et al., 2005; Wallis et al., 2008; Sherwood & Bonello, 2016; Cale et al., 2017; He et al., 2022), our emphasis on compound inducibility, or inducible variation of terpenoids, has shown differential proportional changes both locally and systemically, suggesting that both timing and magnitude of accumulation of specialized metabolites are important in the expression of SIR. Specifically, we found enhanced systemic inducibility of monoterpenes like α-pinene and β-pinene, and volatiles like benzaldehyde, in response to pathogenic attack. Indeed, two weeks after the challenge inoculation, the systemic inducibility of these and other terpenoids had increased manifold in pathogen induced trees. The local inducibility of terpenoids differed between induction and challenge points, with the latter expressing higher local inducibility than that at the induction point. One possible explanation is that the host allocates fewer resources to constitutive accumulation of terpenoids near the base of the stem, which includes the induction point,

compared to further up the stem. This appears consistent with reports that constitutive levels of monoterpenes decrease basipetally along the stem with increasing distance from the crown, which leads to increasing susceptibility to bark-beetle and associated pathogenic attacks (Goodsman et al., 2013). Here, it is important to note that stem induction with *D. pinea* also causes higher systemic accumulation of specific antimicrobial stilbenes and flavonoids in Austrian pine, possibly due to trade-offs between the two metabolic pathways (Wallis et al., 2008). However, this has been studied only at two weeks post-induction (Bonello & Blodgett, 2003; Wallis et al., 2008). Thus, the declines observed in Fig. 3.11 over time may reflect such tradeoffs with phenolics accumulation. Therefore, we hypothesize that terpenoid inducibility is more important very early in the interaction, while phenolics accumulation becomes more important in later stages.

The spatial and temporal inducibility α-pinene, β-pinene, and benzaldehyde with increasing incubation time was consistently significant across all analyses. Such statistical significance was reflected in biological significance, through the fungistatic activity of these compounds demonstrated in our bioassay against *D. pinea* at biologically relevant concentrations. While the accumulation of α-pinene and β-pinene has been repeatedly implicated as a defense mechanism against insect feeding and pathogenic invasion (Wallis et al., 2008; Zhao et al., 2010; Lackus et al., 2018), a potential involvement in defense-related signaling has also been suggested, for example in *Arabidopsis thaliana* (Riedlmeier et al., 2017). In another example, exposure of wheat seedlings to β-pinene induced accumulation of reactive oxygen species (ROS), enhanced lipid peroxidation, and led to loss of membrane integrity (Chowhan et al., 2014), indicating a potential role in ROS signaling. However, the temporary fungistatic effects of α-pinene demonstrated in our fungal bioassays clearly suggest that this compound is involved in directly hindering fungal activity and has, therefore, potentially complementary roles in SIR as both a signaling molecule and an antifungal compound. Temporary inhibitory effects of α-pinene have also been reported on feeding behavior of insect pests such as the red turpentine beetle (*Dendroctonus valens*) on Manchurian red pine (*P. tabuliformis*) (Xu et al., 2016). At the same time, increased accumulation of benzaldehyde can also directly inhibit the growth of fungal pathogens, or indirectly via toxic derivatives such as cyanogenic glycosides or hydrogen cyanide (Christensen & Jaroszewski, 2001; Huang et al., 2022). However, benzaldehyde also acts as an intermediate in the phenylalanine ammonia lyase pathway for the biosynthesis of salicylic acid

(Ding & Ding, 2020). We speculate that upon induction it is likely that, α-pinene, β-pinene, and benzaldehyde might be involved in induced resistance, via direct effects on the pathogen as well as being linked with the signaling mechanism underlying SIR.

Importantly, this is the first report of dodecanol and n-dodecyl acrylate accumulation as an induced defense response in Austrian pine. Dodecanol is a fatty acid alcohol that has been tested as a co-adjuvant for plant based pesticidal essential oils (Gonzalez Audino et al., 2007), and also reportedly as an induced defense response in *Arabidopsis thaliana* leaf cuticle upon insect feeding (Ahuja et al., 2016). Additionally, its fungistatic behavior has also been demonstrated against *Saccharomyces cerevisiae* (Yamawaki et al., 2018), and it is exploited for larvicidal activity against *Culex tarsalis* (Kubo, 2006). Limonene and its derivative, citronellal, are also induced upon herbivory by leafcutters as a defense response in citrus, Chinese cabbage, and tobacco (Hummelbrunner & Isman, 2001; Verza et al., 2017; Du et al., 2014). N-dodecyl acrylate has been shown to have inhibitory effects in bacterial bioassays (Seong-Soo et al., 2010), and has been reported as a potential biomarker for phylum-level identification of some Zygomycetes (Guo et al., 2021). However, the direct effects and mechanisms of n-dodecyl acrylate and dodecanol in plant defense against pathogenic attack is not known. Importantly, limonene did not accumulate consistently across incubation time, although it was clustered with the aforementioned compounds. As such, we speculate that these detected compounds might be both directly and indirectly involved in early SIR in Austrian pine against *D. pinea*.

According to the source/sink hypothesis by Honkanen & Haukioja (1994), damage to plant tissues alters the ability of host meristems to acquire resources. As mentioned above, this hypothesis has been tested by using a vertical continuum of competing sinks of phloem carbohydrates along lodgepole pine (*P. contorta*) stems, with the implication that constitutive monoterpene levels decrease towards the base of the stem (Goodsman et al., 2013). In our study, this would entail higher levels of constitutive terpenoids at the upstream challenge point, compared to the induction point, which would remain unchanged if our treatments had no effects or had similar effects to each other. In contrast, we demonstrate a strong association between progressive SIR response over time and the accumulation and inducibility of specific terpenoids and non-terpenoids within the challenge point. A possible explanation for this observation would be the existence of a systemic signaling molecule/s that induce/s terpenoid biosynthesis at the

challenge point before challenge inoculation, by direct transport of carbohydrates, and/or terpenoid intermediates.

In conclusion, our experiment and prior work in this pathosystem strongly suggest that SIR expression occurs via early with the induction of specific monoterpenes and non-terpenoids, and is later followed by the accumulation of sesquiterpenes, diterpenoid resin acids, and phenolic compounds (such as stilbenes, flavonoids, lignin). We also confirmed that SIR is likely a generalized phenomenon in the Austrian pine – *D. pinea* pathosystem, in response to infection and wounding, one that intensifies with increasing time of incubation. Our ongoing work on characterizing the role of phenolic compounds in this same system will further reveal possible tradeoffs between the phenolic and terpenoid metabolic pathways, and how these metabolic crosstalks influence SIR expression in this pathosystem. Finally, the ultimate resistance phenotype has been described as being plastic and organ-dependent, where SIR and SIS can be expressed, concurrently, on different parts of the same tree, specifically stem and shoots, respectively (Blodgett et al. 2007; Sherwood & Bonello, 2016). Since our experiment was limited to the main stem, it would be interesting if concurrent SIS expression in shoots can also be documented as early as 12 h after induction. Regardless, our findings advance our understanding of systemic mechanisms and the involvement of terpenoids in SIR expression in trees.

CHAPTER 4
PHYTOHORMONE CROSSTALK MEDIATES SYSTEMIC INDUCED RESISTANCE IN AUSTRIAN PINE

4.1 Introduction

The ability of plants to resist pathogenic invasions depends on rapid deployment of defense-associated anatomical and physiological adjustments. These changes are regulated by underlying metabolic responses that are known to involve crosstalk among various phytohormone signaling pathways. Abiotic and biotic stress responses in plants are modulated by jasmonic acid (JA), salicylic acid (SA), abscisic acid (ABA), pipecolic acid (PA), and ethylene mediated signaling pathways (Mohamed et al., 2020; Savatin et al., 2014; Santino et al., 2013). Specifically, SA and PA - mediated signaling and defense responses have been associated with systemic acquired resistance (SAR) in herbaceous model and crop plants against biotrophic pathogens, while JA - mediated signaling has been associated with responses to necrotrophic pathogens, pest damage, and abiotic stress (Arévalo-Marin et al., 2020; Santino et al., 2013; Pieterse et al., 2012).

JA, its precursors, and derivatives are produced from lipids via the oxylipin cycle upon pest or pathogenic invasion (Gfeller et al., 2010). JA biosynthesis is initiated with the synthesis and subsequent conversion of α-linoleic acid to 12-oxo-phytodieonic acid (OPDA) in chloroplasts, which is then translocated to the peroxisome. JA can also be metabolized into other bioactive forms like methyl jasmonate (MeJA) through JA carboxyl methyltransferase (JMT) activity, or into amino acid conjugates such as jasmonoyl isoleucine (JAIleu) via JA conjugate synthase (JAR1) activity, in the cytosol (Pieterse et al., 2012). Interestingly, OPDA, MeJA and JAIleu have also been associated with induced tolerance to abiotic stress and defense against biotic stress such as pest and pathogenic invasion (Zhang et al., 2017; Li et al., 2017; Aubert et al., 2015; Wasternack 2004), while ABA and ethylene also have been associated with abiotic stress responses (Kumar et al, 2019; Kazan, 2015).

In coniferous trees like pine and spruce, like in all plants, the efficiency of host defenses may be influenced by prior interactions elsewhere on the tree (systemic) with the same or different pathogens, often referred to as an induction event. When the mediators of a systemic response are unknown (i.e., in cases unlike SAR), as is true for most tree species to date, enhanced systemic protection as the result of an induction event is referred to as systemic induced resistance (SIR, Bonello et al, 2006). Conversely, induction events may also culminate in the host becoming weaker and more susceptible to future invasions, which is referred to as systemic induced susceptibility (SIS, Bonello et al. 2006). SIR and SIS have been demonstrated repeatedly in the Austrian pine – *Diplodia pinea* (APDP) pathosystem, as well as the involvement of secondary metabolites like phenolics and terpenoids in SIR expression, which has been discussed and described in Chapters 1 and 3.

In this study, we used the APDP pathosystem to test the hypothesis that phytohormone crosstalk is involved in SIR by undertaking the following objectives/ questions: (1) What are the systemic patterns in gene regulation in response to *D. pinea* that help explain the expression of SIR? And (2) what are the main features of hormone signal transduction involved in the early stages of the interaction (0.5 – 7 days post-induction)? In order to answer these questions, we used the experimental model from Chapter 2 to test the levels of various phytohormones and gene expression patterns in Austrian phloem, after trees have been induced earlier by pathogenic infection, or wounding, at a downstream, systemic location on the stem. We found significant levels of JA, and its precursor, OPDA, along with other JA intermediates, such as methyl jasmonate and jasmonoyl isoleucine were significantly induced, coupled with nuanced gene expression of JA, ABA, and auxin signaling pathways.

4.2 Materials and methods

4.2.1 Plant and fungal material

Five-year-old, open pollinated Austrian pine trees growing in 3-gallon plastic pots (from Willoway Nurseries, Madison, OH) were maintained with regular fertigation and drip irrigation twice daily and moved to a greenhouse six weeks prior to experimentation, to allow for acclimation. *D. pinea* strain IS-411, which was used in this study, is the same as used in Chapter 3, and was kindly provided by Prof. Glenn Stanosz (retired, University of Wisconsin, Madison,

WI.) The fungus was cultured on PDA for a week on the benchtop, at room temperature and with exposure to ambient light, before being used in the experiments described below.

4.2.2 Experimental model

The trees were organized in a completely randomized, factorial plot design. As the *main factor*, we induced sixty trees on the opposite sides of the main stem, 5 cm above the soil line (red triangles in Fig. 4.1), by excising a 5 mm diameter plug comprising outer bark and phloem, down to the cambium, using a sterile increment borer. This tissue plug was then replaced with either a 5 mm agar plug taken from the margin of an active culture of *D. pinea* growing on PDA, or a 5 mm agar plug of PDA alone, which constituted the pathogen induction and wound or mock induction, respectively. Thirty control pine trees were left uninduced (non-induced control). We sampled the trees at a distal point 15 cm above the induction site (red circle in Fig. 4.1) at six separate time points, which constituted the *sub-plot factor* in our design. The time points were 12 hours or 0.5 days post induction (dpi), 24 hours or 1 dpi, 36 hours or 1.5 dpi, 48 hours or 2 dpi, 72 hours or 3 dpi, and 134 hours or 7 dpi, with six trees sampled at each time point. Sampling was conducted by peeling off a strip of bark/phloem around the stem from a ~ 1 cm stem length, and by collecting plugs of phloem from the peeled bark/phloem using a sterile 5 mm diameter

increment borer. Samples were subsequently stored in -80 °C until further use for RNA extractions and phytohormone assays (Fig. 4.1).

4.2.3 Extraction of phytohormones from ground phloem

Frozen bark/phloem plugs were ground to a fine powder in liquid nitrogen with a mortar and pestle. Phytohormone extraction was based on the protocol by Rodrigues et al. 2021. For each sample, 100 mg of cold, homogenized tissue was transferred to a 2 mL screw-capped tube containing 1 mL of ice-cold 70:30 (v/v) LC-MS Optima water and methanol, amended with

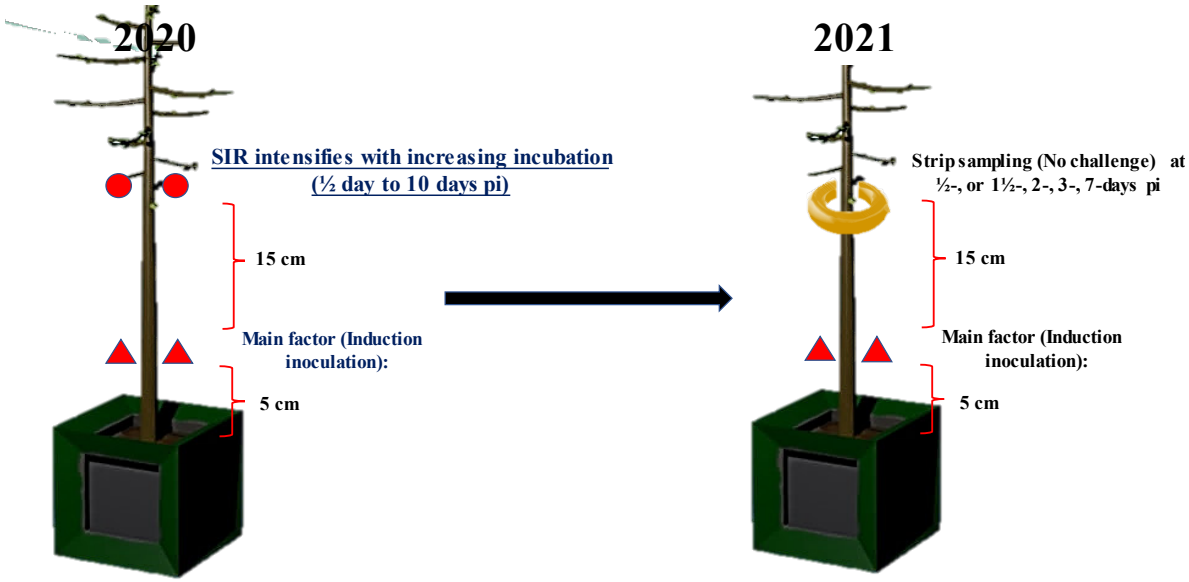

Figure 4.1. Schematic of treatment application and sampling strategy. In the experiment conducted in 2020 and described in Chapter 3 (left), Austrian pine stems were induced 5 cm above soil line by either inoculating them with *D. pinea*, wounding (mock), or leaving them untreated (red triangles). Stems were then challenged 15 cm above the induction location with *D. pinea* after 12 h, 72 h, and 10 days incubations (red circle). In 2021 (*right*), Austrian pine stems were induced as in 2020. Phloem was then sampled 15 cm upstream of induction after ½, or 1, 1½, 2, 3, 7 days incubation to conduct all analyses described in this chapter.

internal standards based on targeted phytohormones: salicylic acid-d_4 (500 ng mL^{-1}), (±)-jasmonic acid-d_5 (2000 ng mL^{-1}), (±)-abscisic acid-d_6 (500 ng mL^{-1}), d_6-2-cis-4-trans-ABA (20 ng mL^{-1}), d_2-gibberellin A3 (10 ng mL^{-1}), d_5-trans-zeatin (50 ng mL^{-1}), and d_2-gibberellin A4 (10 ng mL^{-1}). Tubes were vortexed at low speed and at 4 °C for 15 minutes, followed by

centrifugation at 13,000 rpm at 4°C for 20 min. The supernatant was then transferred to a fresh 2 mL tube and concentrated in a Speedvac vacuum drier at room temperature for 90 min. The resultant brownish-orange concentrate was reconstituted in 100 µl. of 70:30 (v/v) LC-MS Optima water and methanol and sonicated for 10 min at 4°C until thoroughly resuspended. The resuspended extract was then centrifuged at 13,000 rpm at 4°C for 15 min and transferred to amber vials for subsequent UPLC-QqQ-MS/MS based identification and quantification.

4.2.4 Acquisition of UPLC-MS/MS data

Acquisition of MS/MS data was conducted on a Waters ACQUITY H-Class™ triple-quadrupole (TDQ) system after separation using an inline ACQUITY H-Class UPLC system with a CORTECS™ Solid core C18 column, 90 Å, 2.7 µm, 2.1 mm x 100 mm, fitted with a Waters ACQUITY Van-Guard™ pre-column, 130 Å, 1.7µm, 2.1 mm x 5 mm. The binary solvent gradient of water + 0.1% formic acid (solvent A), and acetonitrile + 0.1% formic acid (solvent B), was applied as follows: 0-1.22 min hold at 10% B, linear 10-100% B gradient between 1.22-4.64 min, 4.64-5.6 min hold at 100% B, linear 100-10% B gradient between 5.6-5.62 min, 5.62-6.66 min hold at 10% B, with an equilibration time of 2 min between runs and a constant flow rate of 0.5 mL/min. Compounds were soft-fragmented using electrospray ionization (ESI) in both positive (ES+) and negative modes (ES-).

The TQD tandem mass spectrometer was calibrated to a resolution of 11.6/14.8 (min/min) on MS1 with an ion energy of 0.3 (arbitrary units), and a resolution of 12.1/15.0 (min/min) with an ion energy of 1.7 (arbitrary units) on MS2 scans. Measurements were carried out using capillary voltage of 3570-3900 V and cone voltage of 43-(-42.25) V for ES+ and capillary voltage of 3570-3600 V and cone voltage of 36-(-42.25) V for ES-, and a source temperature of 150°C for both ionization modes. Spectral acquisition methods were developed using Waters IntelliStart™ for the 15 targeted phytohormones; (±)-JA, (±)-JA-d5 (IS), MeJA, jasmonoyl-isoleucine, 12-oxo phytodienoic acid, SA, SA-d4 (IS), methyl salicylate, (+)-ABA-d6 (IS), (+)-ABA, gibberellic acid GA_3, gibberellic acid GA_4, 3-indole acetic acid (IAA), indole-3-carboxylic acid (I3CA), and trans-zeatin-d_5 (IS). All compounds were acquired from Cayman Chemicals? (Michigan, USA). The UPLC-MS/MS data were collected and visualized on Waters MassLynx. Targeted phytohormone standard curves were obtained in Waters TargetLynx using a quadratic regression fit, due to saturation effects at higher concentrations. The presence of compounds was confirmed

if visible peaks were observed for two out of three MRM transitions of tested phytohormones, and subsequently the response or peak area of the transition with highest peak area among all transitions for a given compound, was used for quantification.

4.2.5 Statistical analyses of phytohormone concentrations

We compared phytohormone concentrations at the systemic location using a two-way fully factorial MANOVA in the stats package (R core team, 2021), followed by pairwise comparisons between treatment combinations. Significantly variable concentrations of phytohormones were then subjected to individual ANOVAs, with the significance threshold set at $\alpha = 0.05$.

We also investigated relationships between phytohormones and/or treatment factors. Data were organized into a multivariate matrix of the order $X \in Q^{p \times q}$, where p represented all the tested phytohormones and q represented all replicates of various treatment factors, i.e., type of induction and time of sampling. We attempted to uncover significant associations via PCA using the *princomp* function in the R *stats* package (R core team, 2021), that uses scaled z-scores to compute Euclidean distance between data pairs for multidimensional projection. A Scree-plot was also generated to identify the minimum number of components required to maximize the variance of the scaled and normalized data.

Next, we conducted a Spearman's rank correlation analysis to test for significance of associations and their directions among phytohormones, using the *corr* function in the R *stats* package (R core team, 2021).

4.2.6 RNA extraction and gene expression analysis

RNA extraction was carried out following a standard CTAB protocol (Chang et al., 1993) modified for pine samples (extraction in 500 µl buffer preheated at 65˚C for one hour), from five biological replicates of each of the eighteen treatment combinations, corresponding to induction type and time of incubation before sampling, for a total of ninety samples. RNA extracts were then treated with amplification-grade DnaseI per the manufacturer's instructions (Invitrogen, ThermoFisher Scientific, Waltham, MA, USA) and then purified with the RNeasy Plant Mini Kit per manufacturer's instructions (Qiagen, Germantown, MD, USA). Samples were quantified spectrophotometrically using a NanoDrop (Thermo Scientific, Wilmington, Delaware, USA) and sent to the Yale Center for Genome Analysis (YCGA, New Haven, CT, USA) for quality control assessment and sequencing. The concentration and purity of RNA were further assessed using a Bioanalyzer (Agilent Technologies, Inc., Santa Clara, CA, USA). The cDNA libraries were subsequently generated by the ribodepletion method using TruSeq® Stranded Total RNA with Ribo-Zero Plant (Illumina, San Diego, CA, USA), and subjected to 150-bp paired-end sequencing on an Illumina NovaSeq® 6000 (Illumina, San Diego, CA, USA), with a targeted depth of 30 million reads per sample.

4.2.7 Transcriptome assembly and annotation, and expression analysis

The RNAseq data were analyzed using a pipeline that included read preprocessing, *de novo* transcriptome assembly, differential expression, and functional enrichment analysis (Fig. 4.2).

Raw reads were subjected to trimming of adapter sequences and poor-quality bases using *TrimGalore* v. 0.6.7 (https://www.bioinformatics.babraham.ac.uk/projects/trim_galore/) with options "—quality 30 —length 50" to trim bases with a Phred quality score below 30 and remove reads with a post-trimming length below 50 bp. Next, we performed read error correction using *rcorrector v.* 1.0.5 (Song & Florea, 2015), and rRNA removal using *SortMeRNA* v. 4.3.4

(Kopylova et al., 2012). Contaminant reads were inferred using *Kraken2 v. 2.1.2* (Wood et al., 2019) with the "Standard Database" version 20220926 (containing Refseq archaea, bacteria, viral, plasmid, human, and univec_core sequences as the databases of potential contaminants) and options "—confidence 0.5 —unclassified-out" to output reads that were not classified as contaminants, which were used for the next steps. *Kraken2* results were visualized using *KronaTools v.* 2.8.1 (Ondov et al., 2011). Reads that were not classified by *Kraken2* were normalized with *Orna* v. 2.0 in batches of 10 samples (20 FASTQ files) per Orna run. Raw and processed read quality was assessed using *FastQC v.* 0.12.1 (http://www.bioinformatics.babraham.ac.uk/projects/fastqc/), and results of *FastQC* and the aforementioned read processing tools were summarized using *MultiQC* v. 1.13 (Ewels et al., 2016).

Next, a series of transcriptomes were assembled with *Trinity* v. 2.13.2 (Haas et al., 2013), *rnaSPAdes* v. 3.15.5 (Bushmanova et al., 2019), and *Trans-AbySS* v. 2.0.1 (Robertson et al., 2010). Separate assemblies were created for normalized reads (with reads from all samples assembled together) and non-normalized reads (with separate assemblies for each batch of 5 samples) as well as for k-mer sizes 55, 75, and "auto" for *rnaSPAdes*, k-mer sizes 32, 64, and 96 for *Trans-AbySS*, and for *de novo* and reference-guided (using the *Pinus taeda* GCA_000404065.3 genome assembly as the reference) run-modes for *Trinity*. For all assemblies, a minimum contig length threshold of 300 bp was used to remove short transcripts. The resulting 152 assemblies (i.e., all combinations of k-mer sizes, run modes, and read normalization) were progressively merged using *EviGene* v. 2022.01.20 (Gilbert, 2016) in three rounds. In the first round, all normalized assemblies were merged (resulting in assembly 1A) and non-normalized assemblies were merged separately for each assembler (resulting in assemblies 1B-D); in the second round, assemblies 1B-D were merged (resulting in assembly 2); and in round 3, assembly 1A and 2 were merged.

The merged transcriptome assembly was filtered prior to annotation by retaining only transcripts with a valid coding frame of at least 100 codons (as identified by *TransDecoder* v. 5.5.0, (https://github.com/TransDecoder/TransDecoder), and by retaining only transcripts with a mean across-sample TPM (transcripts per million) of at least 0.1 *and* with a TPM of at least 1.0 in at least 1 sample after quantifying expression levels with *Kallisto* v. 0.48.0 (Bray et al., 2016).

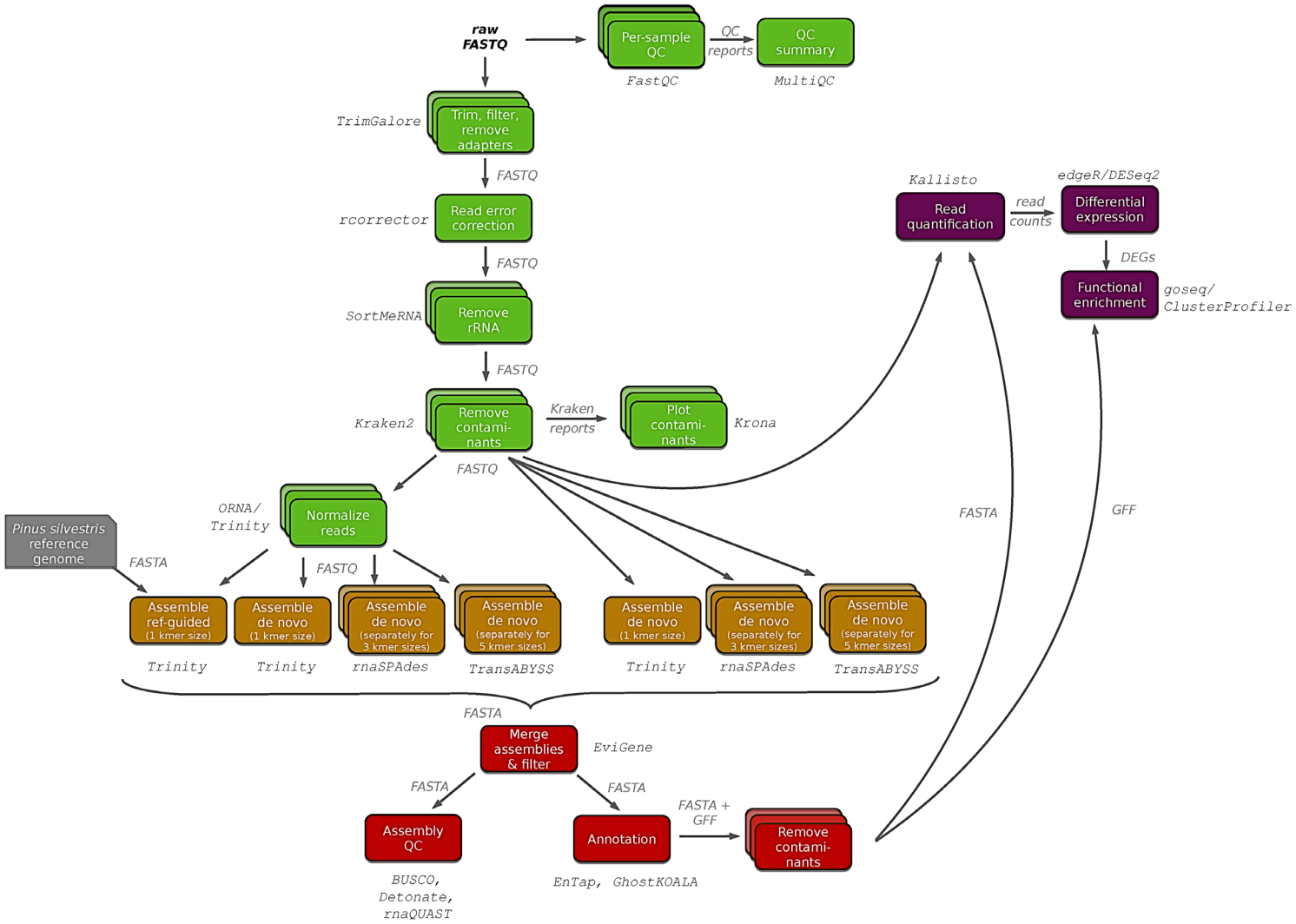

Figure 4.2. RNA-seq workflow used for quality control, assembly, annotation, differential expression, and gene set enrichment and analyses for classification of raw reads.

TransDecoder-predicted amino acid sequences for the primary transcript for each gene (as identified by *EviGene*) in the filtered transcriptome were annotated in three rounds using *EnTAP* v 0.10 (Hart et al., 2019). In the first round, assignment of gene families, protein domains, GO terms and KEGG pathways was done using *EggNOG-mapper* v. 0.12.7 (Cantalapiedra et al., 2021), against the EggNOG database v. 4.1 (Huerta-Cepas et al., 2019) as shipped with *EnTAP*, and with *Interproscan* v. 5.55-88.0 (Payasan-Laffose et al., 2022), against the InterPro database downloaded on 2023-02-01); additionally, similarity searching was done using *DIAMOND* v. 0.9.10 (Buchfink et al., 2014) against the UniProt/SwissProt (release 2022-05), OrthoDB (v. 11), STRING (v. 11), and NCBI RefSeq Plant (downloaded on 2023-02-01) databases. Transcripts without a similarity search hit in the first *EnTap* round were subjected to a second round with DIAMOND similarity searching against the NCBI NR database (downloaded on 2023-02-01), after which annotations from both rounds were combined. Finally, in a third *EnTap* round, similarity searching was performed against the Dicots PLAZA v. 5.0 () and TAIR v. 10 databases to generate an additional annotation file (Poole, 2007). In all three rounds, similarity searches were done with *DIAMOND*'s "—more-sensitive" option, and the following thresholds: a query coverage threshold of 80%, a target coverage threshold of 60%, and an E-value threshold of 1×10^{-5}.

EnTAP annotations were also used for a final round of filtering of the assembly, removing potential contaminant transcripts. First, *EnTAP* itself was instructed to identify contaminants (using the "contam" keyword in the *EnTAP* configuration file) if the source of the best hit in the similarity search was any of the following taxonomic groups in the NCBI taxonomy: "bacteria", "viruses", "archaea", "opisthokonta", "amoebozoa", "ancyromonadida", "122pusozoan", "breviatea", "crums", "cryptophyceae", "discoba", "glaucocystophyceae", "haptista", "hemimastigophora", "malawimonadida", "metamonada", "rhodelphea", "rhodophyta", or "sar". Second, we identified as contaminants transcripts that did not have a similarity search hit (i.e., passing the thresholds details above) while having an EggNOG annotation from "Animals", "Fungi, "Bacteria", "Arthropoda", "Opisthokonts", "Mammals", "Fishes", "Aves", "Archaea", "Nematodes", or "Apicomplexa". All transcripts from genes for which the primary transcript was identified as a contaminant were removed from the final transcriptome assembly.

Expression quantification was performed with the pseudoalignment approach implemented in *Kallisto* v. 0.48.0, using the processed reads (see details above) and the final transcriptome as inputs. *Kallisto*'s output files were imported into R and transcript-specific counts were summed across genes using the "*tximport*" function from the R/Bioconductor package *tximport* v. 1.26.0 (Soneson et al.,2015) with additional argument "*countsFromAbundance = 'lengthScaledTPM'*", after which the resulting object was converted to a DESeq2 object using *tximeta*'s *DESeqDataSetFromTximport()* function.

4.2.8 Differential gene expression analysis

We inferred differential expression using the R/Bioconductor package *DESeq2 v1.37* (Love et al., 2014). A principal component analysis was conducted of the first 500 most variable genes using the *prcomp()* function of stats package to visualize possible clustering of different treatment sample groups. Differential expression analyses were based on a total of 18 pairwise comparisons: the three pairwise combinations of the three treatment levels (pathogen-induction with *D. pinea*, mock-induction or wounding, non-induced control) at each of the six time points (0.5, 1, 1.5 , 2, 3, or 7 dpi). Genes were considered differentially expressed genes (DEGs) when they had a Benjamini-Hochberg adjusted p-value < 0.05 and an absolute $\log_2$-fold change > 0.5. DEGs were further filtered if they had annotations on all three platforms: KEGG orthologs, EGGNOG and ENTAP annotations. The KO orthologs of upregulated and down regulated genes for selected DE comparisons were used to reconstruct metabolic pathways using the KEGG reconstruct pathway tool, and the biological relevance of observed differential metabolic gene expression were investigated across general annotated plant pathways.

We also conducted functional enrichment analysis of different gene functions corresponding to their respective Gene Ontology (GO) (Ashburner 2000) terms. A global GO annotated gene list was used to test for significance of annotation of DEGs to respective GO terms, among respective DE comparisons of our study using the R/Bioconductor *topGO* package's Fisher's exact test (Alexa & Rahnenfuhrer, 2023), with a false discovery rate (FDR) threshold of 0.05.

4.3 Results

4.3.1 Validation of phytohormone identification and quantification

Mass transitions detected for various phytohormones, along with their retention times, are shown in Table 4.1.

Table 4.1. Multiple reaction monitoring (MRM) transitions of 15 phytohormones determined using Waters IntelliStart™. ES±: electrospray ionization, tR: retention time (min), CE: collision energy, CV: collision voltage.

Compound identity	Ion mode	MRM traces	tR	CE	CV
(±)-JA	ES-	209.16 > 59.01*	3.65	12	34
	ES+	211.16 > 133.09	3.7	14	20
		211.16 > 151.12	3.65		
MeJA	ES+	225.16 > 133.10	4.25	16	40
		225.16 > 151.13*	4.2	14	
		225.16 > 147.16	4.2		
jasmonoyl-isoleucine	ES-	322.26 > 130.09*	3.88	20	44
		322.26 > 172.12	3.9	14	
	ES+	324.26 > 86.09	3.9	24	24
12-oxo phytodienoic acid	ES+	293.26 > 40.98	4.55	50	28
		293.26 > 81.07*	4.55	26	
		293.26 > 92.66	4.55	22	
(±)-JA-d5 **(DIS)** ‡	ES-	214.16 > 62.04*	5.4	12	32
	ES+	216.16 > 135.35	5.38	16	20
		216.16 > 153.38	5.38	14	
(+)-ABA	ES-	263.23 > 153.06*	3.4	12	36
	ES+	265.16 > 187.08	3.3	14	18
		265.16 > 229.17	3.3		

(continued)

(+)-ABA-d6 **(DIS)** ‡	ES-	269.26 > 159.11*	4.41	12	32
		269.26 > 210.25	4.4		
		269.26 > 207.13	4.4	20	
SA	ES+	139.00 > 65.01	4.9	22	20
	ES-	139.00 > 121.77	4.86	24	
		137.00 > 93.10*	4.86		
methyl salicylate	ES-	151.03 > 79.00	2.5	24	28
		151.03 > 92.02*	2.5	26	
SA-d4 **(DIS)** ‡	ES+	144.03 > 116.00	4.52	18	62
	ES-	143.06 > 97.16*	4.55	18	44
		143.06 > 71.06	4.55	28	
Gibberellic acid GA3	ES-	345.20 > 143.10	5.23	30	54
		345.20 > 221.17	5.22	22	
		345.20 > 239.19	5.22	14	
Gibberellin A4	ES-	331.20 > 213.16	5.37	30	48
		331.20 > 243.21	5.4	18	
		331.20 > 257.20	5.4	22	
3-indole acetic acid	ES-	195.04 > 127.06	4.07	16	30
		195.04 > 107.06	4.1	14	
indole-3-carboxylic acid	ES-	159.10 > 140.86*	3.07	12	48
	ES+	162.00 > 91.04	3.65	22	24
		162.00 > 116.10	3.65		
trans-Zeatin-d5 **(DIS)** ‡	ES-	223.16 > 223.77	4.2	20	70
	ES+	225.16 > 136.94*	4.22	24	32
		225.16 > 45.99	4.2	18	

* Used for quantification.

‡ DIS: deuterated internal standard.

The identities of compounds were confirmed based on the presence of at least two mass traces (MRM) and quantified by peak integration using the APEX TRACKER™ and retention time of the MRM trace with the highest response. Using this process, we detected ten phytohormones in Austrian pine phloem, plus all four deuterated internal standards. The calibration curves of targeted compounds along with QC parameters such as limit of detection (*LoD*), limit of quantification (*LoQ*), and limit of blank (*LoB*) are shown in Table 4.2.

Table 4.2. Response (calibration) curves for all phytohormone standards detected in this study. LoD: limit of detection, LoQ: limit of quantification, LoB: limit of blank. The best fit for all standards was quadratic due to saturation effects at the highest concentration.

Phytohormone analyte	Conc. Range (ng/mL)	Quadratic regression	R^2	LoD (ng/mL)	LoQ (ng/mL)	LoB (ng/mL)
(±)-JA	10-1000	$-2e\text{-}10x^2 + 0.0009x - 82.246$	1.00	1.5359	4.6543	0.0009
MeJA	10-1000	$-1e\text{-}10x^2 + 0.0008x - 65.674$	1.00	1.5147	4.5901	0.0017
jasmonoyl-isoleucine	5-500	$-9e\text{-}11x^2 + 0.0004x + 19.45$	1.00	0.7527	2.2809	0.0025
12-oxo Phytodienoic acid	10-1000	$-2e\text{-}10x^2 + 0.001x - 124.04$	1.00	1.5172	4.5974	0.0012
(+)-ABA	10-1000	$-2e\text{-}10x^2 + 0.0009x - 92.027$	0.99	1.5076	4.5685	0.0015
indole-3-carboxylic acid	5-500	$0.0052183x^2+2.3612x+86.624$	0.99	0.4707	0.8355	0.0022
(±)-JA-d5 (IS)	1-100	$-2e\text{-}11x^2 + 0.0002x - 2.2893$	0.99	0.2026	0.4565	0.0005
(+)-ABA-d6 (IS)	1-100	$1e\text{-}10x^2 + 6E\text{-}05x + 1.878$	0.99	0.1198	0.4813	0.0011
SA-d4 (IS)	1-100	6E-10x2 + 3E-05x + 3.0054	0.99	0.2465	0.5622	0.0013
trans-Zeatin-d5 (IS)	1-100	$47.4336x^2+3292.4x+19236.6$	0.99	0.3216	0.6855	0.0007

4.3.2 Phytohormone quantification in systemic tissues post induction.

The concentrations of detected phytohormones by treatment and time are shown in Fig. 4.3. **At 0.5 dpi**, MeJA and OPDA were significantly higher in pathogen-induced trees than mock-induced and non-induced trees (Fig. 4.3). At **1 dpi** and 1.5 dpi, MeJA, JA, and OPDA were significantly higher in pathogen-induced trees than mock-induced and non-induced trees (Fig.

4.3). At **2 dpi**, **3 dpi**, and **7 dpi**, MeJA, JA, Ja-Ileu, and OPDA were significantly higher in pathogen-induced trees than in mock-induced and non-induced trees (Fig. 4.3). I3CA was lower in pathogen and mock-induced trees, between 1.5 dpi and **3 dpi**. Systemic levels of ABA were highest between 1.5 dpi and **7 dpi** in mock-induced trees compared to pathogen-induced and control trees (Fig. 4.3)

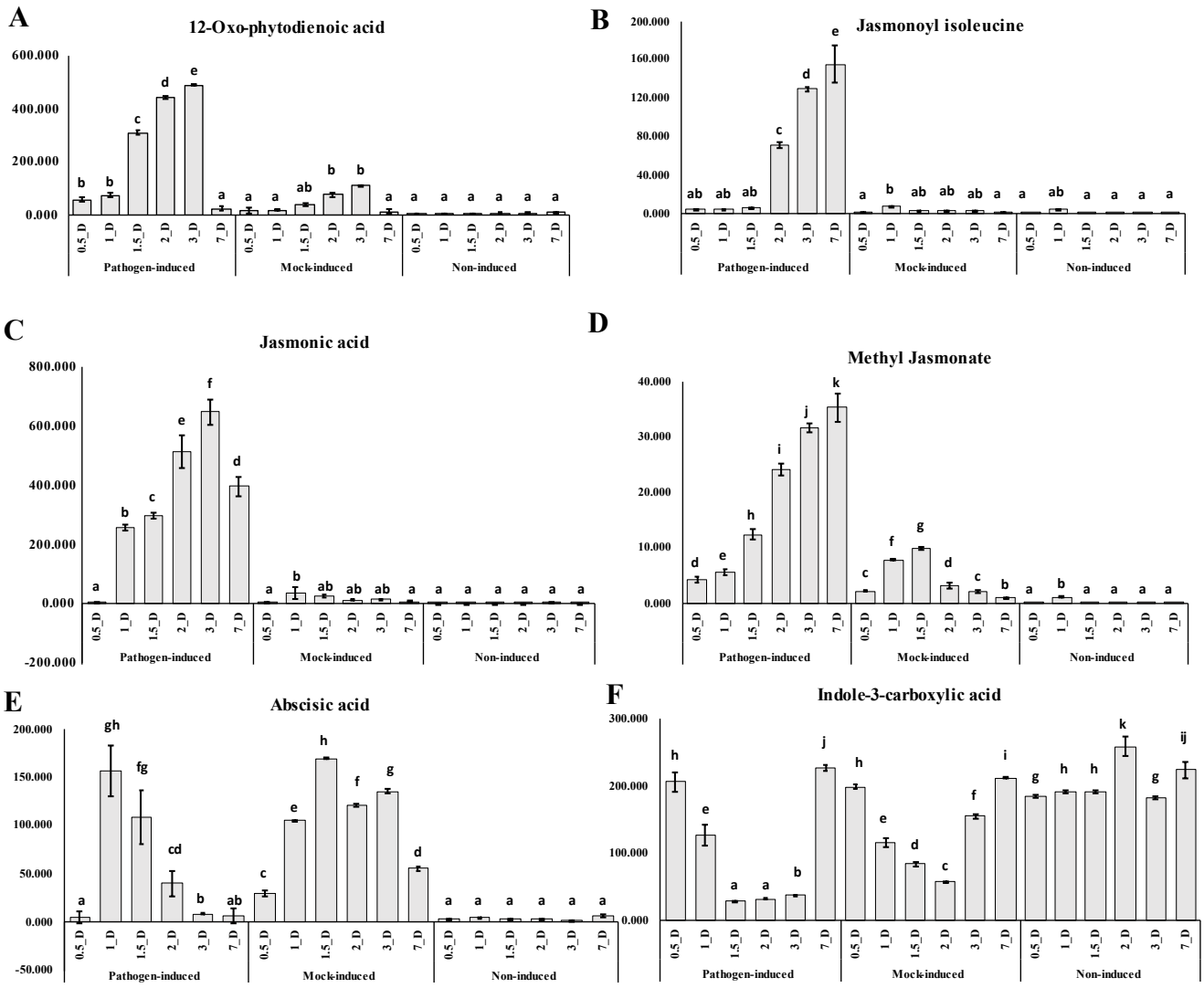

Figure 4.3. Concentrations (ng g^{-1} FW) of detected phytohormones (± SE) in systemic phloem tissue, at 0.5 dpi, or 1 dpi, 1.5 dpi, 2 dpi, 3 dpi, 7 dpi, by induction treatment. Lower case lettering indicates significant differences in accumulation of six phytohormone compounds by time within treatment, and across treatments ($p < 0.05$).

Overall, phytohormones were significantly affected by induction treatment, incubation time, and their interactions (MANOVA), and this was also true for the individual compounds (ANOVA) (Table 4.3).

Table 4.3. MANOVA and ANOVA tables of concentrations (ng g^{-1} FW) of various phytohormones showing significant main effects and interactions of induction type and time of incubation. (* for $p < 0.05$, ** for $p < 0.01$, *** for $p < 0.001$). Subscripts to F-values are degrees of freedom.

MANOVA (global)					
Induction		**Incubation**		**Induction x Incubation**	
F_2	***PR*(>F)**	**F_5**	***PR*(>F)**	**F_{10}**	***PR*(>F)**
153.585	< 2.2e-16 ***	45.736	< 2.2e-16 ***	26.856	< 2.2e-16 ***

INDIVIDUAL ANOVA						
Compounds	**Induction**		**Incubation**		**Induction x Incubation**	
	F_2	***PR*(>F)**	**F_5**	***PR*(>F)**	**F_{10}**	***PR*(>F)**
JA (JA)	1683.52	< 2.2e-16 ***	266.83	< 2.2e-16 ***	286.48	< 2.2e-16 ***
MeJA (MeJA)	284.67	< 2.2e-16 ***	20.758	8.837e-13 ***	45.736	< 2.2e-16 ***
jasmonyl isoleucine (JA-Ileu)	105.804	< 2.2e-16 ***	21.689	3.535e-13 ***	23.513	< 2.2e-16 ***
12-oxo-phytodieonic acid (OPDA)	249.928	< 2.2e-16 ***	45.674	< 2.2e-16 ***	45.477	< 2.2e-16 ***
ABA (ABA)	582.52	< 2.2e-16 ***	76.899	< 2.2e-16 ***	88.044	< 2.2e-16 ***

(continued)

indole-3-carboxylic acid (I3CA)	91.789	< 2.2e-16 ***	42.497	< 2.2e-16 ***	19.353	< 2.2e-16 ***

Phytohormones could also grouped into distinct clusters (CI = 95%) using PCA by generating a global biplot of the z-scores using the first two principal components, which together explained ~80% of the total variance (Fig. 4.4). Among the phytohormones, JA, MeJA, JAIleu, and OPDA showed responses in opposition to I3CA. Clusters corresponding to pathogen-induced trees that were sampled at 1.5 dpi, 2 dpi, and 3 dpi, were the most distinct (Fig. 4.4). Clusters for all mock-induced and control trees were not distinguishable from each other between the selected principal components and were considered not significantly different (Fig. 4.4). Clusters for pathogen-induced trees that were sampled at 0.5 dpi and 1 dpi were not significantly distinct from each other and were also relatively close to the mock-induced and non-induced groups, while pathogen-induced trees sampled at 7 dpi had the most variance among samples (Fig. 4.4).

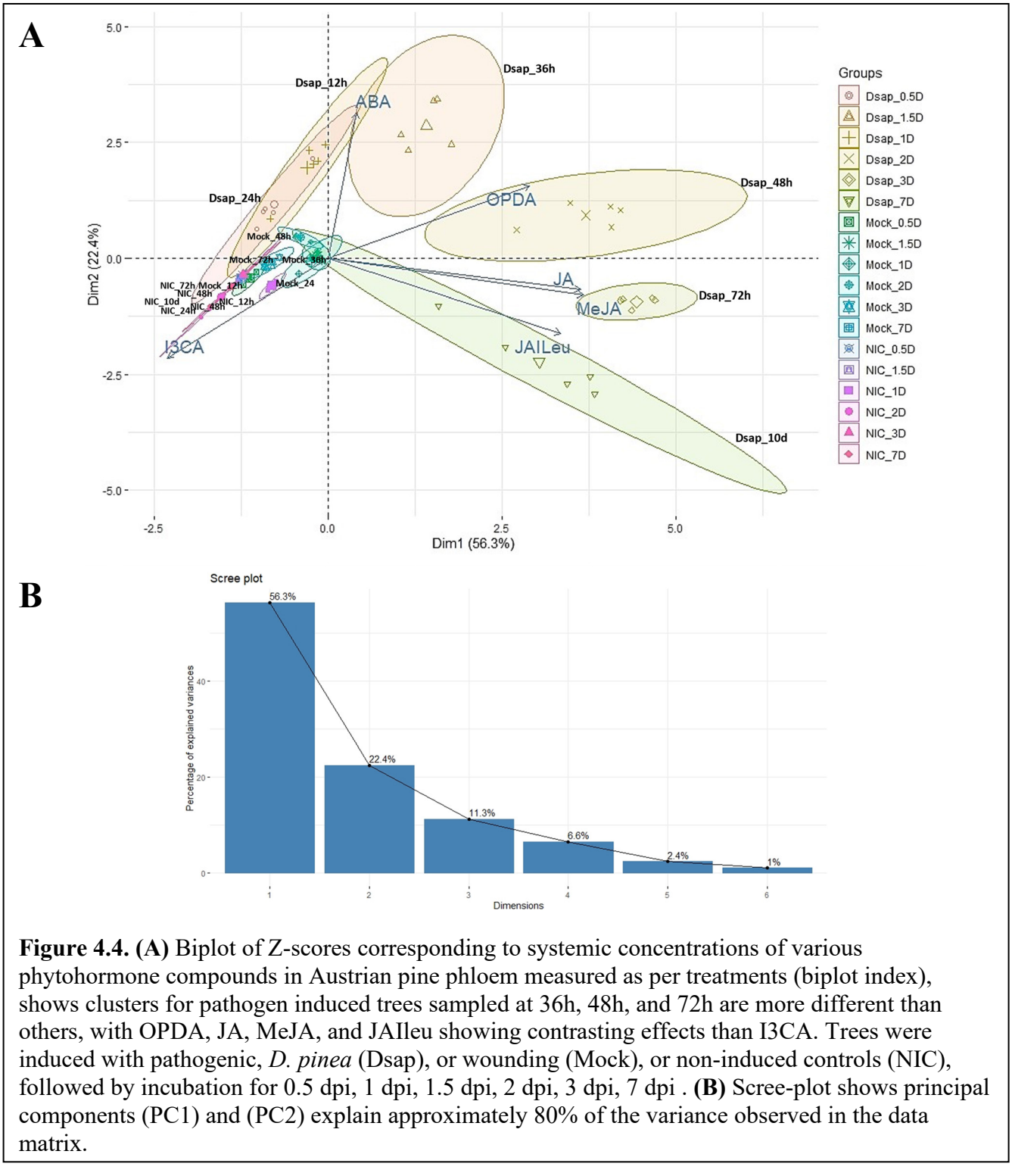

Figure 4.4. (A) Biplot of Z-scores corresponding to systemic concentrations of various phytohormone compounds in Austrian pine phloem measured as per treatments (biplot index), shows clusters for pathogen induced trees sampled at 36h, 48h, and 72h are more different than others, with OPDA, JA, MeJA, and JAIleu showing contrasting effects than I3CA. Trees were induced with pathogenic, *D. pinea* (Dsap), or wounding (Mock), or non-induced controls (NIC), followed by incubation for 0.5 dpi, 1 dpi, 1.5 dpi, 2 dpi, 3 dpi, 7 dpi . **(B)** Scree-plot shows principal components (PC1) and (PC2) explain approximately 80% of the variance observed in the data matrix.

To confirm the co-regulated nature of certain phytohormones evidenced by the PCA, we also conducted Spearman's correlation analyses at each incubation time (Fig. 4.5). **At 0.5 dpi**,

significant negative correlations were observed between I3CA and MeJA, I3CA and JA-Ileu (Fig. 4.5). Significant positive correlations were established between MeJA and JA-Ileu, JA and ABA, followed by JA-Ileu and ABA (Fig. 5,). **At 1 dpi**, significant negative correlations were observed between MeJA and OPDA, MeJA and ABA, and JA and I3CA (Fig. 4.5). The only significant positive correlations occurred between JA and OPDA, and ABA and OPDA, (Fig. 4.5). **After 1.5 dpi and 2 dpi**, significant negative correlations occurred between I3CA and other phytohormones (Fig. 4.5). **After 1.5 dpi**, positive correlations were observed between JA, OPDA, MeJA, JA-Ileu, as well as with ABA after **2 dpi** ($p < 0.05$) (Fig. 4.5). **At 3 dpi**, significant negative correlations were observed between I3CA and JA, MeJA, JA-Ileu, and OPDA (Fig. 4.5). Strong and significant positive correlations were observed between JA, MeJA, JA-Ileu, and OPDA (Fig. 4.5). After **7 dpi**, there were no significant `negative correlations, however, significant positive correlations were observed between MeJA and JA-Ileu, MeJA and JA, JA-Ileu and JA, OPDA and JA.

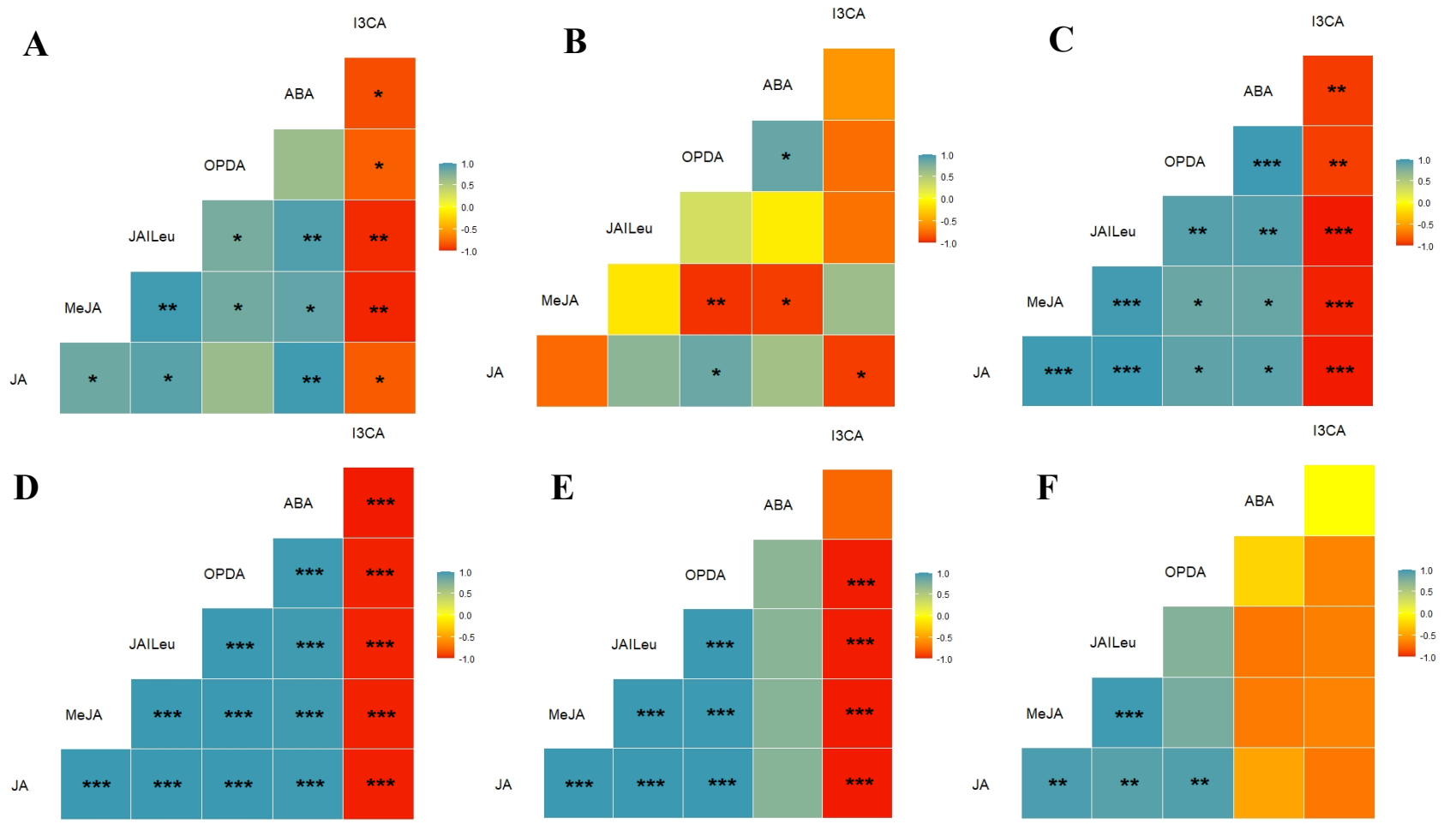

Figure 4.5. Heatmaps of correlation coefficients among the systemic levels six phytohormones in Austrian pine phloem over increasing incubation time, 0.5 dpi **(A)**, 1 dpi **(B)**, 1.5 dpi **(C)**, 2 dpi **(D)**, 3 dpi **(E)**, 7 dpi **(F)** post induction with *D. pinea*. Row labels: JA- jasmonic acid, MeJA- methyl jasmonate, JA-Ileu- jasmonoyl isoleucine, OPDA- 12-oxo-phytodieonic acid, ABA- abscisic acid, I3CA- indole-3-carboxylic acid. Heat color represent strength of correlation, with blue cells indicating strong positive correlation, yellow cells indicate no correlation and red cells indicate strong negative correlations. Significance of correlation indicated by * for $\alpha < 0.05$, ** for $\alpha < 0.01$, and *** for $\alpha < 0.001$.

4.3.3 Transcriptome assembly and annotation

Across a total of ninety samples, 2.958 billion 150-bp paired-end reads (per-sample mean: 32.9 million, range: 23.5-75.3 million) were received from the sequencer, of which 2.553 billion (per-sample mean: 28.4 million, range: 19.0-55.3 million) remained after quality, rRNA, and contaminant filtering.

The initial, merged transcriptome contained 3,909,115 transcripts and 537,656 genes. After removing sequences with a valid coding frame shorter than 100 amino acids as well as lowly expressed and likely contaminant sequences, the final transcriptome used for the differential gene expression analysis contained 2,166,751 transcripts and 52,729 genes. Out of 52,729 genes, 18,183 genes only had a similarity search annotation, 8,756 genes only had an EggNOG-based annotation, 27,411 genes had an Interproscan-based annotation, 6,792 genes had a similarity search and both EggNOG/Interproscan-based annotation, and 19,102 genes had a KEGG ortholog number assigned.

4.3.4 Differential gene expression and enrichment of phytohormones-associated pathways

Significant numbers of DEG were observed in pathogen-induced trees compared to other induction types (Fig. 4.6A). A high proportion of DEGs was expressed and suppressed in pathogen-induced trees compared to mock-induced and non-induced trees at 1.5 dpi and 2 dpi, respectively. Relatively higher numbers of DEGs were also observed in pathogen-induced trees compared to non-induced trees at 3 dpi. We found five GO terms associated with phytohormone pathways among our DEGs, namely, response to hormone, cellular response to hormone stimulus, hormone mediated signaling pathway, response to JA, and response to ABA (Fig. 4.6B). The list of DEGs that were annotated to at least one of the phytohormone related GO terms were significantly enriched across all of our study comparisons (Fig. 4.6B). A relatively high number of DEGs was significantly enriched for phytohormone associated pathways in pathogen-induced trees compared to non-induced trees at 2 dpi and 3 dpi, and at 1.5 dpi and 2 dpi compared to non-induced trees (Fig. 4.6B). We further investigated the investigated

annotations of high and low expressed gene sets on KEGG reconstructed pathways of plant hormone signal transduction, for our DE comparisons.

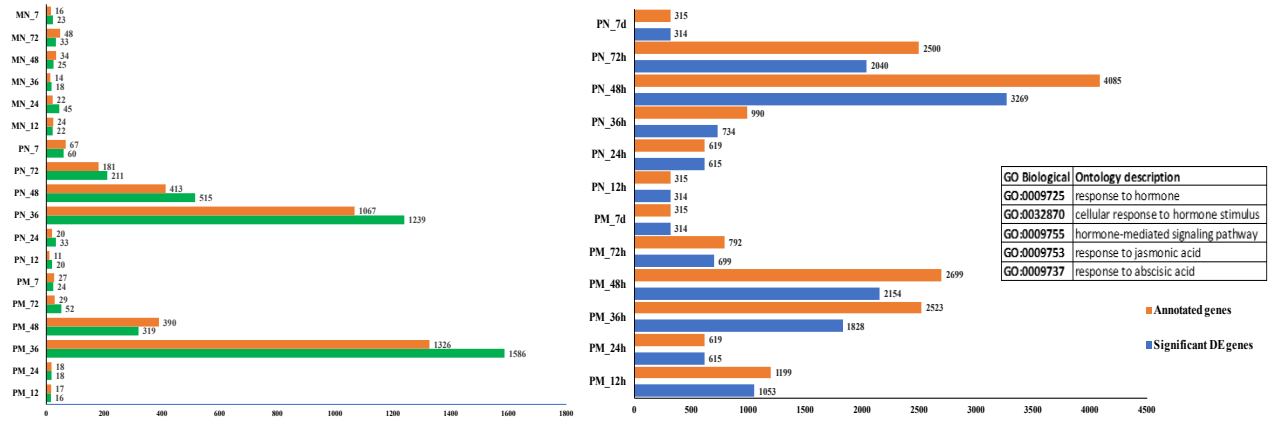

Figure 4.6. (A) Differentially expressed genes retained for the biological comparisons of the study; pathogen-induced versus mock-induced Austrian pine trees (PM), pathogen-induced induced versus non-induced trees (PN), mock-induced vs. non-induced trees (MN); after either 0.5 dpi (_12), or 1 dpi (_24), 1.5 dpi (_36), 2 dpi (_48), 3 dpi (_72), 7 dpi (_7). **(B)** Number of DE genes in different study comparisons that were significantly enriched (Fisher's exact test, $\alpha < 0.05$) (*blue bars*) out of the total number of DE genes (*orange bars*) in the comparison annotated to the Gene Ontology terms mentioned in the figure legend.

At 0.5 dpi, however, we found 8-fold expression of endochitinase B (*ChiB*), and heightened JA signaling as indicated by 3-fold increase in myelocytomatosis (*MYC2*), and almost a 20-fold increase in jasmonate-*ZIM* domain proteins (*JAZ*) in pathogen-induced vs. non-induced trees (Fig. 4.7, Table 4.4). We also found around a 10-fold increase in catalase (*CAT1*) genes in pathogen-induced vs. non-induced trees. We found an over 500-fold increase in PR genes, along with forty-nine DEGs annotated to disease resistance protein in pathogen-induced vs. non-induced trees (Fig. 4.7, Table 4.4). In pathogen-induced vs. mock-induced trees, we did not find any significant DEGs in phytohormone signal transduction pathways; however, we found enhanced expressions of thirty-eight disease resistance DEGs (Fig. 4.7, Table 4.4). In mock-induced vs. non-induced trees, we found suppressed *MYC2* and *COI-1*, enhanced *JAZ* genes in JA signal transduction pathway, while we also found suppressed ABA binding factor (*ABF*) and enhanced pyrabactin resistance, and pyrabactin resistance-like genes (*PYR/PYRL*) (Table 4.4).

At 1 dpi, we observed higher expression of endochitinase B (*ChiB*) in pathogen-induced vs. mock-induced and non-induced trees again. In JA signal transduction pathway between

pathogen-induced trees compared to non-induced trees, we observed suppressed *JAZ* and enhanced *MYC2* transcription factors, while in ABA signaling, we found suppressed protein phosphatase 2C (*PP2C*) genes, and a 3-fold decrease in *ABF*. We also found enhanced small auxin-induced RNA (*SAUR*) genes related to auxin signal transduction and suppressed (4-fold) non-expressor of pathogenesis-related (*NPR*) protein and enhanced *PR* proteins (5-fold) along with forty-six disease resistance DEGs in pathogen-induced trees compared to non-induced trees (Fig. 4.7, Table 4.4). In mock-induced trees compared to non-induced trees, we found suppressed *MYC2* and *JAZ* in JA signal transduction, while in ABA signaling, we found suppressed *ABF* and *PP2C*, along with an enhanced (8-fold) *SAUR* gene and eight enhanced *CAT* genes related to oxidative stress (Table 4.4).

At 1.5 dpi, we found higher expression of endochitinase B (*ChiB*) in pathogen-induced vs. mock-induced and non-induced trees again, as well as differences in disease resistance DEGs such as *NPR* and *PR* in pathogen-induced compared to mock-induced, and *NPR* and *bZIP* family transcription factors (*TGA*) genes in pathogen-induced vs. non-induced trees. We also found JA signal transduction DEGs such as enhanced *JAZ*, *MYC2*, and *COI-1*, genes in pathogen-induced vs. non-induced trees, while we found enhanced *JAZ* and *MYC2*, but suppressed *COI-1* in pathogen-induced vs. mock-induced trees in pathogen-induced trees compared to non-induced trees (Fig. 4.7, Table 4.4). In ABA signaling, we found differences suppressed Sucrose non-fermenting-related protein kinase (*SnRK2*) genes and enhanced *PP2C* and *ABF*, genes in pathogen-induced compared to non-induced trees, while we found suppressed *ABF*, *SnRK2*, and *PYR/PYL* and enhanced *PP2C* genes in pathogen-induced trees compared to mock-induced trees (Fig. 4.7, Table 4.4). In auxin signaling, we found suppressed auxin transport response inhibitor (*TIR1*), auxin resistant family (*AUX1*), auxin responsive factor (*ARF*), and *SAUR* in pathogen-induced vs. non-induced trees, while in mock-induced vs. pathogen-induced trees, we found suppressed auxin-responsive Gretchen Hagen3 family (*GH3*), *AUX1*, SAUR, and Auxin/Indole-3-Acetic Acid family (*AUX/IAA*) genes (Fig. 4.7, Table 4.4). In mock-induced trees compared to non-induced trees, we also found suppressed *JAZ* and enhanced *COI-1* in the JA signal transduction pathway (Table 4.4).

At 2 dpi, we did not find any recognition related DEGs in both pathogen-induced and mock-induced trees vs. non-induced trees, however, we found suppressed *NPR1* and enhanced *PR1* in

pathogen-induced trees compared to both mock-induced and non-induced trees (Fig. 4.7, Table 4.4). In JA signal transduction, we found enhanced *JAZ* and *MYC2*, and suppressed *COI-1*, while in ABA signaling, we found suppressed *SnRK2*, *ABF*, and *PP2C* in pathogen-induced trees compared to both mock-induced and non-induced trees (Fig. 4.7, Table 4.4). In auxin signal transduction, we found enhanced *SAUR* and *GH3*, and suppressed *TIR1*, *AUX1*, and *AUX/IAA* genes in pathogen-induced vs. mock-induced trees, while we found suppressed *GH3*, *TIR1*, *AUX1*, and *AUX/IAA*, but enhanced *SAUR* in pathogen-induced vs. non-induced trees (Fig. 4.7, Table 4.4). In the diterpenoid-gibberellin pathway, we found enhanced gibberellin insensitive Dwarf (*GID1*), *GID2*, and *DELLA* genes in pathogen-induced vs. non-induced trees. In mock-induced vs. non-induced trees, we found enhanced *JAZ* in JA-signal transduction, while we also found suppressed *ABF* and enhanced PYR/PYL in ABA signal transduction, and also enhanced *CAT* genes related to oxidative stress.

At 3 dpi, we noted enhanced *JAZ* in pathogen-induced trees compared to both mock-induced and non-induced trees, while we also found enhanced *MYC2* and *COI-1* genes in pathogen-induced vs. non-induced trees (Fig. 4.7, Table 4.4). In ABA signaling, we found suppressed *ABF* and *PYR/PYL* in pathogen-induced vs. mock-induced trees, further suppressed *ABF* and *PP2C* in pathogen-induced vs. non-induced trees (Fig. 4.7, Table 4.4). In auxin signaling, we found suppressed *ARF* and enhanced *SAUR* in pathogen-induced vs. mock-induced trees, while we found suppressed *AUX1* and *ARF i*n pathogen-induced vs. non-induced trees (Fig. 4.7, Table 4.4). We also found enhanced *PR* genes in pathogen-induced vs. non-induced trees. In mock-induced vs. non-induced trees, we found enhanced JA-signaling related *JAZ*, and auxin-signaling related *SAUR*, while we also found suppressed *ABF* and *PYR/PYL* in ABA signaling (Table 4.4).

At 7 dpi, we found enhanced JAZ in pathogen-induced vs. non-induced trees, but in pathogen-induced vs. mock-induced trees *JAZ* genes were suppressed. We also found enhanced *COI-1* in pathogen-induced trees compared to both mock-induced and non-induced trees, along with enhanced *MYC2* in pathogen-induced compared to non-induced trees (Fig. 4.7, Table 4.4). In ABA signaling, we found suppressed *PYR/PYL* in pathogen-induced vs. both mock-and non-induced trees, as well as suppressed *DELLA* in pathogen-induced vs. non-induced trees (Fig. 4.7, Table 4.4). We did not find any significant phytohormone signal transduction DEGs in mock-induced vs. non-induced trees at this time.

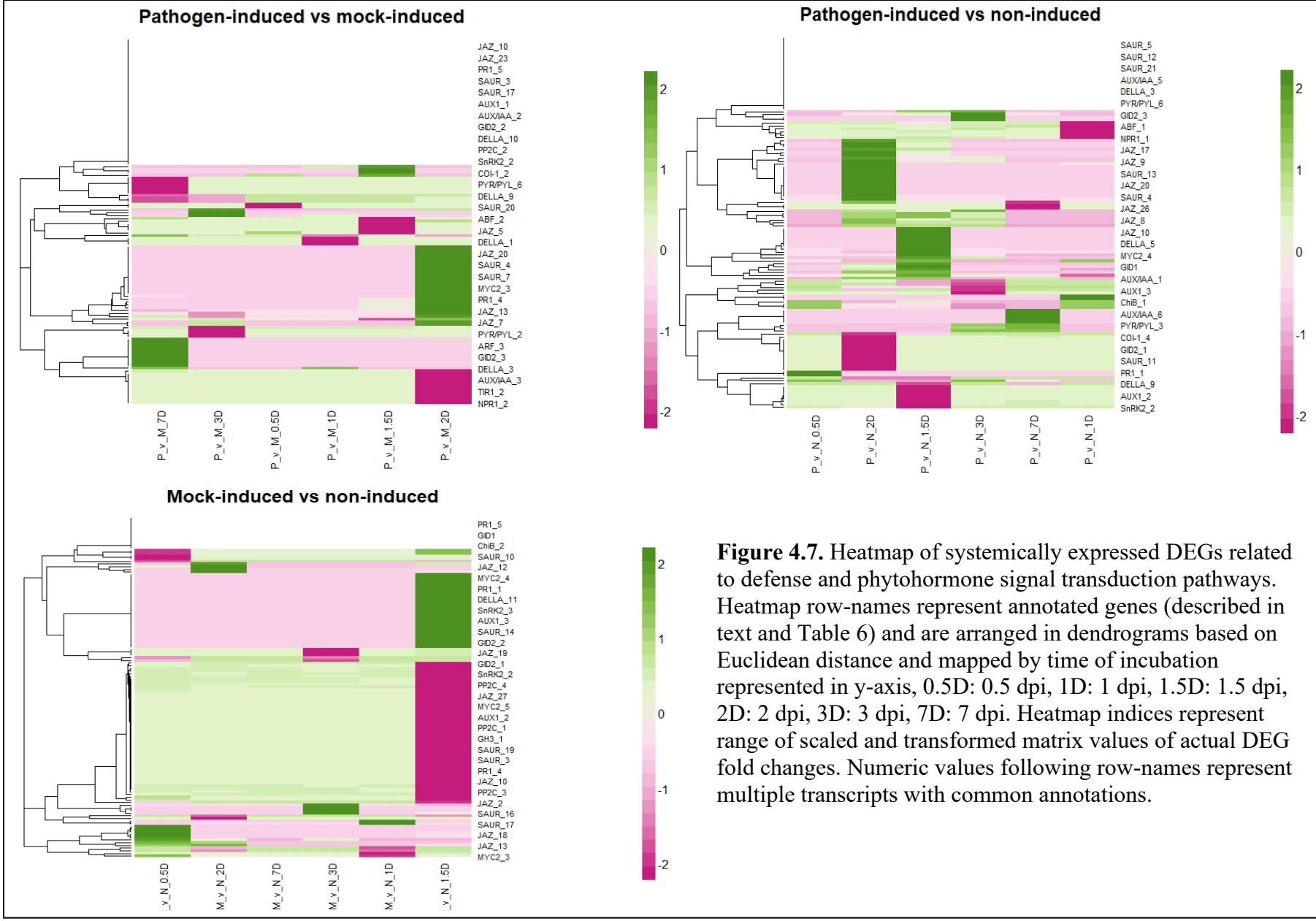

Figure 4.7. Heatmap of systemically expressed DEGs related to defense and phytohormone signal transduction pathways. Heatmap row-names represent annotated genes (described in text and Table 6) and are arranged in dendrograms based on Euclidean distance and mapped by time of incubation represented in y-axis, 0.5D: 0.5 dpi, 1D: 1 dpi, 1.5D: 1.5 dpi, 2D: 2 dpi, 3D: 3 dpi, 7D: 7 dpi. Heatmap indices represent range of scaled and transformed matrix values of actual DEG fold changes. Numeric values following row-names represent multiple transcripts with common annotations.

Table 4.4. Annotated DEGs related to defense and phytohormone signal transduction in systemic phloem tissue of Austrian pine, separated by treatment and measured at 0.5 dpi, or 1 dpi, 1.5 dpi, 2 dpi, 3 dpi, 7 dpi. Green font: enhanced DEGs; red font: suppressed DEGs.

Pathogen-induced vs. mock-induced					
0.5 dpi					
	base Mean	**log2 Fold Change**	**p-value**	**actual Fold Change**	**KEGG ortholog**
ENDOCHITINASE B (ChiB)	**329.49**	**2.80**	**1E-03**	**8**	**K20547**
CATALASE (CAT1)	**14.72**	**2.63**	**2E-02**	**7**	**K03781**
JA- ASSOCIATED ZIM DOMAIN PROTEIN (JAZ)	**40.96**	**2.19**	**1E-02**	**5**	**K13464**
PATHOGENESIS-RELATED (PR1)	**48.38**	**2.15**	**4E-02**	**5**	**K13449**
	33.25	**3.83**	**9E-03**	**15**	**K13449**

(continued)

	7.83	6.34	1E-03	40	K13449
1 dpi					
	base Mean	**log2 Fold Change**	**p-value**	**actual Fold Change**	**KEGG ortholog**
ENDOCHITINASE B (ChiB)	415.37	3.99	2E-02	16	K20547
SMALL AUXIN UPREGULATED RNA (SAUR)	198.60	-0.68	4E-02	-2	K14488
GIBBERELLIN INSENSITIVE DWARF 2 (GID2)	328.56	-0.57	4E-02	-3	K14495
1.5 dpi					
	base Mean	**log2 Fold Change**	**p-value**	**actual Fold Change**	**KEGG ortholog**
ENDOCHITINASE B (ChiB)	3199.15	5.94	1E-12	35	K20547
	329.49	3.43	6E-05	12	K20547
CATALASE (CAT1)	4.53	20.57	8E-09	423	K03781
	6.89	7.26	1E-05	53	K03781
	6.27	4.70	2E-03	22	K03781
	3.79	3.39	4E-02	11	K03781

(continued)

	8.23	3.29	1E-02	11	K03781
	13.27	2.98	5E-03	9	K03781
	4.36	2.88	2E-02	8	K03781
	14.72	2.59	3E-02	7	K03781
	11.35	2.55	7E-03	6	K03781
	32.68	1.70	3E-02	3	K03781
	17.82	1.56	2E-02	2	K03781
	26.78	1.55	2E-02	2	K03781
JA- ASSOCIATED ZIM DOMAIN PROTEIN (JAZ)	50.17	3.96	1E-05	16	K13464
	669.73	3.80	9E-09	14	K13464
	14.33	3.62	8E-04	13	K13464
	71.43	3.48	5E-05	12	K13464
	77.34	3.29	2E-04	11	K13464
	178.28	3.08	7E-06	9	K13464
	19.81	2.81	1E-02	8	K13464
	22.01	2.03	4E-02	4	K13464
	721.45	1.96	4E-05	4	K13464

(continued)

	511.56	1.65	5E-02	3	K13464
	1378.42	1.63	2E-03	3	K13464
	656.39	1.37	4E-02	2	K13464
CORONATINE INSENSITIVE (COI-1)	7807.37	-0.42	2E-02	-6	K13463
	1557.26	2.15	3E-08	5	K13422
MYELOCYTOMATOSIS 2 (MYC2)	3700.17	1.68	7E-07	3	K13422
	228.85	1.52	2E-03	2	K13422
ABA BINDING FACTOR (ABF)	555.25	-0.80	4E-07	-2	K14432
Sucrose non-fermenting-related protein kinase (SnRK2)	538.39	-0.65	3E-03	-2	K14498
PROTEIN PHOSPHATASE 2C (PP2C)	13.45	2.32	3E-02	5	K14497
PYRABACTIN RESISTANCE-LIKE GENES (PYR/PYL)	155.74	1.77	1E-02	3	K14496
	276.06	-0.48	3E-02	-4	K14496

(continued)

ETHYLENE RESPONSE FACTOR (ERF1/2)	35.64	4.47	3E-10	20	K14516
ETHYLENE BINDING FACTOR (EBF1/2)	2707.57	1.40	3E-07	2	K14515
SMALL AUXIN UPREGULATED RNA (SAUR)	2.01	5.76	5E-02	33	K14488
	171.83	-0.76	4E-03	-2	K14488
AUXIN-RESPONSIVE Gretchen Hagen3 (GH3)	16.25	2.18	1E-02	5	K14487
	8220.69	-0.56	3E-03	-3	K14484
	509.66	-0.65	4E-02	-2	K14484
	2976.33	-0.59	2E-02	-3	K13946
	1257.93	-0.36	4E-03	-8	K14485
2 dpi					
	base Mean	**log2 Fold Change**	**p-value**	**actual Fold Change**	**KEGG ortholog**
JA- ASSOCIATED ZIM DOMAIN PROTEIN (JAZ)	71.43	2.63	2E-03	7	K13464
	50.17	2.43	6E-03	6	K13464
	669.73	2.07	2E-03	4	K13464
	77.34	2.05	2E-02	4	K13464
	77.34	2.05	2E-02	4	K13464

(continued)

	106.67	1.89	3E-02	4	K13464
	1378.42	1.47	5E-03	2	K13464
	226.25	1.25	5E-02	2	K13464
	721.45	1.01	3E-02	1	K13464
	630.45	0.72	4E-03	1	K13464
	6695.60	0.62	5E-03	0	K13464
	6695.60	0.62	5E-03	0	K13464
	570.27	0.28	5E-02	0	K13464
CORONATINE INSENSITIVE (COI-1)	2542.06	-0.67	9E-03	-2	K13463
	7807.37	-0.67	2E-04	-2	K13463
MYELOCYTOMATOSIS 2 (MYC2)	228.85	2.56	1E-03	7	K13422
	1557.26	1.87	2E-04	4	K13422
PROTEIN PHOSPHATASE 2C (PP2C)	1704.56	0.83	3E-03	1	K14497
	196.82	-1.28	4E-04	-1	K14497
Sucrose non-fermenting-related protein kinase (SnRK2)	1207.97	-0.45	3E-02	-5	K14498

(continued)

AUXIN RESISTANT 1 (AUX1)	406.37	-1.31	3E-04	-1	K13946
Auxin/Indole-3-Acetic Acid (AUX/IAA) family	935.57	0.78	3E-02	1	K14484
	4.67	4.86	1E-03	24	K14488
	5.81	3.32	2E-02	11	K14488
	501.33	1.30	9E-03	2	K14488
	91.59	1.14	6E-03	1	K14488
SMALL AUXIN UPREGULATED RNA (SAUR)	301.38	1.04	3E-02	1	K14488
	198.60	-1.28	1E-04	-1	K14488
	172.20	-1.48	2E-02	0	K14488
	16.68	-1.68	4E-02	0	K14488
	9.04	-2.07	3E-02	0	K14488
NON-EXPRESSOR OF PR (NPR1)	2207.93	0.63	4E-03	0	K14508
	7.83	4.87	5E-03	24	K13449
PATHOEGENSIS-RELATED 1 (PR1)	33.25	2.87	4E-02	8	K13449
	48.38	2.37	2E-02	6	K13449
3 dpi					

(continued)

	base Mean	log2 Fold Change	p-value	actual Fold Change	KEGG ortholog
JA- ASSOCIATED ZIM DOMAIN PROTEIN (JAZ)	178.28	2.77	6E-05	8	K13464
	50.17	1.81	4E-02	3	K13464
	71.43	1.68	5E-02	3	K13464
	669.73	1.57	2E-02	2	K13464
	773.78	-0.56	2E-02	-3	K13464
ABA BINDING FACTOR (ABF)	555.25	-0.34	3E-02	-8	K14432
PYRABACTIN RESISTANCE-LIKE GENES (PYR/PYL)	59.11	-0.81	5E-02	-2	K14496
SMALL AUXIN UPREGULATED RNA (SAUR)	25.08	2.20	5E-03	5	K14488
DELLA	2642.14	-0.45	3E-02	-5	K14494
7 dpi					
	base Mean	**log2 Fold Change**	**p-value**	**actual Fold Change**	**KEGG ortholog**
JA- ASSOCIATED ZIM DOMAIN PROTEIN (JAZ)	773.78	-0.47	4E-02	-5	K13464

(continued)

CORONATINE INSENSITIVE (COI-1)	7807.37	7.43	2E-02	55	K13463
PYRABACTIN RESISTANCE-LIKE GENES (PYR/PYL)	443.96	-0.72	5E-02	-2	K14496
	93.01	-1.73	4E-02	-3	K14496
	14.59	-2.11	4E-02	-4	K14496
	4.45	-5.35	1E-03	-29	K14496
Pathogen-induced vs. non-induced					
0.5 dpi					
	base Mean	**log2 Fold Change**	**p-value**	**actual Fold Change**	**KEGG ortholog**
ENDOCHITINASE B (ChiB)	329.49	2.90	7E-04	8	K20547
	3199.15	2.09	1E-02	4	K20547
	3199.15	1.99	2E-02	4	K20547
MYELOCYTOMATOSIS 2 (MYC2)	228.85	1.56	1E-03	2	K13422
	1557.26	1.47	2E-04	2	K13422
JA- ASSOCIATED ZIM DOMAIN PROTEIN (JAZ)	19.81	4.20	9E-04	18	K13464

(continued)

	14.33	2.86	1E-02	8	K13464
	669.73	2.70	5E-05	7	K13464
	71.43	2.45	4E-03	6	K13464
	511.56	2.42	4E-03	6	K13464
	656.39	2.29	7E-04	5	K13464
	9.93	2.27	3E-02	5	K13464
	226.25	2.25	4E-04	5	K13464
	106.67	2.21	1E-02	5	K13464
	28.28	2.10	6E-03	4	K13464
	77.34	2.06	2E-02	4	K13464
	1378.42	1.82	5E-04	3	K13464
	178.28	1.70	1E-02	3	K13464
	721.45	1.67	5E-04	3	K13464
PATHOGENESIS-RELATED (PR1)	65.81	22.85	4E-19	522	K13449
Auxin/Indole-3-Acetic Acid (AUX/IAA)	324.70	-0.64	3E-02	-2	K14484
AUXIN RESPONSE FACTOR (ARF)	558.30	-0.81	3E-02	-2	K14486
1 dpi					

(continued)

	base Mean	log2 Fold Change	p-value	actual Fold Change	KEGG ortholog
ENDOCHITINASE B (ChiB)	287.05	2.92	6E-04	9	K20547
	3959.66	3.88	4E-03	15	K20547
JA- ASSOCIATED ZIM DOMAIN PROTEIN (JAZ)	180.32	-0.64	1E-02	-2	K13464
MYELOCYTOMATOSIS 2 (MYC2)	1116.91	2.51	3E-02	6	K13422
	3700.17	3.72	3E-02	14	K13422
	1557.26	1.87	2E-02	4	K13422
SMALL AUXIN UPREGULATED RNA (SAUR)	15.64	2.26	4E-02	5	K14488
	17.83	1.44	2E-02	2	K14488
PROTEIN PHOSPHATASE 2C (PP2C)	894.63	-0.42	1E-02	-6	K14497
ABA BINDING FACTOR (ABF)	234.00	-0.59	2E-02	-3	K14432
NON-EXPRESSOR OF PR (NPR1)	2207.93	-0.53	2E-02	-4	K14508
PATHOEGENSIS-RELATED 1 (PR1)	48.38	2.16	4E-02	5	K13449
1.5 dpi					

(continued)

	base Mean	log2 Fold Change	p-value	actual Fold Change	KEGG ortholog
ENDOCHITINASE B (ChiB)	3199.15	4.19	6E-07	18	K20547
	329.49	2.31	7E-03	5	K20547
JA- ASSOCIATED ZIM DOMAIN PROTEIN (JAZ)	669.73	2.94	9E-06	9	K13464
	178.28	2.22	1E-03	5	K13464
	50.17	2.20	1E-02	5	K13464
	22.01	1.95	5E-02	4	K13464
	77.34	1.85	3E-02	3	K13464
	656.39	1.83	7E-03	3	K13464
	226.25	1.78	5E-03	3	K13464
	71.43	1.71	4E-02	3	K13464
	721.45	1.69	4E-04	3	K13464
	1378.42	1.27	1E-02	2	K13464
	773.78	-0.77	1E-03	-2	K13464
CORONATINE INSENSITIVE (COI-1)	2542.06	2.65	7E-04	7	K13463
MYELOCYTOMATOSIS 2 (MYC2)	1557.26	2.18	2E-08	5	K13422

(continued)

	3700.17	1.66	9E-07	3	K13422
	228.85	1.56	1E-03	2	K13422
PROTEIN PHOSPHATASE 2C (PP2C)	13.45	2.14	5E-02	5	K14497
Sucrose non-fermenting-related protein kinase (SnRK2)	538.39	-0.51	2E-02	-4	K14498
	458.59	-0.67	3E-02	-2	K14498
ABA BINDING FACTOR (ABF)	239.88	-0.65	2E-02	-2	K14432
	555.25	-0.78	7E-07	-2	K14432
GIBBERELLIN INSENSITIVE DWARF 2 (GID2)	7.94	3.67	5E-04	13	K14495
DELLA	759.56	-0.42	2E-02	-6	K14494
AUXIN RESISTANT 1 (AUX1)	2976.33	-0.69	6E-03	-2	K13946
AUXIN TRANSPORT INHIBITOR RESPONSE 1 (TIR1)	1257.93	-0.28	2E-02	-13	K14485
	983.82	-0.72	3E-04	-2	K14485
AUXIN RESPONSE FACTOR (ARF)	1312.85	-0.31	5E-02	-10	K14486
	789.05	-0.39	5E-02	-7	K14486
SMALL AUXIN UPREGULATED RNA (SAUR)	171.83	-0.69	9E-03	-2	K14488

(continued)

NON-EXPRESSOR OF PR (NPR1)	2207.93	1.78	4E-04	3	K14508
TGACG-Binding bZIP superfamily (TGA)	2363.60	2.49	5E-02	6	K14431
2 dpi					
	base Mean	**log2 Fold Change**	**p-value**	**actual Fold Change**	**KEGG ortholog**
JA- ASSOCIATED ZIM DOMAIN PROTEIN (JAZ)	50.17	4.23	4E-06	18	K13464
	77.34	3.84	1E-05	15	K13464
	71.43	3.59	3E-05	13	K13464
	669.73	3.47	2E-07	12	K13464
	178.28	3.05	1E-05	9	K13464
	511.56	3.01	3E-04	9	K13464
	656.39	3.00	1E-05	9	K13464
	226.25	2.90	5E-06	8	K13464
	106.67	2.80	1E-03	8	K13464
	1378.42	2.34	7E-06	5	K13464
	14.33	2.25	4E-02	5	K13464

(continued)

	721.45	1.80	2E-04	3	K13464
	28.28	1.60	3E-02	3	K13464
CORONATINE INSENSITIVE (COI-1)	2542.06	-0.76	3E-03	-2	K13463
	7807.37	-0.76	2E-05	-2	K13463
MYELOCYTOMATOSIS 2 (MYC2)	228.85	2.16	1E-05	5	K13422
	1557.26	1.47	2E-04	2	K13422
	196.82	-1.30	4E-04	-2	K14497
Sucrose non-fermenting-related protein kinase (SnRK2)	240.51	-1.41	1E-04	-2	K14497
	13.45	-2.21	4E-02	-5	K14497
	458.59	-1.47	1E-06	-2	K14498
ABA BINDING FACTOR (ABF)	239.88	-1.43	3E-07	-2	K14432
GIBBERELLIN INSENSITIVE DWARF 1 (GID1)	639.76	0.57	5E-02	0	K14493
GIBBERELLIN INSENSITIVE DWARF 2 (GID2)	7.94	2.59	2E-02	7	K14495
AUXIN TRANSPORT INHIBITOR RESPONSE 1 (TIR1)	983.82	-0.47	2E-02	-5	K14485
AUXIN RESPONSE FACTOR (ARF)	324.70	-0.79	9E-03	-2	K14484
	1839.76	-0.47	2E-03	-5	K14486
AUXIN-RESPONSIVE Gretchen Hagen3 (GH3)	257.83	2.07	5E-04	4	K14487

(continued)

	5.81	4.29	4E-03	18	K14488
	93.04	1.53	9E-03	2	K14488
	301.38	1.28	8E-03	2	K14488
PATHGENSIS-RELATED 1 (PR1)	7.83	4.87	5E-03	24	K13449
	33.25	2.87	4E-02	8	K13449
3 dpi					
	base Mean	**log2 Fold Change**	**p-value**	**actual Fold Change**	**KEGG ortholog**
	19.81	3.25	4E-03	11	K13464
	669.73	2.75	3E-05	8	K13464
	178.28	2.70	1E-04	7	K13464
	50.17	2.37	8E-03	6	K13464
JA- ASSOCIATED ZIM DOMAIN PROTEIN (JAZ)	71.43	2.25	8E-03	5	K13464
	721.45	1.70	4E-04	3	K13464
	1927.34	0.80	5E-03	1	K13464
	6695.60	0.71	1E-03	1	K13464
	773.78	-0.63	7E-03	-3	K13464

(continued)

CORONATINE INSENSITIVE (COI-1)	1170.29	11.43	2E-03	131	K13463
MYELOCYTOMATOSIS 2 (MYC2)	1116.91	7.67	3E-03	59	K13422
	3700.17	2.67	5E-02	7	K13422
PROTEIN PHOSPHATASE 2C (PP2C)	196.82	-0.75	4E-02	-2	K14497
	239.88	-0.58	4E-02	-3	K14432
AUXIN RESISTANT 1 (AUX1)	406.37	-0.76	4E-02	-2	K13946
AUXIN RESPONSE FACTOR (ARF)	558.30	-0.95	9E-03	-1	K14486
PATHOGENESIS-RELATED (PR1)	61.23	1.33	3E-02	2	K13449
7 dpi					
	base Mean	**log2 Fold Change**	**p-value**	**actual Fold Change**	**KEGG ortholog**
JA- ASSOCIATED ZIM DOMAIN PROTEIN (JAZ)	19.81	3.75	2E-03	14	K13464
	9.93	2.62	1E-02	7	K13464
	773.78	-0.66	4E-03	-2	K13464
CORONATINE INSENSITIVE (COI-1)	7807.37	7.36	4E-02	54	K13463

(continued)

MYELOCYTOMATOSIS 2 (MYC2)	228.85	8.93	2E-02	80	K13422
DELLA	582.68	-0.63	8E-03	-3	K14494

Mock-induced vs. non-induced					
0.5 dpi					
	base Mean	**log2 Fold Change**	**p-value**	**actual Fold Change**	**KEGG ortholog**
JA- ASSOCIATED ZIM DOMAIN PROTEIN (JAZ)	19.81	3.91	2E-03	15	K13464
	669.73	2.34	4E-04	5	K13464
	721.45	1.75	3E-04	3	K13464
	226.25	1.52	2E-02	2	K13464
	656.39	1.39	4E-02	2	K13464
MYELOCYTOMATOSIS 2 (MYC2)	3700.17	-0.81	2E-02	-2	K13422
CORONATINE INSENSITIVE (COI-1)	7807.37	-0.37	4E-02	-7	K13463

(continued)

ABA BINDING FACTOR (ABF)	555.25	-0.42	7E-03	-6	K14432
PYRABACTIN RESISTANCE-LIKE GENES (PYR/PYL)	4.45	5.62	9E-04	32	K14496
SMALL AUXIN UPREGULATED RNA (SAUR)	7.45	1.57	2E-02	2	K14488
	275.94	-0.74	5E-02	-2	K14488
AUXIN RESPONSE FACTOR (ARF)	1312.85	-0.32	4E-02	-10	K14486
	789.05	-0.40	4E-02	-6	K14486
GIBBERELLIN INSENSITIVE DWARF 2 (GID2)	328.56	-0.67	1E-02	-2	K14495
CATALASE (CAT1)	4.36	2.87	2E-02	8	K03781
1 dpi					
	base Mean	**log2 Fold Change**	**p-value**	**actual Fold Change**	**KEGG ortholog**
MYELOCYTOMATOSIS 2 (MYC2)	1116.91	-0.46	4E-02	-5	K13422
	3700.17	-0.75	3E-02	-2	K13422
JA- ASSOCIATED ZIM DOMAIN PROTEIN (JAZ)	760.94	-0.37	2E-02	-7	K13464

(continued)

SMALL AUXIN UPREGULATED RNA (SAUR)	4.23	2.74	5E-02	8	K14488
DELLA	9.89	1.64	9E-03	3	K14494
	1970.57	-0.62	2E-04	-3	K14494
ABA BINDING FACTOR (ABF)	234.00	-0.51	4E-02	-4	K14432
CATALASE (CAT1)	11.41	4.53	1E-02	21	K03781
	4.24	4.16	6E-03	17	K03781
	4.93	3.90	2E-02	15	K03781
	3.43	3.64	1E-02	13	K03781
	18.04	2.09	4E-02	4	K03781
	32.68	2.01	1E-02	4	K03781
1.5 dpi					
	base Mean	**log2 Fold Change**	**p-value**	**actual Fold Change**	**KEGG ortholog**
JA- ASSOCIATED ZIM DOMAIN PROTEIN (JAZ)	6695.60	-0.44	4E-02	-5	K13464
CORONATINE INSENSITIVE (COI-1)	2542.06	2.42	4E-03	6	K13463
	7807.37	2.24	2E-02	5	K13463
	1170.29	2.12	4E-02	4	K13463

(continued)

ABA BINDING FACTOR (ABF)	239.88	-0.61	3E-02	-3	K14432
SMALL AUXIN UPREGULATED RNA (SAUR)	198.60	-0.71	3E-02	-2	K14488
AUXIN RESPONSE FACTOR (ARF)	1312.85	-0.41	8E-03	-6	K14486
2 dpi					
	base Mean	**log2 Fold Change**	**p-value**	**actual Fold Change**	**KEGG ortholog**
JA- ASSOCIATED ZIM DOMAIN PROTEIN (JAZ)	656.39	2.28	8E-04	5	K13464
	77.34	1.79	4E-02	3	K13464
	226.25	1.65	1E-02	3	K13464
	669.73	1.41	3E-02	2	K13464
ABA BINDING FACTOR (ABF)	239.88	-0.56	4E-02	-3	K14432
	234.00	-0.66	8E-03	-2	K14432
PYRABACTIN RESISTANCE-LIKE GENES (PYR/PYL)	93.01	1.83	3E-02	3	K14496
CATALASE (CAT1)	3.35	3.90	5E-02	15	K03781
3 dpi					

(continued)

	base Mean	log2 Fold Change	p-value	actual Fold Change	KEGG ortholog
JA- ASSOCIATED ZIM DOMAIN PROTEIN (JAZ)	178.28	2.77	6E-05	8	K13464
	50.17	1.81	4E-02	3	K13464
	71.43	1.68	5E-02	3	K13464
	669.73	1.57	2E-02	2	K13464
	773.78	-0.56	2E-02	-3	K13464
ABA BINDING FACTOR (ABF)	555.25	-0.34	3E-02	-8	K14432
PYRABACTIN RESISTANCE-LIKE GENES (PYR/PYL)	59.11	-0.81	5E-02	-2	K14496
DELLA	2642.14	-0.45	3E-02	-5	K14494
SMALL AUXIN UPREGULATED RNA (SAUR)	25.08	2.20	5E-03	5	K14488
At 7 dpi, we did not find any significant annotated DEGs					

4.4 Discussion

We previously conducted an experiment (described in Chapter 3) that demonstrated SIR expression after prior induction with the pathogen *D. pinea,* and to a lesser extent after mock-induction (Chapter 3, Fig. 3.1). While the previous experiment demonstrated SIR expression after 0.5 dpi, 3 dpi, and 10 dpi, this study increased the temporal resolution by using six different time points: 12 hours or 0.5 dpi, 24 hours or 1 dpi, 36 hours or 1.5 dpi, 48 hours or 2 dpi, 72 hours or 3 dpi, and 136 hours or 7 dpi. However, the same experimental design as the previous study design was used (Fig. 4.1). Our goal was to track systemic shifts in phytohormone signaling and gene expression associated with early host's responses underlying SIR. In the current study, we found distinct and profound shifts in accumulation of auxin, JA, and ABA, in addition to clear effects on the expression of genes underlying their biosynthesis or modification, in response to pathogenic induction. For example, we found evidence of pathogen recognition (*ChiB*) with elevated ABA levels and *PR* proteins at 0.5 dpi, followed by increase in defense protein synthesis and JA response at 1 dpi through 7 dpi via *JAZ*, *COI-1*, and *MYC2*, while auxin signaling was reduced between 1 dpi and 3 dpi and increased again by 7 dpi as indicated by *AUX/IAA*, *SAUR*, and *ARF* DEGs.

JA has been associated with priming of defense and suppression of the hypersensitive response against necrotrophic pathogens (Rossi et al., 2011; Arévalo-Marín et al., 2021). The stress response hormone, ABA, reportedly suppresses JA accumulation and signaling (Mauch-Mani and Mauch, 2005), while the primary growth hormone auxin has been known to operate synergistically with JA signaling for defense against necrotrophic pathogens (Kazan and Manners, 2009). Taken together, this evidence suggests that the systemic changes in auxin, JA, and ABA accumulation in Austrian pine phloem between 12 h and 7 days of incubation following induction with *D. pinea* are an integral component in SIR signaling and the elicitation of defense responses, such those described in Chapter 3.

4.4.1 Effects of time of induction

In order to better understand the dynamic aspects of all the processes we analyzed, we synthesized all information in Fig. 4.8, based on mean fold-change in accumulation of quantified phytohormones at different times in pathogen-induced vs. mock-induced and non-induced trees,

as well as gene expression patterns associated with defense and phytohormone signal transduction pathways.

At 0.5 dpi (Fig. 4.8), we found evidence of systemic fungal pathogenic recognition via endochitinase (*ChiB*) in pathogen-induced vs. mock-induced and non-induced trees. We also noticed a stark ABA response in pathogen-induced trees with an almost 25-fold increase compared to mock-induced trees, and 700-fold increase in pathogen-induced vs. non-induced trees. In the latter comparison, we also noticed an over 400-fold increase in systemic JAILeu and 175-fold increase in systemic JA levels, besides over 40-fold increase in MeJA and 50-fold increase in OPDA. While ABA is an established stress hormone that is also associated with hydraulic stress occurring in the plant vascular tissues (Kuromori et al., 2018), endochitinase proteins can reportedly trigger various defense response cascades like JA and ET signaling, upon recognition of pathogenic attack, but they have also been described as essential for salinity and drought stress (Chen et al., 2016; Kwon et al., 2006). At this time point, we did not find any significant differences in gene expression related to phytohormone accumulation compared to mock-induced and non-induced trees. However, we found highly expressed catalase (*CAT*) DEGs in pathogen-induced compared to mock- and non-induced trees. Catalase is involved in cytosolic and apoplastic neutralization of peroxide and other ROS species, which are also known to trigger ABA signaling (Bi et al., 2017; Kar et al., 2011). We also found highly expressed defense protein genes in pathogen-induced trees compared to mock-induced and non-induced trees, and a highly expressed *PR* protein gene in pathogen-induced trees compared to non-induced trees. *PR* proteins are members of a broader protein family known as the cysteine-rich secretory proteins, antigen 5, and pathogenesis-related-1 (*CAP*) protein superfamily that are located both intracellularly and intercellularly, are involved in defenses against pathogens (Gibbs et al., 2008; Agrios, 2005), and can be induced upon wounding and by pathogen elicitors like fungal spores, chitin, chitosan, glycoproteins, lipids, and polysaccharides (Walton, 1997).

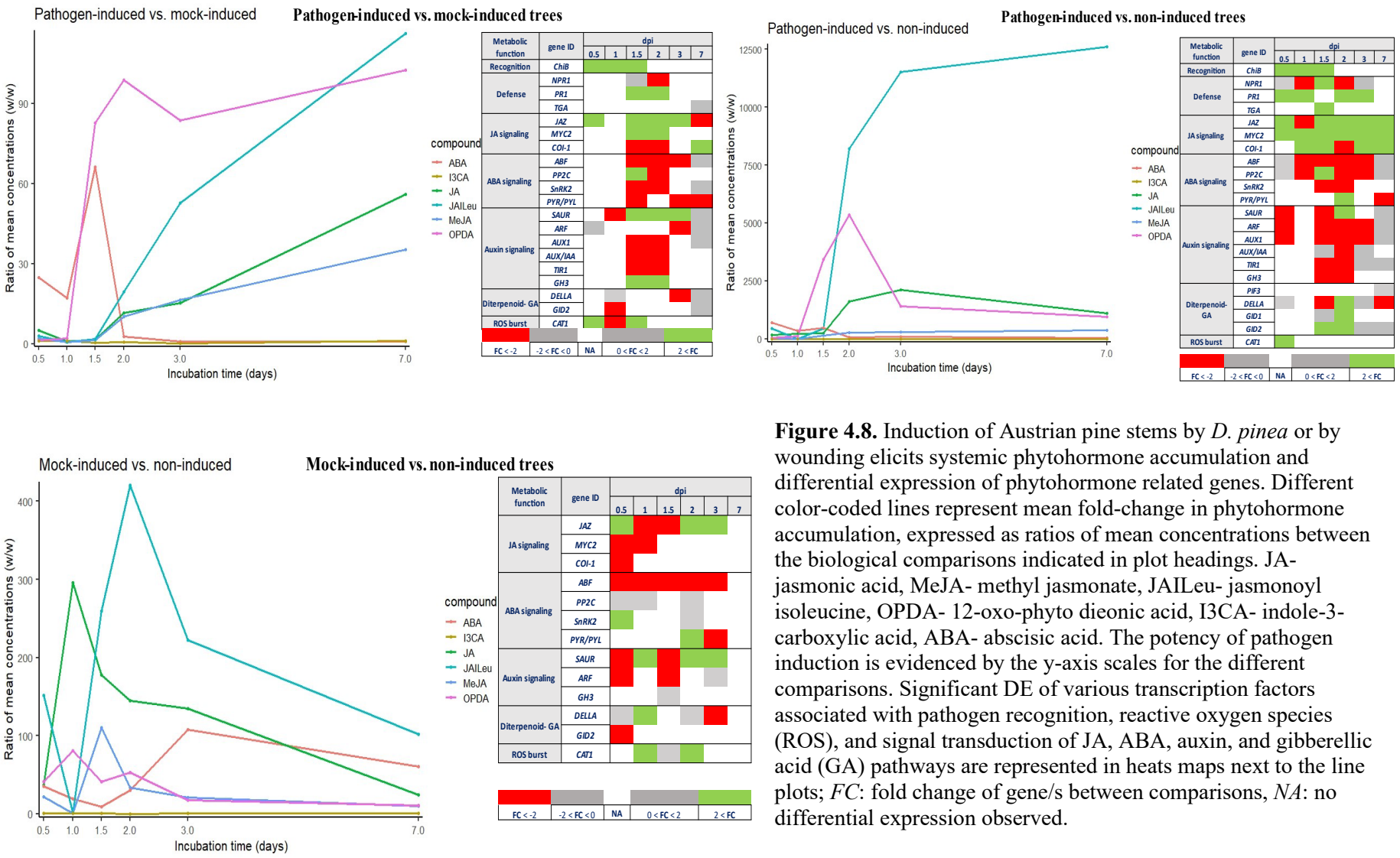

Figure 4.8. Induction of Austrian pine stems by *D. pinea* or by wounding elicits systemic phytohormone accumulation and differential expression of phytohormone related genes. Different color-coded lines represent mean fold-change in phytohormone accumulation, expressed as ratios of mean concentrations between the biological comparisons indicated in plot headings. JA- jasmonic acid, MeJA- methyl jasmonate, JAILeu- jasmonoyl isoleucine, OPDA- 12-oxo-phyto dieonic acid, I3CA- indole-3-carboxylic acid, ABA- abscisic acid. The potency of pathogen induction is evidenced by the y-axis scales for the different comparisons. Significant DE of various transcription factors associated with pathogen recognition, reactive oxygen species (ROS), and signal transduction of JA, ABA, auxin, and gibberellic acid (GA) pathways are represented in heats maps next to the line plots; *FC*: fold change of gene/s between comparisons, *NA*: no differential expression observed.

Interestingly, we also noticed an over 150-fold increase in JA-Ileu, and an over 20-fold increase in JA, OPDA, MeJA, and ABA in mock-induced trees compared to non-induced trees. This suggests that a generalized systemic defense response is deployed upon wounding or pathogenic induction by accumulation of ABA, JA and JA-Ileu, along with increases in *PR* proteins within 12 hours after pathogenic induction of Austrian pine, while a stronger oxidative stress upon pathogenic induction might induce higher ABA levels, systemically.

At 1 dpi (Fig. 4.8)*, ChiB* was still sustained in pathogen-induced vs. mock-induced and non-induced trees. We also noticed a 17-fold increase in ABA accumulation, and a 2-fold increase in OPDA in pathogen-induced vs mock-induced trees, while we did not find any DE of JA and ABA signaling genes. However, we found lower expression of catalase, the auxin family protein *SAUR*, and the diterpenoid- gibberellin TFs, *GID2* and *DELLA* in pathogen induced compared to mock-induced trees. The inhibition of *GID2* proteins is mediated by an increased accumulation of *DELLA* proteins that results in suppression of downstream GA-mediated growth (Achard and Genschik, 2009). In contrast, we found an over 200-fold increase in JA and over 100-fold increase in OPDA levels, accompanied by suppressed *JAZ* activity and enhanced *COI-1* in pathogen-induced vs. non-induced trees. *JAZ* suppression is involved in enhanced activity of downstream JA signaling genes like *COI-1*, *JAR*, *TPL* through MeJA and JAIleu biosynthesis as bioactive forms, while JA-Ileu can reportedly also bind to the SCF^{COI-1}-*JAZ* complex followed by its degradation that results in enhanced downstream JA signaling genes like *VSP* that are involved in defense response against wounding damage (Li et al., 2021; Santino et al., 2013). Additionally, we also found suppressed *NPR* and higher expression of *PR* protein genes in pathogen-induced trees compared to non-induced trees along with several other defense proteins. ABA accumulation also was over 300-fold higher in pathogen-induced vs. non-induced trees, while we noticed suppression of *ABF* and *PP2C* DEGs. The accumulation of ABA activates *PYL/ABA* membrane receptors that results in inhibition of *PP2C* activity, which in turn allows *SnRK2* activation for downstream ABA effects on signaling proteins such as *ABI*, *ABF*, and *ABRE* (Ng et al., 2014). We also found enhanced *SAUR* proteins in pathogen-induced vs. non-induced trees. These proteins have been associated with signaling of primary growth and elongation in plants and can result in enhanced auxin transport (Stortenbeker and Bemer, 2018). *De novo* accumulation of JA, ABA and ET is known to be induced by wounding, either via

wound-activated surface potential changes and/or triggering of various receptor-like kinases (Savatin et al., 2014; Finkelstein 2013). Interestingly, we also noticed an over 250-fold increase in JA in mock-induced compared to non-induced trees. We suggest that at 1 dpi, a common response due to wounding or pathogenic-induction is generated via sustained accumulation of ABA and JA along with JA signaling, besides suppressed auxin and GA pathways, while sustained pathogenic recognition also results in higher accumulation of disease resistance *PR* proteins.

At 1.5 dpi (Fig. 4.8), systemic *ChiB* activity was still observed in pathogen-induced vs. mock-induced and non-induced trees. Also, we found manifold increase in JA, MeJA, OPDA, and JAIleu in both pathogen-induced and mock-induced trees compared to non-induced trees. This was also accompanied by enhanced *COI-1* and suppressed *JAZ* in pathogen-induced vs. mock-induced trees. However, we found all three JA related TFs, *COI-1*, *JAZ*, and *MYC2*, to be enhanced in pathogen-induced vs. non-induced trees. MeJA and JA-Ileu are reported bioactive forms of JA, and at low concentrations trigger *JAZ* mediated suppression of *MYC2* and *COI-1* mediated downstream JA signaling (Santino et al., 2013). The involvement of *JAZ* proteins in positive regulation of ABA signaling has also been described through protein-protein interactions with ABA insensitive (ABI) transcription factors (Zhao et al., 2023). We also found an over 450-fold increase in ABA accumulation in pathogen-induced vs. non-induced trees, an over 60-fold increase in pathogen-induced vs. mock-induced trees, and 9-fold increase in mock-induced vs. non-induced trees. Meanwhile, *ABF* was suppressed in pathogen-induced trees compared to other induction types, along with enhanced *PP2C* and suppressed *SnRK2* in pathogen-induced vs. non-induced trees. On the other hand, auxin signaling was most enhanced in mock-induced, followed by pathogen-induced trees compared to non-induced trees. Lower auxin concentration promotes activation of *AUX/IAA* that leads to repression of *TIR1* and *ARF* mediated signaling of various plant growth and differentiation processes (Lavy and Estelle, 2016). At the same time, we also found enhanced *NPR* and *TGA* protein genes in pathogen-induced compared to non-induced trees, along with a 3-fold higher number of expressed defense protein genes than earlier incubation times. Basic *PR* proteins with higher isoelectric points are usually located intracellularly in vacuoles and their activation and translocation is attributed to JA pathways (Ji et al., 2021; Joshi et al., 2021). This suggests that by **1.5 dpi**, pathogen recognition patterns were sustained along with systemic defense responses via continued accumulation of *PR*- proteins,

ABA, along with JA and its precursor, OPDA and intermediates, MeJA, JA-Ileu upon earlier pathogenic induction, and to a lesser extent due to wounding.

At 2 dpi (Fig. 4.8)**,** we did not find systemic differential expression of any pathogen recognition patterns between pathogen-induced, mock-induced, and non-induced trees. We also found manifold responses of JA and related compounds such as OPDA, MeJA, and JA-Ileu in pathogen-induced trees compared to mock- and non-induced trees, with an almost 100-fold increase in OPDA accumulation in pathogen-induced trees compared to mock-induced trees, and over 8000-fold increase of JA-Ileu in pathogen-induced trees compared to non-induced trees. This was accompanied by higher expression of *MYC2*, *COI-1* and suppressed *JAZ*, indicating a heightened response in JA signaling and likely accumulation of JA, MeJA, and JA-Ileu. We continued observing the reducing margins of ABA levels between different induction types than earlier incubation times. ABA levels were 60-fold higher in pathogen-induced trees than non-induced trees and 3-fold higher than mock-induced trees. Meanwhile, ABA signaling in pathogen-induced vs. mock-induced trees were suppressed as indicated by *ABF*, *PP2C*, and *SnRK2*, while in pathogen-induced vs. non-induced trees, we noticed suppressed *SnRK2* and *PYR/PYL*, and enhanced *ABF* and *PP2C*. In auxin signal transduction, we observed suppression of AUX, *TIR1*, *AUX/IAA*, and enhancement of *SAUR* and *GH3* in pathogen-induced vs. mock-induced trees, and an overall enhanced auxin signal transduction via *AUX1*, *SAUR*, *TIR1*, *GH3* TFs in pathogen-induced vs. non-induced trees, though we did not find differential accumulation of any auxin associated compounds at this time. *SAUR* genes are known to induce plant growth by regulating cell wall acidification through inhibition of *PP2C* (Stortenbeker and Bemer, 2018). Therefore, a possible crosstalk of AUX/ABA pathways might be occurring by suppression of various targeted *PR* type proteins. In terms of defense proteins, we found enhanced *NPR* and *PR* protein DEGs in pathogen-induced compared to mock-induced trees, as well as enhanced *PR* genes and suppressed *NPR* genes in pathogen-induced vs. non-induced trees. It appears that after 48 hours of incubation, the systemic defense response associated with *PR* proteins is similar to the response after 36 hours, although JA signaling is more prominent along with a less prominent and nuanced auxin-ABA signaling in pathogen-induced trees.

At 3 dpi (Fig. 4.8), we found sustained manifold increase in stress hormone accumulation in both pathogen-induced and mock-induced trees compared to non-induced trees. Among the

highest, we noted an over 80-fold increase in OPDA and over 50-fold increase in JA-Ileu between pathogen-induced and mock-induced trees, while OPDA was over 1400-fold higher, JA-Ileu was over 10,000-fold higher, JA was over 2000-fold higher, and MeJA was over 300-fold higher in pathogen-induced vs. non-induced trees. Meanwhile, the JA signal transduction was enhanced in pathogen-induced vs. non-induced trees as indicated by *COI-1*, *JAZ*, and *MYC2*, while we only found enhanced *JAZ* in pathogen-induced vs. mock-induced trees. Interestingly, we still found an over 90-fold increase in ABA in pathogen-induced vs. non-induced trees, and over 100-fold increase in mock-induced vs. non-induced trees, while ABA signal transduction seemed suppressed as indicated by suppressed *ABF* and *PYR/PYL* in pathogen-induced vs. mock-induced trees, though we found enhanced *PYR/PYL* and suppressed *ABF* and *PP2C* in pathogen-induced vs. non-induced trees. Besides not finding any differential change in auxin accumulation between different induction types, auxin signal transduction activity was indicated only by enhanced *TIR1* and *AUX/IAA* and suppressed *AUX* and *ARF* in pathogen-induced vs. non-induced trees, while we found suppressed *SAUR* and *ARF* in pathogen-induced vs. mock-induced trees. In terms of defense protein genes, we found enhanced *NPR* and *PR* protein genes in pathogen-induced vs. non-induced trees, while the number defense protein DEGs reduced significantly between pathogen-induced vs. mock- and non-induced trees than earlier incubation times. Thus, at 72 hours, the systemic defense response is less intense than at earlier times, likely due to the absence of sustained recognition of the pathogen, either locally or at the induction point, and lesser accumulation of defense proteins, while JA signaling continues to gain prominence systemically upon pathogenic induction and wounding, along with a less prominent and nuanced response in auxin-ABA signal transduction pathways.

Finally, **at 7 dpi** (Fig. 4.8), stress hormone accumulation was still manifold higher in both types of induced trees. For instance, we found an over 12,000-fold increase in JA-Ileu, over 1000-fold increase in JA, over 900-fold increase in OPDA, and over 300-fold increase in MeJA in pathogen-induced vs. non-induced trees, while compared to mock-induced trees, we found an over 100-fold increase in JA-Ileu and OPDA, and over 30-fold increase in JA and MeJA in pathogen-induced trees. Meanwhile, we found enhanced *COI-1* and suppressed *JAZ* in pathogen-induced vs. mock-induced trees, and we also found enhanced *COI-1*, *JAZ*, and *MYC2* in pathogen-induced vs. non-induced trees, which indicated sustained JA signal transduction due to induction at 7 dpi. In ABA signal transduction, we found no differential accumulation between

induced trees, however, ABA levels were 33-fold higher in pathogen-induced, and 61-fold higher in mock-induced trees, as compared to non-induced trees. Besides, we also found enhanced *ABF* and *SnRK2* and suppressed *PYR/PYL* in pathogen-induced vs. mock-induced trees, while we found enhanced *ABF* and *PP2C* and suppressed *PYR/PYL* in pathogen-induced vs. non-induced trees. At 7 dpi, we found no differences in auxin accumulation between pathogen-induced, mock-induced, and non-induced trees, indicating a revived intensity of auxin signal transduction between 3 dpi and 7 dpi. This was also indicated by enhanced *ARF*, *SAUR*, *AUX/IAA* in pathogen-induced vs. mock-induced trees, while in pathogen-induced vs. non-induced trees, we found enhanced *ARF*, *AUX/IAA*, *TIR1* and suppressed *SAUR*. While we did not detect the two tested GA compounds (GA_3 and GA_4), we found an enhanced diterpenoid- gibberellin signal transduction pathway at 7 dpi, as indicated by enhanced *GID1* and *PIF3* and suppressed *DELLA* in pathogen-induced vs. non-induced trees, while we found enhanced *GID2* suppressed *DELLA* in pathogen-induced vs. mock-induced trees. We also found systemic DE of defense proteins that were lower in numbers than earlier incubation times, besides, we also found enhanced *TGA* and ARR-B DEGs in pathogen-induced vs. mock-induced trees, while we also found enhanced *TGA* and *PR* proteins in pathogen-induced vs. non-induced trees. It seems that at 7 dpi, SIR responses are still mediated with fewer defense proteins and progressively intense JA signaling, and prominent accumulation of JA-Ileu in pathogen-induced trees.

4.5 Conclusion

The concurrent synergistic and antagonistic interactions, or crosstalk, of various phytohormones like AUX, JA, ABA, and GAs appear inextricably linked with the SIR response in Austrian pine induced by inoculation with *D. pinea,* but also in response to wounding. In this study, we confirm the elicitation of systemic defense responses by pathogenic infection, and, to a much lesser extent, wounding alone. The differential metabolic responses in trees upon the perception of *D. pinea*, compared to an abiotic stressor like mechanical wounding, depends on the accuracy and sustainability of recognition of pathogen-associated molecular patterns (PAMPS) versus damage-associated molecular patterns (DAMPS), respectively. A prior study had suggested that an active pathogen recognition system was operational in the expression of SIR in Austrian pine, demonstrated by SIR elicitation by both live and killed mycelium, and to a lesser degree by protein extracts from *D. pinea* (Bonello and Blodgett, 2003).

Our study shows that presence of an active infection triggers systemic responses within 0.5 days including activation of *ChiB* and *PR* proteins. This respose is sustained for at least a week. However, recognition-related gene responses disappear after 2 dpi without a challenge infection at the systemic location. Wounding or pathogenic inoculation also causes rapid systemic induction of oxidative stress, which may induce an intense ABA signal transduction by 0.5 dpi. Gradually, ABA signaling declines in prominence upon successful SIR expression over a week and simultaneously, a progressive JA signal transduction occurs after 1 dpi by wounding or pathogenic inoculation and is heightened over a week. This is reflected by manifold changes in systemic accumulation of JA, OPDA, MeJA, and JA-Ileu by 0.5 dpi in both pathogen-induced and wound-induced Austrian pines that subsequently triggers DE of JA-signaling genes by 1 dpi. The JA signaling intensifies progressively over a week, and JA, JA-Ileu, and MeJA remain as bioactive forms, with JA-Ileu progressive levels mediating SIR after 1 week post induction. Therefore, we conclude that circumstantial evidence shows JA and its intermediates OPDA, MeJA, and JA-Ileu to be pivotal in long-distance signaling of SIR in Austrian pines.

CHAPTER 5
CONCLUSIONS

The overarching goal of this dissertation was to enhance our understanding of the nature and mechanisms of abiotic and biotic stress responses in tree hosts that results in susceptibility during an adverse environment- pathogen invasion, as well as the nature and mechanisms of stress responses that results in successful resistance to recurring attacks by SIR expression. I did so by studying Austrian pine responses at the gene, biochemical, and physiological levels to gain an integrated understanding of the intricate mechanisms governing such interactions. The study was separated into four linked objectives, (1) investigating mechanisms of host susceptibility and pathogenic aggressiveness under CC conditions, (2) finding early evidence of SIR expression against pathogenic attack, (3) investigating the role of terpenoids and other plant volatile compounds in SIR, and (4) investigating forms of signaling mediating SIR expression.

5.1 Mechanisms of abiotic stress induced host susceptibility and pathogenic aggressiveness

Prolonged exposure to high temperatures and low water availability, implied as the impacts of CC in temperate regions, can be detrimental to forest health either directly, or, by weaking trees' metabolism and defense against invading pests and pathogens. While ample evidence exists reporting non-virulent fungi causing aggressive infections in hosts that have been predisposed to abiotic stress, as well as increased spread of insect pests like bark beetles in drought stressed trees, rarely have the mechanisms underlying these phenomena been studied in detail. In Chapter

2, we found that under normal conditions of temperature and water availability, the necrotrophic pathogen, *D. pinea* caused severe symptoms in Austrian pines compared with *D. scrobiculata* infection, however, both pathogens produced similarly severe symptoms under CC. This led to the investigation of the host and pathogen transcriptome after 3 days, revealing key areas of metabolic regulation that contribute to increased susceptibility of hosts to pathogenic attacks by *Diplodia* spp., upon prior exposure to CC, or susceptibility due to aggressive attack by *D. pinea* under normal conditions of temperature and water availability. We found that suppressed primary metabolism, defense, and jasmonic acid-related signaling pathway in the hosts leads to increased susceptibility of Austrian pines, while enhanced primary metabolism in *D. pinea* leads to an aggressive pathogenesis by *D. pinea*. Further, while *D. scrobiculata* infection produced heightened defenses in Austrian pines, we found that suppression of host primary metabolism, phytohormone signaling, and defense related pathways under CC stress leads to enhanced aggressiveness of *D. scrobiculata* infection. Our integrated model in Chapter 2 portrays a comparative metabolic overview of host susceptibility and pathogen aggressiveness in the pathosystem, at the expanse of a prevalent abiotic stressors like high temperatures and low water availability, i.e., climate change.

5.2 Extending the evidence of SIR and its mechanisms

In conifers like pine and spruce, SIR has been an important form of immediate resistance against recurring attacks of pests and pathogens. Evidence of SIR has also been repeatedly demonstrated using the APDP pathosystem, however, only upon challenge inoculation at 8 days after induction of hosts (Sherwood and Bonello, 2016). In Chapter 3, we found evidence of SIR when trees were challenged within 0.5 days of induction by the pathogen, besides, a progressively stronger response is generated upon challenge within 10 days of induction by *D. pinea*, and also to a

much lesser extent upon wounding. Along with existing literature, our results confirm that SIR is an important mechanism of immediate response in tree-pathogen interactions. Further, we also found manifold induction of terpenoids along with SIR, within 0.5 days of induction by *D. pinea*, along with co-regulation of various monoterpenes, sesquiterpenes, and other plant volatile compounds in the presence of pathogen, such as α-pinene and a cluster of β-pinene, limonene, benzaldehyde, dodecanol, and n-dodecyl acrylate, that were also fungistatic *in vitro*. Interestingly, this dissertation is also the first report of dodecanol and n-dodecyl acrylate in conifer defense. Our study confirmed the involvement of terpenoids in SIR expression in the pathosystem, with a nuanced role of several compounds, and suggested potential roles of α-pinene and β-pinene in SIR signaling.

5.3 Nature of SIR signaling in the P. nigra- D. pinea pathosystem

Phytohormones are indispensable for communication of plant metabolic cues, and they orchestrate transduction of interconnected cellular cascades, some of which have been discussed as systemic signaling molecules/ mechanisms for mediating resistance to abiotic and biotic stresses (Vlot et al., 2020). Stress hormones like JA and ABA have been well-documented for mediating responses against abiotic stress as well as pathogenic attack by necrotrophic fungi, while their role in SIR expression is not known. In Chapter 4, we show evidence of systemic induction of pathogenic recognition patterns upon live inoculation of Austrian pines with *D. pinea*, in conjunction with earlier reports in the pathosystem demonstrating dead and live mycelia along with fungal protein extracts as potential elicitors of systemic induction of defenses (Bonello and Blodgett, 2003). We also found manifold systemic accumulation of ABA and enhancement of ROS related gene expression within 0.5 days of induction, followed by JA mediated systemic response within 1 day of induction that intensifies up to 10 days of induction.

We also reported MeJA as the bioactive form of JA signaling up to 3 days of induction, whereas JA-Ileu was the major bioactive form after 7 days of induction, indicating their roles in early and latent signaling of JA that mediates the SIR response observed in the study.

5.4 Future directions

The strides and advancements made regarding the nature and mechanisms of resistance and signaling in response to abiotic and biotic stresses in the APDP pathosystem will serve as an excellent platform for testing means of induced resistance involving other necrotrophic pathogens, and also open the door for investigating the nature of induced resistance in tree-biotrophic fungal pathogen interactions. Also, this dissertation proposes a number of candidate elicitors, such as monoterpenes and stress hormones, that can be used for testing induction of resistance, that can be optimized for devising efficient pest and disease management strategies in both natural and artificial settings. Furthermore, in line with earlier reports that suggested multiple routes of SIR signaling in the pathosystem (Bonello and Blodgett, 2003; Sherwood and Bonello, 2016), we propose the involvement of three distinct routes of SIR signaling, involving the phloem mediating transportation of signaling solutes, the xylem mediating a rapid hydraulic stress resulting in systemic induction of ABA and ROS, as well as aerial routes involving volatile compounds such as terpenoids and stress hormone derivatives. Ultimately, a more granular understanding of these basic mechanisms will greatly enhance the possibilities of applying this knowledge to tree improvement through breeding and conservation, contributing to better management of these recalcitrant issues.

CHAPTER 6
BIBLIOGRAPHY

Achard, P., & Genschik, P. (2009). Releasing the brakes of plant growth: how GAs shutdown DELLA proteins. *Journal of Experimental Botany*, *60*(4), 1085–1092. https://doi.org/10.1093/jxb/ern301

Adams, H.D., Guardiola-Claramonte, M., Barron-Gafford, G.A., Villegas, J.C., Breshears, D.D., Zou, C.B., Troch, P.A., and Huxman, T.E. (2009). Temperature sensitivity of drought-induced tree mortality portends increased regional die-off under global-change-type drought. *Proceedings of the National Academy of Sciences of the United States of America* 106**,** 7063-7066.

Agrios, G. N. (2005). *chapter six - How plants defend themselves against pathogens* (G. N. B. T.-P. P. (Fifth E. AGRIOS (ed.); pp. 207–248). Academic Press. https://doi.org/https://doi.org/10.1016/B978-0-08-047378-9.50012-9

Alexa A, Rahnenfuhrer J (2023). *topGO: Enrichment Analysis for Gene Ontology*. R package version 2.52.0.

Alexa, A., and Rahnenfuhrer, J. (2021). "topGO: Enrichment Analysis for Gene Ontology.", in: *R package version 2.46.0*.

Allen, C. D., Macalady, A. K., Chenchouni, H., Bachelet, D., McDowell, N., Vennetier, M., Kitzberger, T., Rigling, A., Breshears, D. D., Hogg, E. H. (Ted), Gonzalez, P., Fensham, R., Zhang, Z., Castro, J., Demidova, N., Lim, J.-H., Allard, G., Running, S. W., Semerci, A., & Cobb, N. (2010). A global overview of drought and heat-induced tree mortality reveals emerging climate change risks for forests. *Forest Ecology and Management*, *259*(4), 660–684. https://doi.org/https://doi.org/10.1016/j.foreco.2009.09.001

Arévalo-Marín, D. F., Briceño-Robles, D. M., Mosquera, T., Melgarejo, L. M., & Sarmiento, F. (2021). Jasmonic acid priming of potato uses hypersensitive response-dependent defense and delays necrotrophic phase change against Phytophthora infestans. *Physiological and Molecular Plant Pathology*, *115*, 101680. https://doi.org/https://doi.org/10.1016/j.pmpp.2021.101680

Aubert, Y., Widemann, E., Miesch, L., Pinot, F., & Heitz, T. (2015). CYP94-mediated jasmonoyl-isoleucine hormone oxidation shapes jasmonate profiles and attenuates defence

responses to Botrytis cinerea infection. *Journal of Experimental Botany*, *66*(13), 3879–3892. https://doi.org/10.1093/jxb/erv190

Babady, N.E., Pang, Y.-P., Elpeleg, O., and Isaya, G. (2007). Cryptic proteolytic activity of dihydrolipoamide dehydrogenase. *Proceedings of the National Academy of Sciences* 104**,** 6158-6163.

Barto, E.K., Enright, S., Eyles, A., Wallis, C.M., Chorbadjian, R., Hansen, R., Herms, D.A., Bonello, P., and Cipollini, D.F. (2008). Effects of soil fertility on systemic protein defense responses of Austrian pine to attack by a fungal pathogen and an insect defoliator. *Journal of Chemical Ecology* 34**,** 1392-1400.

Bauer, H., Ache, P., Lautner, S., Fromm, J., Hartung, W., Al-Rasheid, K. A. S., Sonnewald, S., Sonnewald, U., Kneitz, S., Lachmann, N., Mendel, R. R., Bittner, F., Hetherington, A. M., & Hedrich, R. (2013). The Stomatal Response to Reduced Relative Humidity Requires Guard Cell-Autonomous ABA Synthesis. *Current Biology*, *23*(1), 53–57. https://doi.org/10.1016/j.cub.2012.11.022

Beattie, G. A. (2011). Water Relations in the Interaction of Foliar Bacterial Pathogens with Plants. *Annual Review of Phytopathology*, *49*(1), 533–555. https://doi.org/10.1146/annurev-phyto-073009-114436

Behnke, K., Ehlting, B., Teuber, M., Bauerfeind, M., Louis, S., Hänsch, R., … & Schnitzler, J. (2007). Transgenic, non-isoprene emitting poplars don't like it hot. The Plant Journal, 51(3), 485-499. https://doi.org/10.1111/j.1365-313x.2007.03157.x

Behnke, K., Kleist, E., Uerlings, R., Wildt, J., Rennenberg, H., & Schnitzler, J.-P. (2009). RNAi-mediated suppression of isoprene biosynthesis in hybrid poplar impacts ozone tolerance. *Tree Physiology*, *29*(5), 725–736. https://doi.org/10.1093/treephys/tpp009

Bentz, B.J., Regniere, J., Fettig, C.J., Hansen, E.M., Hayes, J.L., Hicke, J.A., Kelsey, R.G., Negron, J.F., and Seybold, S.J. (2010). Climate change and bark beetles of the western United States and Canada: Direct and indirect effects. *Bioscience* 60**,** 602-613.

Bhargava, S., and Sawant, K. (2013). Drought stress adaptation: metabolic adjustment and regulation of gene expression. *Plant Breeding* 132**,** 21-32.

Bi, C., Ma, Y., Wu, Z., Yu, Y.-T., Liang, S., Lu, K., & Wang, X.-F. (2017). Arabidopsis ABI5 plays a role in regulating ROS homeostasis by activating CATALASE 1 transcription in seed germination. *Plant Molecular Biology*, *94*(1), 197–213. https://doi.org/10.1007/s11103-017-0603-y

Bihon, W., Slippers, B., Burgess, T., Wingfield, M.J. and Wingfield, B.D. (2011), Diplodia scrobiculata found in the southern hemisphere. Forest Pathology, 41: 175-181. https://doi.org/10.1111/j.1439-0329.2010.00649.x

Blodgett, J. T., & Bonello, P. (2003). The aggressiveness of Sphaeropsis sapinea on Austrian pine varies with isolate group and site of infection. *Forest Pathology*, *33*(1), 15–19. https://doi.org/https://doi.org/10.1046/j.1439-0329.2003.00303.x

Blodgett, J. T., Eyles, A., & Bonello, P. (2007). Organ-dependent induction of systemic resistance and systemic susceptibility in Pinus nigra inoculated with Sphaeropsis sapinea and Diplodia scrobiculata. *Tree Physiology*, *27*(4), 511–517. https://doi.org/10.1093/treephys/27.4.511

Blodgett, J.T., Kruger, E.L., and Stanosz, G.R. (1997a). Effects of moderate water stress on disease development by *Sphaeropsis sapinea* on red pine. *Phytopathology* 87**,** 422-428.

Blodgett, J.T., Kruger, E.L., and Stanosz, G.R. (1997b). *Sphaeropsis sapinea* and water stress in a red pine plantation in central Wisconsin. *Phytopathology* 87**,** 429-434.

Blumenstein, K., Bußkamp, J., Langer, G. J., & Terhonen, E. (2022). Diplodia tip blight pathogen's virulence empowered through host switch. In *Frontiers in Fungal Biology (*Vol. 3). https://www.frontiersin.org/articles/10.3389/ffunb.2022.939007

Blumenstein, K., Bußkamp, J., Langer, G.J., Langer, E.J., and Terhonen, E. (2021). The Diplodia tip blight pathogen *Sphaeropsis sapinea* is the most common fungus in Scots pines' mycobiome, irrespective of health status—A case study from Germany. *Journal of Fungi* 7**,** 607.

Boccardo, N.A., Segretin, M.E., Hernandez, I., Mirkin, F.G., Chacón, O., Lopez, Y., Borrás-Hidalgo, O., and Bravo-Almonacid, F.F. (2019). Expression of pathogenesis-related proteins in transplastomic tobacco plants confers resistance to filamentous pathogens under field trials. *Scientific Reports* 9**,** 2791.

Boege, K. (2004). Induced responses in three tropical dry forest plant species – direct and indirect effects on herbivory. *Oikos*, *107*(3), 541–548. https://doi.org/https://doi.org/10.1111/j.0030-1299.2004.13272.x

Bolger, A.M., Lohse, M., and Usadel, B. (2014). Trimmomatic: a flexible trimmer for Illumina sequence data. *Bioinformatics*.

Boncan, D. A. T., Tsang, S. S. K., Li, C., Lee, I. H. T., Lam, H.-M., Chan, T.-F., & Hui, J. H. L. (2020). Terpenes and Terpenoids in Plants: Interactions with Environment and Insects. In *International Journal of Molecular Sciences* (Vol. 21, Issue 19). https://doi.org/10.3390/ijms21197382

Bonello, P., & Blodgett, J. T. (2003). Pinus nigra–Sphaeropsis sapinea as a model pathosystem to investigate local and systemic effects of fungal infection of pines. *Physiological and Molecular Plant Pathology*, *63*(5), 249–261. https://doi.org/https://doi.org/10.1016/j.pmpp.2004.02.002

Bonello, P., Gordon, T. R., Herms, D. A., Wood, D. L., & Erbilgin, N. (2006). Nature and ecological implications of pathogen-induced systemic resistance in conifers: A novel hypothesis. *Physiological and Molecular Plant Pathology*, *68*(4–6), 95–104. https://doi.org/10.1016/j.pmpp.2006.12.002

Bonello, Gordon, & Storer. (2001). Systemic induced resistance in Monterey pine. *Forest Pathology*, *31*(2), 99–106. https://doi.org/https://doi.org/10.1046/j.1439-0329.2001.00230.x

Bostock, R.M., Pye, M.F., and Roubtsova, T.V. (2014). Predisposition in plant disease: exploiting the nexus in abiotic and biotic stress perception and response. *Annual Review of Phytopathology* 52**,** 517-549.

Bray, N. L., Pimentel, H., Melsted, P., & Pachter, L. (2016). Near-optimal probabilistic RNA-seq quantification. *Nature Biotechnology*, *34*(5), 525–527. https://doi.org/10.1038/nbt.3519

Buchfink, B., Xie, C., & Huson, D. H. (2015). Fast and sensitive protein alignment using DIAMOND. *Nature Methods*, *12*(1), 59–60. https://doi.org/10.1038/nmeth.3176

Buchfink, B., Xie, C., and Huson, D.H. (2014). Fast and sensitive protein alignment using DIAMOND. *Nature Methods* 12**,** 59-60.

Bushmanova, E., Antipov, D., Lapidus, A., & Prjibelski, A. D. (2019). rnaSPAdes: a de novo transcriptome assembler and its application to RNA-Seq data. *GigaScience*, *8*(9), giz100. https://doi.org/10.1093/gigascience/giz100

Cale, J. A., Muskens, M., Najar, A., Ishangulyyeva, G., Hussain, A., Kanekar, S. S., Klutsch, J. G., Taft, S., & Erbilgin, N. (2017). Rapid monoterpene induction promotes the susceptibility of a novel host pine to mountain pine beetle colonization but not to beetle-vectored fungi. *Tree Physiology*, *37*(12), 1597–1610. https://doi.org/10.1093/treephys/tpx089

Castells, A. A. (2015). *The role of terpenes in the defensive responses of conifers against herbivores and pathogens*. PhD thesis, 1–184. Universitat Autònoma de Barcelona, Bellaterra, Barcelona, Spain

Celedon, J. M., & Bohlmann, J. (2019). Oleoresin defenses in conifers: chemical diversity, terpene synthases and limitations of oleoresin defense under climate change. *New Phytologist*, *224*(4), 1444–1463. https://doi.org/https://doi.org/10.1111/nph.15984

Chakraborty, S., Whitehill, J. G. A., Hill, A. M. Y. L., Opiyo, S. O., Cipollini, D. O. N., Herms, D. A., & Bonello, P. (2014). Effects of water availability on emerald ash borer larval performance and phloem phenolics of Manchurian and black ash. *Plant, Cell & Environment*, *37*(4), 1009–1021. https://doi.org/https://doi.org/10.1111/pce.12215

Chandra, S., & Sharma, I. P. (2023). Chapter 4 - Elicitins as microbe-associated molecular patterns and their role in plant defense. In D. Chandra & P. B. T.-U. P.-M. S. Bhatt (Eds.), *Developments in Applied Microbiology and Biotechnology* (pp. 77–86). Academic Press. https://doi.org/https://doi.org/10.1016/B978-0-323-99896-3.00001-1

Chang, S., Puryear, J., and Cairney, J. (1993). A simple and efficient method for isolating RNA from pine trees. *Plant Molecular Biology Reporter* 11**,** 113-116.

Chaves, M.M., Maroco, J.P., and Pereira, J.S. (2003). Understanding plant responses to drought - from genes to the whole plant. *Functional Plant Biology* 30**,** 239-264.

Chen, J., Piao, Y., Liu, Y., Li, X., & Piao, Z. (2018). Genome-wide identification and expression analysis of chitinase gene family in Brassica rapa reveals its role in clubroot resistance. *Plant Science*, *270*, 257–267. https://doi.org/https://doi.org/10.1016/j.plantsci.2018.02.017

Chen, L., Wang, W.-S., Wang, T., Meng, X.-F., Chen, T., Huang, X.-X., Li, Y., & Hou, B.-K. (2019). Methyl Salicylate Glucosylation Regulates Plant Defense Signaling and Systemic Acquired Resistance. *Plant Physiology*, *180*(4), 2167–2181. https://doi.org/10.1104/pp.19.00091

Cheval, C., Aldon, D., Galaud, J.-P., and Ranty, B. (2013). Calcium/calmodulin-mediated regulation of plant immunity. *Biochimica et Biophysica Acta (BBA) - Molecular Cell Research* 1833**,** 1766-1771.

Chiasson, D., Ekengren, S.K., Martin, G.B., Dobney, S.L., and Snedden, W.A. (2005). Calmodulin-like proteins from *Arabidopsis* and tomato are involved in host defense against *Pseudomonas syringae* pv. tomato. *Plant Molecular Biology* 58**,** 887-897.

Chiu, C. C., & Bohlmann, J. (2022). Mountain Pine Beetle Epidemic: An Interplay of Terpenoids in Host Defense and Insect Pheromones. *Annual Review of Plant Biology*, *73*(1), 475–494. https://doi.org/10.1146/annurev-arplant-070921-103617

Choi, H. W., & Klessig, D. F. (2016). DAMPs, MAMPs, and NAMPs in plant innate immunity. *BMC Plant Biology*, *16*(1), 232. https://doi.org/10.1186/s12870-016-0921-2

Choi, W.-G., Hilleary, R., Swanson, S. J., Kim, S.-H., & Gilroy, S. (2016). Rapid, Long-Distance Electrical and Calcium Signaling in Plants. *Annual Review of Plant Biology*, *67*(1), 287–307. https://doi.org/10.1146/annurev-arplant-043015-112130

Chowhan, N., Bali, A. S., Singh, H. P., Batish, D. R., & Kohli, R. K. (2014). Reactive oxygen species generation and antioxidant defense system in hydroponically grown wheat (Triticum aestivum) upon β-pinene exposure: an early time course assessment. *Acta Physiologiae Plantarum*, *36*(12), 3137–3146. https://doi.org/10.1007/s11738-014-1654-1

Christensen, J., & Jaroszewski, J. W. (2001). Natural Glycosides Containing Allopyranose from the Passion Fruit Plant and Circular Dichroism of Benzaldehyde Cyanohydrin Glycosides1. *Organic Letters*, *3*(14), 2193–2195. https://doi.org/10.1021/ol016044+

Chung, I. M., Kim, J. J., Lim, J. D., Yu, C. Y., Kim, S. H., & Hahn, S. J. (2006). Comparison of resveratrol, SOD activity, phenolic compounds and free amino acids in Rehmannia glutinosa under temperature and water stress. *Environmental and Experimental Botany*, *56*(1), 44–53. https://doi.org/https://doi.org/10.1016/j.envexpbot.2005.01.001

Cipollini, D., & Heil, M. (2023). Costs and benefits of induced resistance to herbivores and pathogens in plants. In *CABI Reviews*. CABI Reviews. https://doi.org/10.1079/PAVSNNR20105005

Clifford, M.J., Royer, P.D., Cobb, N.S., Breshears, D.D., and Ford, P.L. (2013). Precipitation thresholds and drought-induced tree die-off: insights from patterns of *Pinus edulis* mortality along an environmental stress gradient. *New Phytologist* 200**,** 413-421.

De Wet, J., Burgess, T., Slippers, B., Preisig, O., Wingfield, B. D., & Wingfield, M. J. (2003). Multiple gene genealogies and microsatellite markers reflect relationships between morphotypes of Sphaeropsis sapinea and distinguish a new species of Diplodia. *Mycological Research*, *107*(5), 557–566. https://doi.org/https://doi.org/10.1017/S0953756203007706

Delvas, N., Bauce, É., Labbé, C., Ollevier, T., & Bélanger, R. (2011). Phenolic compounds that confer resistance to spruce budworm. *Entomologia Experimentalis et Applicata*, *141*(1), 35–44. https://doi.org/https://doi.org/10.1111/j.1570-7458.2011.01161.x

Desprez-Loustau, M.L., Marcais, B., Nageleisen, L.M., Piou, D., and Vannini, A. (2006). Interactive effects of drought and pathogens in forest trees. *Annals of Forest Science* 63**,** 597-612.

Dievart, A., Gottin, C., Périn, C., Ranwez, V., & Chantret, N. (2020). Origin and Diversity of Plant Receptor-Like Kinases. *Annual Review of Plant Biology*, *71*(1), 131–156. https://doi.org/10.1146/annurev-arplant-073019-025927

Ding, P., & Ding, Y. (2020). Stories of Salicylic Acid: A Plant Defense Hormone. *Trends in Plant Science*, *25*(6), 549–565. https://doi.org/10.1016/j.tplants.2020.01.004

Dixit, G., Praveen, A., Tripathi, T., Yadav, V. K., & Verma, P. C. (2017). Herbivore-responsive cotton phenolics and their impact on insect performance and biochemistry. *Journal of Asia-Pacific Entomology*, *20*(2), 341–351. https://doi.org/https://doi.org/10.1016/j.aspen.2017.02.002

Djami-Tchatchou, A.T., Harrison, G.A., Harper, C.P., Wang, R., Prigge, M.J., Estelle, M., and Kunkel, B.N. (2020). Dual role of auxin in regulating plant defense and bacterial virulence gene expression during *Pseudomonas syringae* PtoDC3000 pathogenesis. *Molecular Plant-Microbe Interactions* 33**,** 1059-1071.

Du, M., Zhai, Q., Deng, L., Li, S., Li, H., Yan, L., Huang, Z., Wang, B., Jiang, H., Huang, T., Li, C.-B., Wei, J., Kang, L., Li, J., & Li, C. (2014). Closely Related NAC Transcription Factors of Tomato Differentially Regulate Stomatal Closure and Reopening during Pathogen Attack . *The Plant Cell*, *26*(7), 3167–3184. https://doi.org/10.1105/tpc.114.128272

Eccel, E., Maresi, G., and Ambrosi, P. (2003). "Deficit idrici e disseccamenti da *Sphaeropsis sapinea* su pino nero in Trentino", in: *III Convegno Nazionale SISEF: Alberi e Foreste per il Terzo Millennio*, eds. P. De Angelis, A. Macuz & G. Bucci (Viterbo, Italy: Società Italiana di Selvicoltura ed Ecologia Forestale), 351-356 (in Italian with abstract in English).

Eleftherianos, I., Vamvatsikos, P., Ward, D., & Gravanis, F. (2006). Changes in the levels of plant total phenols and free amino acids induced by two cereal aphids and effects on aphid fecundity. *Journal of Applied Entomology*, *130*(1), 15–19. https://doi.org/https://doi.org/10.1111/j.1439-0418.2005.01017.x

Erbilgin, N. (2019). Phytochemicals as mediators for host range expansion of a native invasive forest insect herbivore. *New Phytologist*, *221*(3), 1268–1278. https://doi.org/https://doi.org/10.1111/nph.15467

Ewels, P., Magnusson, M., Lundin, S., & Käller, M. (2016). MultiQC: summarize analysis results for multiple tools and samples in a single report. *Bioinformatics*, *32*(19), 3047–3048. https://doi.org/10.1093/bioinformatics/btw354

Eyles, A., Bonello, P., Ganley, R., & Mohammed, C. (2010). Induced resistance to pests and pathogens in trees. *New Phytologist*, *185*(4), 893–908. https://doi.org/https://doi.org/10.1111/j.1469-8137.2009.03127.x

Eyles, A., Chorbadjian, R., Wallis, C., Hansen, R., Cipollini, D., Herms, D., & Bonello, P. (2007). Cross-induction of systemic induced resistance between an insect and a fungal pathogen in Austrian pine over a fertility gradient. *Oecologia*, *153*(2), 365–374. https://doi.org/10.1007/s00442-007-0741-z

Fabre, B., Piou, D., Desprez-Loustau, M.L., and Marcais, B. (2011). Can the emergence of pine Diplodia shoot blight in France be explained by changes in pathogen pressure linked to climate change? *Global Change Biology* 17**,** 3218-3227.

Falcone Ferreyra, M. L., Rius, S., & Casati, P. (2012). Flavonoids: biosynthesis, biological functions, and biotechnological applications. In *Frontiers in Plant Science (*Vol. 3). https://www.frontiersin.org/articles/10.3389/fpls.2012.00222

Finkelstein, R. (2013). Abscisic Acid Synthesis and Response. *The Arabidopsis Book*, *2013*(11). https://doi.org/10.1199/tab.0166

Franceschi, V. R., Krokene, P., Christiansen, E., & Krekling, T. (2005). Anatomical and chemical defenses of conifer bark against bark beetles and other pests. New Phytologist, 167(2), 353-376. https://doi.org/10.1111/j.1469-8137.2005.01436.x

Gallé, A., Lautner, S., Flexas, J., & Fromm, J. (2015). Environmental stimuli and physiological responses: The current view on electrical signalling. *Environmental and Experimental Botany*, *114*, 15–21. https://doi.org/https://doi.org/10.1016/j.envexpbot.2014.06.013

Gallou, A., Lucero Mosquera, H. P., Cranenbrouck, S., Suárez, J. P., & Declerck, S. (2011). Mycorrhiza induced resistance in potato plantlets challenged by Phytophthora infestans. *Physiological and Molecular Plant Pathology*, *76*(1), 20–26. https://doi.org/https://doi.org/10.1016/j.pmpp.2011.06.005

Gautam, A. K., Singh, P. K., & Aravind, M. (2020). Defensive Role of Plant Phenolics Against Pathogenic Microbes for Sustainable Agriculture BT - Plant Phenolics in Sustainable Agriculture: Volume 1 (R. Lone, R. Shuab, & A. N. Kamili (eds.); pp. 579–594). *Springer Singapore*. https://doi.org/10.1007/978-981-15-4890-1_25

Gfeller, A., Dubugnon, L., Liechti, R., & Farmer, E. E. (2010). Jasmonate Biochemical Pathway. *Science Signaling*, *3*(109), cm3–cm3. https://doi.org/10.1126/scisignal.3109cm3

Ghosh, S. K., Slot, J. C., Visser, E. A., Naidoo, S., Sovic, M. G., Conrad, A. O., Kyre, B., Vijayakumar, V., & Bonello, P. (2022). Mechanisms of Pine Disease Susceptibility Under Experimental Climate Change . In *Frontiers in Forests and Global Change* (Vol. 5). https://www.frontiersin.org/articles/10.3389/ffgc.2022.872584

Gibbs, G. M., Roelants, K., & O'Bryan, M. K. (2008). The CAP Superfamily: Cysteine-Rich Secretory Proteins, Antigen 5, and Pathogenesis-Related 1 Proteins—Roles in Reproduction, Cancer, and Immune Defense. *Endocrine Reviews*, *29*(7), 865–897. https://doi.org/10.1210/er.2008-0032

Gilbert, D. (2016). Gene-omes built from mRNA seq not genome DNA [version 1; not peer reviewed]. *F1000Research* 5**,** 1695 (poster).

Gilbert, Donald (2013) Gene-omes built from mRNA seq not genome DNA. 7th annual arthropod genomics symposium. Notre Dame. http://arthropods.eugenes.org/EvidentialGene/about/EvigeneRNA2013poster.pdf and http://globalhealth.nd.edu/7th-annual-arthropod-genomics-symposium/ and doi:10.7490/f1000research.1112594.1

Goh, C.-H., Ko, S.-M., Koh, S., Kim, Y.-J., & Bae, H.-J. (2012). Photosynthesis and Environments: Photoinhibition and Repair Mechanisms in Plants. *Journal of Plant Biology*, *55*(2), 93–101. https://doi.org/10.1007/s12374-011-9195-2

Goodsman, D.W., Lusebrink, I., Landhäusser, S.M., Erbilgin, N., Lieffers, V.J. (2013). Variation in carbon availability, defense chemistry and susceptibility to fungal invasion along the stems of mature trees. *New Phytologist*. doi.org/10.1111/nph.12019

Gordon T, Reynolds GJ, Kirkpatrick SC, Storer AJ, Wood DL, Fernandez DM, McPherson B (2020) Monterey pine forest made a remarkable recovery from pitch canker. California Agriculture 74 (3):169-173. https://doi.org/10.3733/ca.2020a0019

Gordon, T. R., Kirkpatrick, S. C., Aegerter, B. J., Fisher, A. J., Storer, A. J., & Wood, D. L. (2011). Evidence for the occurrence of induced resistance to pitch canker, caused by Gibberella circinata (anamorph Fusarium circinatum), in populations of Pinus radiata. *Forest Pathology*, *41*(3), 227–232. https://doi.org/https://doi.org/10.1111/j.1439-0329.2010.00678.x

Gossner, M. M., Perret-Gentil, A., Britt, E., Queloz, V., Glauser, G., Ladd, T., Roe, A. D., Cleary, M., Liziniewicz, M., Nielsen, L. R., Ghosh, S. K., Bonello, P., & Eisenring, M. (2023). A glimmer of hope – ash genotypes with increased resistance to ash dieback pathogen show cross-resistance to emerald ash borer. *New Phytologist*, *n/a*(n/a). https://doi.org/https://doi.org/10.1111/nph.19068

Grabherr, M.G., Haas, B.J., Yassour, M., Levin, J.Z., Thompson, D.A., and Amit, I. (2011). Full-length transcriptome assembly from RNA-Seq data without a reference genome. *Nature Biotechnology*

Guo, Y., Jud, W., Weikl, F., Ghirardo, A., Junker, R. R., Polle, A., Benz, J. P., Pritsch, K., Schnitzler, J. P., & Rosenkranz, M. (2021). Volatile organic compound patterns predict

fungal trophic mode and lifestyle. *Communications Biology*, *4*(1), 1–12. https://doi.org/10.1038/s42003-021-02198-8

Haas, B. J., Papanicolaou, A., Yassour, M., Grabherr, M., Blood, P. D., Bowden, J., Couger, M. B., Eccles, D., Li, B., Lieber, M., MacManes, M. D., Ott, M., Orvis, J., Pochet, N., Strozzi, F., Weeks, N., Westerman, R., William, T., Dewey, C. N., … Regev, A. (2013). De novo transcript sequence reconstruction from RNA-seq using the Trinity platform for reference generation and analysis. *Nature Protocols*, *8*(8), 1494–1512. https://doi.org/10.1038/nprot.2013.084

Haddad, I., Hiller, K., Frimmersdorf, E., Benkert, B., Schomburg, D., & Jahn, D. (2009). An emergent self-organizing map based analysis pipeline for comparative metabolome studies. *In Silico Biology*, *9*(4), 163–178. https://doi.org/10.3233/ISB-2009-0396

Harris, J.M., Balint-Kurti, P., Bede, J.C., Day, B., Gold, S., Goss, E.M., Grenville-Briggs, L.J., Jones, K.M., Wang, A., Wang, Y., Mitra, R.M., Sohn, K.H., and Alvarez, M.E. (2020). What are the top 10 unanswered questions in molecular plant-microbe interactions? *Molecular Plant-Microbe Interactions* 33**,** 1354-1365.

Hart, A. J., Ginzburg, S., Xu, M. (Sam), Fisher, C. R., Rahmatpour, N., Mitton, J. B., Paul, R., & Wegrzyn, J. L. (2020). EnTAP: Bringing faster and smarter functional annotation to non-model eukaryotic transcriptomes. *Molecular Ecology Resources*, *20*(2), 591–604. https://doi.org/https://doi.org/10.1111/1755-0998.13106

Hart, A.J., Ginzburg, S., Xu, M., Fisher, C.R., Rahmatpour, N., Mitton, J.B., Paul, R., and Wegrzyn, J.L. (2020). EnTAP: Bringing faster and smarter functional annotation to non-model eukaryotic transcriptomes. *Molecular Ecology Resources* 20**,** 591-604.

He, X., Jiang, Y., Chen, S., Chen, F., & Chen, F. (2023). Terpenoids and Their Possible Role in Defense Against a Fungal Pathogen Alternaria tenuissima in Chrysanthemum morifolium Cultivars. *Journal of Plant Growth Regulation*, *42*(2), 1144–1157. https://doi.org/10.1007/s00344-022-10619-z

Hernandez-Escribano, L., Visser, E.A., Iturritxa, E., Raposo, R., and Naidoo, S. (2020). The transcriptome of *Pinus pinaster* under *Fusarium circinatum* challenge. *BMC Genomics* 21**,** 28.

Herre, E.A., Mejia, L.C., Kyllo, D.A., Rojas, E., Maynard, Z., Butler, A., and Van Bael, S.A. (2007). Ecological implications of anti-pathogen effects of tropical fungal endophytes and mycorrhizae. *Ecology* 88**,** 550-558.

Hlaiem, S., Yangui, I., Ezzine, O. et al. First report of Diplodia scrobiculata causal agent of Tetraclinis articulata branch canker in Tunisia. J Plant Pathol 105, 369 (2023). https://doi.org/10.1007/s42161-022-01284-y

Honkanen, T., Haukioja, E. (1994). Why does a branch suffer more after branch-wide than after tree-wide defoliation? *Oikos*. doi.org/10.2307/3545832

Hou, S., Liu, Z., Shen, H., & Wu, D. (2019). Damage-Associated Molecular Pattern-Triggered Immunity in Plants. In *Frontiers in Plant Science (*Vol. 10). https://www.frontiersin.org/articles/10.3389/fpls.2019.00646

Huang, X., Xiao, Y., Köllner, T.G., Zhang, W., Wu, J., Wu, J., Guo, Y., Zhang, Y. (2013). Identification and characterization of (E)-*β*-caryophyllene synthase and *α*/*β*-pinene synthase potentially involved in constitutive and herbivore-induced terpene formation in cotton. *Plant Physiology and Biochemistry*. doi.org/10.1016/j.plaphy.2013.10.017

Huang, X. Q., Li, R., Fu, J., & Dudareva, N. (2022). A peroxisomal heterodimeric enzyme is involved in benzaldehyde synthesis in plants. *Nature Communications*, *13*(1). https://doi.org/10.1038/s41467-022-28978-2

Huang, H., Nguyen Thi Thu, T., He, X., Gravot, A., Bernillon, S., Ballini, E., and Morel, J.-B. (2017). Increase of fungal pathogenicity and role of plant glutamine in nitrogen-induced susceptibility (NIS) to rice blast. *Frontiers in Plant Science* 8.

Huber, A. E., & Bauerle, T. L. (2016). Long-distance plant signaling pathways in response to multiple stressors: the gap in knowledge. *Journal of Experimental Botany*, *67*(7), 2063–2079. https://doi.org/10.1093/jxb/erw099

Huerta-Cepas, J., Szklarczyk, D., Forslund, K., Cook, H., Heller, D., Walter, M.C., Rattei, T., Mende, D.R., Sunagawa, S., Kuhn, M., Jensen, L.J., Von Mering, C., and Bork, P. (2016). EGGNOG 4.5: A hierarchical orthology framework with improved functional annotations for eukaryotic, prokaryotic and viral sequences. *Nucleic Acids Research* 44**,** D286-D293.

Huerta-Cepas, J., Szklarczyk, D., Heller, D., Hernández-Plaza, A., Forslund, S. K., Cook, H., Mende, D. R., Letunic, I., Rattei, T., Jensen, L. J., von Mering, C., & Bork, P. (2019). eggNOG 5.0: a hierarchical, functionally and phylogenetically annotated orthology resource based on 5090 organisms and 2502 viruses. *Nucleic Acids Research*, *47*(D1), D309–D314. https://doi.org/10.1093/nar/gky1085

Hummelbrunner, L.A., Isman, M.B. (2001). Acute, sublethal, antifeedant, and synergistic effects of monoterpenoid essential oil compounds on the tobacco cutworm, *Spodoptera litura* (Lep., Noctuidae). *Journal of Agricultural and Food Chemistry*. doi.org/10.1021/jf000749t

Hutnik, R. J., McClenahen, J. R., Long, R. P., & Davis, D. D. (2014). Mercury Accumulation in *Pinus nigra* (Austrian Pine). *Northeastern Naturalist*, *21*(4), 529–540. https://doi.org/10.1656/045.021.0402

Jain, M., Amera, G. M., Muthukumaran, J., & Singh, A. K. (2022). Insights into biological role of plant defense proteins: A review. *Biocatalysis and Agricultural Biotechnology*, *40*, 102293. https://doi.org/https://doi.org/10.1016/j.bcab.2022.102293

Ji, N., Wang, J., Zuo, X., Li, Y., Li, M., Wang, K., Jin, P., & Zheng, Y. (2021). PpWRKY45 is involved in methyl jasmonate primed disease resistance by enhancing the expression of jasmonate acid biosynthetic and pathogenesis-related genes of peach fruit. *Postharvest Biology and Technology*, *172*, 111390. https://doi.org/https://doi.org/10.1016/j.postharvbio.2020.111390

Joo, S.S., Kim, Y.B., Lee, D.I. (2010). Antimicrobial and antioxidant properties of secondary metabolites from white rose flower. *Plant Pathology Journal*. doi.org/10.5423/PPJ.2010.26.1.057

Joshi, V., Joshi, N., Vyas, A., & Jadhav, S. K. (2021). *25 - Pathogenesis-related proteins: Role in plant defense* (S. B. T.-B. A. and S. M. Jogaiah (ed.); pp. 573–590). Woodhead Publishing. https://doi.org/https://doi.org/10.1016/B978-0-12-822919-4.00025-9

Jung, S. C., Martinez-Medina, A., Lopez-Raez, J. A., & Pozo, M. J. (2012). Mycorrhiza-Induced Resistance and Priming of Plant Defenses. *Journal of Chemical Ecology*, *38*(6), 651–664. https://doi.org/10.1007/s10886-012-0134-6

Kanehisa, M., and Sato, Y. (2020). KEGG Mapper for inferring cellular functions from protein sequences. *Protein Science* 29**,** 28-35.

Kanehisa, M., Sato, Y., and Morishima, K. (2016). BlastKOALA and GhostKOALA: KEGG tools for functional characterization of genome and metagenome sequences. *Journal of Molecular Biology* 428**,** 726-731.

Kar, R. K. (2011). Plant responses to water stress: Role of reactive oxygen species. *Plant Signaling & Behavior*, *6*(11), 1741–1745. https://doi.org/10.4161/psb.6.11.17729

Kassambara, A., Mundt, F. (2020). *Factoextra: extract and visualize the results of multivariate data analyses*. R package *v.1.0.7*. URL https://CRAN.R-project.org/package=factoextra

Katsir, L., Schilmiller, A.L., Staswick, P.E., He, S.Y., and Howe, G.A. (2008). COI1 is a critical component of a receptor for jasmonate and the bacterial virulence factor coronatine. *Proceedings of the National Academy of Sciences* 105**,** 7100-7105.

Kazan, K. (2015). Diverse roles of jasmonates and ethylene in abiotic stress tolerance. *Trends in Plant Science*, *20*(4), 219–229. https://doi.org/10.1016/j.tplants.2015.02.001

Kazan, K., & Manners, J. M. (2009). Linking development to defense: auxin in plant–pathogen interactions. *Trends in Plant Science*, *14*(7), 373–382. https://doi.org/https://doi.org/10.1016/j.tplants.2009.04.005

Kim, S.-H., Shackel, K. A., & Lieth, J. H. (2004). Bending Alters Water Balance and Reduces Photosynthesis of Rose Shoots. *Journal of the American Society for Horticultural Science Jashs*, *129*(6), 896–901. https://doi.org/10.21273/JASHS.129.6.0896

Kısa, D., Elmastaş, M., Öztürk, L., & Kayır, Ö. (2016). Responses of the phenolic compounds of Zea mays under heavy metal stress. *Applied Biological Chemistry*, *59*(6), 813–820. https://doi.org/10.1007/s13765-016-0229-9

Klutsch, J.G., Najar, A., Cale, J.A., Erbilgin, N. (2016). Direction of interaction between mountain pine beetle (*Dendroctonus ponderosae*) and resource-sharing wood-boring beetles depends on plant parasite infection. *Oecologia*. doi.org/10.1007/s00442-016-3559-8

Klutsch, J.G., Najar, A., Sherwood, P., Bonello, P., Erbilgin, N. (2017). A native parasitic plant systemically induces resistance in jack pine to a fungal symbiont of invasive mountain pine beetle. *Journal of Chemical Ecology*. doi.org/10.1007/s10886-017-0845-9

Kolbe, A.R., Brutnell, T.P., Cousins, A.B., and Studer, A.J. (2018). Carbonic anhydrase mutants in *Zea mays* have altered stomatal responses to environmental signals. *Plant Physiology* 177**,** 980-989.

Kopylova, E., Noé, L., & Touzet, H. (2012). SortMeRNA: fast and accurate filtering of ribosomal RNAs in metatranscriptomic data. *Bioinformatics*, *28*(24), 3211–3217. https://doi.org/10.1093/bioinformatics/bts611

Koricheva, J., Larsson, S., Haukioja, E., and Keinanen, M. (1998). Regulation of woody plant secondary metabolism by resource availability: hypothesis testing by means of meta-analysis. *Oikos* 83**,** 212-226.

Kranner, I., Minibayeva, F. V., Beckett, R. P., & Seal, C. E. (2010). What is stress? Concepts, definitions and applications in seed science. *New Phytologist*, *188*(3), 655–673. https://doi.org/10.1111/j.1469-8137.2010.03461.x

Krokene, P. (2015). *Chapter 5 - Conifer Defense and Resistance to Bark Beetles* (F. E. Vega & R. W. B. T.-B. B. Hofstetter (eds.); pp. 177–207). Academic Press. https://doi.org/https://doi.org/10.1016/B978-0-12-417156-5.00005-8

Krokene, P., Solheim, H., Krekling, T., & Christiansen, E. (2003). Inducible anatomical defense responses in Norway spruce stems and their possible role in induced resistance. *Tree Physiology*, *23*(3), 191–197. https://doi.org/10.1093/treephys/23.3.191

Kubo, I. 2006. New concept to search for alternate insect control agents from plants. *Advances in Phytomedicine*. doi.org/10.1016/S1572-557X(06)03004-2

Kuc J (1983) Induced Systemic Resistance in Plants to Diseases Caused by Fungi and Bacteria. In: Bailey JA, Deverall BJ (eds) The Dynamics of Host Defence. Academic Press, Sydney, pp 191-221.

Kumar, M., Kesawat, M. S., Ali, A., Lee, S.-C., Gill, S. S., & Kim, H. U. (2019). Integration of Abscisic Acid Signaling with Other Signaling Pathways in Plant Stress Responses and Development. In *Plants* (Vol. 8, Issue 12). https://doi.org/10.3390/plants8120592

Kunert, N., Hajek, P., Hietz, P., Morris, H., Rosner, S., & Tholen, D. (2022). Summer temperatures reach the thermal tolerance threshold of photosynthetic decline in temperate conifers. *Plant Biology*, *24*(7), 1254–1261. https://doi.org/https://doi.org/10.1111/plb.13349

Kuromori, T., Seo, M., & Shinozaki, K. (2018). ABA Transport and Plant Water Stress Responses. *Trends in Plant Science*, *23*(6), 513–522. https://doi.org/10.1016/j.tplants.2018.04.001

Kwon, Y., Kim, S.-H., Jung, M.-S., Kim, M.-S., Oh, J.-E., Ju, H.-W., Kim, K., Vierling, E., Lee, H., & Hong, S.-W. (2007). Arabidopsis hot2 encodes an endochitinase-like protein that is essential for tolerance to heat, salt and drought stresses. *The Plant Journal*, *49*(2), 184–193. https://doi.org/https://doi.org/10.1111/j.1365-313X.2006.02950.x

La Porta, N., Capretti, P., Thomsen, I.M., Kasanen, R., Hietala, A.M., and Von Weissenberg, K. (2008). Forest pathogens with higher damage potential due to climate change in Europe. *Canadian Journal of Plant Pathology* 30**,** 177-195.

Labboun, S., Tercé-Laforgue, T., Roscher, A., Bedu, M., Restivo, F.M., Velanis, C.N., Skopelitis, D.S., Moshou, P.N., Roubelakis-Angelakis, K.A., Suzuki, A., and Hirel, B. (2009). Resolving the role of plant glutamate dehydrogenase. I. In vivo real time nuclear magnetic resonance spectroscopy experiments. *Plant and Cell Physiology* 50**,** 1761-1773.

Lackus, N.D., Lackner, S., Gershenzon, J., Unsicker, S.B., Köllner, T.G. (2018). The occurrence and formation of monoterpenes in herbivore-damaged poplar roots. *Scientific Reports*. doi.org/10.1038/s41598-018-36302-6

Lavy, M., & Estelle, M. (2016). Mechanisms of auxin signaling. *Development*, *143*(18), 3226–3229. https://doi.org/10.1242/dev.131870

Leba, L.-J., Cheval, C., Ortiz-Martín, I., Ranty, B., Beuzón, C.R., Galaud, J.-P., and Aldon, D. (2012). CML9, an *Arabidopsis* calmodulin-like protein, contributes to plant innate immunity through a flagellin-dependent signalling pathway. *The Plant Journal* 71**,** 976-989.

Lebeda, A., & Burdon, J. J. (2022). Studying Wild Plant Pathosystems to Understand Crop Plant Pathosystems: Status, Gaps, Challenges, and Perspectives. *Phytopathology®*, *113*(3), 365–380. https://doi.org/10.1094/PHYTO-01-22-0018-PER

Li, R., Tee, C.S., Jiang, Y.L., Jiang, X.Y., Venkatesh, P.N., Sarojam, R., Ye, J. (2015). A terpenoid phytoalexin plays a role in basal defense of *Nicotiana benthamiana* against potato virus X. *Scientific Reports*. doi.org/10.1038/srep09682

Li, D., Halitschke, R., Baldwin, I. T., & Gaquerel, E. (2023). Information theory tests critical predictions of plant defense theory for specialized metabolism. *Science Advances*, *6*(24), eaaz0381. https://doi.org/10.1126/sciadv.aaz0381

Li, G., Chen, T., Zhang, Z., Li, B., & Tian, S. (2020). Roles of Aquaporins in Plant-Pathogen Interaction. In *Plants* (Vol. 9, Issue 9). https://doi.org/10.3390/plants9091134

Li, J., Brader, G.N., and Palva, E.T. (2004). The WRKY70 transcription factor: a node of convergence for jasmonate-mediated and salicylate-mediated signals in plant defense. *The Plant Cell* 16**,** 319-331.

Li, M., Yu, G., Cao, C., & Liu, P. (2021). Metabolism, signaling, and transport of jasmonates. *Plant Communications*, *2*(5), 100231. https://doi.org/https://doi.org/10.1016/j.xplc.2021.100231

Li, Q., Zheng, J., Li, S., Huang, G., Skilling, S. J., Wang, L., Li, L., Li, M., Yuan, L., & Liu, P. (2017). Transporter-Mediated Nuclear Entry of Jasmonoyl-Isoleucine Is Essential for Jasmonate Signaling. *Molecular Plant*, *10*(5), 695–708. https://doi.org/10.1016/j.molp.2017.01.010

Lichtenthaler, H. K. (1996). Vegetation Stress: an Introduction to the Stress Concept in Plants. *Journal of Plant Physiology*, *148*(1), 4–14. https://doi.org/https://doi.org/10.1016/S0176-1617(96)80287-2

Lipiec, J., Doussan, C., Nosalewicz, A., & Kondracka, K. (2013). Effect of drought and heat stresses on plant growth and yield: A review. *International Agrophysics*, *27*(4), 463–477. https://doi.org/10.2478/intag-2013-0017

Liu, P.-P., von Dahl, C. C., & Klessig, D. F. (2011). The Extent to Which Methyl Salicylate Is Required for Signaling Systemic Acquired Resistance Is Dependent on Exposure to Light

after Infection. *Plant Physiology*, *157*(4), 2216–2226. https://doi.org/10.1104/pp.111.187773

Liu, Q., Luo, L., & Zheng, L. (2018). Lignins: Biosynthesis and Biological Functions in Plants. In *International Journal of Molecular Sciences* (Vol. 19, Issue 2). https://doi.org/10.3390/ijms19020335

Logemann, E., Reinold, S., Somssich, I.E., and Hahlbrock, K. (1997). A novel type of pathogen defense-related cinnamyl alcohol dehydrogenase. *Biological Chemistry* 378**,** 909-914.

Lohse, M., Nagel, A., Herter, T., May, P., Schroda, M., Zrenner, R., Tohge, T., Fernie, A.R., Stitt, M., and Usadel, B. (2014). Mercator: A fast and simple web server for genome scale functional annotation of plant sequence data. *Plant, Cell and Environment* 37**,** 1250-1258.

López-Villamor, A., Zas, R., Pérez, A., Cáceres, Y., Nunes da Silva, M., Vasconcelos, M., Vázquez-González, C., Sampedro, L., Solla, A. (2021). Traumatic resin ducts induced by methyl jasmonate in *Pinus* spp. *Trees - Structure and Function*. doi.org/10.1007/s00468-020-02057-9

Love, M. I., Huber, W., & Anders, S. (2014). Moderated estimation of fold change and dispersion for RNA-seq data with DESeq2. *Genome Biology*, *15*(12), 550. https://doi.org/10.1186/s13059-014-0550-8

Luchi, N., Longa, C.M.O., Danti, R., Capretti, P., and Maresi, G. (2014). *Diplodia sapinea*: the main fungal species involved in the colonization of pine shoots in Italy. *Forest Pathology* 44**,** 372-381.

Luchi, N., Ma, R., Capretti, P., & Bonello, P. (2005). Systemic induction of traumatic resin ducts and resin flow in Austrian pine by wounding and inoculation with Sphaeropsis sapinea and Diplodia scrobiculata. *Planta*, *221*(1), 75–84. https://doi.org/10.1007/s00425-004-1414-3

Luchi, N., Mancini, V., Feducci, M., Santini, A., and Capretti, P. (2012). *Leptoglossus occidentalis* and *Diplodia pinea*: a new insect-fungus association in Mediterranean forests. *Forest Pathology* 42**,** 246-251.

Ma, W., Smigel, A., Tsai, Y.-C., Braam, J., and Berkowitz, G.A. (2008). Innate immunity signaling: cytosolic Ca^{2+} elevation is linked to downstream nitric oxide generation

through the action of calmodulin or a calmodulin-like protein. *Plant Physiology* 148**,** 818-828.

Manzanos, T., Aragonés, A., & Iturritxa, E. (2017). *Diplodia scrobiculata*: a latent pathogen of *Pinus radiata* reported in northern Spain. *Phytopathologia Mediterranea*, 56(2), 274–277. http://www.jstor.org/stable/44809345

Marchiosi, R., dos Santos, W. D., Constantin, R. P., de Lima, R. B., Soares, A. R., Finger-Teixeira, A., Mota, T. R., de Oliveira, D. M., Foletto-Felipe, M. de P., Abrahão, J., & Ferrarese-Filho, O. (2020). Biosynthesis and metabolic actions of simple phenolic acids in plants. *Phytochemistry Reviews*, *19*(4), 865–906. https://doi.org/10.1007/s11101-020-09689-2

Mauch-Mani, B., & Mauch, F. (2005). The role of abscisic acid in plant–pathogen interactions. *Current Opinion in Plant Biology*, *8*(4), 409–414. https://doi.org/https://doi.org/10.1016/j.pbi.2005.05.015

Mehdi, K., Thierie, J., and Penninckx, M.J. (2001). γ-Glutamyl transpeptidase in the yeast *Saccharomyces cerevisiae* and its role in the vacuolar transport and metabolism of glutathione. *Biochemical Journal* 359**,** 631-637.

Michaud, M., and Jouhet, J. (2019). Lipid trafficking at membrane contact sites during plant development and stress response. *Frontiers in Plant Science* 10.

Miedes, E., Vanholme, R., Boerjan, W., and Molina, A. (2014). The role of the secondary cell wall in plant resistance to pathogens. *Frontiers in Plant Science* 5.

Miller, B., Madilao, L.L., Ralph, S., Bohlmann, J. (2005). Insect-induced conifer defense. White pine weevil and methyl jasmonate induce traumatic resinosis, *de novo* formed volatile emissions, and accumulation of terpenoid synthase and putative octadecanoid pathway transcripts in sitka spruce. *Plant Physiology*. doi.org/10.1104/pp.104.050187

Mohamed, H. I., El-Shazly, H. H., & Badr, A. (2020). *Role of Salicylic Acid in Biotic and Abiotic Stress Tolerance in Plants BT - Plant Phenolics in Sustainable Agriculture: Volume 1* (R. Lone, R. Shuab, & A. N. Kamili (eds.); pp. 533–554). Springer Singapore. https://doi.org/10.1007/978-981-15-4890-1_23

Molitor, A., Zajic, D., Voll, L. M., Pons-Kühnemann, J., Samans, B., Kogel, K.-H., & Waller, F. (2011). Barley Leaf Transcriptome and Metabolite Analysis Reveals New Aspects of Compatibility and Piriformospora indica–Mediated Systemic Induced Resistance to Powdery Mildew. *Molecular Plant-Microbe Interactions®*, *24*(12), 1427–1439. https://doi.org/10.1094/MPMI-06-11-0177

Morris, H., Hietala, A.M., Jansen, S., Ribera, J., Rosner, S., Salmeia, K.A., Schwarze, F.W.M.R. (2020). Using the CODIT model to explain secondary metabolites of xylem in defence systems of temperate trees against decay fungi. *Annals of Botany*. doi.org/10.1093/aob/mcz138

Moss, G.P., Smith, P.A.S., Tavernier, D. (1995). Glossary of class names of organic compounds and reactive intermediates based on structure (IUPAC recommendations 1995). *Pure and Applied Chemistry*. doi.org/10.1351/pac199567081307

Mott, G. A., Thakur, S., Smakowska, E., Wang, P. W., Belkhadir, Y., Desveaux, D., & Guttman, D. S. (2016). Genomic screens identify a new phytobacterial microbe-associated molecular pattern and the cognate Arabidopsis receptor-like kinase that mediates its immune elicitation. *Genome Biology*, *17*(1), 98. https://doi.org/10.1186/s13059-016-0955-7

Naidoo, S., Visser, E.A., Zwart, L., Toit, Y.D., Bhadauria, V., and Shuey, L.S. (2018). Dual RNA-sequencing to elucidate the plant-pathogen duel. *Current Issues in Molecular Biology* 27**,** 127-142.

Naikoo, M. I., Dar, M. I., Raghib, F., Jaleel, H., Ahmad, B., Raina, A., Khan, F. A., & Naushin, F. (2019). *Chapter 9 - Role and Regulation of Plants Phenolics in Abiotic Stress Tolerance: An Overview* (M. I. R. Khan, P. S. Reddy, A. Ferrante, & N. A. B. T.-P. S. M. Khan (eds.); pp. 157–168). Woodhead Publishing. https://doi.org/https://doi.org/10.1016/B978-0-12-816451-8.00009-5

Natita, W., Wiboonsak, W., Dusadee, S. (2016). Appropriate learning rate and neighborhood function of self-organizing map (SOM) for specific humidity pattern classification over Southern Thailand. *International Journal of Modeling and Optimization*. doi.org/10.7763/ijmo.2016.v6.504

Neilson, E. H., Goodger, J. Q. D., Woodrow, I. E., & Møller, B. L. (2013). Plant chemical defense: at what cost? *Trends in Plant Science*, *18*(5), 250–258. https://doi.org/https://doi.org/10.1016/j.tplants.2013.01.001

Newman, M.-A., Sundelin, T., Nielsen, J., & Erbs, G. (2013). MAMP (microbe-associated molecular pattern) triggered immunity in plants . In *Frontiers in Plant Science* (Vol. 4). https://www.frontiersin.org/articles/10.3389/fpls.2013.00139

Ng, L. M., Melcher, K., Teh, B. T., & Xu, H. E. (2014). Abscisic acid perception and signaling: structural mechanisms and applications. *Acta Pharmacologica Sinica*, *35*(5), 567–584. https://doi.org/10.1038/aps.2014.5

Nguyen, Q.-M., Iswanto, A. B., Son, G. H., & Kim, S. H. (2021). Recent Advances in Effector-Triggered Immunity in Plants: New Pieces in the Puzzle Create a Different Paradigm. In *International Journal of Molecular Sciences* (Vol. 22, Issue 9). https://doi.org/10.3390/ijms22094709

Nicaise, V., Roux, M., & Zipfel, C. (2009). Recent Advances in PAMP-Triggered Immunity against Bacteria: Pattern Recognition Receptors Watch over and Raise the Alarm. *Plant Physiology*, *150*(4), 1638–1647. https://doi.org/10.1104/pp.109.139709

Niraula, P.M., Zhang, X., Jeremic, D., Lawrence, K.S., and Klink, V.P. (2021). Xyloglucan endotransglycosylase/hydrolase increases tightly-bound xyloglucan and chain number but decreases chain length contributing to the defense response that *Glycine max* has to *Heterodera glycines*. *PLOS ONE* 16**,** e0244305.

NIST. (2017). *NIST mass spectral database for NIST/EPA/NIH and mass spectral search program (version 2.3)*. Maryland, USA: The National Institute of Standards and Technology NIST. URL http://www.nist.gov/srd/

Noor, W., Majeed, G., Lone, R., Tyub, S., Kamili, A. N., & Azeez, A. (2023). *Interactive Role of Phenolics and PGPR in Alleviating Heavy Metal Toxicity in Wheat BT - Plant Phenolics in Abiotic Stress Management* (R. Lone, S. Khan, & A. Mohammed Al-Sadi (eds.); pp. 287–320). Springer Nature Singapore. https://doi.org/10.1007/978-981-19-6426-8_14

Ockels, F.S., Eyles, A., McPherson, B.A., Wood, D.L., Bonello, P. (2007). Phenolic chemistry of coast live oak response to *Phytophthora ramorum* infection. *Journal of Chemical Ecology*. doi.org/10.1007/s10886-007-9332-z

Oka, Y., Cohen, Y., & Spiegel, Y. (1999). Local and Systemic Induced Resistance to the Root-Knot Nematode in Tomato by DL-β-Amino-n-Butyric Acid. *Phytopathology®*, *89*(12), 1138–1143. https://doi.org/10.1094/PHYTO.1999.89.12.1138

Oksanen, A.J., Blanchet, F.G., Friendly, M., Kindt, R., Legendre, P., Mcglinn, D., Minchin, P.R., Hara, R.B.O., Simpson, G.L., Solymos, P. et al. (2020). *Vegan: community ecology package.* R package *v.2.4.3*. URL https://CRAN.R-project.org/package=vegan

Ondov, B. D., Bergman, N. H., & Phillippy, A. M. (2011). Interactive metagenomic visualization in a Web browser. *BMC Bioinformatics*, *12*(1), 385. https://doi.org/10.1186/1471-2105-12-385

Paysan-Lafosse, T., Blum, M., Chuguransky, S., Grego, T., Pinto, B. L., Salazar, G. A., Bileschi, M. L., Bork, P., Bridge, A., Colwell, L., Gough, J., Haft, D. H., Letunić, I., Marchler-Bauer, A., Mi, H., Natale, D. A., Orengo, C. A., Pandurangan, A. P., Rivoire, C., … Bateman, A. (2023). InterPro in 2022. *Nucleic Acids Research*, *51*(D1), D418–D427. https://doi.org/10.1093/nar/gkac993

Pichersky, E., & Lewinsohn, E. (2011). Convergent Evolution in Plant Specialized Metabolism. *Annual Review of Plant Biology*, *62*(1), 549–566. https://doi.org/10.1146/annurev-arplant-042110-103814

Pieterse, C. M. J., Van der Does, D., Zamioudis, C., Leon-Reyes, A., & Van Wees, S. C. M. (2012). Hormonal Modulation of Plant Immunity. *Annual Review of Cell and Developmental Biology*, *28*(1), 489–521. https://doi.org/10.1146/annurev-cellbio-092910-154055

Pieterse, C. M. J., Van der Does, D., Zamioudis, C., Leon-Reyes, A., & Van Wees, S. C. M. (2012). Hormonal Modulation of Plant Immunity. *Annual Review of Cell and Developmental Biology*, *28*(1), 489–521. https://doi.org/10.1146/annurev-cellbio-092910-154055

Pieterse, C. M. J., Zamioudis, C., Berendsen, R. L., Weller, D. M., Van Wees, S. C. M., & Bakker, P. A. H. M. (2014). Induced Systemic Resistance by Beneficial Microbes. *Annual Review of Phytopathology*, *52*(1), 347–375. https://doi.org/10.1146/annurev-phyto-082712-102340

Plant Disease Diagnostic Clinic. (2008). *Diplodia Tip Blight: Sphaeropsis sapinea*. 1–3.

Plata-Rueda, A., Campos, J. M., da Silva Rolim, G., Martínez, L. C., Dos Santos, M. H., Fernandes, F. L., Serrão, J. E., & Zanuncio, J. C. (2018). Terpenoid constituents of cinnamon and clove essential oils cause toxic effects and behavior repellency response on granary weevil, Sitophilus granarius. *Ecotoxicology and Environmental Safety*, *156*, 263–270. https://doi.org/https://doi.org/10.1016/j.ecoenv.2018.03.033

Polishchuk, O.V. (2021). Stress-related changes in the expression and activity of plant carbonic anhydrases. *Planta* 253**,** 58.

Poole, R. L. (2007). The TAIR database. *Methods in molecular biology (Clifton, N.J.)*, 406, 179–212. https://doi.org/10.1007/978-1-59745-535-0_8

Potvin, C. (2000). "ANOVA: Experimental Layout and Analysis," in *Design and analysis of ecological experiments,* eds. S.M. Scheiner & J. Gurevitch. 2nd ed ed (New York: Oxford University Press), xvi, 415 p.

Prates, H.T., Santos, J.P., Waquil, J.M., Fabris, J.D., Oliveira, A.B., Foster, J.E. (1998). Insecticidal activity of monoterpenes against *Rhyzopertha dominica* (F.) and *Tribolium castaneum* (Herbst). *Journal of Stored Products Research*. doi.org/10.1016/S0022-474X(98)00005-8

R Core Team. (2021). R: A language and environment for statistical computing. R Foundation for Statistical Computing, Vienna, Austria. https://www.R-project.org/

R Core Team. (2022). *R: a language and environment for statistical computing*. Vienna, Austria: R Foundation for Statistical Computing. URL http://www.R-project.org/

Ramírez-Zavaleta, C. Y., García-Barrera, L. J., Rodríguez-Verástegui, L. L., Arrieta-Flores, D., & Gregorio-Jorge, J. (2022). An Overview of PRR- and NLR-Mediated Immunities: Conserved Signaling Components across the Plant Kingdom That Communicate Both Pathways. In *International Journal of Molecular Sciences* (Vol. 23, Issue 21). https://doi.org/10.3390/ijms232112974

Rathore, J. S., & Ghosh, C. (2018). *Pathogen-Associated Molecular Patterns and Their Perception in Plants BT - Molecular Aspects of Plant-Pathogen Interaction* (A. Singh & I. K. Singh (eds.); pp. 79–113). Springer Singapore. https://doi.org/10.1007/978-981-10-7371-7_4

René, A., Abasq, M.-L., Hauchard, D., & Hapiot, P. (2010). How Do Phenolic Compounds React toward Superoxide Ion? A Simple Electrochemical Method for Evaluating Antioxidant Capacity. *Analytical Chemistry*, *82*(20), 8703–8710. https://doi.org/10.1021/ac101854w

Riedlmeier, M., Ghirardo, A., Wenig, M., Knappe, C., Koch, K., Georgii, E., Dey, S., Parker, J. E., Schnitzler, J.-P., & Vlot, A. C. (2017). Monoterpenes Support Systemic Acquired Resistance within and between Plants. *The Plant Cell*, *29*(6), 1440–1459. https://doi.org/10.1105/tpc.16.00898

Rieseberg, T. P., Dadras, A., Fürst-Jansen, J. M. R., Dhabalia Ashok, A., Darienko, T., de Vries, S., Irisarri, I., & de Vries, J. (2023). Crossroads in the evolution of plant specialized metabolism. *Seminars in Cell & Developmental Biology*, *134*, 37–58. https://doi.org/https://doi.org/10.1016/j.semcdb.2022.03.004

Rizzo, J., Stanchev, L.D., Da Silva, V.K.A., Nimrichter, L., Pomorski, T.G., and Rodrigues, M.L. (2019). Role of lipid transporters in fungal physiology and pathogenicity. *Computational and Structural Biotechnology Journal* 17**,** 1278-1289.

Robertson, G., Schein, J., Chiu, R., Corbett, R., Field, M., Jackman, S. D., Mungall, K., Lee, S., Okada, H. M., Qian, J. Q., Griffith, M., Raymond, A., Thiessen, N., Cezard, T., Butterfield, Y. S., Newsome, R., Chan, S. K., She, R., Varhol, R., … Birol, I. (2010). De novo assembly and analysis of RNA-seq data. *Nature Methods*, *7*(11), 909–912. https://doi.org/10.1038/nmeth.1517

Robinson, M.D., Mccarthy, D.J., and Smyth, G.K. (2010). edgeR: a Bioconductor package for differential expression analysis of digital gene expression data. *Bioinformatics* 6, 139–140.

Rodrigues, A. M., Langer, S., Carrasquinho, I., Bergström, E., Larson, T., Thomas-Oates, J., & António, C. (2021). Pinus pinaster Early Hormonal Defence Responses to Pinewood Nematode (Bursaphelenchus xylophilus) Infection. In *Metabolites* (Vol. 11, Issue 4). https://doi.org/10.3390/metabo11040227

Rossi, F. R., Gárriz, A., Marina, M., Romero, F. M., Gonzalez, M. E., Collado, I. G., & Pieckenstain, F. L. (2011). The Sesquiterpene Botrydial Produced by Botrytis cinerea Induces the Hypersensitive Response on Plant Tissues and Its Action Is Modulated by Salicylic Acid and Jasmonic Acid Signaling. *Molecular Plant-Microbe Interactions®*, *24*(8), 888–896. https://doi.org/10.1094/MPMI-10-10-0248

Sade, N., Shatil-Cohen, A., Attia, Z., Maurel, C., Boursiac, Y., Kelly, G., Granot, D., Yaaran, A., Lerner, S., & Moshelion, M. (2014). The Role of Plasma Membrane Aquaporins in Regulating the Bundle Sheath-Mesophyll Continuum and Leaf Hydraulics . *Plant Physiology*, *166*(3), 1609–1620. https://doi.org/10.1104/pp.114.248633

Saijo, Y., Loo, E. P., & Yasuda, S. (2018). Pattern recognition receptors and signaling in plant–microbe interactions. *The Plant Journal*, *93*(4), 592–613. https://doi.org/https://doi.org/10.1111/tpj.13808

Santamaria, O., Smith, D.R., and Stanosz, G.R. (2011). Interaction between *Diplodia pinea* and *D. scrobiculata* in red and jack pine seedlings. *Phytopathology* 101**,** 334-339.

Santino, A., Taurino, M., De Domenico, S., Bonsegna, S., Poltronieri, P., Pastor, V., & Flors, V. (2013). Jasmonate signaling in plant development and defense response to multiple (a)biotic stresses. *Plant Cell Reports*, *32*(7), 1085–1098. https://doi.org/10.1007/s00299-013-1441-2

Savatin, D. V, Gramegna, G., Modesti, V., & Cervone, F. (2014). Wounding in the plant tissue: the defense of a dangerous passage. In *Frontiers in Plant Science* (Vol. 5). https://www.frontiersin.org/articles/10.3389/fpls.2014.00470

Schoenherr, A. P., Rizzo, E., Jackson, N., Manosalva, P., & Gomez, S. K. (2019). Mycorrhiza-Induced Resistance in Potato Involves Priming of Defense Responses Against Cabbage Looper (Noctuidae: Lepidoptera). *Environmental Entomology*, *48*(2), 370–381. https://doi.org/10.1093/ee/nvy195

Shabala, S., & Pottosin, I. (2014). Regulation of potassium transport in plants under hostile conditions: implications for abiotic and biotic stress tolerance. *Physiologia Plantarum*, *151*(3), 257–279. https://doi.org/https://doi.org/10.1111/ppl.12165

Shah, J., and Zeier, J. (2013). Long-distance communication and signal amplification in systemic acquired resistance. *Frontiers in Plant Science* 4.

Shalaby, S., & Horwitz, B. A. (2015). Plant phenolic compounds and oxidative stress: integrated signals in fungal–plant interactions. *Current Genetics*, *61*(3), 347–357. https://doi.org/10.1007/s00294-014-0458-6

Sherwood, P., & Bonello, P. (2013). Austrian pine phenolics are likely contributors to systemic induced resistance against Diplodia pinea. *Tree Physiology*, *33*(8), 845–854. https://doi.org/10.1093/treephys/tpt063

Sherwood, P., & Bonello, P. (2016). Testing the systemic induced resistance hypothesis with Austrian pine and Diplodia sapinea. *Physiological and Molecular Plant Pathology*, *94*, 118–125. https://doi.org/https://doi.org/10.1016/j.pmpp.2016.06.002

Sherwood, P., Villari, C., Capretti, P., & Bonello, P. (2015). Mechanisms of induced susceptibility to Diplodia tip blight in drought-stressed Austrian pine. *Tree Physiology*, *35*(5), 549–562. https://doi.org/10.1093/treephys/tpv026

Shimizu, T., Nakano, T., Takamizawa, D., Desaki, Y., Ishii-Minami, N., Nishizawa, Y., Minami, E., Okada, K., Yamane, H., Kaku, H., & Shibuya, N. (2010). Two LysM receptor molecules, CEBiP and OsCERK1, cooperatively regulate chitin elicitor signaling in rice. *The Plant Journal*, *64*(2), 204–214. https://doi.org/https://doi.org/10.1111/j.1365-313X.2010.04324.x

Singh, H.P., Batish, D.R., Kaur, S., Arora, K., Kohli, R.K. (2006). *α*-Pinene inhibits growth and induces oxidative stress in roots. *Annals of Botany*. doi.org/10.1093/aob/mcl213

Singh, A., Guest, D., & Copeland, L. (2015). Associations Between Glucosinolates, White Rust, and Plant Defense Activators in Brassica Plants: A Review. *International Journal of Vegetable Science*, *21*(3), 297–313. https://doi.org/10.1080/19315260.2013.832465

Singh, S. K. (2018). *Explorations of Plant's Chemodiversity: Role of Nitrogen-Containing Secondary Metabolites in Plant Defense BT - Molecular Aspects of Plant-Pathogen Interaction* (A. Singh & I. K. Singh (eds.); pp. 309–332). Springer Singapore. https://doi.org/10.1007/978-981-10-7371-7_14

Slippers, B., and Wingfield, M.J. (2007). Botryosphaeriaceae as endophytes and latent pathogens of woody plants: diversity, ecology and impact. *Fungal Biology Reviews* 21**,** 90-106.

Smith, D. R., & Stanosz, G. R. (2006). A Species-Specific PCR Assay for Detection of Diplodia pinea and D. scrobiculata in Dead Red and Jack Pines with Collar Rot Symptoms. *Plant Disease*, *90*(3), 307–313. https://doi.org/10.1094/PD-90-0307

Soneson, C., Love, M. I., Robinson, M. D. (2015) Differential analyses for RNA-seq: transcript-level estimates improve gene-level inferences [version 1; peer review: 2 approved]. *F1000Research*, 4:1521. https://doi.org/10.12688/f1000research.7563.1

Song, L., & Florea, L. (2015). Rcorrector: efficient and accurate error correction for Illumina RNA-seq reads. *GigaScience*, *4*(1), s13742-015-0089-y. https://doi.org/10.1186/s13742-015-0089-y

Sphaeropsis sapinea (Sphaeropsis blight). (2023). In *CABI Compendium*. CABI Compendium. https://doi.org/10.1079/cabicompendium.19160

Stamp, N. (2003). Out of the Quagmire of Plant Defense Hypotheses. *The Quarterly Review of Biology*, *78*(1), 23–55. https://doi.org/10.1086/367580

Stanke, M., Diekhans, M., Baertsch, R., and Haussler, D. (2008). Using native and syntenically mapped cDNA alignments to improve de novo gene finding. *Bioinformatics* 24**,** 637-644.

Stortenbeker, N., & Bemer, M. (2019). The SAUR gene family: the plant's toolbox for adaptation of growth and development. *Journal of Experimental Botany*, *70*(1), 17–27. https://doi.org/10.1093/jxb/ery332

Sturrock, R.N., Frankel, S.J., Brown, A.V., Hennon, P.E., Kliejunas, J.T., Lewis, K.J., Worrall, J.J., and Woods, A.J. (2011). Climate change and forest diseases. *Plant Pathology* 60**,** 133-149.

Sun, L., & Zhang, J. (2020). Regulatory role of receptor-like cytoplasmic kinases in early immune signaling events in plants. *FEMS Microbiology Reviews*, *44*(6), 845–856. https://doi.org/10.1093/femsre/fuaa035

Sun, T., & Zhang, Y. (2021). Short- and long-distance signaling in plant defense. *The Plant Journal*, *105*(2), 505–517. https://doi.org/https://doi.org/10.1111/tpj.15068

Survila, M., Davidsson, P.R., Pennanen, V., Kariola, T., Broberg, M., Sipari, N., Heino, P., and Palva, E.T. (2016). Peroxidase-generated apoplastic ROS impair cuticle integrity and contribute to DAMP-elicited defenses. *Frontiers in Plant Science* 7.

Swett, C. L., Kirkpatrick, S. C., & Gordon, T. R. (2015). Evidence for a Hemibiotrophic Association of the Pitch Canker Pathogen Fusarium circinatum with Pinus radiata. *Plant Disease*, *100*(1), 79–84. https://doi.org/10.1094/PDIS-03-15-0270-RE

Taiz, L., Zeiger, E., Møller, M., & Murphy, A. (2018). Fundamentals of plant physiology. *Sinauer Associates*. ISBN 9781605357904, 7th edition, 116-118.

Takahashi, F., & Shinozaki, K. (2019). Long-distance signaling in plant stress response. *Current Opinion in Plant Biology*, *47*, 106–111. https://doi.org/https://doi.org/10.1016/j.pbi.2018.10.006

Tan, S. Y., & Yip, A. (2018). Hans Selye (1907-1982): Founder of the stress theory. *Singapore Medical Journal*, *59*(4), 170–171. https://doi.org/10.11622/smedj.2018043

Tang, S., Lomsadze, A., and Borodovsky, M. (2015). Identification of protein coding regions in RNA transcripts. *Nucleic Acids Research* 43**,** 1-10.

Thimm, O., Bläsing, O., Gibon, Y., Nagel, A., Meyer, S., Krüger, P., Selbig, J., Müller, L.A., Rhee, S.Y., and Stitt, M. (2004). MAPMAN: A user-driven tool to display genomics data sets onto diagrams of metabolic pathways and other biological processes. *Plant Journal* 37**,** 914-939.

Tholl, D. (2015). *Biosynthesis and Biological Functions of Terpenoids in Plants BT - Biotechnology of Isoprenoids* (J. Schrader & J. Bohlmann (eds.); pp. 63–106). Springer International Publishing. https://doi.org/10.1007/10_2014_295

Tibebu B. Defense Mechanisms of Plants to Insect Pests: From Morphological to Biochemical Approach. *Trends Tech Sci Res*. 2018; 2(2): 555584. DOI: 10.19080/TTSR.2018.02.555584

Toyota, M., Spencer, D., Sawai-Toyota, S., Jiaqi, W., Zhang, T., Koo, A. J., Howe, G. A., & Gilroy, S. (2018). Glutamate triggers long-distance, calcium-based plant defense signaling. *Science*, *361*(6407), 1112–1115. https://doi.org/10.1126/science.aat7744

Treena, B. I., Gordon, T. R., Wingfield, M. J., & Wingfield, B. D. (2004). Geographic isolation of *Diplodia scrobiculata* and its association with native *Pinus radiata*. *Mycological Research*, *108*(12)**,** 1399- 1406. https://doi.org/10.1017/S0953756204001443

Tronchet, M., Balagué, C., Kroj, T., Jouanin, L., and Roby, D. (2010). Cinnamyl alcohol dehydrogenases-C and D, key enzymes in lignin biosynthesis, play an essential role in disease resistance in Arabidopsis. *Molecular Plant Pathology* 11**,** 83-92.

Tsuda, K., & Katagiri, F. (2010). Comparing signaling mechanisms engaged in pattern-triggered and effector-triggered immunity. *Current Opinion in Plant Biology*, *13*(4), 459–465. https://doi.org/https://doi.org/10.1016/j.pbi.2010.04.006

Ullah, A., Klutsch, J.G., Erbilgin, N. (2021). Production of complementary defense metabolites reflects a co-evolutionary arms race between a host plant and a mutualistic bark beetle-fungal complex. *Plant Cell and Environment*. doi.org/10.1111/pce.14100

Usha Rani, P., & Pratyusha, S. (2014). Role of castor plant phenolics on performance of its two herbivores and their impact on egg parasitoid behaviour. *BioControl*, *59*(5), 513–524. https://doi.org/10.1007/s10526-014-9590-y

Vadez, V., Kholova, J., Choudhary, S., Zindy, P., Terrier, M., L., K., Pasala, R., & Turner, N. (2018). *Chapter 5.2 Responses to Increased Moisture Stress and Extremes: Whole Plant Response to Drought under Climate Change*.

Van Bel, A.J.E., Gaupels, F. (2004). Pathogen-induced resistance and alarm signals in the phloem. *Molecular Plant Pathology*. doi.org/10.1111/J.1364-3703.2004.00243.X

Van Der Nest, M.A., Bihon, W., De Vos, L., Naidoo, K., Roodt, D., Rubagotti, E., Slippers, B., Steenkamp, E.T., Markus Wilken, P., Wilson, A., Wingfield, M.J., and Wingfield, B.D. (2014). Draft genome sequences of *Diplodia sapinea*, *Ceratocystis manginecans*, and *Ceratocystis moniliformis*. *IMA Fungus* 5**,** 135-140.

van Loon, L. C. (1985). Pathogenesis-related proteins. *Plant Molecular Biology*, *4*(2), 111–116. https://doi.org/10.1007/BF02418757

VanHook, A. M. (2015). Plants kill pathogens with cyanide. *Science Signaling*, *8*(395), ec272–ec272. https://doi.org/10.1126/scisignal.aad4595

Verza, S.S., Nagamoto, N.S., Forti, L.C., Noronha, N.C. (2011). Preliminary studies on the effects of *d*-limonene to workers of the leaf-cutting ant *Atta sexdens rubropilosa* and its implications for control. *Bulletin of Insectology* 64(1): 27–32.

Vidhyasekaran, P. (2014). *PAMP Signaling in Plant Innate Immunity BT - PAMP Signals in Plant Innate Immunity: Signal Perception and Transduction* (P. Vidhyasekaran (ed.); pp. 17–161). Springer Netherlands. https://doi.org/10.1007/978-94-007-7426-1_2

Vincenzo Lattanzio, Veronica M. T. Lattanzio, and A. C. (2015). Role of phenolics in the resistance mechanisms of plants against fungal pathogens and insects. In *Phytochemistry* (Vol. 661, Issue 2).

Visser, E.A., Wegrzyn, J.L., Myburg, A.A., and Naidoo, S. (2018). Defence transcriptome assembly and pathogenesis related gene family analysis in *Pinus tecunumanii* (low elevation). *BMC Genomics* 19**,** 1-13.

Visser, E.A., Wegrzyn, J.L., Steenkamp, E.T., Myburg, A.A., and Naidoo, S. (2019). Dual RNA-seq analysis of the pine-*Fusarium circinatum* interaction in resistant (*Pinus tecunumanii*) and susceptible (*Pinus patula*) hosts. *Microorganisms* 7**,** 315.

Vlot, A. C., Sales, J. H., Lenk, M., Bauer, K., Brambilla, A., Sommer, A., Chen, Y., Wenig, M., & Nayem, S. (2021). Systemic propagation of immunity in plants. *New Phytologist*, *229*(3), 1234–1250. https://doi.org/https://doi.org/10.1111/nph.16953

Vos, C., Schouteden, N., van Tuinen, D., Chatagnier, O., Elsen, A., De Waele, D., Panis, B., & Gianinazzi-Pearson, V. (2013). Mycorrhiza-induced resistance against the root–knot nematode Meloidogyne incognita involves priming of defense gene responses in tomato. *Soil Biology and Biochemistry*, *60*, 45–54. https://doi.org/https://doi.org/10.1016/j.soilbio.2013.01.013

Wallis, C., Eyles, A., Chorbadjian, R. A., Riedl, K., Schwartz, S., Hansen, R., Cipollini, D., Herms, D. A., & Bonello, P. (2011). Differential effects of nutrient availability on the secondary metabolism of Austrian pine (Pinus nigra) phloem and resistance to Diplodia pinea. *Forest Pathology*, *41*(1), 52–58. https://doi.org/10.1111/j.1439-0329.2009.00636.x

Wallis, C., Eyles, A., Chorbadjian, R., McSpadden Gardener, B., Hansen, R., Cipollini, D., Herms, D. A., & Bonello, P. (2008). Systemic induction of phloem secondary metabolism and its relationship to resistance to a canker pathogen in Austrian pine. *New Phytologist*, *177*(3), 767–778. https://doi.org/https://doi.org/10.1111/j.1469-8137.2007.02307.x

Wallis, C., Lewandowski, D.J., Bonello, P. (2016). Diplodia Tip Blight of Two-Needled Pines. Ohioline. The Ohio State University Extension. https://ohioline.osu.edu/factsheet/plpath-tree-03

Walters, D. (2010). Plant defense: Warding off attack by pathogens, herbivores and parasitic plants. *John Wiley & Sons*, Incorporated. ISBN 9781444328554.

Walton, J. D. (1997). *13 - Biochemical Plant Pathology* (P. M. Dey & J. B. B. T.-P. B. Harborne (eds.); pp. 487–502). Academic Press. https://doi.org/https://doi.org/10.1016/B978-012214674-9/50014-X

Wang, Q., Xin, Z., Li, J., Hu, L., Lou, Y., Lu, J. (2015). (*E*)-*β*-caryophyllene functions as a host location signal for the rice white-backed planthopper *Sogatella furcifera*. *Physiological and Molecular Plant Pathology*. doi.org/10.1016/j.pmpp.2015.07.002

Wang, D., Eyles, A., Mandich, D., & Bonello, P. (2006). Systemic aspects of host–pathogen interactions in Austrian pine (Pinus nigra): A proteomics approach. *Physiological and Molecular Plant Pathology*, *68*(4), 149–157. https://doi.org/https://doi.org/10.1016/j.pmpp.2006.09.005

Wang, G., & Fiers, M. (2010). Receptor-like proteins: Searching for functions. *Plant Signaling & Behavior*, *5*(5), 540–542. https://doi.org/10.4161/psb.11030

War, A. R., Sharma, H. C., Paulraj, M. G., War, M. Y., & Ignacimuthu, S. (2011). Herbivore induced plant volatiles: Their role in plant defense for pest management. *Plant Signaling & Behavior*, *6*(12), 1973–1978. https://doi.org/10.4161/psb.6.12.18053

Wasternack, C. (2004). *9 - Jasmonates—Biosynthesis and Role in Stress Responses and Developmental Processes* (L. D. B. T.-P. C. D. P. Noodén (ed.); pp. 143–155). Academic Press. https://doi.org/https://doi.org/10.1016/B978-012520915-1/50012-6

Wehrens, R., Kruisselbrink, J. (2018). Flexible self-organizing maps in *kohonen* 3.0. *Journal of Statistical Software*. doi.org/10.18637/jss.v087.i07

Whitehill, J. G. A., Rigsby, C., Cipollini, D., Herms, D. A., & Bonello, P. (2014). Decreased emergence of emerald ash borer from ash treated with methyl jasmonate is associated with

induction of general defense traits and the toxic phenolic compound verbascoside. *Oecologia*, *176*(4), 1047–1059. https://doi.org/10.1007/s00442-014-3082-8

Wilkinson, S. W., Magerøy, M. H., López Sánchez, A., Smith, L. M., Furci, L., Cotton, T. E. A., Krokene, P., & Ton, J. (2019). Surviving in a Hostile World: Plant Strategies to Resist Pests and Diseases. *Annual Review of Phytopathology*, *57*(1), 505–529. https://doi.org/10.1146/annurev-phyto-082718-095959

Williams, A.P., Allen, C.D., Macalady, A.K., Griffin, D., Woodhouse, C.A., Meko, D.M., Swetnam, T.W., Rauscher, S.A., Seager, R., Grissino-Mayer, H.D., Dean, J.S., Cook, E.R., Gangodagamage, C., Cai, M., and Mcdowell, N.G. (2013). Temperature as a potent driver of regional forest drought stress and tree mortality. *Nature Climate Change* 3**,** 292-297.

Wood, D. E., Lu, J., & Langmead, B. (2019). Improved metagenomic analysis with Kraken 2. *Genome Biology*, *20*(1), 257. https://doi.org/10.1186/s13059-019-1891-0

Wright, C. A., & Beattie, G. A. (2004). Pseudomonas syringae pv. tomato cells encounter inhibitory levels of water stress during the hypersensitive response of Arabidopsis thaliana. *Proceedings of the National Academy of Sciences*, *101*(9), 3269–3274. https://doi.org/10.1073/pnas.0400461101

Xu, L., Shi, Z., Wang, B., Lu, M., Sun, J. (2016). Pine defensive monoterpene *α*-pinene influences the feeding behavior of *Dendroctonus valens* and its gut bacterial community structure. *International Journal of Molecular Sciences*. doi.org/10.3390/ijms17111734

Yamawaki, C., Oyama, M., Yamaguchi, Y., Ogita, A., Tanaka, T., Fujita, K.I. (2019). Curcumin potentiates the fungicidal effect of dodecanol by inhibiting drug efflux in wild-type budding yeast. *Letters in Applied Microbiology*. doi.org/10.1111/lam.13083

Yu, Y., Gui, Y., Li, Z., Jiang, C., Guo, J., & Niu, D. (2022). Induced Systemic Resistance for Improving Plant Immunity by Beneficial Microbes. In *Plants* (Vol. 11, Issue 3). https://doi.org/10.3390/plants11030386

Zagrobelny, M., Bak, S., Rasmussen, A. V., Jørgensen, B., Naumann, C. M., & Lindberg Møller, B. (2004). Cyanogenic glucosides and plant–insect interactions. *Phytochemistry*, *65*(3), 293–306. https://doi.org/https://doi.org/10.1016/j.phytochem.2003.10.016

Zhang, Z., Yang, T., Mi, N., Wang, Y., Li, G., Wang, L., Xie, Y. (2016). Antifungal activity of monoterpenes against wood white-rot fungi. *International Biodeterioration and Biodegradation*. doi.org/10.1016/j.ibiod.2015.10.018

Zhang, L., Zhang, F., Melotto, M., Yao, J., & He, S. Y. (2017). Jasmonate signaling and manipulation by pathogens and insects. *Journal of Experimental Botany*, *68*(6), 1371–1385. https://doi.org/10.1093/jxb/erw478

Zhao, T., Krokene, P., Björklund, N., Lngström, B., Solheim, H., Christiansen, E., Borg-Karlson, A.K. (2010). The influence of *Ceratocystis polonica* inoculation and methyl jasmonate application on terpene chemistry of Norway spruce, Picea abies. *Phytochemistry*. doi.org/10.1016/j.phytochem.2010.05.017

Zhao, Z., Meng, G., Zamin, I., Wei, T., Ma, D., An, L., & Yue, X. (2023). Genome-Wide Identification and Functional Analysis of the TIFY Family Genes in Response to Abiotic Stresses and Hormone Treatments in Tartary Buckwheat (Fagopyrum tataricum). In *International Journal of Molecular Sciences* (Vol. 24, Issue 13). https://doi.org/10.3390/ijms241310916

Zheng, Z., Qamar, S.A., Chen, Z., and Mengiste, T. (2006). Arabidopsis WRKY33 transcription factor is required for resistance to necrotrophic fungal pathogens. *The Plant Journal* 48**,** 592-605.

Zhu, X., Wang, Y., Su, Z., Lv, L., and Zhang, Z. (2018). Silencing of the Wheat Protein Phosphatase 2A Catalytic Subunit TaPP2Ac Enhances Host Resistance to the Necrotrophic Pathogen Rhizoctonia cerealis. *Frontiers in Plant Science* 9.

APPENDIX A1
MECHANISMS OF PINE DISEASE SUSCEPTIBILITY UNDER EXPERIMENTAL CLIMATE CHANGE

Greenhouse and growth chamber conditions for growing and maintaining pine trees:

In Autumn 2016, 40 samplings were transferred to a greenhouse, where they were exposed to supplemental lighting on a 14 h photoperiod, while the temperature was maintained at a near constant 19° C to keep them from entering dormancy. On December 6, 2016, the saplings were repotted into 2 gal containers using a potting mix consisting of Com-Til compost (provided by Department of Public Utilities, city of Columbus, OH), pine bark, and organic matter (1:1:1 = v:v:v) comprised primarily of composted yard waste.

In the absence of information on well characterized conditions of heat and drought that have resulted in enhanced susceptibility of Austrian pine to *D. sapinea* in European forest environments, we decided to expose seedlings to combinations of heat and drought corresponding as much as possible to conditions that have led to widespread mortality of piñon pine (*P. edulis*) in the southwestern US and that were previously tested experimentally in the Biosphere 2 facility (Adams et al., 2009). The ambient conditions included weekly mean minima of 10.9 – 20.8 ºC and maxima of 22.8 – 34.2 ºC (Adams et al., 2009). Furthermore, Clifford et al. (Clifford et al., 2013) showed that in similar piñon pine ecosystems, extensive pine mortality was associated with field-measured vapor pressure deficits (VPD) > ~1.7 kPa. Adams et al. (Adams et al., 2009) also showed that a 4.3 ºC increase reduced survival times of trees subjected to complete water deprivation from a mean of 25 weeks to a mean of 18 weeks. At death, trees had a pre-dawn twig water potential below -8 MPa. This is much more severe than the levels of sub-lethal water deprivation imposed on our experimental trees described above [mean of -2.5 – 3 MPa (Sherwood et al., 2015)] or those measured by Blodgett and Stanosz (Blodgett et al., 1997a; b) and which resulted in increased susceptibility of red pine (*P. resinosa*) to *D. pinea*.

We conducted our experiments in Conviron E15 environmental chambers, which allow for different temperature and RH conditions. On January 10, 2017, 20 saplings were moved into the CCT growth chamber, while 20 were moved into the CT chamber. (Eventually, only 18 trees in each chamber were

used – see “inoculation treatments” below.) Trees in the CT chamber were watered to field capacity throughout the experiment while water was withheld by watering each tree with 250-500 ml of water twice a week in the CCT chamber.

In preliminary tests, it had been noted that the pines were showing symptoms of reduced growth in the climate chambers, compared to growth observed in the greenhouse. Monitoring over several days revealed that CO_2 concentration dropped to minimal levels during the day due to consumption of the gas by actively photosynthesizing plants in the crowded chambers. Therefore, the chambers were outfitted with a custom-made automatic CO_2 monitoring and delivery system, composed of a RAD-0501 CO_2 monitor and controller system (CO2meter.com) connected to a CO_2 tank with plastic tubing. Both the controller and tank were placed in the growth chamber and released the CO_2 as needed. A HOBO MX CO_2 logger (MX1102) was also placed in the chamber at tree crown level. Delivery of CO_2 was set to achieve 400 ppm in the chambers during the day. No effort was made to control CO_2 levels at night.

Because the trees started showing symptoms of excessive desiccation due to heat and drought-induced stress in the CCT chamber, on 16 February 2017, the maximum temperatures were lowered by 5 ºC in each chamber, to 23 ºC in the CT chamber and 28 ºC in the CCT chamber.

Pre-dawn needle water potentials were measured with a Scholander pressure bomb (PMS Instrument Co., Corvallis, OR). On February 14, 2017, they averaged -0.1 kPa and -1.3 kPa for the pines in the CT and CCT chambers, respectively; on March 1, 2017, they averaged -0.3 kPa and -2.0 kPa, respectively; on March 3, 2017, they averaged -0.3 kPa and -2.0 kPa, respectively; and on March 8, 2017, they averaged -0.1 kPa and -2.4 kPa, respectively (N = 6 for each mean).

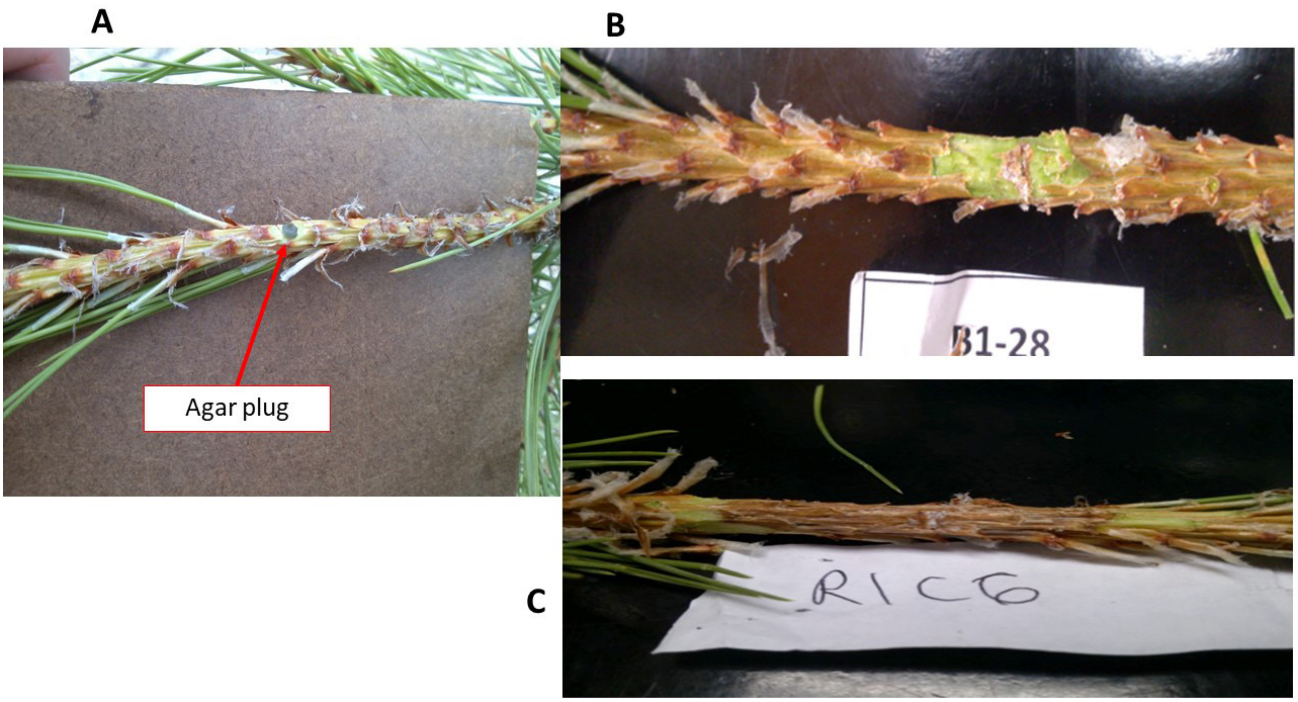

Figure A1.1. **(A)** Inoculations were performed by placing a plug of colonized agar (*Diplodia pinea* or *D. scrobiculata*) or axenic agar (mock) into a small shallow wound near the tip of a shoot, which was then wrapped with parafilm. **(B)** Typical outcome of a mock inoculation after 2 weeks. **(C)** Extensive lesion produced after 2 weeks by D. scrobiculata inoculation under CCT.

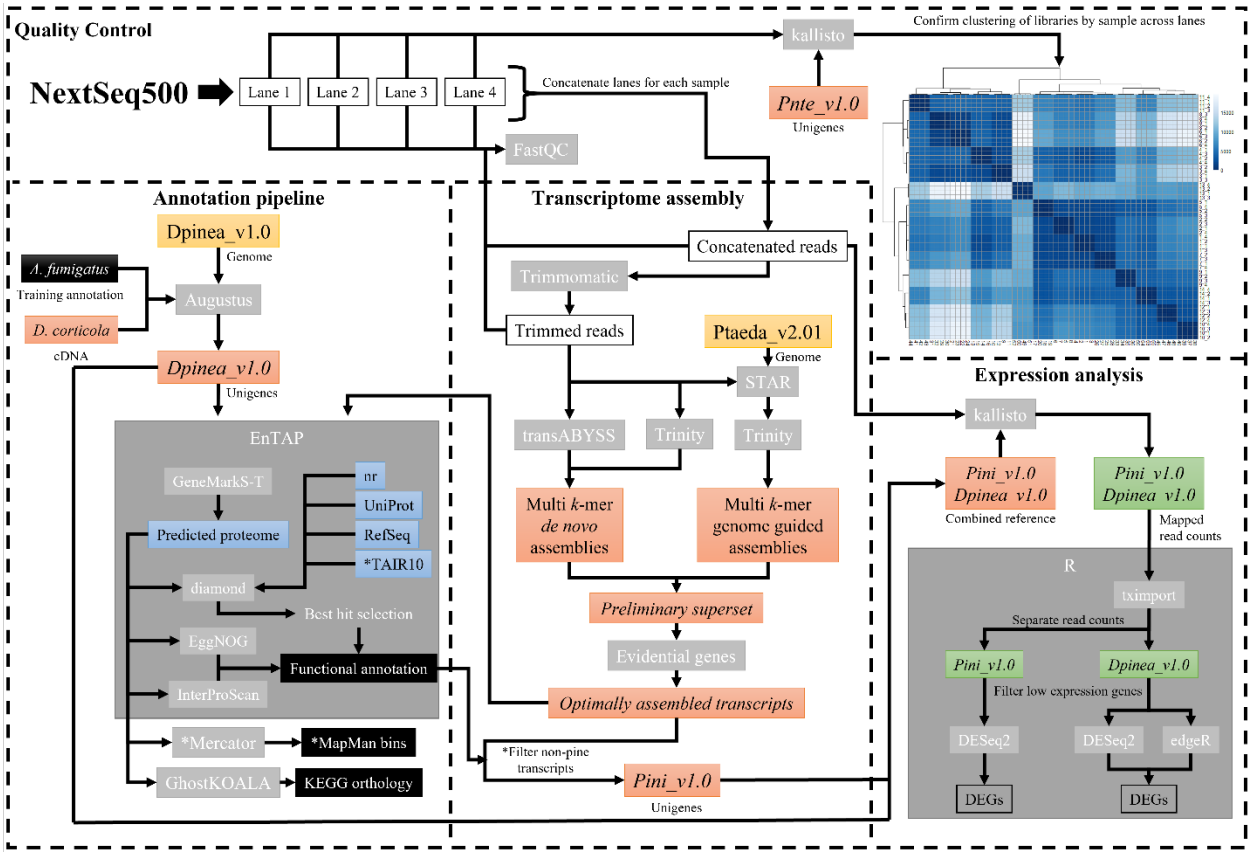

Figure A1.2. Bioinformatics analysis flow diagram. Grey boxes represent programs, black boxes represent annotations, yellow boxes represent genomic sequences, orange boxes represent transcriptomic/unigene sequences blue boxes represent protein sequence, colorless boxes represent RNAseq read libraries. Dpinea_v1.0 = *Diplodia pinea* v1.0 assembly, Pini_v1.0 = *Pinus nigra* v1.0 assembly, Pnte_v1.0 = *Pinus tecunumanii* v1.0 assembly, Ptaeda_v2.01 = *Pinus taeda* v2.01 assembly.

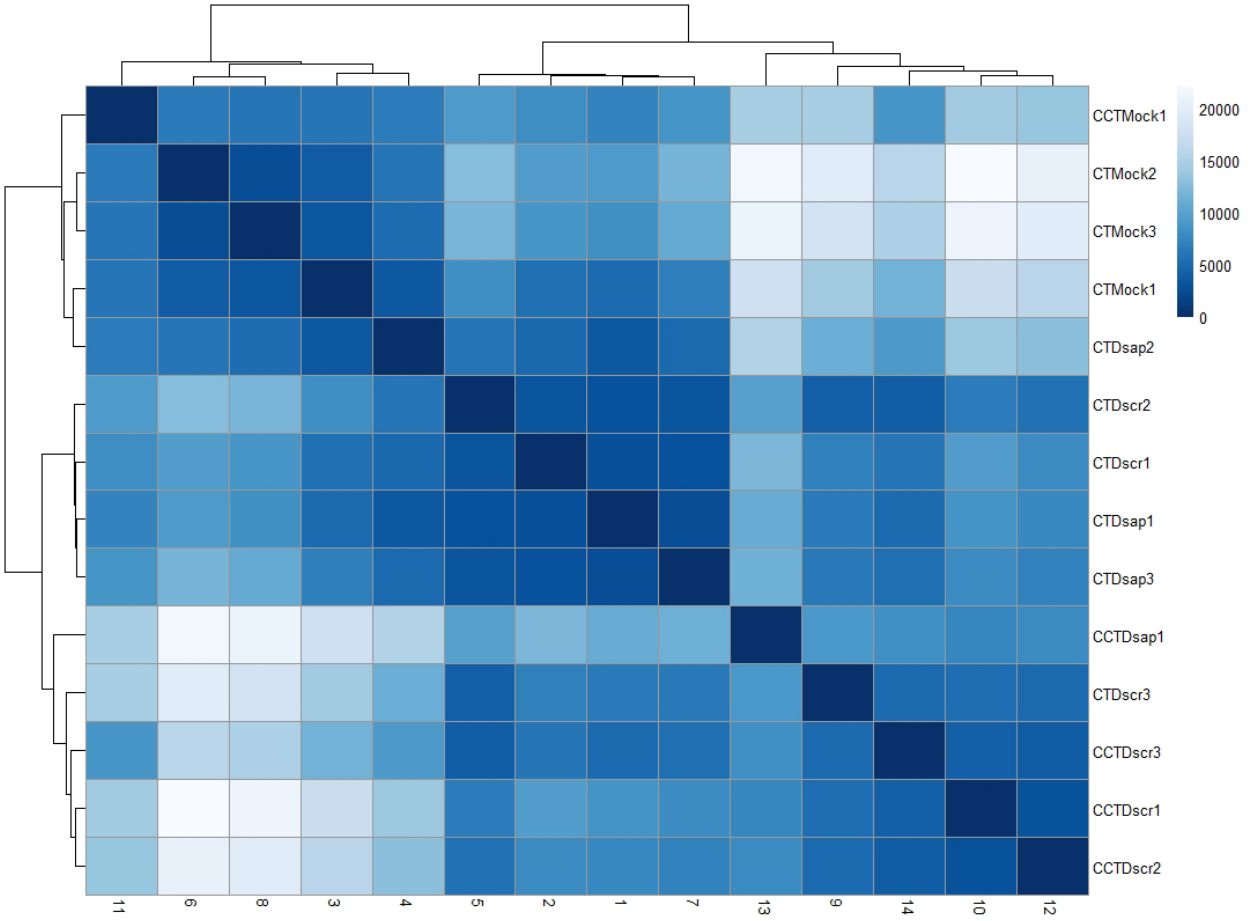

Figure A1.3. Poisson distribution of normalized RNA from Austrian pine from various sample treatments showed strong correlation between identical treatment types. Vertical axis indicates treatment type followed by replicate number with the corresponding sample number plotted on the horizontal axis. Treatment labels: CCT: climate change treatment, CT: control climate treatment, Dsap: *D. pinea*, Dscr: *D. scrobiculata*.

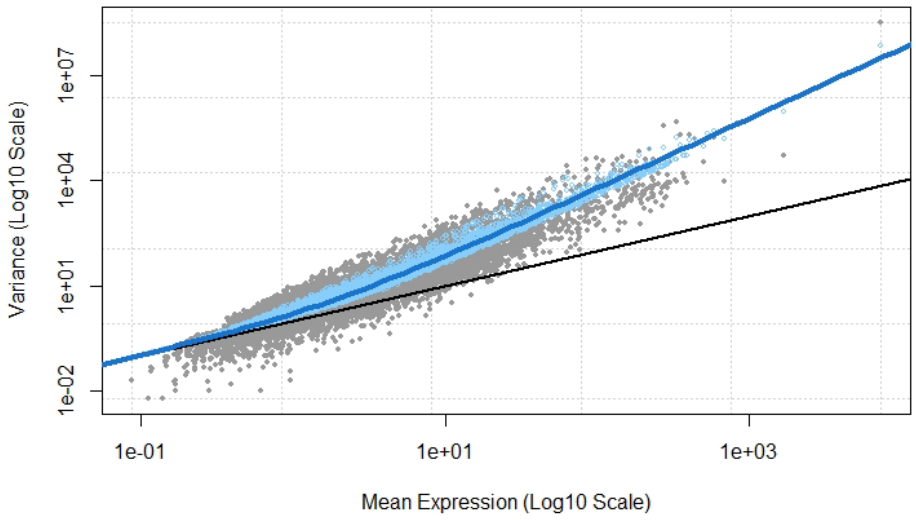

Figure A1.4. Mean variance plot of count data for all *Diplodia* spp. genes. Black line indicates the expected trend of dispersion, whereas blue line indicates shows higher than normal dispersion of counts with increased expression.

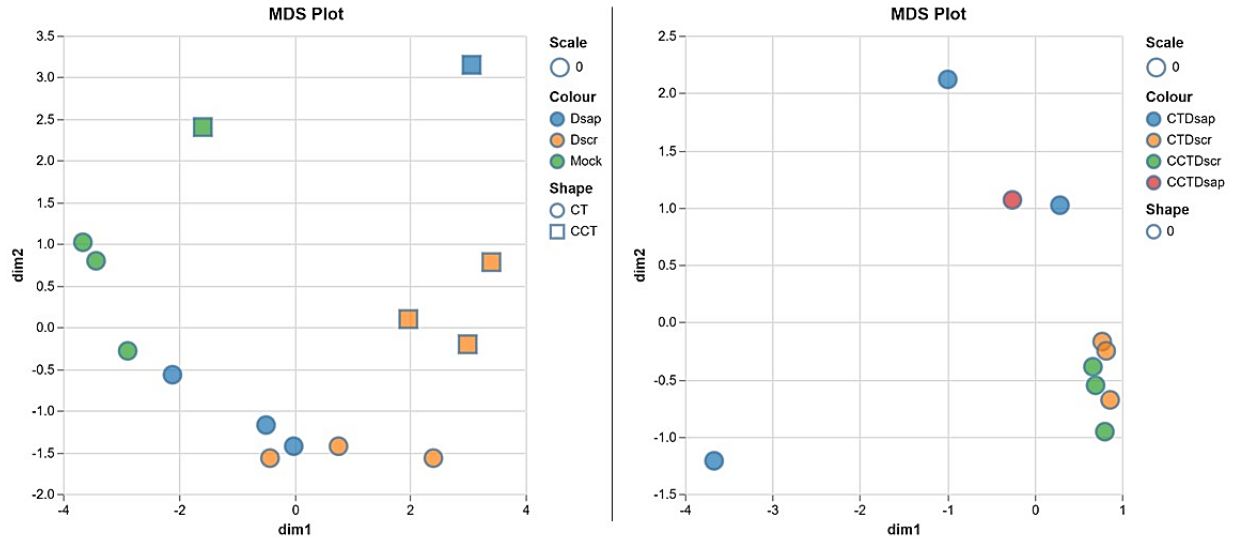

Figure A1.5. Multi-dimensional scaling (MDS) plot for respective treatment comparisons of the host (LEFT) and the pathogen (RIGHT). For host comparisons, legend shape indicates climate treatment, while legend color indicates inoculation treatment. For pathogen comparisons, legend color indicates treatment combination. Treatment labels: CCT: climate change treatment, CT: control climate treatment, Dsap: *D. pinea*, Dscr: *D. scrobiculata*.

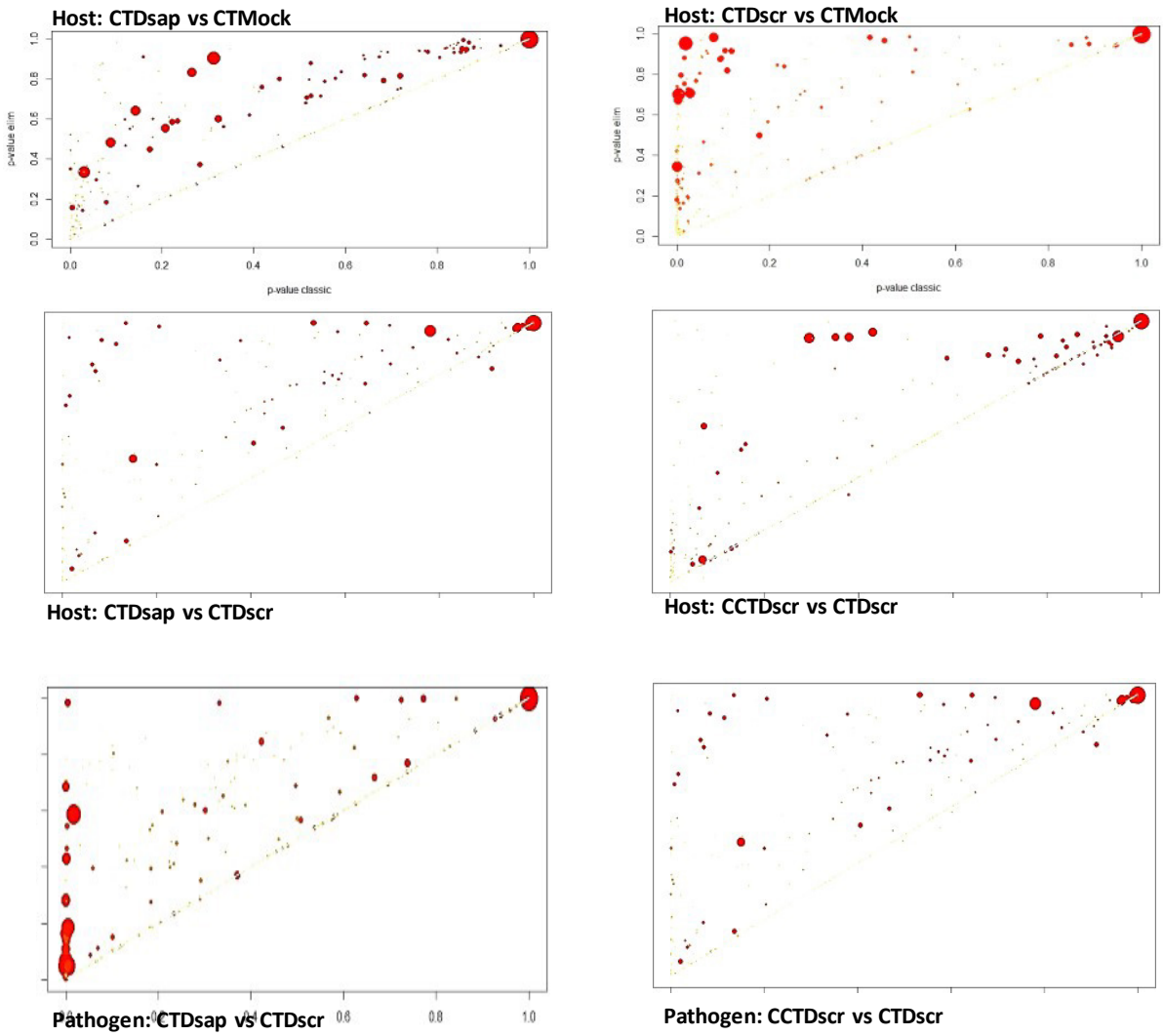

Figure A1.6. Scatter plot shows comparison of GO enrichment analysis results (adjusted p-value) from Kolmogorov-Smirnov elimination (elimKS) method on the Y-axis versus the results (adjusted p-value) from classic Fisher test on the X-axis. Plot points represent respective GO terms, and size of plot points indicate the significantly enriched GO terms. Enriched GO terms are better separated along the X-axis than the Y-axis in all comparisons, and thus the classic Fisher test results were used for interpretation.

Table A1.1. Details of sequence submission for biological samples of Austrian pine- D. pinea / D. scrobiculata to NCBI.

Accession	Sample Name	SPUID	Organism	Tax ID	Cultivar	Isolate	url
SAMN26565493	APDS_L1	APDS_L1	Pinus nigra	58042	not applicable	Pinus nigra and Diplodia sapinea dual transcriptome	26565493: https://www.ncbi.nlm.nih.gov/biosample/26565493
SAMN26565494	APDS_L2	APDS_L2	Pinus nigra	58042	not applicable	Pinus nigra and Diplodia sapinea dual transcriptome	26565494: https://www.ncbi.nlm.nih.gov/biosample/26565494
SAMN26565495	APDS_L3	APDS_L3	Pinus nigra	58042	not applicable	Pinus nigra and Diplodia sapinea dual transcriptome	26565495: https://www.ncbi.nlm.nih.gov/biosample/26565495
SAMN26565496	APDS_L4	APDS_L4	Pinus nigra	58042	not applicable	Pinus nigra and Diplodia sapinea dual transcriptome	26565496: https://www.ncbi.nlm.nih.gov/biosample/26565496
SAMN26565497	APDS_L5	APDS_L5	Pinus nigra	58042	not applicable	Pinus nigra and Diplodia sapinea dual transcriptome	26565497: https://www.ncbi.nlm.nih.gov/biosample/26565497
SAMN26565498	APDS_L6	APDS_L6	Pinus nigra	58042	not applicable	Pinus nigra and Diplodia sapinea dual transcriptome	26565498: https://www.ncbi.nlm.nih.gov/biosample/26565498
SAMN26565499	APDS_L7	APDS_L7	Pinus nigra	58042	not applicable	Pinus nigra and Diplodia sapinea dual transcriptome	26565499: https://www.ncbi.nlm.nih.gov/biosample/26565499

(continued)

SAMN26565500	APDS_L8	APDS_L8	Pinus nigra	58042	not applicable	Pinus nigra and Diplodia sapinea dual transcriptome	26565500: https://www.ncbi.nlm.nih.gov/biosample/26565500
SAMN26565501	APDS_L9	APDS_L9	Pinus nigra	58042	not applicable	Pinus nigra and Diplodia scrobiculata dual transcriptome	26565501: https://www.ncbi.nlm.nih.gov/biosample/26565501
SAMN26565502	APDS_L10	APDS_L10	Pinus nigra	58042	not applicable	Pinus nigra and Diplodia scrobiculata dual transcriptome	26565502: https://www.ncbi.nlm.nih.gov/biosample/26565502
SAMN26565503	APDS_L11	APDS_L11	Pinus nigra	58042	not applicable	Pinus nigra and Diplodia scrobiculata dual transcriptome	26565503: https://www.ncbi.nlm.nih.gov/biosample/26565503
SAMN26565504	APDS_L12	APDS_L12	Pinus nigra	58042	not applicable	Pinus nigra and Diplodia scrobiculata dual transcriptome	26565504: https://www.ncbi.nlm.nih.gov/biosample/26565504
SAMN26565505	APDS_L13	APDS_L13	Pinus nigra	58042	not applicable	Pinus nigra and Diplodia scrobiculata dual transcriptome	26565505: https://www.ncbi.nlm.nih.gov/biosample/26565505
SAMN26565506	APDS_L14	APDS_L14	Pinus nigra	58042	not applicable	Pinus nigra and Diplodia scrobiculata dual transcriptome	26565506: https://www.ncbi.nlm.nih.gov/biosample/26565506
SAMN26565507	APDS_L15	APDS_L15	Pinus nigra	58042	not applicable	Pinus nigra and Diplodia scrobiculata dual transcriptome	26565507: https://www.ncbi.nlm.nih.gov/biosample/26565507
SAMN26565508	APDS_L16	APDS_L16	Pinus nigra	58042	not applicable	Pinus nigra and Diplodia scrobiculata dual transcriptome	26565508: https://www.ncbi.nlm.nih.gov/biosample/26565508
SAMN26565509	APDS_L17	APDS_L17	Pinus nigra	58042	not applicable	Pinus nigra transcriptome	26565509: https://www.ncbi.nlm.nih.gov/biosample/26565509

(continued)

SAMN26565510	APDS_L18	APDS_L18	Pinus nigra	58042	not applicable	Pinus nigra transcriptome	26565510: https://www.ncbi.nlm.nih.gov/biosample/26565510
SAMN26565511	APDS_L19	APDS_L19	Pinus nigra	58042	not applicable	Pinus nigra transcriptome	26565511: https://www.ncbi.nlm.nih.gov/biosample/26565511
SAMN26565512	APDS_L20	APDS_L20	Pinus nigra	58042	not applicable	Pinus nigra transcriptome	26565512: https://www.ncbi.nlm.nih.gov/biosample/26565512
SAMN26565513	APDS_L21	APDS_L21	Pinus nigra	58042	not applicable	Pinus nigra transcriptome	26565513: https://www.ncbi.nlm.nih.gov/biosample/26565513
SAMN26565514	APDS_L22	APDS_L22	Pinus nigra	58042	not applicable	Pinus nigra transcriptome	26565514: https://www.ncbi.nlm.nih.gov/biosample/26565514
SAMN26565515	APDS_L23	APDS_L23	Pinus nigra	58042	not applicable	Pinus nigra transcriptome	26565515: https://www.ncbi.nlm.nih.gov/biosample/26565515
SAMN26565516	APDS_L24	APDS_L24	Pinus nigra	58042	not applicable	Pinus nigra transcriptome	26565516: https://www.ncbi.nlm.nih.gov/biosample/26565516
SAMN26565517	APDS_L25	APDS_L25	Pinus nigra	58042	not applicable	Pinus nigra and Diplodia sapinea dual transcriptome	26565517: https://www.ncbi.nlm.nih.gov/biosample/26565517
SAMN26565518	APDS_L26	APDS_L26	Pinus nigra	58042	not applicable	Pinus nigra and Diplodia sapinea dual transcriptome	26565518: https://www.ncbi.nlm.nih.gov/biosample/26565518
SAMN26565519	APDS_L27	APDS_L27	Pinus nigra	58042	not applicable	Pinus nigra and Diplodia sapinea dual transcriptome	26565519: https://www.ncbi.nlm.nih.gov/biosample/26565519

(continued)

SAMN26565520	APDS_L28	APDS_L28	Pinus nigra	58042	not applicable	Pinus nigra and Diplodia sapinea dual transcriptome	26565520: https://www.ncbi.nlm.nih.gov/biosample/26565520
SAMN26565521	APDS_L29	APDS_L29	Pinus nigra	58042	not applicable	Pinus nigra and Diplodia sapinea dual transcriptome	26565521: https://www.ncbi.nlm.nih.gov/biosample/26565521
SAMN26565522	APDS_L30	APDS_L30	Pinus nigra	58042	not applicable	Pinus nigra and Diplodia sapinea dual transcriptome	26565522: https://www.ncbi.nlm.nih.gov/biosample/26565522
SAMN26565523	APDS_L31	APDS_L31	Pinus nigra	58042	not applicable	Pinus nigra and Diplodia sapinea dual transcriptome	26565523: https://www.ncbi.nlm.nih.gov/biosample/26565523
SAMN26565524	APDS_L32	APDS_L32	Pinus nigra	58042	not applicable	Pinus nigra and Diplodia sapinea dual transcriptome	26565524: https://www.ncbi.nlm.nih.gov/biosample/26565524
SAMN26565525	APDS_L33	APDS_L33	Pinus nigra	58042	not applicable	Pinus nigra and Diplodia scrobiculata dual transcriptome	26565525: https://www.ncbi.nlm.nih.gov/biosample/26565525
SAMN26565526	APDS_L34	APDS_L34	Pinus nigra	58042	not applicable	Pinus nigra and Diplodia scrobiculata dual transcriptome	26565526: https://www.ncbi.nlm.nih.gov/biosample/26565526
SAMN26565527	APDS_L35	APDS_L35	Pinus nigra	58042	not applicable	Pinus nigra and Diplodia scrobiculata dual transcriptome	26565527: https://www.ncbi.nlm.nih.gov/biosample/26565527
SAMN26565528	APDS_L36	APDS_L36	Pinus nigra	58042	not applicable	Pinus nigra and Diplodia scrobiculata dual transcriptome	26565528: https://www.ncbi.nlm.nih.gov/biosample/26565528
SAMN26565529	APDS_L37	APDS_L37	Pinus nigra	58042	not applicable	Pinus nigra and Diplodia scrobiculata dual transcriptome	26565529: https://www.ncbi.nlm.nih.gov/biosample/26565529

(continued)

SAMN26565530	APDS_L38	APDS_L38	Pinus nigra	58042	not applicable	Pinus nigra and Diplodia scrobiculata dual transcriptome	26565530: https://www.ncbi.nlm.nih.gov/biosample/26565530
SAMN26565531	APDS_L39	APDS_L39	Pinus nigra	58042	not applicable	Pinus nigra and Diplodia scrobiculata dual transcriptome	26565531: https://www.ncbi.nlm.nih.gov/biosample/26565531
SAMN26565532	APDS_L40	APDS_L40	Pinus nigra	58042	not applicable	Pinus nigra and Diplodia scrobiculata dual transcriptome	26565532: https://www.ncbi.nlm.nih.gov/biosample/26565532
SAMN26565533	APDS_L41	APDS_L41	Pinus nigra	58042	not applicable	Pinus nigra transcriptome	26565533: https://www.ncbi.nlm.nih.gov/biosample/26565533
SAMN26565534	APDS_L42	APDS_L42	Pinus nigra	58042	not applicable	Pinus nigra transcriptome	26565534: https://www.ncbi.nlm.nih.gov/biosample/26565534
SAMN26565535	APDS_L43	APDS_L43	Pinus nigra	58042	not applicable	Pinus nigra transcriptome	26565535: https://www.ncbi.nlm.nih.gov/biosample/26565535
SAMN26565536	APDS_L44	APDS_L44	Pinus nigra	58042	not applicable	Pinus nigra transcriptome	26565536: https://www.ncbi.nlm.nih.gov/biosample/26565536
SAMN26565537	APDS_L45	APDS_L45	Pinus nigra	58042	not applicable	Pinus nigra transcriptome	26565537: https://www.ncbi.nlm.nih.gov/biosample/26565537
SAMN26565538	APDS_L46	APDS_L46	Pinus nigra	58042	not applicable	Pinus nigra transcriptome	26565538: https://www.ncbi.nlm.nih.gov/biosample/26565538
SAMN26565539	APDS_L47	APDS_L47	Pinus nigra	58042	not applicable	Pinus nigra transcriptome	26565539: https://www.ncbi.nlm.nih.gov/biosample/26565539

(continued)

SAMN26565540	APDS_L48	APDS_L48	Pinus nigra	58042	not applicable	Pinus nigra transcriptome	26565540: https://www.ncbi.nlm.nih.gov/biosample/26565540
SAMN26565541	APDS_L49	APDS_L49	Pinus nigra	58042	not applicable	Pinus nigra and Diplodia sapinea dual transcriptome	26565541: https://www.ncbi.nlm.nih.gov/biosample/26565541
SAMN26565542	APDS_L50	APDS_L50	Pinus nigra	58042	not applicable	Pinus nigra and Diplodia sapinea dual transcriptome	26565542: https://www.ncbi.nlm.nih.gov/biosample/26565542
SAMN26565543	APDS_L51	APDS_L51	Pinus nigra	58042	not applicable	Pinus nigra and Diplodia sapinea dual transcriptome	26565543: https://www.ncbi.nlm.nih.gov/biosample/26565543
SAMN26565544	APDS_L52	APDS_L52	Pinus nigra	58042	not applicable	Pinus nigra and Diplodia sapinea dual transcriptome	26565544: https://www.ncbi.nlm.nih.gov/biosample/26565544
SAMN26565545	APDS_L53	APDS_L53	Pinus nigra	58042	not applicable	Pinus nigra and Diplodia sapinea dual transcriptome	26565545: https://www.ncbi.nlm.nih.gov/biosample/26565545
SAMN26565546	APDS_L54	APDS_L54	Pinus nigra	58042	not applicable	Pinus nigra and Diplodia sapinea dual transcriptome	26565546: https://www.ncbi.nlm.nih.gov/biosample/26565546
SAMN26565547	APDS_L55	APDS_L55	Pinus nigra	58042	not applicable	Pinus nigra and Diplodia sapinea dual transcriptome	26565547: https://www.ncbi.nlm.nih.gov/biosample/26565547
SAMN26565548	APDS_L56	APDS_L56	Pinus nigra	58042	not applicable	Pinus nigra and Diplodia sapinea dual transcriptome	26565548: https://www.ncbi.nlm.nih.gov/biosample/26565548
SAMN26565549	APDS_L57	APDS_L57	Pinus nigra	58042	not applicable	Pinus nigra and Diplodia scrobiculata dual transcriptome	26565549: https://www.ncbi.nlm.nih.gov/biosample/26565549

(continued)

SAMN26565550	APDS_L58	APDS_L58	Pinus nigra	58042	not applicable	Pinus nigra and Diplodia scrobiculata dual transcriptome	26565550: https://www.ncbi.nlm.nih.gov/biosample/26565550
SAMN26565551	APDS_L59	APDS_L59	Pinus nigra	58042	not applicable	Pinus nigra and Diplodia scrobiculata dual transcriptome	26565551: https://www.ncbi.nlm.nih.gov/biosample/26565551
SAMN26565552	APDS_L60	APDS_L60	Pinus nigra	58042	not applicable	Pinus nigra and Diplodia scrobiculata dual transcriptome	26565552: https://www.ncbi.nlm.nih.gov/biosample/26565552
SAMN26565553	APDS_L61	APDS_L61	Pinus nigra	58042	not applicable	Pinus nigra and Diplodia scrobiculata dual transcriptome	26565553: https://www.ncbi.nlm.nih.gov/biosample/26565553
SAMN26565554	APDS_L62	APDS_L62	Pinus nigra	58042	not applicable	Pinus nigra and Diplodia scrobiculata dual transcriptome	26565554: https://www.ncbi.nlm.nih.gov/biosample/26565554
SAMN26565555	APDS_L63	APDS_L63	Pinus nigra	58042	not applicable	Pinus nigra and Diplodia scrobiculata dual transcriptome	26565555: https://www.ncbi.nlm.nih.gov/biosample/26565555
SAMN26565556	APDS_L64	APDS_L64	Pinus nigra	58042	not applicable	Pinus nigra and Diplodia scrobiculata dual transcriptome	26565556: https://www.ncbi.nlm.nih.gov/biosample/26565556
SAMN26565557	APDS_L65	APDS_L65	Pinus nigra	58042	not applicable	Pinus nigra transcriptome	26565557: https://www.ncbi.nlm.nih.gov/biosample/26565557
SAMN26565558	APDS_L66	APDS_L66	Pinus nigra	58042	not applicable	Pinus nigra transcriptome	26565558: https://www.ncbi.nlm.nih.gov/biosample/26565558
SAMN26565559	APDS_L67	APDS_L67	Pinus nigra	58042	not applicable	Pinus nigra transcriptome	26565559: https://www.ncbi.nlm.nih.gov/biosample/26565559

(continued)

SAMN26565560	APDS_L68	APDS_L68	Pinus nigra	58042	not applicable	Pinus nigra transcriptome	26565560: https://www.ncbi.nlm.nih.gov/biosample/26565560
SAMN26565561	APDS_L69	APDS_L69	Pinus nigra	58042	not applicable	Pinus nigra transcriptome	26565561: https://www.ncbi.nlm.nih.gov/biosample/26565561
SAMN26565562	APDS_L70	APDS_L70	Pinus nigra	58042	not applicable	Pinus nigra transcriptome	26565562: https://www.ncbi.nlm.nih.gov/biosample/26565562
SAMN26565563	APDS_L71	APDS_L71	Pinus nigra	58042	not applicable	Pinus nigra transcriptome	26565563: https://www.ncbi.nlm.nih.gov/biosample/26565563
SAMN26565564	APDS_L72	APDS_L72	Pinus nigra	58042	not applicable	Pinus nigra transcriptome	26565564: https://www.ncbi.nlm.nih.gov/biosample/26565564
SAMN26565565	APDS_L73	APDS_L73	Pinus nigra	58042	not applicable	Pinus nigra and Diplodia scrobiculata dual transcriptome	26565565: https://www.ncbi.nlm.nih.gov/biosample/26565565
SAMN26565566	APDS_L74	APDS_L74	Pinus nigra	58042	not applicable	Pinus nigra and Diplodia scrobiculata dual transcriptome	26565566: https://www.ncbi.nlm.nih.gov/biosample/26565566
SAMN26565567	APDS_L75	APDS_L75	Pinus nigra	58042	not applicable	Pinus nigra and Diplodia scrobiculata dual transcriptome	26565567: https://www.ncbi.nlm.nih.gov/biosample/26565567
SAMN26565568	APDS_L76	APDS_L76	Pinus nigra	58042	not applicable	Pinus nigra and Diplodia scrobiculata dual transcriptome	26565568: https://www.ncbi.nlm.nih.gov/biosample/26565568
SAMN26565569	APDS_L77	APDS_L77	Pinus nigra	58042	not applicable	Pinus nigra and Diplodia scrobiculata dual transcriptome	26565569: https://www.ncbi.nlm.nih.gov/biosample/26565569

(continued)

SAMN26565570	APDS_L78	APDS_L78	Pinus nigra	58042	not applicable	Pinus nigra and Diplodia scrobiculata dual transcriptome	26565570: https://www.ncbi.nlm.nih.gov/biosample/26565570
SAMN26565571	APDS_L79	APDS_L79	Pinus nigra	58042	not applicable	Pinus nigra and Diplodia scrobiculata dual transcriptome	26565571: https://www.ncbi.nlm.nih.gov/biosample/26565571
SAMN26565572	APDS_L80	APDS_L80	Pinus nigra	58042	not applicable	Pinus nigra and Diplodia scrobiculata dual transcriptome	26565572: https://www.ncbi.nlm.nih.gov/biosample/26565572
SAMN26565573	APDS_L81	APDS_L81	Pinus nigra	58042	not applicable	Pinus nigra transcriptome	26565573: https://www.ncbi.nlm.nih.gov/biosample/26565573
SAMN26565574	APDS_L82	APDS_L82	Pinus nigra	58042	not applicable	Pinus nigra transcriptome	26565574: https://www.ncbi.nlm.nih.gov/biosample/26565574
SAMN26565575	APDS_L83	APDS_L83	Pinus nigra	58042	not applicable	Pinus nigra transcriptome	26565575: https://www.ncbi.nlm.nih.gov/biosample/26565575
SAMN26565576	APDS_L84	APDS_L84	Pinus nigra	58042	not applicable	Pinus nigra transcriptome	26565576: https://www.ncbi.nlm.nih.gov/biosample/26565576
SAMN26565577	APDS_L85	APDS_L85	Pinus nigra	58042	not applicable	Pinus nigra transcriptome	26565577: https://www.ncbi.nlm.nih.gov/biosample/26565577
SAMN26565578	APDS_L86	APDS_L86	Pinus nigra	58042	not applicable	Pinus nigra transcriptome	26565578: https://www.ncbi.nlm.nih.gov/biosample/26565578
SAMN26565579	APDS_L87	APDS_L87	Pinus nigra	58042	not applicable	Pinus nigra transcriptome	26565579: https://www.ncbi.nlm.nih.gov/biosample/26565579

(continued)

SAMN26565580	APDS_L88	APDS_L88	Pinus nigra	58042	not applicable	Pinus nigra transcriptome	26565580: https://www.ncbi.nlm.nih.gov/biosample/26565580
SAMN26565581	APDS_L89	APDS_L89	Pinus nigra	58042	not applicable	Pinus nigra and Diplodia scrobiculata dual transcriptome	26565581: https://www.ncbi.nlm.nih.gov/biosample/26565581
SAMN26565582	APDS_L90	APDS_L90	Pinus nigra	58042	not applicable	Pinus nigra and Diplodia scrobiculata dual transcriptome	26565582: https://www.ncbi.nlm.nih.gov/biosample/26565582
SAMN26565583	APDS_L91	APDS_L91	Pinus nigra	58042	not applicable	Pinus nigra and Diplodia scrobiculata dual transcriptome	26565583: https://www.ncbi.nlm.nih.gov/biosample/26565583
SAMN26565584	APDS_L92	APDS_L92	Pinus nigra	58042	not applicable	Pinus nigra and Diplodia scrobiculata dual transcriptome	26565584: https://www.ncbi.nlm.nih.gov/biosample/26565584
SAMN26565585	APDS_L93	APDS_L93	Pinus nigra	58042	not applicable	Pinus nigra and Diplodia scrobiculata dual transcriptome	26565585: https://www.ncbi.nlm.nih.gov/biosample/26565585
SAMN26565586	APDS_L94	APDS_L94	Pinus nigra	58042	not applicable	Pinus nigra and Diplodia scrobiculata dual transcriptome	26565586: https://www.ncbi.nlm.nih.gov/biosample/26565586
SAMN26565587	APDS_L95	APDS_L95	Pinus nigra	58042	not applicable	Pinus nigra and Diplodia scrobiculata dual transcriptome	26565587: https://www.ncbi.nlm.nih.gov/biosample/26565587
SAMN26565588	APDS_L96	APDS_L96	Pinus nigra	58042	not applicable	Pinus nigra and Diplodia scrobiculata dual transcriptome	26565588: https://www.ncbi.nlm.nih.gov/biosample/26565588
SAMN26565589	APDS_L97	APDS_L97	Pinus nigra	58042	not applicable	Pinus nigra and Diplodia sapinea dual transcriptome	26565589: https://www.ncbi.nlm.nih.gov/biosample/26565589

(continued)

SAMN26565590	APDS_L98	APDS_L98	Pinus nigra	58042	not applicable	Pinus nigra and Diplodia sapinea dual transcriptome	26565590: https://www.ncbi.nlm.nih.gov/biosample/26565590
SAMN26565591	APDS_L99	APDS_L99	Pinus nigra	58042	not applicable	Pinus nigra and Diplodia sapinea dual transcriptome	26565591: https://www.ncbi.nlm.nih.gov/biosample/26565591
SAMN26565592	APDS_L100	APDS_L100	Pinus nigra	58042	not applicable	Pinus nigra and Diplodia sapinea dual transcriptome	26565592: https://www.ncbi.nlm.nih.gov/biosample/26565592
SAMN26565593	APDS_L101	APDS_L101	Pinus nigra	58042	not applicable	Pinus nigra and Diplodia sapinea dual transcriptome	26565593: https://www.ncbi.nlm.nih.gov/biosample/26565593
SAMN26565594	APDS_L102	APDS_L102	Pinus nigra	58042	not applicable	Pinus nigra and Diplodia sapinea dual transcriptome	26565594: https://www.ncbi.nlm.nih.gov/biosample/26565594
SAMN26565595	APDS_L103	APDS_L103	Pinus nigra	58042	not applicable	Pinus nigra and Diplodia sapinea dual transcriptome	26565595: https://www.ncbi.nlm.nih.gov/biosample/26565595
SAMN26565596	APDS_L104	APDS_L104	Pinus nigra	58042	not applicable	Pinus nigra and Diplodia sapinea dual transcriptome	26565596: https://www.ncbi.nlm.nih.gov/biosample/26565596
SAMN26565597	APDS_L105	APDS_L105	Pinus nigra	58042	not applicable	Pinus nigra and Diplodia scrobiculata dual transcriptome	26565597: https://www.ncbi.nlm.nih.gov/biosample/26565597
SAMN26565598	APDS_L106	APDS_L106	Pinus nigra	58042	not applicable	Pinus nigra and Diplodia scrobiculata dual transcriptome	26565598: https://www.ncbi.nlm.nih.gov/biosample/26565598
SAMN26565599	APDS_L107	APDS_L107	Pinus nigra	58042	not applicable	Pinus nigra and Diplodia scrobiculata dual transcriptome	26565599: https://www.ncbi.nlm.nih.gov/biosample/26565599

(continued)

SAMN26565600	APDS_L108	APDS_L108	Pinus nigra	58042	not applicable	Pinus nigra and Diplodia scrobiculata dual transcriptome	26565600: https://www.ncbi.nlm.nih.gov/biosample/26565600
SAMN26565601	APDS_L109	APDS_L109	Pinus nigra	58042	not applicable	Pinus nigra and Diplodia scrobiculata dual transcriptome	26565601: https://www.ncbi.nlm.nih.gov/biosample/26565601
SAMN26565602	APDS_L110	APDS_L110	Pinus nigra	58042	not applicable	Pinus nigra and Diplodia scrobiculata dual transcriptome	26565602: https://www.ncbi.nlm.nih.gov/biosample/26565602
SAMN26565603	APDS_L111	APDS_L111	Pinus nigra	58042	not applicable	Pinus nigra and Diplodia scrobiculata dual transcriptome	26565603: https://www.ncbi.nlm.nih.gov/biosample/26565603
SAMN26565604	APDS_L112	APDS_L112	Pinus nigra	58042	not applicable	Pinus nigra and Diplodia scrobiculata dual transcriptome	26565604: https://www.ncbi.nlm.nih.gov/biosample/26565604

Table A1.2. List of DE genes for various treatment comparisons of Austrian pine and *Diplodia* spp. RNAseq.

HOST: CTDsap vs CTMock						
UP						
label	**ID**	**annotation**	**log2FoldChange**	**actualFC**	**padj**	**KO**
T_11	PiniT23N_TRINITY_DN26330_c2_g2_i3	receptor-like protein kinase	2.744	8	0.005433007	
T_26	PiniA43_J3675585598115451737602	calcium-binding protein	5.739	33	5.51802E-07	K13448

T_27	PiniT29N_TRINITY_DN26174_c0_g1_i6	calcium-binding protein	5.535	31	4.25488E-05	K13448
T_33	PiniT21G_TRINITY_GG_35834_c0_g1_i1	glucan endo-1-3-beta-glucosidase	3.402	12	7.49078E-06	
T_34	PiniT31G_TRINITY_GG_47165_c0_g1_i8	Serine threonine-protein kinase	2.277	5	0.00017139	
T_35	PiniT27N_TRINITY_DN36321_c2_g3_i1	Pathogenesis-related protein	2.271	5	0.002482143	K13449
T_36	PiniT21N_TRINITY_DN22363_c1_g2_i5	calcium-binding protein PBP1-like	2.413	6	0.000165872	
T_43	PiniT25G_TRINITY_GG_501_c0_g1_i3	jasmonate ZIM binding protein JAZ	6.702	45	0.000123204	K13464
T_44	PiniT27_TRINITY_DN40705_c0_g1_i6	jasmonate ZIM binding protein JAZ	5.814	34	6.954E-06	K13464
T_47	PiniA45_S350420775339842346199	Transcription factor	4.013	16	9.71472E-05	K9286
T_49	PiniA51_J261579013823144041461287	gibberellin receptor GID1	2.398	5	0.000723028	
T_50	PiniA51_R261120512341337672394266	phosphatase 2C PP2C	2.292	5	0.016376662	K14497
T_61	PiniT23N_TRINITY_DN23320_c1_g1_i3	Cinnamyl alcohol dehydrogenase	2.777	8	6.0273E-08	K83
T_65	PiniT29N_TRINITY_DN36015_c0_g2_i1	peroxidase	3.011	9	1.20131E-06	K43
T_71	PiniA21_R766127218901671102515645 8	beta-glucosidase	3.089	10	5.77255E-06	K1188
T_75	PiniT21G_TRINITY_GG_43300_c0_g1_i1	4-coumarate--CoA ligase	2.320	5	0.005736845	K194
T_76	PiniA37_R435313818361267790128088 5	4-coumarate--CoA ligase-like	2.908	8	0.000424855	K194
T_82	PiniT31G_TRINITY_GG_36100_c0_g1_i1	The primary product of this enzyme is 4,2',4',6'- tetrahydroxychalcone (also termed naringenin-chalcone or chalcone) which can under specific conditions spontaneously isomerize into naringenin	4.844	23	3.03587E-07	K66
T_83	PiniT21G_TRINITY_GG_37613_c0_g1_i1	The primary product of this enzyme is 4,2',4',6'- tetrahydroxychalcone (also termed naringenin-chalcone or chalcone) which can under specific conditions spontaneously isomerize into naringenin	4.039	16	3.50344E-05	K66

T_84	PiniT25N_TRINITY_DN36430_c1_g2_i1	The primary product of this enzyme is 4,2',4',6'- tetrahydroxychalcone (also termed naringenin-chalcone or chalcone) which can under specific conditions spontaneously isomerize into naringenin	3.215	10	0.01454034	K66
T_85	PiniT27N_TRINITY_DN24283_c0_g2_i3	The primary product of this enzyme is 4,2',4',6'- tetrahydroxychalcone (also termed naringenin-chalcone or chalcone) which can under specific conditions spontaneously isomerize into naringenin	2.373	6	0.010521123	K66
T_86	PiniT25G_TRINITY_GG_55719_c0_g2_i4	The primary product of this enzyme is 4,2',4',6'- tetrahydroxychalcone (also termed naringenin-chalcone or chalcone) which can under specific conditions spontaneously isomerize into naringenin	2.267	5	0.004305095	K66
T_88	PiniA75_J8904341530356598342 49	flavonoid	3.637	13	4.70623E-06	K528
	PiniT23N_TRINITY_DN17427_c0_g1_i4	Helix-loop-helix DNA-binding domain	8.256	68	1.32047E-05	
	PiniT23G_TRINITY_GG_26716_c0_g1_i1	Inherit from euNOG: glutamine dumper	7.805	61	0.000751705	
	PiniT31G_TRINITY_GG_22027_c0_g1_i3	12-oxophytodienoate reductase	7.774	60	1.02989E-05	K5894
	PiniA21_R77093757141354653557244	40s ribosomal protein s13	7.499	56	0.000128839	K2953
	PiniT23N_TRINITY_DN26011_c0_g4_i4	Transcription factor	6.978	49	0.000207654	K9286
	PiniA47_J30970601127252003021189	Transcription factor	6.977	49	0.000780416	K9422
	PiniT29G_TRINITY_GG_32304_c0_g1_i1	SRG1-like	6.919	48	3.10819E-09	
	PiniT25_TRINITY_DN33687_c0_g2_i3	calcium-binding protein PBP1-like	6.840	47	0.000247746	K16465
	PiniA71_R116517317582264343606	1-aminocyclopropane-1-carboxylate synthase	6.819	46	0.0002759	K1762
	PiniT25G_TRINITY_GG_55111_c0_g1_i3	glucose-6-phosphate phosphate translocator	6.813	46	0.000201667	K15283
	PiniT27N_TRINITY_DN23582_c0_g1_i7	Transcription factor	6.783	46	0.000281302	K9286
	PiniT21_TRINITY_DN11649_c0_g1_i1	branching enzyme	6.754	46	0.002435687	K7

	PiniA23_R70778881448907582028761	adp-ribosylation factor	6.685	45	0.000929628	K7937
	PiniA71_S37721053713044	40S ribosomal protein S14	6.628	44	0.000647226	K2955
	PiniA61_S1854694797150581018772	polygalacturonase	6.551	43	7.16542E-05	
	PiniT31N_TRINITY_DN37217_c1_g1_i1	acid-thiol ligase activity	6.450	42	9.61242E-08	
	PiniT31N_TRINITY_DN21543_c0_g1_i1	Acetyltransferase (GNAT) family	6.432	41	7.84995E-09	
	PiniT31_TRINITY_DN36904_c2_g2_i9	Transcription factor	6.411	41	0.001130391	K9286
	PiniT21G_TRINITY_GG_16215_c0_g1_i1	WRKY transcription factor	6.355	40	0.000287025	
	PiniT21N_TRINITY_DN20512_c0_g1_i6	12-oxophytodienoate reductase	6.322	40	1.57869E-09	K5894
	PiniA61_R18864548011301795794	Inhibitor	6.218	39	0.003047159	K12462
	PiniA75_R862044151431198945073 83	polygalacturonase	6.218	39	2.54293E-11	
	PiniA49_R30764791201107482747874	NADH flavin oxidoreductase NADH oxidase family protein	6.216	39	0.000914413	K354
	PiniT21N_TRINITY_DN21273_c2_g3_i8	Transcription factor	6.189	38	2.45866E-07	K9422
	PiniA21_R78450941669343221558759	coproporphyrinogen III oxidase	6.149	38	0.01122741	K228
	PiniA21_S77362971853948652889218	Pyruvate decarboxylase	6.148	38	0.004605584	K1568
	PiniA71_R1091844141057110837263	Phospholipase A1-Igamma3	6.147	38	2.24836E-05	
	PiniA47_R3043613137915781618818 11	12-oxophytodienoate reductase	6.095	37	8.66075E-10	K5894
	PiniA21_R77717761729772007579840	Aldehyde dehydrogenase	6.016	36	0.00246178	K129
	PiniT25N_TRINITY_DN19484_c0_g1_i1	GTP-binding Protein	6.003	36	0.002818086	K4513
	PiniA21_R7773928712349431624624	Peptidyl-prolyl cis-trans isomerase	5.985	36	0.008914902	K9568
	PiniA55_J2304658708586421805431	60S ribosomal protein l26	5.980	36	0.000265592	K2898

	PiniA27_J60558136091060615708433	ribosomal protein L32'	5.969	36	0.000172697	K2912
	PiniA25_R6792263200539151326745	nadh-ubiquinone oxidoreductase	5.903	35	0.012005947	K3934
	PiniA37_J4350377971121303890032	S-formylglutathione hydrolase	5.891	35	0.011220812	K17
	PiniA71_R1139898106115488622247	ubiquitin	5.856	34	0.000791783	K877
	PiniA23_R73281841358347906463694	nucleolin protein Nsr1	5.853	34	0.003408696	K11294
	PiniT21_TRINITY_DN20231_c0_g1_i1	peroxisomal membrane protein	5.761	33	0.008129496	K14171
	PiniT27G_TRINITY_GG_14522_c1_g1_i2	calcium-binding protein PBP1-like	5.755	33	0.007119285	K16465
	PiniT21G_TRINITY_GG_31614_c0_g1_i1	Nodulation-signaling pathway 2	5.745	33	1.12952E-11	
	PiniA75_R8639472900309190773511	Plant lipoxygenase may be involved in a number of diverse aspects of plant physiology including growth and development, pest resistance, and senescence or responses to wounding (By similarity)	5.724	33	2.79065E-07	K15718
	PiniT31G_TRINITY_GG_40535_c3_g1_i3	1-aminocyclopropane-1-carboxylate synthase	5.669	32	1.59344E-08	K1762
	PiniT27G_TRINITY_GG_4397_c0_g1_i5	chitinase	5.658	32	3.14741E-05	K2547
	PiniA21_R77948071126229617229912	May mediate the reduction of outer membrane cytochrome b5 (By similarity)	5.658	32	0.004562206	K326
	PiniA71_R1085880140756223972475	Ocs element-binding factor	5.647	32	2.55787E-13	
	PiniA39_R4083221139212944014230 33	Glycosyltransferase	5.618	32	3.00802E-09	K8238
	PiniA25_R64786051724642450458 9574	Phospholipase A1-Igamma3	5.617	32	1.12552E-05	
	PiniA21_R77567841562731321598810	rab gdp-dissociation inhibitor	5.580	31	0.002915442	K17255
	PiniT31N_TRINITY_DN34363_c0_g1_i3	Aluminum-activated malate transporter	5.580	31	0.0033672	
	PiniA23_R71154311479403835651924	curved dna-binding protein	5.468	30	0.01121768	
	PiniT21G_TRINITY_GG_18391_c0_g1_i1	Transcription factor	5.462	30	7.14038E-12	K9286

	PiniT27N_TRINITY_DN20445_c2_g1_i3	Transcription factor	5.435	30	0.001858739	K9286
	PiniA71_S113063996619608412921	jasmonate-zim-domain protein 1	5.430	29	8.30984E-07	
	PiniA21_R769937511022003311164088	40S ribosomal protein S1	5.418	29	0.000812068	K2984
	PiniT21_TRINITY_DN23126_c0_g1_i1	NADPH-dependent methylglyoxal reductase GRE2	5.404	29	0.011451974	
	PiniT21_TRINITY_DN12645_c0_g1_i1	Dihydroxy-acid dehydratase	5.293	28	0.02266522	K1687
	PiniA51_R278418410047584238950	The proteasome is a multicatalytic proteinase complex which is characterized by its ability to cleave peptides with Arg, Phe, Tyr, Leu, and Glu adjacent to the leaving group at neutral or slightly basic pH. The proteasome has an ATP-dependent proteolytic activity (By similarity)	5.282	28	0.015372217	K2726
	PiniT29G_TRINITY_GG_32049_c0_g1_i1	Late embryogenesis abundant protein	5.232	27	2.9834E-05	
	PiniA21_R78428799172675333375705	protoplast secreted protein 2	5.204	27	0.031839339	K389
	PiniA23_S6990379222678946514001	Phosphorylase is an important allosteric enzyme in carbohydrate metabolism. Enzymes from different sources differ in their regulatory mechanisms and in their natural substrates. However, all known phosphorylases share catalytic and structural properties (By similarity)	5.169	27	0.013416772	K688
	PiniA21_S432911565410646	thioesterase	5.091	26	0.001293673	
	PiniT27G_TRINITY_GG_2293_c1_g1_i5	UDP-glycosyltransferase	5.080	26	1.65993E-09	K13496
	PiniT21_TRINITY_DN12930_c0_g1_i1	serine threonine-protein phosphatase	5.076	26	0.024403473	K6269
	PiniA25_R67187261397194111947639	protein phosphatase PP2A regulatory subunit A	5.062	26	0.034395674	K3456
	PiniA65_R15045722242511841427838	phospholipase A1-Ibeta2, chloroplastic-like	5.061	26	0.000322813	

	PiniA21_S77007021724398941686879	Plays an important role in the de novo pathway and in the salvage pathway of purine nucleotide biosynthesis. Catalyzes the first	5.054	26	0.036976928	K1939
	PiniT21N_TRINITY_DN21387_c2_g5_i2	Transcription factor	5.051	26	0.001654034	K9286
	PiniA21_S210854181813570	attachment protein	5.041	25	0.04022858	K15296
	PiniT21_TRINITY_DN14173_c0_g1_i1	Catalyzes the removal of a penultimate prolyl residue from the N-termini of peptides (By similarity)	5.031	25	0.019047549	K14213
	PiniA23_R6993002147564069141104 33	Transcription factor	5.028	25	1.0307E-10	K9286
	PiniA21_R78893881221281312207179	3 complex	5.018	25	0.024848526	K5757
	PiniA21_S78021391372435355099627	3-ketoacyl-coA thiolase	5.018	25	0.028835827	K7513
	PiniA21_R78221091192236774391145	regulatory subunit	5.017	25	0.026291432	K364
	PiniA27_R61634281530590711685899	BAHD acyltransferase	5.005	25	9.38314E-08	
	PiniT21_TRINITY_DN35082_c0_g1_i1	Arp2 3 complex	4.993	25	0.033223281	K18584
	PiniA45_S34197061355380321496711	E3 ubiquitin-protein ligase	4.977	25	1.36046E-08	
	PiniA21_R78192871227273598966 79	vacuolar ATP synthase subunit d	4.951	25	0.026470727	K2146
	PiniA39_S41949921031184511597910	Seems to be required for maximal rate of protein biosynthesis. Enhances ribosome dissociation into subunits and stabilizes the binding of the initiator Met-tRNA(I) to 40 S ribosomal subunits (By similarity)	4.944	24	0.013133607	K3236
	PiniT21N_TRINITY_DN22363_c1_g2_i1	calcium-binding protein PBP1-like	4.932	24	0.000102198	K16465
	PiniT27_TRINITY_DN42212_c1_g2_i1	Transcription factor	4.914	24	6.24456E-09	K9286
	PiniT29G_TRINITY_GG_8114_c4_g1_i1	Mitogen-activated protein kinase kinase kinase	4.910	24	8.95612E-12	
	PiniT21_TRINITY_DN27772_c1_g2_i5	calcium-binding protein PBP1-like	4.885	24	0.005024032	K16465

	PiniA75_R958030202682130281879	cytochrome P450	4.876	24	1.00777E-07	K9832
	PiniT29N_TRINITY_DN27650_c0_g1_i8	phosphatase 2C	4.868	24	0.002000787	
	PiniT23_TRINITY_DN34067_c0_g3_i2	Protein IN2-1 homolog	4.867	24	6.81381E-07	K799
	PiniT21_TRINITY_DN29598_c2_g1_i4	diphosphate synthase	4.816	23	1.39628E-07	K412
	PiniT21_TRINITY_DN429_c0_g1_i1	t-complex protein 1	4.785	23	0.038119385	K9494
	PiniT23N_TRINITY_DN22640_c0_g1_i4	Core component of nucleosome. Nucleosomes wrap and compact DNA into chromatin, limiting DNA accessibility to the cellular machineries which require DNA as a template. Histones thereby play a central role in transcription regulation, DNA repair, DNA replication and chromosomal stability. DNA accessibility is regulated via a complex set of post-translational modifications of histones, also called histone code, and nucleosome remodeling	4.716	22	0.000707342	K11253
	PiniT23N_TRINITY_DN21993_c0_g3_i3	E3 ubiquitin-protein ligase	4.714	22	4.83941E-09	K16281
	PiniA21_R8019990855117941841641	NADH flavin oxidoreductase NADH oxidase family protein	4.676	22	0.043286284	K354
	PiniT21_TRINITY_DN38861_c0_g1_i1	Component of the eukaryotic translation initiation factor 3 (eIF-3) complex, which is involved in protein synthesis and, together with other initiation factors, stimulates binding of mRNA and methionyl-tRNAi to the 40S ribosome (By similarity)	4.664	22	0.039109188	K3253
	PiniA21_S36161692114586	The proteasome is a multicatalytic proteinase complex which is characterized by its ability to cleave peptides with Arg, Phe, Tyr, Leu, and Glu adjacent to the leaving group at neutral or slightly basic pH. The proteasome has an ATP-dependent proteolytic activity (By similarity)	4.647	22	0.042131838	K2725
	PiniT21G_TRINITY_GG_32334_c0_g1_i1	auxin-induced protein	4.618	21	1.07847E-07	
	PiniT21G_TRINITY_GG_41795_c1_g1_i1	1-aminocyclopropane-1-carboxylate synthase	4.617	21	1.99038E-08	K1762

	PiniT29N_TRINITY_DN33485_c1_g1_i1	chitinase	4.609	21	2.53745E-05	K2547
	PiniT21_TRINITY_DN39282_c0_g1_i1	guanine nucleotide-binding protein	4.607	21	0.034244006	K463
	PiniT21N_TRINITY_DN20945_c0_g4_i2	loosening and extension of plant cell walls by disrupting non-covalent bonding between cellulose microfibrils and matrix glucans. No enzymatic activity has been found	4.590	21	0.0086028	
	PiniT29G_TRINITY_GG_4825_c0_g1_i3	flavonol 3-O-glucosyltransferase activity	4.579	21	6.2317E-09	
	PiniA75_R885439183562016789061	1-aminocyclopropane-1-carboxylate synthase	4.553	21	6.11113E-08	K2772
	PiniA41_R401549811069927329910 14	60S ribosomal protein L5	4.540	21	0.001059579	K2932
	PiniT27N_TRINITY_DN6730_c0_g1_i1	trafficking protein particle complex subunit 3	4.499	20	0.040933256	K232
	PiniT21_TRINITY_DN1463_c0_g1_i1	Component of the eukaryotic translation initiation factor 3 (eIF-3) complex, which is involved in protein synthesis and, together with other initiation factors, stimulates binding of mRNA and methionyl-tRNAi to the 40S ribosome (By similarity)	4.487	20	0.047571547	K3251
	PiniT21N_TRINITY_DN21887_c0_g3_i5	Transcription factor	4.445	20	0.000133543	K9286
	PiniA21_R7888922117521206549162	Component of the eukaryotic translation initiation factor 3 (eIF-3) complex	4.440	20	0.027880287	K3248
	PiniT21N_TRINITY_DN23354_c3_g1_i11	phosphatase 2C	4.398	19	0.000590884	
	PiniT29N_TRINITY_DN26849_c0_g3_i4	WRKY transcription factor	4.373	19	4.0414E-05	
	PiniA75_R976749154117382849462	Serine threonine-protein kinase	4.346	19	0.005181575	
	PiniT21_TRINITY_DN27220_c1_g4_i3	Transcription factor	4.341	19	9.84953E-07	
	PiniA55_R2265244106230027939177	inositol oxygenase	4.315	19	0.008325679	K469
	PiniT31G_TRINITY_GG_47097_c0_g1_i1	Glutathione S-transferase	4.303	19	2.28405E-06	K799
	PiniT25G_TRINITY_GG_14836_c1_g1_i3	calcium-binding protein PBP1-like	4.267	18	0.037644268	K16465

	PiniA27_R6100343178512526117383 16	ATP-dependent RNA helicase which is a subunit of the eIF4F complex involved in cap recognition and is required for mRNA binding to ribosome. In the current model of translation initiation, eIF4A unwinds RNA secondary structures in the 5'-UTR of mRNAs which is necessary to allow efficient binding of the small ribosomal subunit, and subsequent scanning for the initiator codon (By similarity)	4.263	18	0.004984681	K3257
	PiniT23G_TRINITY_GG_15584_c0_g1_i1	polygalacturonase QRT3-like	4.262	18	5.9668E-05	
	PiniT21G_TRINITY_GG_20956_c0_g1_i1	loosening and extension of plant cell walls by disrupting non-covalent bonding between cellulose microfibrils and matrix glucans. No enzymatic activity has been found	4.249	18	0.009513376	
	PiniA61_S18121454294484711466	glucan endo-1-3-beta-glucosidase	4.223	18	5.96972E-05	
	PiniA27_R62736941755304532814529	ATP-citrate synthase subunit 1	4.218	18	0.024210638	K1648
	PiniA37_S45254317462061192313813	Core component of nucleosome. Nucleosomes wrap and compact DNA into chromatin, limiting DNA accessibility to the cellular machineries which require DNA as a template. Histones thereby play a central role in transcription regulation, DNA repair, DNA replication and chromosomal stability. DNA accessibility is regulated via a complex set of post-translational modifications of histones, also called histone code, and nucleosome remodeling	4.210	18	0.00620993	K11252
	PiniT29N_TRINITY_DN28923_c2_g1_i1	chaperone protein dnaJ 11	4.190	18	0.000647791	
	PiniT23N_TRINITY_DN25285_c1_g2_i2	Aluminum-activated malate transporter	4.168	17	0.011854409	
	PiniA21_R77912591649327126900003	phosphoenolpyruvate carboxykinase	4.153	17	0.008201816	K161
	PiniT29N_TRINITY_DN34926_c0_g1_i8	ADP,ATP carrier protein	4.150	17	1.30215E-08	K5863
	PiniA27_R60830257991155905348619	40s ribosomal protein S17	4.123	17	0.005535742	K2962
	PiniA75_R888770192625453708302	auxin responsive protein	4.011	16	0.000357355	K14487

	PiniA65_R14387341160135011508245	Glutathione S-transferase	3.999	16	0.001707204	K799
	PiniA21_R77577541137857784901478	Catalyzes the initial reaction in the xylose utilization pathway by reducing D-xylose into xylitol. Xylose is a major component of hemicelluloses such as xylan. Most fungi utilize D- xylose via three enzymatic reactions, xylose reductase (XR), xylitol dehydrogenase (XDH), and xylulokinase, to form xylulose 5- phosphate, which enters pentose phosphate pathway	3.998	16	0.024009271	K17743
	PiniA33_R49754973042463323248805 27	Plant lipoxygenase may be involved in a number of diverse aspects of plant physiology including growth and development, pest resistance, and senescence or responses to wounding (By similarity)	3.983	16	9.19461E-06	K15718
	PiniT31N_TRINITY_DN25413_c0_g1_i1	Sugar carrier protein	3.958	16	4.92113E-07	
	PiniA35_S4738958571202131246336	polygalacturonase QRT3-like	3.944	16	2.45866E-07	
	PiniT31G_TRINITY_GG_9285_c0_g1_i6	jasmonate-zim-domain protein 10	3.932	15	8.90267E-07	K13464
	PiniA65_J1447093150090019396290	U-box domain-containing protein	3.862	15	0.008682272	
	PiniA35_R4703674815755714371277	WRKY transcription factor	3.856	15	6.72145E-05	
	PiniT23N_TRINITY_DN25329_c0_g1_i4	Late embryogenesis abundant protein	3.833	15	0.000268623	
	PiniA71_R107379818422383507352 73	1-aminocyclopropane-1-carboxylate synthase	3.829	15	8.73683E-07	K1762
	PiniT21N_TRINITY_DN21085_c2_g1_i2	protein BPS1, chloroplastic-like	3.814	15	1.94789E-05	
	PiniA31_R53075582091204121139897 45	Lignin degradation and detoxification of lignin-derived products (By similarity)	3.795	14	0.000425467	K599
	PiniA41_R39924861655137143092424	UDP-Glycosyltransferase	3.775	14	0.003962135	K13691
	PiniA21_R77098179731498821807202	60S ribosomal protein L8	3.746	14	0.010054846	K2936
	PiniA75_R8644062079487446507486	reductase	3.727	14	1.73323E-11	K597

	PiniT21G_TRINITY_GG_6568_c0_g1_i1	UDP-glycosyltransferase 74B1-like	3.684	14	0.02109289	K13691
	PiniT29_TRINITY_DN40218_c0_g1_i5	jasmonate-zim-domain protein 1	3.673	13	2.79065E-07	
	PiniA75_R88422715885971066194	Glutamate-gated receptor that probably acts as non- selective cation channel	3.651	13	0.00989104	K5387
	PiniT21N_TRINITY_DN23659_c1_g1_i5	beta-fructofuranosidase	3.647	13	4.30878E-07	K1193
	PiniT25G_TRINITY_GG_12937_c0_g1_i1	gibberellin	3.642	13	3.63791E-06	K4125
	PiniA27_R62049451149708786040710	DNA-binding protein ESCAROLA-like	3.639	13	0.005137783	
	PiniA39_R40682942274155947337795 54	Lignin degradation and detoxification of lignin-derived products (By similarity)	3.634	13	0.000296096	K599
	PiniA21_R76936017741690635718288	60S ribosomal protein L27	3.612	13	0.010649635	K291
	PiniT27G_TRINITY_GG_22224_c2_g1_i5	glutathione peroxidase	3.577	13	0.000633956	K432
	PiniA21_R778672184352984626699 5	Transcription factor	3.575	13	0.002213258	
	PiniA31_R53042761960388694552823 86	12-oxophytodienoate reductase	3.569	13	1.15423E-05	K5894
	PiniT21G_TRINITY_GG_4553_c0_g1_i1	Lipase class 3 family protein	3.564	13	0.014924107	
	PiniT21N_TRINITY_DN22060_c0_g2_i2	biosynthesis protein	3.545	13	5.74549E-10	K6215
	PiniT23N_TRINITY_DN22939_c3_g3_i1	nac domain	3.540	13	0.002679812	
	PiniT31G_TRINITY_GG_51582_c2_g1_i13	wound-induced protein	3.518	12	3.32853E-06	
	PiniA61_R18717381240281601660710	60s ribosomal protein	3.513	12	0.010001115	K293
	PiniT21_TRINITY_DN34821_c0_g1_i1	Translation initiation factor	3.484	12	0.014491148	K3263
	PiniT21_TRINITY_DN26603_c0_g1_i4	receptor-like protein kinase	3.469	12	0.000601292	
	PiniT29G_TRINITY_GG_4333_c0_g1_i1	chitinase	3.468	12	0.009434803	K2547
	PiniA21_R76575422381250130437398 94	atp sulfurylase	3.460	12	1.2859E-09	K13811

	PiniT29N_TRINITY_DN23023_c4_g4_i1	Retrotransposon protein	3.446	12	0.029138785	
	PiniT21N_TRINITY_DN19582_c0_g1_i6	xyloglucan galactosyltransferase	3.418	12	1.01898E-07	K2888
	PiniT27_TRINITY_DN43259_c0_g1_i3	Pathogenesis-related protein	3.380	11	7.51271E-05	K13449
	PiniT21N_TRINITY_DN22106_c0_g2_i3	thaumatin-like protein	3.378	11	0.000330881	
	PiniT25G_TRINITY_GG_7267_c1_g1_i3	Transcription factor	3.368	11	0.000311065	
	PiniT29G_TRINITY_GG_9765_c0_g1_i6	chitinase	3.365	11	7.32519E-05	K2547
	PiniT25_TRINITY_DN31382_c2_g1_i2	chaperone protein dnaJ 11	3.361	11	5.01707E-12	
	PiniA75_R87895385123012650416	Late embryogenesis abundant protein	3.357	11	0.000723028	
	PiniT23_TRINITY_DN32807_c2_g1_i2	Pleiotropic drug resistance protein	3.317	11	2.50541E-08	
	PiniT23G_TRINITY_GG_14546_c0_g1_i1	UDP-Glycosyltransferase	3.301	11	0.001128226	K13691
T_21	PiniT27G_TRINITY_GG_52956_c1_g1_i5	carbonic anhydrase_t1	3.296	11	8.29676E-15	K1674
	PiniA33_R49813201696132004815586 44	WRKY transcription factor	3.292	11	3.71516E-05	
	PiniT29G_TRINITY_GG_50531_c0_g1_i2	Glutathione S-transferase	3.289	11	6.92593E-06	K799
	PiniT29G_TRINITY_GG_40005_c0_g1_i4	pleiotropic drug resistance	3.279	11	8.95612E-12	
	PiniA65_R1459946205070951420325	Lignin degradation and detoxification of lignin-derived products (By similarity)	3.273	11	5.982E-06	K599
	PiniT27N_TRINITY_DN36736_c1_g1_i1	May be involved in modulation of pathogen defense and leaf cell death (By similarity)	3.268	11	0.003932325	K8472
	PiniA45_S339114315311182001209841	1-aminocyclopropane-1-carboxylate oxidase	3.236	10	0.006682176	K5933
	PiniT25G_TRINITY_GG_34287_c0_g1_i2	Glutathione S-transferase	3.230	10	3.4313E-05	K799
	PiniT31N_TRINITY_DN37205_c2_g2_i1	Potassium transporter	3.226	10	6.68664E-08	K3549
	PiniA65_R1430542109010791121695 24	Glutathione S-transferase	3.226	10	0.000220876	K799

	PiniT23N_TRINITY_DN25082_c1_g1_i7	Transcription factor	3.200	10	4.55632E-05	
	PiniT21G_TRINITY_GG_15208_c0_g1_i1	synthase	3.192	10	0.001654034	
	PiniT25G_TRINITY_GG_39833_c0_g1_i1	Inherit from euNOG: NAD dependent epimerase dehydratase family protein	3.181	10	0.000295119	K22419
	PiniA75_R8714521440132815625828	DJ-1/PfpI family	3.175	10	1.46294E-05	
	PiniA71_S8408157114131	Catalyzes the formation of formate and 2-keto-4- methylthiobutyrate (KMTB) from 1,2-dihydroxy-3-keto-5- methylthiopentene (DHK-MTPene) (By similarity)	3.173	10	0.047176919	K8967
	PiniT29N_TRINITY_DN30545_c0_g1_i1	beta-1,3-galactosyltransferase 7-like	3.170	10	5.7099E-08	K2855
	PiniA49_R2804484126473447311331 61	VQ motif	3.167	10	3.81933E-05	
	PiniA71_R10729101471256081450350	serine acetyltransferase	3.157	10	8.90267E-07	K64
	PiniT23N_TRINITY_DN24724_c0_g1_i9	Protein IN2-1 homolog	3.147	10	1.09502E-08	K799
	PiniT23N_TRINITY_DN25643_c1_g1_i6	calcium-binding protein PBP1-like	3.141	10	0.030709843	K16465
	PiniT29G_TRINITY_GG_52447_c1_g1_i1	Shikimate kinase	3.113	10	3.0062E-07	K891
	PiniT21G_TRINITY_GG_8902_c0_g1_i1	chitinase	3.102	10	0.007239636	K1183
	PiniT27G_TRINITY_GG_35221_c0_g1_i1	UDP-Glycosyltransferase	3.101	10	1.59246E-07	
	PiniT21N_TRINITY_DN20210_c0_g1_i5	Acetyltransferase (GNAT) family	3.089	10	5.63018E-05	
	PiniA49_R28041612196119074784709	Ubiquinol oxidase	3.081	9	3.12138E-06	K17893
	PiniT27G_TRINITY_GG_32375_c0_g1_i1	glutathione peroxidase	3.069	9	0.027960912	K432
	PiniA65_J14485502275449061426525	Transcription factor	3.036	9	4.22717E-13	
	PiniT21G_TRINITY_GG_12296_c0_g1_i1	cytokinin	3.026	9	0.000437367	K279
	PiniA61_R17393231800187866668827	Transcription factor	3.021	9	1.54764E-05	K9422

	PiniA65_R1430880158110459031013092	12-oxophytodienoate reductase	3.019	9	0.000140939	K5894
	PiniA61_R172315331502865131002512	Plant lipoxygenase may be involved in a number of diverse aspects of plant physiology including growth and development, pest resistance, and senescence or responses to wounding (By similarity)	3.016	9	0.003408696	K15718
	PiniA51_R26079391887125935597163	Lignin degradation and detoxification of lignin-derived products (By similarity)	3.001	9	0.003562584	K599
	PiniT25G_TRINITY_GG_19932_c0_g1_i5	bidirectional sugar transporter	2.973	9	1.23723E-05	K15382
	PiniT23_TRINITY_DN33151_c1_g1_i1	response to low sulfur	2.958	9	0.049997191	
	PiniA55_R220682426561495192847850	riboflavin biosynthesis protein	2.950	9	4.54966E-06	K14652
	PiniA25_R64742094058226507037644 22	RNA helicase	2.945	9	0.000120269	K1325
	PiniT31N_TRINITY_DN35089_c0_g1_i9	cysteine synthase	2.939	9	3.0062E-07	K1334
	PiniT27N_TRINITY_DN30231_c0_g1_i1	nac domain	2.925	9	0.00021356	
	PiniT21_TRINITY_DN28039_c4_g1_i1	bidirectional sugar transporter	2.923	9	0.003221358	K15382
	PiniA21_J77292661118403913391691	fructose-bisphosphate aldolase	2.919	9	0.000345683	K1623
	PiniA21_R76656595510161721246731 37	ABC transporter C family member	2.904	8	0.000133543	
	PiniA45_R352549175992052280555	synthetase	2.894	8	0.000383783	K22133
	PiniT23_TRINITY_DN29602_c1_g1_i10	Mitogen-activated protein kinase kinase kinase	2.891	8	0.00459266	
	PiniT25_TRINITY_DN33687_c0_g2_i1	calcium-binding protein PBP1-like	2.889	8	0.043102889	K16465
	PiniT29_TRINITY_DN36239_c0_g1_i2	RING-H2 finger protein	2.880	8	0.000245722	
	PiniT23_TRINITY_DN30829_c3_g1_i2	Transcription factor	2.863	8	8.8068E-05	K9422
	PiniT25G_TRINITY_GG_35989_c0_g1_i1	Pleiotropic drug resistance protein	2.836	8	5.46951E-06	

	PiniT25N_TRINITY_DN34611_c0_g1_i1	LRR receptor-like serine threonine-protein kinase	2.813	8	3.61439E-06	
	PiniT31G_TRINITY_GG_23238_c0_g1_i5	Allene oxide synthase	2.811	8	0.022715982	K1723
	PiniA47_R30920042949811901667280	Cysteine-rich receptor-like protein kinase	2.806	8	0.030936251	
	PiniA61_R1916259111633521486427	Elongation factor	2.794	8	0.031502462	K3234
	PiniT29G_TRINITY_GG_12639_c0_g1_i1	BAHD acyltransferase	2.787	8	2.8707E-06	
	PiniA29_R5678435187277785712226646	nac domain	2.768	8	1.07655E-05	
	PiniA75_R8660781565175956217457	12-oxophytodienoate reductase	2.763	8	0.003336403	K5894
	PiniT25G_TRINITY_GG_41648_c0_g1_i2	1-aminocyclopropane-1-carboxylate oxidase	2.757	8	0.027914712	K5933
	PiniT31_TRINITY_DN30069_c0_g1_i1	U-box domain-containing protein	2.750	8	0.022017321	
	PiniT27_TRINITY_DN34189_c1_g3_i1	Short-chain type dehydrogenase	2.729	7	0.008534597	K59
	PiniA43_R35836751830232141528949	LRR receptor-like serine threonine-protein kinase	2.726	7	0.002435687	
	PiniA75_R8738991514412516530935	F-box kelch-repeat protein	2.716	7	2.39613E-06	
	PiniT23_TRINITY_DN34118_c0_g1_i1	1-aminocyclopropane-1-carboxylate oxidase	2.709	7	0.008813409	K5933
	PiniT21G_TRINITY_GG_29087_c0_g1_i1	Transcription factor	2.699	7	0.005396443	K9422
	PiniT21G_TRINITY_GG_27256_c0_g1_i1	receptor kinase	2.697	7	0.003904886	
	PiniT21N_TRINITY_DN17438_c0_g1_i1	receptor-like protein kinase	2.695	7	0.001596758	
	PiniT31G_TRINITY_GG_4183_c0_g1_i2	germin-like protein	2.687	7	0.003082169	
	PiniT25_TRINITY_DN29778_c0_g1_i3	Transcription factor	2.685	7	2.31697E-06	K9422
	PiniA33_R4976658394421990283442782	ABC transporter	2.672	7	1.4482E-05	K5658
	PiniT25N_TRINITY_DN32043_c0_g1_i2	gamma-glutamyltranspeptidase	2.664	7	1.1991E-09	K18592

	PiniA55_J2324014191529212768381	polygalacturonase QRT3-like	2.656	7	0.00220874	
	PiniA35_R4669934147631586325146 58	Myb-related protein	2.651	7	1.23692E-06	K9422
	PiniT27G_TRINITY_GG_4941_c3_g1_i3	Sucrose-cleaving enzyme that provides UDP-glucose and fructose for various metabolic pathways (By similarity)	2.647	7	1.9923E-05	K695
	PiniT23G_TRINITY_GG_14227_c0_g1_i1	1-aminocyclopropane-1-carboxylate oxidase	2.645	7	0.009096755	K5933
	PiniA43_S3848810175985133495565	Disease resistance protein	2.632	7	0.000664198	
	PiniT25G_TRINITY_GG_3461_c3_g1_i4	3-ketoacyl-coa thiolase	2.630	7	2.79065E-07	K7513
	PiniT21N_TRINITY_DN22436_c0_g1_i4	Allene oxide synthase	2.611	7	0.025874704	K1723
	PiniA45_J3368201174081607185 6485	serine threonine-protein kinase	2.609	7	1.10301E-06	
	PiniT21_TRINITY_DN26914_c1_g1_i1	benzyl alcohol O-benzoyltransferase-like	2.605	7	1.39915E-05	K19861
	PiniA51_R2598860197920360411368 48	UDP-glucoronosyl and UDP-glucosyl transferase	2.600	7	0.036323691	K13691
	PiniA29_R5752120144613584925029 39	U-box domain-containing protein	2.599	7	0.034038687	
	PiniA41_R3781259175133270452901291	Electron carrier protein. The oxidized form of the cytochrome c heme group can accept an electron from the heme group of the cytochrome c1 subunit of cytochrome reductase. Cytochrome c then transfers this electron to the cytochrome oxidase complex, the final protein carrier in the mitochondrial electron-transport chain (By similarity)	2.590	7	1.20206E-07	K8738
	PiniT29N_TRINITY_DN30582_c0_g6_i1	cytochrome P450	2.580	7	0.002290229	K2665
	PiniT25N_TRINITY_DN35687_c0_g1_i2	thaumatin-like protein	2.580	7	0.000842759	
	PiniT29G_TRINITY_GG_23556_c0_g1_i1	bidirectional sugar transporter	2.576	7	0.005304756	K15382
	PiniT21N_TRINITY_DN22042_c0_g3_i1	chitinase	2.570	7	0.046999506	K1183
	PiniT21G_TRINITY_GG_14764_c0_g1_i1	wound-induced protein	2.560	7	0.008135845	

	PiniT21_TRINITY_DN23881_c0_g1_i2	3-methyl-2-oxobutanoate	2.558	7	2.98855E-05	K66
	PiniA71_R10723031601171925738630	C2 domain of PTEN tumour-suppressor protein	2.546	6	1.10148E-08	K111
	PiniA21_R768910918856347775097239	oxidoreductase, 2OG-Fe(II) oxygenase family protein	2.525	6	1.62657E-07	
	PiniT31G_TRINITY_GG_32739_c0_g1_i2	Prephenate dehydratase	2.524	6	7.11138E-08	K5359
	PiniT21_TRINITY_DN23822_c0_g1_i1	Polyamine oxidase	2.496	6	0.02711604	K13366
	PiniA75_R8788651983147707163881	Galacturonosyltransferase	2.493	6	2.88786E-11	K2867
	PiniA65_S14939601706144037437099	Arogenate dehydratase prephenate dehydratase	2.488	6	4.91148E-07	K5359
	PiniA61_R1846673178616947991892	Phospholipase A1-Igamma3	2.478	6	0.006541196	
	PiniA71_R10694393488666159166442	Plant lipoxygenase may be involved in a number of diverse aspects of plant physiology including growth and development, pest resistance, and senescence or responses to wounding (By similarity)	2.469	6	7.32519E-05	K454
	PiniA23_R6992067286292370532491 51	subtilisin-like	2.469	6	5.79988E-08	
	PiniA29_R5668071255820324784319630	phosphoenolpyruvate carboxykinase	2.466	6	7.48052E-05	K161
	PiniT27N_TRINITY_DN21576_c0_g1_i3	defense response	2.441	6	0.001330528	
	PiniT25_TRINITY_DN35119_c0_g2_i2	anion transporter	2.435	6	4.16726E-09	
	PiniT29G_TRINITY_GG_25005_c1_g1_i3	calcium-binding protein PBP1-like	2.428	6	0.013069055	K16465
	PiniT25G_TRINITY_GG_942_c0_g1_i2	lob domain-containing protein	2.426	6	0.000385178	
	PiniT23G_TRINITY_GG_55991_c0_g1_i1	WRKY transcription factor	2.425	6	0.014164639	
	PiniT31G_TRINITY_GG_49636_c2_g1_i14	Inherit from euNOG: maternal effect embryo arrest 59	2.416	6	0.003955897	
	PiniT23N_TRINITY_DN23289_c1_g3_i7	WRKY transcription factor	2.412	6	6.76469E-08	K18835

	PiniT27G_TRINITY_GG_44107_c7_g1_i9	auxin-induced protein	2.407	6	3.00925E-06	
	PiniT21N_TRINITY_DN18240_c0_g1_i1	sugar transport protein	2.387	6	2.25196E-05	
	PiniA71_R10710501114294511549928	4,5-DOPA dioxygenase	2.348	6	0.005947066	K15777
	PiniT27G_TRINITY_GG_30055_c0_g1_i2	nac domain	2.348	6	1.83787E-05	
	PiniA75_R8690861991201743812436	Aminotransferase	2.342	5	0.002254365	K815
	PiniT23G_TRINITY_GG_43933_c0_g1_i1	anthocyanidin reductase	2.336	5	0.038061291	K8695
	PiniT21N_TRINITY_DN22135_c0_g1_i10	polyubiquitin	2.315	5	0.007119285	K877
	PiniA71_S1235825183376449610640l7	Iaa-amino acid hydrolase	2.313	5	1.76813E-09	K2164
	PiniA55_S225425315528537394602	synthase	2.296	5	0.01300419	
	PiniA39_R40925722393716632909462	LRR receptor-like serine threonine-protein kinase	2.294	5	0.008882016	
	PiniA65_R1502135840291130337168	tyrosine specific protein phosphatase family protein	2.293	5	9.99953E-08	K1845
	PiniA65_R1432297225810182321421923	UDP-arabinose 4-epimerase	2.286	5	1.38497E-14	K12448
	PiniT27N_TRINITY_DN36321_c2_g3_i1	Pathogenesis-related protein	2.277	5	0.008135845	K13450
	PiniA21_R76601312017185370732l7610	Proline dehydrogenase	2.267	5	5.7115E-07	K318
	PiniT29G_TRINITY_GG_7779_c1_g1_i1	Rhamnose biosynthetic enzyme	2.265	5	3.01526E-08	K12451

DOWN						
label	**ID**	**annotation**	**log2FoldChange**	**actualFC**	**padj**	**KO**

T_1	PiniA39_R43765201399180538171825 7	ATP synthase delta chain ATPF1D	-3	-7.941326	0.017315891	
T_2	PiniT29_TRINITY_DN24089_c0_g1_i2	Photosystem II psb27	-3	-7.964068	0.0067706	
T_46	PiniA51_R27752171848192062043855	auxin-responsive protein	-3	-7.184555	0.003862703	K14484
T_78	PiniA43_J36990671149143963060448	reductase	-3	-9.406854	0.008269849	K9753
	PiniA55_S2468034717375822095742	phosphatidylinositol 4-kinase type 2-beta	-20	-410.2024	2.24262E-12	
	PiniA71_R11642564917202424922	histone h2a	-8	-58.7651	0.020594888	K11251
	PiniA49_S3090416775266142605246	phosphatidylethanolamine-binding protein	-7	-55.77737	0.000813968	
	PiniA39_J41616401093211783253098	1-aminocyclopropane-1-carboxylate oxidase	-6	-34.35819	1.06071E-08	K5933
	PiniT25_TRINITY_DN32793_c1_g1_i6	amino acid	-6	-34.28058	0.013330044	
	PiniA47_S3051217869115496208150	kDa class I heat shock	-6	-34.09225	6.92593E-06	K13993
	PiniT31N_TRINITY_DN34912_c0_g1_i1	heavy metal-associated domain containing protein, expressed	-5	-26.80867	0.006486245	
	PiniA37_S4349833895103594287865	temperature-induced	-5	-26.24422	0.001283965	K398
	PiniT23_TRINITY_DN30996_c1_g1_i1	zinc knuckle (CCHC-type) family protein	-5	-26.15515	0.000124681	
	PiniT21G_TRINITY_GG_30935_c0_g1_i1	phosphate-induced protein 1 conserved region domain containing protein, expressed	-5	-25.07951	0.001055636	
	PiniT27_TRINITY_DN34410_c1_g1_i3	resistance protein	-5	-25.02997	0.040671646	

	PiniT21_TRINITY_DN29644_c1_g1_i15	auxin-induced protein	-5	-25.01599	0.001658961	K14488
	PiniT27_TRINITY_DN28742_c0_g1_i12	transcription elongation regulator	-5	-22.78307	0.049765183	
	PiniT23N_TRINITY_DN22856_c0_g1_i9	heavy metal-associated domain containing protein, expressed	-5	-21.34238	0.008753703	
	PiniA61_R18563961485118441351985	Transmembrane amino acid transporter protein	-5	-20.51445	0.011787611	
	PiniT23N_TRINITY_DN25882_c0_g1_i5	phosphate-induced protein 1 conserved region domain containing protein, expressed	-4	-19.75378	0.033523505	
	PiniT23N_TRINITY_DN25297_c0_g1_i6	auxin-induced protein	-4	-19.64474	0.024008697	K14488
	PiniT25_TRINITY_DN41786_c0_g1_i3	Pfam:DUF26	-4	-19.43975	0.000662029	
	PiniA45_S28589325635855	Plant protein 1589 of unknown function (A_thal_3526)	-4	-18.01206	0.015936017	
	PiniA71_R119312615321644246128 8	auxin-induced protein	-4	-16.43177	0.019821745	
	PiniT25_TRINITY_DN40005_c1_g1_i7	histone H3	-4	-16.36307	0.011341233	K11253
	PiniA51_R2599461926167665217633	Gibberellin regulated protein	-4	-16.22559	0.000499095	
	PiniA31_R5497571224327803871584	Potassium channel	-4	-16.09152	0.006665054	K21867
	PiniA27_J6114525898157365825365	Retrotransposon protein	-4	-15.9503	0.049058315	
	PiniT21N_TRINITY_DN21796_c0_g1_i11	cytochrome P450	-4	-14.86834	0.006170098	K266
	PiniT25_TRINITY_DN29745_c0_g1_i13	NA	-4	-14.60437	0.001623226	

	PiniA21_S78710301098749697419131	PMEI	-4	-14.60024	0.036000392	
	PiniA35_R4818956139027714433289	E3 ubiquitin-protein ligase BAH1-like	-4	-14.24079	0.031425879	K16275
	PiniA23_J701787579517036669520 19	0	-4	-14.22297	4.27333E-05	
	PiniA43_S382984261496603295132	NA	-4	-14.16254	0.017315891	
	PiniT31G_TRINITY_GG_4771_c1_g2_i1	synthase	-4	-13.97188	0.014383862	
	PiniA51_R28779351026234871424993	Polysaccharide biosynthesis protein	-4	-13.88513	0.007606529	
	PiniA47_J3186652379951631550594	Domain of unknown function (DUF3511)	-4	-13.4792	0.008938537	
	PiniA31_R5325445683185042659266	0	-4	-13.05654	0.02109289	
	PiniT25G_TRINITY_GG_33865_c0_g1_i1	Protease inhibitor/seed storage/LTP family	-4	-12.67665	0.046484727	
	PiniA65_R1599241987173681191896	xyloglucan	-3	-12.23963	0.023500325	K8235
	PiniT25G_TRINITY_GG_1827_c0_g1_i4	Ribonuclease	-3	-11.61753	0.003197251	K1166
	PiniA61_R1737637742282071215085	Pfam:DUF584	-3	-11.61374	0.002354818	
	PiniA27_S6096294504118501025043	RING	-3	-11.59768	0.026238906	
	PiniA21_R774137512641218705269765	lob domain-containing protein	-3	-11.5044	0.0067706	
	PiniA65_R14385951480276002148864	Dehydrogenase	-3	-11.44579	0.02109289	

	PiniT25_TRINITY_DN23124_c0_g1_i1	RING	-3	-11.40554	0.044273656	
	PiniA31_R5360571925956631116658	Disease resistance response protein	-3	-11.331	0.005873833	
	PiniA21_R76732766093698611872176	Protease inhibitor/seed storage/LTP family	-3	-11.24011	0.028373078	
	PiniA75_R907088653567679271	auxin-induced protein	-3	-11.08157	0.019872262	K14488
	PiniT29N_TRINITY_DN29155_c0_g2_i3	Universal stress protein	-3	-11.0061	7.14513E-05	
	PiniT21_TRINITY_DN38156_c0_g1_i1	Protease inhibitor seed storage lipid transfer protein	-3	-10.7555	0.00443171	
	PiniT27_TRINITY_DN41968_c2_g3_i2	kDa class I heat shock	-3	-10.74178	0.032387934	K13993
	PiniA65_R15583491785125091424379	Xyloglucan endotransglucosylase hydrolase protein	-3	-10.63317	0.046538278	K8235
	PiniA23_S3222642139919567	phosphate-induced protein 1 conserved region domain containing protein, expressed	-3	-10.52799	0.046475105	
	PiniT27_TRINITY_DN37828_c0_g1_i4	resistance protein	-3	-10.29995	0.003020748	
	PiniT25G_TRINITY_GG_3862_c0_g1_i1	Ribonuclease	-3	-10.05569	0.006009191	K1166
	PiniA21_R768457724306842463502606	amino acid transporter	-3	-10.04134	0.000650678	K1515
	PiniT27G_TRINITY_GG_33213_c0_g1_i1	O-acyltransferase WSD1-like	-3	-10.03946	0.044165621	
	PiniA65_R145905310563396668712 7	glutathione s-transferase	-3	-9.996613	0.026291432	K799
	PiniT31G_TRINITY_GG_7138_c0_g1_i5	Family of unknown function (DUF716)	-3	-9.972852	0.037932977	

	PiniT29N_TRINITY_DN25318_c0_g1_i1	0	-3	-9.882023	0.018219364	
	PiniA71_S111495858428347313621	dCTP pyrophosphatase 1-like	-3	-9.807693	0.01462011	K1694
	PiniT27_TRINITY_DN31718_c0_g1_i1	Abscisic stress ripening protein 2	-3	-9.740254	0.003559548	
	PiniA21_R78095501120322577016965	Transcription factor	-3	-9.498962	0.03467213	
	PiniT23N_TRINITY_DN25408_c0_g1_i7	subtilisin-like protease-like	-3	-9.247163	0.005448113	
	PiniA61_R188518371511145523244	E3 ubiquitin-protein ligase	-3	-9.223501	0.000718676	K16281
	PiniA37_J4533956561225964345556	Basic blue protein	-3	-9.201764	0.042464718	
	PiniT21G_TRINITY_GG_27063_c0_g1_i1	auxin-induced protein	-3	-9.145253	0.033185519	
	PiniT21_TRINITY_DN26253_c0_g1_i3	fiber expressed protein	-3	-9.111795	0.003549718	
	PiniT25N_TRINITY_DN29367_c0_g1_i1	Disease resistance response protein	-3	-9.093372	0.001039071	
	PiniA71_R11604013696752343652	Protease inhibitor/seed storage/LTP family	-3	-9.050934	0.029796084	
	PiniT29G_TRINITY_GG_41627_c0_g1_i6	glycolipid transfer protein	-3	-9.021943	0.012289858	
	PiniT31N_TRINITY_DN33134_c0_g1_i2	peptide transporter	-3	-8.936938	0.049308622	
	PiniA45_R3319519109528414329433396	Sigma factor sigB regulation protein	-3	-8.850639	0.006720632	
	PiniT27_TRINITY_DN43318_c0_g1_i7	kDa class I heat shock	-3	-8.786757	0.007340143	K13993

	PiniT23_TRINITY_DN33870_c0_g2_i4	Dormancy auxin associated	-3	-8.728655	0.003112672	
	PiniA21_R78017591798762621948014	zinc finger	-3	-8.655031	9.4129E-06	
	PiniA65_R1484563177551179618406	Plant-specific domain TIGR01615 family protein	-3	-8.531378	0.01405889	
	PiniT25N_TRINITY_DN35897_c0_g2_i1	kDa class I heat shock	-3	-8.481068	0.014137596	K13993
	PiniT23G_TRINITY_GG_34853_c0_g1_i1	F-box kelch-repeat protein	-3	-8.381431	0.000401241	
	PiniT23G_TRINITY_GG_23770_c0_g1_i1	)-oxidoreductase	-3	-8.305386	0.047176919	
	PiniA47_R30455834913266381839475	Basic blue protein	-3	-8.304388	0.027114007	
	PiniT21G_TRINITY_GG_3248_c0_g1_i1	auxin-induced protein	-3	-8.238775	4.29635E-05	
	PiniA37_S4577509958387733003338	Conserved Protein	-3	-8.177175	0.006594273	
	PiniA27_J62701216861780264820699	NA	-3	-8.176461	0.048804944	
	PiniT21_TRINITY_DN30603_c0_g2_i4	Abscisic stress ripening protein 2	-3	-8.016548	0.003491095	
	PiniA55_J231482968774451162755	auxin-induced protein	-3	-7.911904	0.018447228	K14488
	PiniT21G_TRINITY_GG_9783_c0_g1_i1	zinc finger, C3HC4 type, domain containing protein, expressed	-3	-7.769428	0.016151531	

	PiniA75_S996865102829276829435	Aquaporin	-3	-7.713636	0.006651421	K9873
	PiniT27_TRINITY_DN34445_c0_g1_i5	Heavy-metal-associated domain	-3	-7.69909	0.025994769	
	PiniA51_S27141045352925551046852	kDa class I heat shock	-3	-7.655498	0.011776482	K13993
	PiniT31N_TRINITY_DN35537_c1_g1_i10	Isoflavone reductase	-3	-7.645696	0.038798572	K21568
	PiniT29_TRINITY_DN35347_c0_g1_i5	Universal stress protein	-3	-7.624084	0.025661807	
	PiniA71_R1079970110172737785646	Nuclear transcription factor Y subunit	-3	-7.510132	0.000320329	K866
	PiniT29G_TRINITY_GG_7221_c0_g1_i1	DnaJ domain	-3	-7.505124	0.01828323	
	PiniT25_TRINITY_DN29516_c0_g4_i3	O-acyltransferase WSD1-like	-3	-7.46543	0.041224678	
	PiniT31_TRINITY_DN27472_c1_g1_i1	fiber expressed protein	-3	-7.460918	0.024629531	
	PiniA21_R774828032261978763953856	ABC transporter	-3	-7.435321	0.010347117	
	PiniT25G_TRINITY_GG_60715_c0_g1_i1	Pfam:DUF584	-3	-7.421353	0.012865911	
	PiniT23N_TRINITY_DN21922_c0_g5_i1	Pfam:DUF584	-3	-7.403314	0.00060335	
	PiniT23N_TRINITY_DN23332_c0_g1_i8	Ent-kaurene oxidase	-3	-7.392979	0.048165475	K4122
	PiniT31_TRINITY_DN37339_c0_g1_i2	lob domain-containing protein	-3	-7.382739	0.036317138	
	PiniT25N_TRINITY_DN30040_c0_g2_i5	Xyloglucan endotransglucosylase hydrolase protein	-3	-7.361277	0.035526821	K8235

	PiniA65_R1541823152313668610993	Methyl-CpG binding domain	-3	-7.342742	5.43271E-05	
	PiniT27G_TRINITY_GG_51142_c0_g1_i2	Abscisic stress ripening protein 2	-3	-7.267117	0.016512077	
	PiniT23N_TRINITY_DN21664_c0_g1_i9	Ocs element-binding factor	-3	-7.184344	0.002203626	
	PiniA55_R223602662944385754929	Universal stress protein	-3	-7.037116	4.54673E-05	
	PiniA21_R778445922571058763164994	Ent-kaurenoic acid oxidase	-3	-7.033555	0.00302116	K4123
	PiniA65_S1584605102912548105662 1	rho GDP-dissociation inhibitor	-3	-6.810546	0.018658832	K12462
	PiniA45_R331531339215157512251 31	NA	-3	-6.697965	0.039787595	
	PiniA71_R10958465637091330106	Disease resistance response protein	-3	-6.688454	0.032462704	
	PiniT25G_TRINITY_GG_6287_c0_g1_i3	Transcription factor	-3	-6.679778	0.004228259	
	PiniA47_R31269251242320062428924	Inherit from KOG: Pentatricopeptide repeat-containing protein	-3	-6.647308	0.015090327	
	PiniA65_S1536472147720766726889	Cbl-interacting protein kinase	-3	-6.629149	0.017809297	
	PiniA55_R22362891614871391361646	Cbl-interacting protein kinase	-3	-6.613369	0.000358348	

	PiniT25_TRINITY_DN35883_c0_g1_i3	Calcium-binding peroxygenase involved in the degradation of storage lipid in oil bodies. May be involved in the interaction between oil bodies and vacuoles during seed germination and in the oxylipin signaling pathways and plant defense responses. Can catalyze sulfoxidation of thiobenzamide, hydroxylation of aniline	-3	-6.611745	0.030459593	K17991
	PiniT31_TRINITY_DN35659_c1_g3_i1	Dormancy auxin associated	-3	-6.59262	0.002010801	
	PiniA23_R69727639317603524629246	ABA/WDS induced protein	-3	-6.55571	0.007549921	
	PiniT31_TRINITY_DN41471_c0_g1_i2	oxidoreductase, 2OG-Fe(II) oxygenase family protein	-3	-6.499022	0.001361851	
	PiniT21N_TRINITY_DN19762_c0_g1_i3	0	-3	-6.492249	0.010606625	
	PiniA37_R43998863377712482630106	STYKc	-3	-6.462972	0.03469719	
	PiniT27N_TRINITY_DN31892_c1_g1_i5	heavy metal-associated domain containing protein, expressed	-3	-6.416247	0.016878659	
	PiniA21_R77007951619388592202741 4	0	-3	-6.405192	0.032061411	
	PiniT25_TRINITY_DN23276_c0_g1_i1	Heavy-metal-associated domain	-3	-6.383693	0.007642782	
	PiniA21_R76731892364974039250052	F-box kelch-repeat protein	-3	-6.36971	0.007211021	
	PiniA75_R89070119115342142040	zinc finger CCCH domain-containing protein	-3	-6.30544	0.011248314	
	PiniT25_TRINITY_DN41947_c0_g1_i1	Uncharacterized protein conserved in bacteria (DUF2236)	-3	-6.287483	0.014164639	
	PiniT31N_TRINITY_DN28268_c0_g1_i2	Pfam:DUF584	-3	-6.257932	0.03467213	
	PiniT29_TRINITY_DN42385_c0_g2_i1	ABA/WDS induced protein	-2	-6.220433	0.011399701	

	PiniT29N_TRINITY_DN24484_c0_g1_i1	RING-H2 finger protein	-2	-6.217737	0.003235508	
	PiniA61_R18689171345102111288867	Sulfatase-modifying factor enzyme 1	-2	-6.195393	0.01614816	
	PiniT29_TRINITY_DN37173_c0_g2_i4	0	-2	-6.128482	0.022913216	
	PiniT23G_TRINITY_GG_11276_c0_g1_i1	cytochrome P450	-2	-6.080256	0.026382228	K2618
	PiniT25G_TRINITY_GG_44749_c0_g1_i1	aspartic proteinase	-2	-6.052673	0.041478638	
	PiniA41_R38009576883471382819566	NA	-2	-6.044738	0.015981577	
	PiniT23G_TRINITY_GG_19318_c0_g1_i1	0	-2	-6.041115	1.47761E-06	
	PiniA51_S2811173121984771882912	NA	-2	-6.02258	0.001198545	
	PiniT25_TRINITY_DN31976_c0_g1_i15	BTB POZ domain-containing protein	-2	-5.933833	0.004592229	
	PiniT23_TRINITY_DN21706_c0_g1_i2	Pfam:DUF231	-2	-5.888918	0.039183829	
	PiniA45_R341964580815425108208	Dirigent-like protein	-2	-5.870165	0.030437194	
	PiniA61_S19589061303850961709835	Cbl-interacting protein kinase	-2	-5.862435	0.015277363	

	PiniA21_R77547451062503743180060	BTB POZ domain-containing protein	-2	-5.861771	0.032900413	
	PiniT21_TRINITY_DN27923_c3_g2_i1	Inherit from euNOG: glutamine dumper	-2	-5.859013	0.009654478	
	PiniA51_J27264702277508092033476	transcription initiation factor IIF	-2	-5.827335	0.04356841	K3138
	PiniT21N_TRINITY_DN23444_c1_g1_i2	Somatic embryogenesis receptor kinase	-2	-5.817218	0.019456454	
	PiniA31_R54685331235134682947425	NA	-2	-5.81218	0.048869063	
	PiniT29_TRINITY_DN27277_c0_g1_i1	Protein of unknown function (DUF1279)	-2	-5.809182	0.000792671	
	PiniA71_R1079909203969196369638	sugar transport protein	-2	-5.758176	0.009246846	
	PiniA33_S507760213061927751614639	Pfam:DUF584	-2	-5.726874	0.00309976	
	PiniA23_R7010137122729175966310 38	NA	-2	-5.710332	0.017167777	
	PiniA71_R107224314952791681015017	xyloglucan endotransglucosylase hydrolase protein	-2	-5.673518	0.029926545	K8235
	PiniA51_S2591389673211252249415	thymocyte nuclear protein	-2	-5.632866	0.019680495	
	PiniT27G_TRINITY_GG_26946_c0_g1_i2	ABA/WDS induced protein	-2	-5.619918	0.03260308	
	PiniT31N_TRINITY_DN28700_c0_g1_i8	ABA/WDS induced protein	-2	-5.6128	0.027726512	
	PiniT25_TRINITY_DN40227_c2_g1_i8	Similarities with uniprot P08640 Saccharomyces cerevisiae YIR019c STA1	-2	-5.605238	0.027025452	

	PiniT25_TRINITY_DN40227_c2_g1_i2	NA	-2	-5.597863	0.047014617	K69
	PiniA71_R116835510819453172273	ribonucleoside-diphosphate reductase small	-2	-5.594615	0.043009249	K188
	PiniT21_TRINITY_DN25408_c0_g1_i1	late embryogenesis	-2	-5.567904	0.001283965	
	PiniA47_J3033911810255281614288	auxin-induced protein	-2	-5.539076	0.022977275	K14488
	PiniA21_R766383234662273818436 2112	Homeobox associated leucine zipper	-2	-5.52878	0.005425985	K9338
	PiniA61_J183865370965996973404	Disease resistance response protein	-2	-5.519294	0.004498366	
	PiniA71_R114332675511831733977	glycolipid transfer protein	-2	-5.486948	0.026922512	
	PiniT23N_TRINITY_DN13841_c0_g1_i1	0	-2	-5.468878	0.001876797	
	PiniA29_R58227061769466923952778	secologanin synthase-like	-2	-5.421734	0.045612513	K15639
	PiniA39_R42079301772167133616419	resistance protein	-2	-5.418963	0.01272853	
	PiniT21G_TRINITY_GG_20523_c0_g1_i1	2-oxoacid-dependent dioxygenase	-2	-5.417777	0.018658832	
	PiniA37_R4393056189520719536744 62	cytochrome P450	-2	-5.414355	0.019680495	K15639
	PiniT25G_TRINITY_GG_33991_c0_g1_i1	Set and mynd domain containing	-2	-5.391473	0.017265192	
	PiniT25N_TRINITY_DN31710_c0_g1_i7	Abscisic stress ripening protein 2	-2	-5.389725	0.026315164	
	PiniT31N_TRINITY_DN21192_c0_g1_i4	0	-2	-5.347035	0.016468414	

	PiniT25G_TRINITY_GG_23345_c0_g1_i1	aminotransferase 2	-2	-5.33746	0.003148515	K827
	PiniA41_J38047792469162282063555	Mate efflux family protein	-2	-5.320581	0.00979132	K3327
	PiniT25N_TRINITY_DN34958_c0_g1_i8	ABA/WDS induced protein	-2	-5.305536	0.023207056	
	PiniT27_TRINITY_DN38294_c0_g3_i1	Cyanamide hydratase	-2	-5.260316	0.004296772	K635
	PiniA65_R14955941572298131140311	peroxidase	-2	-5.18544	0.020472428	K43
	PiniT25N_TRINITY_DN18789_c0_g1_i2	NA	-2	-5.179979	0.034038687	
	PiniA65_R150979147112292974257 4	histone h2a	-2	-5.152506	0.000977385	K11251
	PiniT25_TRINITY_DN28406_c0_g3_i2	receptor-like protein kinase	-2	-5.091372	0.01828323	
	PiniA27_R6127268148811462212285 03	Transcription factor	-2	-5.055681	9.8771E-06	K9422
	PiniA25_R6615829156732790663566	phosphatidylcholine 1-acylhydrolase activity	-2	-5.024846	0.02109289	
	PiniA31_J5453992928354592759813	harpin-induced protein 1 domain containing protein, expressed	-2	-4.967217	0.023446854	
	PiniA27_J62350057145150455830648	CASP-like protein	-2	-4.929521	2.67443E-05	
	PiniA65_S12661625133281	Gibberellin regulated protein	-2	-4.890691	0.009602587	
	PiniA43_R35798826531229563275011	Protein of unknown function (DUF1517)	-2	-4.885223	0.045991318	
	PiniA31_R5460971763160711798610	Inherit from euNOG: glutamine dumper	-2	-4.868541	0.020933453	

	PiniA61_S736245148416178	ZnF_C2H2	-2	-4.866641	0.003544107	
	PiniT23N_TRINITY_DN22824_c1_g2_i3	AIG2-like family	-2	-4.863267	0.002313423	K19761
	PiniA47_S3226673519501551878395	Plant protein 1589 of unknown function (A_thal_3526)	-2	-4.850509	0.028978902	
	PiniT21_TRINITY_DN29732_c0_g2_i1	histone H3	-2	-4.800618	0.03363198	K11253
	PiniT31N_TRINITY_DN37411_c1_g1_i2	cellular response to cold	-2	-4.798325	0.013999122	
	PiniA61_R17797111708368511365995	beta-glucosidase	-2	-4.790761	0.007926278	K1188
	PiniT21G_TRINITY_GG_31002_c0_g1_i1	SAM dependent carboxyl methyltransferase	-2	-4.703948	0.036690943	K18886
	PiniT27G_TRINITY_GG_1814_c2_g1_i7	Dormancy auxin associated	-2	-4.673209	0.000757426	
	PiniA23_J709242110212089982986530	NA	-2	-4.67056	0.002435919	
	PiniA65_R15424841519479141401752	Inherit from euNOG: DNAJ heat shock N-terminal domain-containing protein	-2	-4.664207	2.25099E-05	
	PiniA21_R77888171269667962851033	NA	-2	-4.662722	0.039904249	
	PiniT23N_TRINITY_DN23742_c1_g1_i3	serine threonine-protein kinase	-2	-4.660795	0.001592916	
	PiniT21N_TRINITY_DN17864_c0_g1_i1	NA	-2	-4.633822	0.002968853	
	PiniT21N_TRINITY_DN21100_c2_g3_i1	RECEPTOR-like protein	-2	-4.603932	0.013628066	
	PiniT23N_TRINITY_DN23370_c1_g3_i2	Actins are highly conserved proteins that are involved in various types of cell motility and are ubiquitously expressed in all eukaryotic cells	-2	-4.598143	0.001902966	K1355

	PiniA41_S3979607110926604226348 6	short-chain dehydrogenase reductase	-2	-4.575971	0.004899989	
	PiniA55_R22377704221586151339676	NA	-2	-4.57026	0.019321434	
	PiniT27_TRINITY_DN30505_c1_g2_i4	flavonol 3-O-glucosyltransferase activity	-2	-4.531119	0.012185853	
	PiniT25_TRINITY_DN23575_c0_g1_i1	0	-2	-4.50437	0.011220812	

HOST: CTDscr vs CTMock

UP

label	ID	annotation	log2FoldChange	actualFC	padj	KO
T_91	PiniA43_R376357994273452763157	Acetyl-CoA acetyltransferase	7.80	61	0.00021306	K00626
T_90	PiniT23G_TRINITY_GG_43933_c0_g1_i1	anthocyanidin reductase	3.45	12	0.00053892	K08695
T_89	PiniT23G_TRINITY_GG_54742_c0_g1_i1	flavonoid	2.73	7	0.00593342	K05280

T_88	PiniA75_J890434153035659834249	flavonoid	3.68	14	1.3551E-06	K05280
T_87	PiniT27G_TRINITY_GG_29771_c1_g1_i2	The primary product of this enzyme is 4,2',4',6'-tetrahydroxychalcone (also termed naringenin-chalcone or chalcone) which can under specific conditions spontaneously isomerize into naringenin	2.77	8	0.00013687	K00660
T_84	PiniT25N_TRINITY_DN36430_c1_g2_i1	The primary product of this enzyme is 4,2',4',6'-tetrahydroxychalcone (also termed naringenin-chalcone or chalcone) which can under specific conditions spontaneously isomerize into naringenin	3.28	11	0.00644266	K00660
T_83	PiniT21G_TRINITY_GG_37613_c0_g1_i1	The primary product of this enzyme is 4,2',4',6'-tetrahydroxychalcone (also termed naringenin-chalcone or chalcone) which can under specific conditions spontaneously isomerize into naringenin	5.53	31	1.2255E-09	K00660
T_82	PiniT31G_TRINITY_GG_36100_c0_g1_i1	The primary product of this enzyme is 4,2',4',6'-tetrahydroxychalcone (also termed naringenin-chalcone or chalcone) which can under specific conditions spontaneously isomerize into naringenin	5.31	28	4.5453E-09	K00660
T_79	PiniA21_R765347713271832205604392 4	Putative lysophospholipase	2.27	5	1.5153E-07	K18368
T_76	PiniA37_R435313818361267790128088 5	4-coumarate--CoA ligase-like	4.48	20	2.6923E-09	K01904
T_75	PiniT21G_TRINITY_GG_43300_c0_g1_i1	4-coumarate--CoA ligase	3.05	9	6.2568E-05	K01904
T_74	PiniT29_TRINITY_DN38319_c0_g2_i1	4-coumarate-coa ligase	2.17	5	4.2131E-07	K01904
T_71	PiniA21_R766127218901671102515645 8	beta-glucosidase	2.58	7	8.7826E-05	K01188
T_70	PiniT31N_TRINITY_DN29401_c0_g1_i8	beta-glucosidase	3.03	9	4.807E-05	K01188
T_66	PiniT29_TRINITY_DN31718_c0_g1_i4	peroxidase	2.47	6	7.6243E-06	K00430
T_65	PiniT29N_TRINITY_DN36015_c0_g2_i1	peroxidase	3.20	10	6.6345E-08	K00430
T_62	PiniA47_S33567351517935631534640	Cinnamyl alcohol dehydrogenase	2.35	6	0.00251669	K00083

T_61	PiniT23N_TRINITY_DN23320_c1_g1_i3	Cinnamyl alcohol dehydrogenase	3.14	10	1.5671E-10	K00083
T_57	PiniT23_TRINITY_DN29986_c0_g1_i3	Xyloglucan endotransglucosylase hydrolase protein	2.99	9	0.00454858	K14504
T_56	PiniT23G_TRINITY_GG_44796_c0_g1_i1	Xyloglucan endotransglucosylase hydrolase protein	4.73	22	0.00491504	K14504
T_50	PiniA51_R2611205123413376723942 66	phosphatase 2C	2.61	7	0.00256408	K14497
T_49	PiniA51_J2615790138231440414612 87	gibberellin receptor	2.55	6	1.4788E-08	K14493
T_47	PiniA75_R888770192625453708302	Indole-3-acetic acid-amido synthetase	5.11	26	8.8281E-07	K14487
T_45	PiniT31G_TRINITY_GG_9285_c0_g1_i6	jasmonate-zim-domain protein 10	3.18	10	4.8402E-05	K13464
T_44	PiniT27_TRINITY_DN40705_c0_g1_i6	tify 10b	5.32	28	1.9852E-05	K13464
T_43	PiniT25G_TRINITY_GG_501_c0_g1_i3	tify 10b	5.99	36	0.00031874	K13464
T_42	PiniT25_TRINITY_DN28904_c0_g2_i1	Heat shock protein	4.11	17	0.00016997	K04079
T_41	PiniT23G_TRINITY_GG_6460_c0_g1_i1	expansin-like	2.24	5	0.00172451	0
T_40	PiniA23_S71814081550361535958749	This protein promotes the GTP-dependent binding of aminoacyl-tRNA to the A-site of ribosomes during protein biosynthesis (By similarity)	5.21	27	5.4286E-05	K02358
T_40	PiniA61_S194216314591714031647042	domain-containing protein	2.34	5	0.00065084	0
T_39	PiniT23_TRINITY_DN26979_c0_g1_i1	Actins are highly conserved proteins that are involved in various types of cell motility and are ubiquitously expressed in all eukaryotic cells	2.46	6	0.0171391	K05692
T_38	PiniT21G_TRINITY_GG_7371_c0_g1_i1	alcohol dehydrogenase	2.60	7	0.00044162	K18857
T_37	PiniA61_R1916259111633521486427	Elongation factor	2.72	7	0.02237537	K03234
T_37	PiniA61_R1786452208718187428614	enhanced disease susceptibility 1	2.45	6	0.0011693	K18875
T_37	PiniA39_R4149692193199342918206 86	Transcription factor	2.17	5	1.3638E-11	K13422

T_36	PiniT23_TRINITY_DN29602_c1_g1_i10	Mitogen-activated protein kinase kinase kinase	2.81	8	0.00295276	0
T_36	PiniT23N_TRINITY_DN23289_c1_g3_i7	WRKY transcription factor	2.80	8	5.3341E-11	K18835
T_35	PiniT21G_TRINITY_GG_28277_c0_g1_i1	Pathogenesis-related protein	3.14	10	2.5482E-05	K13449
T_35	PiniT21G_TRINITY_GG_9046_c0_g1_i1	gibberellin 20 oxidase	2.98	9	0.00289198	0
T_34	PiniA75_R887414119415948448310	myb-like DNA-binding domain containing protein	3.10	10	0.01581538	K09422
T_33	PiniT27_TRINITY_DN43259_c0_g1_i3	Pathogenesis-related protein	5.26	28	2.3381E-11	K13449
T_33	PiniT21G_TRINITY_GG_6035_c1_g1_i1	Domain of unknown function (DUF966)	3.25	11	6.2403E-08	0
T_32	PiniA75_R8714521440132815625828	DJ-1/PfpI family	3.42	12	9.0865E-07	0
T_31	PiniA21_R7740916963725191965593	calmodulin	6.57	43	1.2445E-07	K02183
T_31	PiniT25_TRINITY_DN37844_c0_g1_i2	Ocs element-binding factor	3.62	13	1.0349E-07	0
T_30	PiniT27N_TRINITY_DN36321_c2_g3_i1	Pathogenesis-related protein	3.81	15	1.5285E-08	K13449
T_29	PiniT25G_TRINITY_GG_51937_c1_g1_i2	peroxidase	4.02	16	4.0749E-06	K00430
T_29	PiniT21_TRINITY_DN26321_c0_g1_i7	calcium-binding protein	2.31	5	0.01703093	K13448
T_28	PiniT25G_TRINITY_GG_13597_c0_g1_i3	transporter	4.24	18	1.7714E-06	0
T_28	PiniT27N_TRINITY_DN34734_c0_g2_i3	calcium-binding protein	2.44	6	0.00018175	K13448
T_27	PiniT29N_TRINITY_DN26174_c0_g1_i6	calcium-binding protein	7.03	49	2.4518E-08	K13448
T_27	PiniT23N_TRINITY_DN25521_c1_g6_i2	Divergent CCT motif	4.48	20	2.5714E-08	K13464
T_26	PiniA43_J3675585598115451737602	calcium-binding protein	5.63	32	3.638E-07	K13448
T_26	PiniA49_S29338022185577381189350	alpha-dioxygenase	4.67	22	2.8435E-10	K10529
T_25	PiniA41_R3808263104520044732087 90	0	4.89	24	3.6725E-07	0

T_24	PiniA23_R7085800188167218897401	NA	5.09	26	2.15E-05	0
T_24	PiniT21N_TRINITY_DN17518_c0_g1_i4	glutamate dehydrogenase	3.02	9	0.003829	K00262
T_23	PiniT31N_TRINITY_DN25797_c0_g1_i2	NA	5.41	29	2.9161E-10	0
T_22	PiniT25G_TRINITY_GG_13184_c0_g1_i2	glucose-methanol-choline (GMC) oxidoreductase family protein	5.75	33	5.0423E-08	0
T_21	PiniA21_R790492010259337458351 8	Acetylglutamate kinase	6.02	36	0.00154694	K12659
T_21	PiniT27G_TRINITY_GG_52956_c1_g1_i5	bifunctional monodehydroascorbate reductase and carbonic anhydrase	4.26	18	2.9456E-25	K01674
T_20	PiniT21N_TRINITY_DN21387_c2_g5_i2	Transcription factor	6.34	40	1.6317E-05	K09286
T_19	PiniT23N_TRINITY_DN25767_c2_g2_i5	PAR1 protein	6.79	46	5.2954E-18	0
	PiniT29N_TRINITY_DN27650_c0_g1_i8	phosphatase 2C	7.17	51	4.4357E-07	0
T_17	PiniA21_S78006431752266165050653	acyl-CoA synthetase	8.23	68	3.3846E-05	K01897
	PiniA61_J18382975481350412379	NA	7.72	60	1.5697E-06	0
T_15	PiniA23_R7253683974277845814957	fatty acid synthase	10.07	101	2.6214E-07	K00667
	PiniA21_R77948071126229617229912	May mediate the reduction of outer membrane cytochrome b5 (By similarity)	8.18	67	4.7071E-06	K00326
T_16	PiniA23_R71254561264207884222355	Fatty acid synthase	8.82	78	1.2581E-06	K00668
T_14	PiniA21_R794725890213152615849 6	3-ketoacyl-acyl carrier protein reductase	5.90	35	0.00246302	K00059
T_13	PiniT25N_TRINITY_DN35824_c1_g3_i4	Short-chain type dehydrogenase	2.80	8	0.00014007	K00059
T_12	PiniA23_R69786511233720610241706	Short-chain type dehydrogenase	3.89	15	1.6404E-07	K00059
T_11	PiniT27_TRINITY_DN34189_c1_g3_i1	Short-chain type dehydrogenase	4.39	19	2.158E-06	K00059
T_92	PiniA21_R7878331125023977203889	farnesyl pyrophosphate synthetase	7.64	58	0.00019319	K00787

	PiniT27_TRINITY_DN35124_c1_g1_i4	Leucine-rich repeat receptor-like protein kinase	40.59	1648	3.6017E-16	0
	PiniA21_R77093757141354653557244	40s ribosomal protein s13	11.21	126	4.4049E-10	K02953
	PiniA23_R70778881448907582028761	adp-ribosylation factor	10.69	114	3.9289E-09	K07937
	PiniT29N_TRINITY_DN29633_c0_g1_i4	Heavy-metal-associated domain	10.69	114	5.6129E-07	0
	PiniA31_S56133691439557405291890	citrate synthase	10.41	108	1.2907E-08	K01647
	PiniA61_R18864548011301795794	Inhibitor	10.29	106	3.624E-08	K12462
	PiniA49_R30764791201107482747874	NADH flavin oxidoreductase NADH oxidase family protein	10.18	104	1.3532E-09	K00354
	PiniA71_S37721053713044	40S ribosomal protein S14	10.17	103	7.5062E-09	K02955
	PiniT25N_TRINITY_DN19484_c0_g1_i1	GTP-binding Protein	10.13	103	1.556E-08	K04513
	PiniA21_R78450941669343221558759	coproporphyrinogen III oxidase	10.10	102	2.4633E-06	K00228
	PiniA21_R78032071460476555482171	Zinc-binding dehydrogenase	10.10	102	1.3159E-08	K07119
	PiniA21_S77362971853948652889218	Pyruvate decarboxylase	10.07	101	1.9752E-07	K01568
	PiniA71_R11651731758226434360 6	1-aminocyclopropane-1-carboxylate synthase	9.99	100	5.1563E-09	K01762
	PiniA55_J2304658708586421805431	60S ribosomal protein l26	9.98	100	1.9788E-11	K02898
	PiniT21_TRINITY_DN23126_c0_g1_i1	NADPH-dependent methylglyoxal reductase GRE2	9.96	99	9.0417E-08	0
	PiniT27_TRINITY_DN37554_c0_g1_i2	AP2	9.95	99	9.2177E-06	0
	PiniT21_TRINITY_DN27810_c0_g1_i12	NA	9.88	98	3.0398E-09	0
	PiniA21_R77717761729772007579840	Aldehyde dehydrogenase	9.81	96	3.3717E-08	K00129
	PiniT21G_TRINITY_GG_15705_c0_g1_i1	Protein of unknown function (DUF679)	9.73	95	5.5231E-08	0
	PiniT25_TRINITY_DN42196_c1_g1_i1	exocyst complex component	9.64	93	4.6801E-06	K07195

	PiniT25G_TRINITY_GG_40922_c0_g1_i5	glyoxalase family	9.62	93	1.3736E-14	0
	PiniT23G_TRINITY_GG_26716_c0_g1_i1	Inherit from euNOG: glutamine dumper	9.60	92	6.9629E-06	0
	PiniA21_R7773928712349431624624	Peptidyl-prolyl cis-trans isomerase	9.58	92	2.3464E-06	K09568

DOWN

label	ID	annotation	log2FoldChange	actualFC	padj	KO
T_78	PiniA43_J36990671149143963060448	reductase	-2.82	-8	0.00859191	K09753
T_77	PiniA33_R511691667343094614006	4-coumarate--CoA ligase-like	-2.29	-5	0.021102991	K01904
T_69	PiniA21_R765266513113371264103458 6	Caffeoyl-coa o-methyltransferase	-2.88	-8	0.000369711	K00588
T_67	PiniT29N_TRINITY_DN31654_c0_g2_i3	peroxidase	-3.15	-10	0.003285816	K00430
T_59	PiniA61_R1872155138042680429533	cyclin d3	-3.01	-9	1.49281E-05	K14505
T_55	PiniA75_R9709901766245285735823	serine threonine-protein kinase	-2.19	-5	0.000180974	K14498
T_54	PiniA65_R156171571057089885447	two-component response regulator	-2.69	-7	0.000100448	K14492
T_53	PiniT21_TRINITY_DN27585_c2_g1_i2	Coronatine-insensitive protein	-2.56	-7	0.009170873	K13463
T_52	PiniA31_J53168841665488113402913	phosphatase 2C	-3.24	-10	0.000345183	K14497

T_51	PiniA23_R6989459203511672451604285	phosphatase 2C	-2.41	-6	1.64275E-05	K14497
T_48	PiniA61_R17940371495519719586877	auxin-responsive protein	-2.14	-5	0.005225337	K14484
T_39	PiniA47_R31864421877247241067754	3-ketoacyl-coa synthase	-2.24	-5	0.023370155	K15397
T_18	PiniA61_R173538615452280171091737	Converts stearoyl-ACP to oleoyl-ACP by introduction of a cis double bond between carbons Delta(9) and Delta(10) of the acyl chain	-5.66	-32	0.000275371	K03921
T_64	PiniA23_R72509651333109945969821	peroxidase	-3.83	-15	0.014958312	K00430
	PiniA31_R54587091691260221124612	cytochrome P450	-38.91	-1514	2.46503E-17	K20562
	PiniA21_J774650748568104308011	Isochorismatase family	-33.91	-1150	1.46575E-11	0
	PiniT23_TRINITY_DN31897_c1_g4_i1	resistance protein	-31.68	-1003	3.32666E-10	0
	PiniT21_TRINITY_DN23497_c0_g1_i1	Non-LTR retroelement reverse transcriptase	-10.03	-101	0.004468376	0
	PiniT25G_TRINITY_GG_34124_c0_g1_i4	Aquaporin	-9.07	-82	0.000177445	K09874
	PiniT31N_TRINITY_DN27123_c0_g1_i2	histone h2a	-8.64	-75	0.000177539	K11251
	PiniT21G_TRINITY_GG_30935_c0_g1_i1	phosphate-induced protein 1 conserved region domain containing protein, expressed	-8.64	-75	2.4535E-07	0
	PiniA21_S787103010987496974191 31	PMEI	-8.22	-68	8.00385E-06	0
	PiniT25G_TRINITY_GG_33865_c0_g1_i1	Protease inhibitor/seed storage/LTP family	-7.46	-56	2.15882E-06	0
	PiniA71_R11642564917202424922	histone h2a	-7.44	-55	0.014065829	K11251
	PiniA71_R11604013696752343652	Protease inhibitor/seed storage/LTP family	-7.42	-55	8.86673E-10	0
	PiniA51_R285050612685307377746	oxidoreductase, 2OG-Fe(II) oxygenase family protein	-7.30	-53	0.002345307	0

	PiniT25G_TRINITY_GG_1827_c0_g1_i4	Ribonuclease	-7.17	-51	1.32891E-11	K01166
	PiniT25_TRINITY_DN29745_c0_g1_i13	NA	-7.06	-50	2.72546E-10	0
	PiniT25_TRINITY_DN26478_c1_g1_i13	NA	-7.02	-49	0.001058052	0
	PiniA51_S280337015371187131814277	auxin-induced protein	-6.97	-49	0.004506005	0
	PiniA45_S28589325635855	Plant protein 1589 of unknown function (A_thal_3526)	-6.88	-47	0.00056334	0
	PiniT21G_TRINITY_GG_44009_c0_g1_i1	UDP-Glycosyltransferase	-6.83	-47	5.08137E-06	K21374
	PiniT21_TRINITY_DN20393_c0_g1_i1	Apurinic endonuclease-redox	-6.71	-45	0.01001117	0
	PiniA31_R54453262001338215286430	0	-6.69	-45	0.00193148	0
	PiniT29_TRINITY_DN24185_c0_g2_i1	Disease resistance response protein	-6.68	-45	8.63585E-05	0
	PiniA47_S3051217869115496208150	kDa class I heat shock	-6.61	-44	2.70951E-06	K13993
	PiniT21G_TRINITY_GG_1390_c0_g1_i1	glucan endo-1,3-beta-glucosidase-like protein	-6.57	-43	0.002330495	0
	PiniT21_TRINITY_DN38156_c0_g1_i1	Protease inhibitor seed storage lipid transfer protein	-6.41	-41	3.16113E-09	0
	PiniT27N_TRINITY_DN31560_c0_g1_i3	RNA helicase	-6.40	-41	0.004370419	K13025
	PiniT23N_TRINITY_DN25882_c0_g1_i5	phosphate-induced protein 1 conserved region domain containing protein, expressed	-6.26	-39	0.001067066	0
	PiniT31G_TRINITY_GG_4771_c1_g2_i1	synthase	-6.13	-38	8.28907E-06	0
	PiniT31N_TRINITY_DN34912_c0_g1_i1	heavy metal-associated domain containing protein, expressed	-6.11	-37	0.00106329	0
	PiniA51_R28779351026234871424993	Polysaccharide biosynthesis protein	-6.06	-37	5.00334E-06	0
	PiniA33_R51140172665440374938107	NA	-6.06	-37	0.00029355	0

	PiniA71_R1193126153216442461288	auxin-induced protein	-5.98	-36	0.000183201	0
	PiniA25_S6722386112369056203553	aspartic proteinase	-5.94	-35	0.001054741	0
	PiniA27_S6096294504118501025043	RING	-5.87	-34	0.000859719	0
	PiniA41_J379171163545482462954	Protein PLANT CADMIUM RESISTANCE	-5.86	-34	0.032635236	0
	PiniA41_S116077106112695	Signal peptidase	-5.76	-33	0.001031612	K12948
	PiniT21N_TRINITY_DN15121_c0_g1_i4	Basic 7S	-5.73	-33	0.004632671	0
	PiniA43_J3625014466749935014 54	auxin-induced protein	-5.71	-33	0.024071556	K14488
	PiniA47_S324560865379162056506	Transcription factor	-5.71	-33	0.032659926	0
	PiniT21G_TRINITY_GG_31623_c0_g1_i1	Lignin degradation and detoxification of lignin-derived products (By similarity)	-5.69	-32	0.000157856	K05909
	PiniT21N_TRINITY_DN23444_c1_g1_i2	Somatic embryogenesis receptor kinase	-5.65	-32	7.00349E-10	0
	PiniT23N_TRINITY_DN22856_c0_g1_i9	heavy metal-associated domain containing protein, expressed	-5.55	-31	0.000818128	0
	PiniA37_J4468420989599401500306	O-methyltransferase	-5.55	-31	1.50624E-05	K00545
	PiniA21_S1435019173323165	glutamate carboxypeptidase	-5.54	-31	8.52545E-06	K01301
	PiniA31_R5360571925956631116658	Disease resistance response protein	-5.51	-30	1.0855E-06	0
	PiniA71_R110891144650182636997	cytochrome b-c1 complex subunit	-5.51	-30	0.001029548	K00419
	PiniA37_S4349833895103594287865	temperature-induced	-5.48	-30	0.000548891	K03098
	PiniT31G_TRINITY_GG_7138_c0_g1_i5	Family of unknown function (DUF716)	-5.46	-30	4.70444E-05	0
	PiniT29_TRINITY_DN33982_c0_g1_i3	Transcription factor	-5.46	-30	0.024639898	0

	PiniA49_S3090416775266142605246	phosphatidylethanolamine-binding protein	-5.43	-29	0.002544712	0
	PiniT23G_TRINITY_GG_35790_c0_g1_i1	phototropism protein	-5.41	-29	0.003699412	0
	PiniA21_R801901453027036469832 8	NA	-5.40	-29	0.000970457	0
	PiniT29_TRINITY_DN42385_c0_g2_i1	ABA/WDS induced protein	-5.39	-29	1.16125E-06	0
	PiniA39_R43162436244758972639	gamma-tocopherol methyltransferase	-5.38	-29	3.72136E-05	K05928
	PiniA21_R774137512641218705269765	lob domain-containing protein	-5.35	-29	4.7012E-06	0
	PiniA37_S45211411023109882257495	BURP domain-containing protein	-5.34	-29	0.025236381	0
	PiniT31G_TRINITY_GG_47387_c0_g1_i1	peroxidase	-5.32	-28	0.003690234	K00430
	PiniT27N_TRINITY_DN22593_c0_g1_i3	Aquaporin	-5.31	-28	0.000348268	K09872
	PiniT31N_TRINITY_DN35984_c0_g2_i15	BURP domain-containing protein	-5.27	-28	0.004467388	0
	PiniA55_R2246453127940462698650	geranylgeranyl pyrophosphate synthase	-5.26	-28	4.70718E-05	K13789
	PiniA71_R11110008756157177361	AWPM-19-like membrane family protein	-5.22	-27	0.005503611	0
	PiniA31_R5325445683185042659266	0	-5.19	-27	0.000218586	0
	PiniA61_R18563961485118441351985	Transmembrane amino acid transporter protein	-5.17	-27	0.002028901	0
	PiniA31_R5497571224327803871584	Potassium channel	-5.16	-27	0.000214561	K21867
	PiniA39_J41616401093211783253098	1-aminocyclopropane-1-carboxylate oxidase	-5.15	-26	7.90246E-08	K05933
	PiniA43_S382984261496603295132	NA	-5.13	-26	0.000646609	0
	PiniA47_R307639738611133627051	Protease inhibitor/seed storage/LTP family	-5.12	-26	1.43063E-06	0

	PiniA47_J3186652379951631550594	Domain of unknown function (DUF3511)	-5.09	-26	6.50925E-05	0
	PiniA39_S87383105511308	Universal stress protein	-5.04	-25	0.000508741	0
	PiniA23_S718414110756839603727 0	LRR receptor-like serine threonine-protein kinase	-5.00	-25	0.006574348	0
	PiniA21_R774828032261978763953856	ABC transporter	-5.00	-25	2.17575E-07	0
	PiniA51_S116709993910337	DUF581 domain containing protein, expressed	-4.98	-25	0.004575474	0
	PiniA55_R22087704922534691754113	Protease inhibitor/seed storage/LTP family	-4.97	-25	9.67564E-05	0
	PiniA51_R2599461926167665217633	Gibberellin regulated protein	-4.94	-24	4.21058E-06	0
	PiniA61_S2797766102610	0	-4.94	-24	0.000255198	0
	PiniA65_R14385951480276002148864	Dehydrogenase	-4.93	-24	0.00017206	0
	PiniA65_R15583491785125091424379	Xyloglucan endotransglucosylase hydrolase protein	-4.90	-24	0.00092933	K08235
	PiniT21_TRINITY_DN20056_c0_g2_i1	Xyloglucan endo-transglycosylase (XET) C-terminus	-4.89	-24	0.000382282	K08235
	PiniA21_R79921799456822440354 9	0	-4.89	-24	0.001616826	0
	PiniT29N_TRINITY_DN29155_c0_g2_i3	Universal stress protein	-4.88	-24	4.33189E-10	0
	PiniT25N_TRINITY_DN35897_c0_g2_i1	kDa class I heat shock	-4.87	-24	4.02935E-06	K13993
	PiniT25N_TRINITY_DN20839_c0_g3_i5	Transcription factor	-4.86	-24	0.008973869	0
	PiniT31N_TRINITY_DN31977_c0_g2_i5	microtubule-associated protein	-4.86	-24	0.00086701	0
	PiniA51_S27141045352925551046852	kDa class I heat shock	-4.85	-24	1.72091E-06	K13993

HOST: CTDsap vs CTDscr

DOWN

label	ID`	annotation	log2FoldChange	actualFC	padj	KO
T_128	PiniA21_R80714061419166226807705	protein beta subunit	-4.683	-22	0.02342	K04536
T_127	PiniT21_TRINITY_DN26914_c1_g2_i5	Heat shock 70 kDa protein	-2.901	-8	0.00032	K04043
T_126	PiniT21N_TRINITY_DN15021_c0_g1_i1	enolase EC 4.2.1.11	-3.429	-12	0.03977	K01689
T_125	PiniA47_R325609392365002361736	The proteasome is a multicatalytic proteinase complex which is characterized by its ability to cleave peptides with Arg, Phe, Tyr, Leu, and Glu adjacent to the leaving group at neutral or slightly basic pH. The proteasome has an ATP-dependent proteolytic activity (By similarity)	-4.408	-19	0.03439	K02728
T_120	PiniT21_TRINITY_DN8628_c0_g1_i1	Bifunctional pyrimidine biosynthesis protein (PyrABCN)	-5.967	-36	0.04429	K11541
T_116	PiniT23N_TRINITY_DN17615_c0_g1_i2	aconitate hydratase	-3.518	-12	0.04057	K01681
T_115	PiniA21_R777162780236565206439	Fumarate hydratase	-4.505	-20	0.0179	K01679
T_114	PiniA27_R627369417553045328145 29	ATP-citrate synthase subunit 1	-3.949	-16	0.01571	K01648
T_113	PiniA21_S1055004130427873	citrate synthase	-4.767	-23	0.02076	K01647
T_112	PiniA21_R777521117286908141812 88	dihydrolipoyl dehydrogenase	-4.060	-16	0.00644	K00382
T_110	PiniT25N_TRINITY_DN18987_c0_g1_i2	Isocitrate dehydrogenase	-3.947	-16	0.01728	K00030
T_105	PiniT29G_TRINITY_GG_50531_c0_g1_i2	Glutathione S-transferase	-2.496	-6	0.00957	K00799
T_104	PiniT25G_TRINITY_GG_34287_c0_g1_i2	Glutathione S-transferase	-2.560	-7	0.01273	K00799

T_103	PiniA65_R143054210901079112169524	Glutathione S-transferase	-3.413	-12	0.00109	K00799
T_102	PiniT31G_TRINITY_GG_3882_c0_g1_i3	Glutathione S-transferase	-5.800	-34	4.58E-13	K00799
T_101	PiniT25G_TRINITY_GG_43132_c0_g1_i3	Glutathione S-transferase	-5.818	-34	0.00092	K00799
T_100	PiniT21_TRINITY_DN12930_c0_g1_i1	serine threonine-protein phosphatase	-4.246	-18	0.0481	K06269
T_100	PiniT21G_TRINITY_GG_2668_c0_g1_i1	glutathione s-transferase	-2.314	-5	0.01293	K00799
T_99	PiniA23_R7197623133326270801979	Glutathione reductase	-5.235	-27	0.00055	K00383
T_99	PiniT25N_TRINITY_DN19484_c0_g1_i1	GTP-binding Protein	-4.129	-17	0.01881	K04513
T_98	PiniA39_S3632492128419626	cell division control protein 42	-6.559	-43	0.00817	K04392
T_98	PiniA25_R66091731439348855120297	isocitrate dehydrogenase NADP	-4.432	-20	0.02075	K00031
T_60	PiniT21_TRINITY_DN28007_c0_g1_i9	Xyloglucan endotransglucosylase hydrolase protein	-2.137	-5	0.0102	K14504
T_40	PiniA23_S71814081550361535958749	This protein promotes the GTP-dependent binding of aminoacyl-tRNA to the A-site of ribosomes during protein biosynthesis (By similarity)	-3.537	-13	0.04823	K02358
T_28	PiniA21_R7740916963725191965593	calmodulin	-3.752	-14	0.02526	K02183
T_25	PiniT21N_TRINITY_DN17518_c0_g1_i4	glutamate dehydrogenase	-3.133	-10	0.03159	K00262
T_17	PiniA21_S78006431752266165050653	acyl-CoA synthetase	-4.646	-22	0.03254	K01897
T_16	PiniA23_R7253683974277845814957	fatty acid synthase	-9.015	-81	0.0002	K00667
T_15	PiniA23_R71254561264207884222355	Fatty acid synthase	-5.753	-33	0.00207	K00668
T_12	PiniA23_R69786511233720610241706	Short-chain type dehydrogenase	-2.716	-7	0.00817	K00059
T_10	PiniT21_TRINITY_DN6910_c0_g1_i1	alanine aminotransferase	-5.863	-34	0.00143	K00814
	PiniA55_S2468034717375822095742	phosphatidylinositol 4-kinase type 2-beta	-22.739	-517	1.07E-14	0

	PiniT25_TRINITY_DN32793_c1_g1_i6	amino acid	-8.757	-77	0.00109	0
	PiniA31_S56133691439557405291890	citrate synthase	-8.515	-73	1.97E-06	K01647
	PiniT29_TRINITY_DN36048_c1_g1_i3	NA	-7.118	-51	0.04322	0
	PiniT23N_TRINITY_DN24810_c2_g1_i3	serine threonine-protein kinase	-6.907	-48	1.15E-05	0
	PiniT21_TRINITY_DN29747_c1_g2_i1	germin-like protein	-6.508	-42	0.00947	0
	PiniT21_TRINITY_DN32746_c0_g1_i1	Required for small ribosomal subunit (SSU) synthesis. Has a role in the processing of early nucleolar and late cytoplasmic pre-RNA species	-6.465	-42	0.02339	K11884
	PiniA29_S574811176767831659925	0	-6.294	-40	0.02288	0
	PiniT29N_TRINITY_DN29633_c0_g1_i4	Heavy-metal-associated domain	-6.262	-39	0.0081	0
	PiniA43_R375910158438933364280	auxin-induced protein	-6.195	-38	0.03252	K14488
	PiniT23N_TRINITY_DN24396_c0_g2_i7	glutathione s-transferase	-6.142	-38	9.92E-06	K00799
	PiniA21_R78032071460476555482171	Zinc-binding dehydrogenase	-6.071	-37	0.00019	K07119
	PiniT21G_TRINITY_GG_20620_c0_g1_i1	Glycosyl hydrolase family 1	-6.048	-37	7.37E-07	K01188
	PiniT21_TRINITY_DN12147_c0_g1_i2	Aaa atpase	-5.778	-33	0.0081	0
	PiniA21_R800934862553041181381	glycosyltransferase family 15 protein	-5.771	-33	0.04823	K03854
	PiniT25G_TRINITY_GG_47577_c0_g1_i1	quinone-oxidoreductase homolog, chloroplastic-like	-5.489	-30	0.00014	K18980
	PiniT21N_TRINITY_DN4915_c0_g1_i1	Required for the sorting and concentration of proteins resulting in the entry of these proteins into the invaginating vesicles of the multivesicular body (MVB). Also required for the proteolytic cleavage of the	-5.450	-30	0.03795	K12194

		transcription factor RIM101 in response to alkaline ambient pH (By similarity)				
	PiniA35_S2777187886085	Quinone oxidoreductase	-5.445	-30	0.03885	0
	PiniA65_J1483743637322780586	0	-5.382	-29	0.02858	0
	PiniT31G_TRINITY_GG_23238_c0_g1_i5	Allene oxide synthase	-5.149	-27	6.54E-05	K01723
	PiniA55_S2474621617359522148357	Carrier protein that may be involved in membrane- trafficking events associated with cell plate formation during cytokinesis. Binds to some hydrophobic molecules such as phosphoinositides and promotes their transfer between the different cellular sites (By similarity)	-5.136	-26	0.00484	0
	PiniT21_TRINITY_DN41575_c0_g1_i1	Catalyzes the synthesis of activated sulfate (By similarity)	-5.133	-26	0.04227	K00860
	PiniA21_S68117369398066	)-reductase	-5.112	-26	0.01385	0
	PiniA21_S175648498910832	4-nitrophenylphosphatase	-5.103	-26	0.02836	K01101
	PiniA65_S142700561127911070786	mago nashi	-5.102	-26	0.04102	K12877
	PiniA21_R76853688122409292290592	Ribosomal protein	-5.074	-26	0.0011	K02865
	PiniA21_S3930798153016104	Galactokinase	-5.002	-25	0.02342	K00849
	PiniT31N_TRINITY_DN28593_c0_g2_i5	response to low sulfur	-4.981	-25	0.02142	0
	PiniT21N_TRINITY_DN18853_c0_g1_i1	40S ribosomal protein S14	-4.957	-25	0.02256	K02955
	PiniT23N_TRINITY_DN25285_c1_g2_i2	Aluminum-activated malate transporter	-4.866	-24	0.01738	0
	PiniA61_S194322683379691654707	NA	-4.779	-23	0.03439	0
	PiniT21_TRINITY_DN37334_c0_g1_i1	UPF0160 domain protein MYG1	-4.776	-23	0.041	0

	PiniA21_R7884993929117037632255	Endosomal cargo receptor (Erp3)	-4.688	-22	0.02424	0
	PiniT23_TRINITY_DN2924_c0_g1_i2	arginine n-methyltransferase	-4.663	-22	0.01864	K11434
	PiniA55_R2374155421294294739	dsDNA-binding protein PDCD5	-4.625	-21	0.03949	K06875
	PiniT21N_TRINITY_DN10708_c0_g1_i1	DNA-dependent RNA polymerase catalyzes the transcription of DNA into RNA using the four ribonucleoside triphosphates as substrates. Common component of RNA polymerases I, II and III which synthesize ribosomal RNA precursors, mRNA precursors and many functional non-coding RNAs, and small RNAs, such as 5S rRNA and tRNAs, respectively. Pol II is the central component of the basal RNA polymerase II transcription machinery. Pols are composed of mobile elements that move relative to each other. In Pol II, RPB5 is part of the lower jaw surrounding the central large cleft and thought to grab the incoming DNA template. Seems to be the major component in this process (By similarity)	-4.604	-21	0.04347	K03013
	PiniA21_R79707411112125282465217	chorismate mutase	-4.600	-21	0.02559	K01850
	PiniT21N_TRINITY_DN8316_c0_g1_i1	ribose-phosphate pyrophosphokinase	-4.567	-21	0.03439	K00948
	PiniT23N_TRINITY_DN24538_c0_g1_i9	Lipase (class 3)	-4.566	-21	6.44E-05	0
	PiniT21_TRINITY_DN23126_c0_g1_i1	NADPH-dependent methylglyoxal reductase GRE2	-4.553	-21	0.01766	0
	PiniA41_S408209075870223420331	Chlorophyllase	-4.513	-20	0.02915	K08099
	PiniA21_R77577541137857784901478	Catalyzes the initial reaction in the xylose utilization pathway by reducing D-xylose into xylitol. Xylose is a major component of hemicelluloses such as xylan. Most fungi utilize D- xylose via three enzymatic reactions, xylose reductase (XR), xylitol dehydrogenase (XDH), and xylulokinase, to form xylulose 5- phosphate, which enters pentose phosphate pathway	-4.415	-19	0.0081	K17743

	PiniT21_TRINITY_DN25809_c2_g1_i1	Electron carrier protein. The oxidized form of the cytochrome c heme group can accept an electron from the heme group of the cytochrome c1 subunit of cytochrome reductase. Cytochrome c then transfers this electron to the cytochrome oxidase complex, the final protein carrier in the mitochondrial electron-transport chain	-4.391	-19	0.02465	K08738
	PiniA47_R30355871103850091864385	response to low sulfur	-4.373	-19	0.00611	0
	PiniA21_S78021391372435355099627	3-ketoacyl-coA thiolase	-4.366	-19	0.04744	K07513
	PiniT25N_TRINITY_DN17049_c1_g1_i2	60S ribosomal protein L5	-4.363	-19	0.00601	K02932
	PiniA35_R4668487117814655438526 91	germin-like protein	-4.304	-19	6.44E-05	0
	PiniT21_TRINITY_DN38861_c0_g1_i1	Component of the eukaryotic translation initiation factor 3 (eIF-3) complex, which is involved in protein synthesis and, together with other initiation factors, stimulates binding of mRNA and methionyl-tRNAi to the 40S ribosome (By similarity)	-4.290	-18	0.04195	K03253
	PiniA65_S164541858810764955377	0	-4.275	-18	0.01571	0
	PiniA21_R78779961213186094747245	Kynurenine aminotransferase	-4.259	-18	0.02929	K14264
	PiniA21_R77014447011424853519358	60s ribosomal protein l20	-4.226	-18	0.00463	K02882
	PiniA33_S5304177811213382293709	Heat Shock Protein	-4.210	-18	0.04422	K03695
	PiniA65_R1459053105633966687127	glutathione s-transferase	-4.206	-18	0.01667	K00799
	PiniT21_TRINITY_DN27810_c0_g1_i12	NA	-4.194	-18	0.00375	0
	PiniA21_R78035741237374907433179	Component of the eukaryotic translation initiation factor 3 (eIF-3) complex, which is involved in protein synthesis and, together with other initiation factors, stimulates binding of mRNA and methionyl-tRNAi to the 40S ribosome (By similarity)	-4.176	-17	0.02526	K15028

	PiniA37_S45254317462061192313813	Core component of nucleosome. Nucleosomes wrap and compact DNA into chromatin, limiting DNA accessibility to the cellular machineries which require DNA as a template. Histones thereby play a central role in transcription regulation, DNA repair, DNA replication and chromosomal stability. DNA accessibility is regulated via a complex set of post-translational modifications of histones, also called histone code, and nucleosome remodeling	-4.174	-17	0.02316	K11252
	PiniT31G_TRINITY_GG_37903_c0_g1_i1	germin-like protein	-4.149	-17	3.51E-05	0
	PiniT23N_TRINITY_DN22640_c0_g1_i4	Core component of nucleosome. Nucleosomes wrap and compact DNA into chromatin, limiting DNA accessibility to the cellular machineries which require DNA as a template. Histones thereby play a central role in transcription regulation, DNA repair, DNA replication and chromosomal stability. DNA accessibility is regulated via a complex set of post-translational modifications of histones, also called histone code, and nucleosome remodeling	-4.137	-17	0.00791	K11253
	PiniA25_R650695775620009255484 9	tumor protein	-4.134	-17	0.02465	0
	PiniT29N_TRINITY_DN36771_c2_g1_i7	Inherit from euNOG: expressed protein	-4.127	-17	0.00947	0
	PiniT21N_TRINITY_DN22485_c1_g4_i3	ribosomal RNA small subunit methyltransferase	-4.098	-17	0.02386	0
	PiniT25N_TRINITY_DN36251_c2_g2_i8	NA	-4.075	-17	0.02465	0
	PiniA61_R18864548011301795794	Inhibitor	-4.070	-17	0.03916	K12462
	PiniT29_TRINITY_DN37492_c0_g2_i4	zinc finger AN1 domain-containing stress-associated protein	-4.043	-16	0.00178	0
	PiniA61_R18717381240281601660710	60s ribosomal protein	-4.040	-16	0.00985	K02930

	PiniT21N_TRINITY_DN15535_c0_g1_i1	Component of the nascent polypeptide-associated complex (NAC), a dynamic component of the ribosomal exit tunnel, protecting the emerging polypeptides from interaction with other cytoplasmic proteins to ensure appropriate nascent protein targeting (By similarity). The NAC complex also promotes mitochondrial protein import by enhancing productive ribosome interactions with the outer mitochondrial membrane and blocks the inappropriate interaction of ribosomes translating non-secretory nascent polypeptides with translocation sites in the membrane of the endoplasmic reticulum (By similarity). EGD1 may act as a transcription factor that exert a negative effect on the expression of several genes that are transcribed by RNA polymerase II (By similarity)	-4.040	-16	0.02142	K01527
	PiniT21_TRINITY_DN8332_c0_g1_i1	rRNA methyltransferase NOP1	-4.017	-16	0.02545	K14563
	PiniA21_R79422821346174245384056	Aldehyde dehydrogenase	-4.008	-16	0.03159	0
	PiniT31G_TRINITY_GG_8810_c0_g1_i2	NA	-4.008	-16	0.01881	0
	PiniT23N_TRINITY_DN19393_c0_g1_i3	NA	-4.007	-16	0.01851	0
	PiniA23_R70778881448907582028761	adp-ribosylation factor	-4.006	-16	0.02929	K07937
	PiniA55_J2304658708586421805431	60S ribosomal protein l26	-3.998	-16	0.01766	K02898
	PiniT21_TRINITY_DN12676_c0_g2_i1	General amino-acid permease GAP1	-3.991	-16	0.03606	K16261
	PiniA27_R61003431785125261173831 6	ATP-dependent RNA helicase which is a subunit of the eIF4F complex involved in cap recognition and is required for mRNA binding to ribosome. In the current model of translation initiation, eIF4A unwinds RNA secondary structures in the 5'-UTR of mRNAs which is necessary to allow efficient binding of the small ribosomal subunit, and subsequent scanning for the initiator codon (By similarity)	-3.985	-16	0.01846	K03257
	PiniT25_TRINITY_DN36639_c3_g2_i2	AWPM-19-like membrane family protein	-3.978	-16	0.01881	0

	PiniA29_S57289281583368001292210	Tubulin is the major constituent of microtubules. It binds two moles of GTP, one at an exchangeable site on the beta chain and one at a non-exchangeable site on the alpha chain (By similarity)	-3.964	-16	0.02142	K07374
	PiniA49_R30764791201107482747874	NADH flavin oxidoreductase NADH oxidase family protein	-3.960	-16	0.00917	K00354
	PiniT23N_TRINITY_DN18839_c0_g1_i4	40S ribosomal protein S9	-3.945	-16	0.02197	K02997
	PiniA21_R76993751102200331116 4088	40S ribosomal protein S1	-3.943	-16	0.02987	K02984
	PiniT31N_TRINITY_DN19391_c0_g1_i3	40s ribosomal protein s23	-3.938	-16	0.02465	K02973
	PiniT23N_TRINITY_DN26447_c3_g1_i10	ubiquitin	-3.930	-15	0.03496	K08770
	PiniA35_R47807901236731624537836	14-3-3 protein	-3.918	-15	0.0098	K06630
	PiniA39_S41949921031184511597910	Seems to be required for maximal rate of protein biosynthesis. Enhances ribosome dissociation into subunits and stabilizes the binding of the initiator Met-tRNA(I) to 40 S ribosomal subunits (By similarity)	-3.900	-15	0.01793	K03236
	PiniT23_TRINITY_DN33151_c1_g1_i1	response to low sulfur	-3.889	-15	0.03153	0
	PiniA21_R78549381213205305832760	Catalyzes the oxidation of 3-carboxy-2-hydroxy-4- methylpentanoate (3-isopropylmalate) to 3-carboxy-4-methyl-2-oxopentanoate. The product decarboxylates to 4-methyl-2 oxopentanoate	-3.887	-15	0.02184	K00052
	PiniT21G_TRINITY_GG_21251_c0_g1_i1	chitinase	-3.845	-15	0.04302	K01183
	PiniA47_S3302759815249422603394	Translation initiation factor	-3.842	-15	0.03435	K03113
	PiniA21_R76936017741690635718288	60S ribosomal protein L27	-3.837	-15	0.02076	K02901
	PiniT21_TRINITY_DN27323_c2_g2_i2	GTP-binding nuclear protein	-3.830	-15	0.00791	K07936
	PiniA39_S43991431041115034052961	TIFY 10A-like	-3.823	-15	0.02465	K13464
	PiniA21_R77717761729772007579840	Aldehyde dehydrogenase	-3.799	-14	0.02925	K00129

	PiniT21_TRINITY_DN34821_c0_g1_i1	Translation initiation factor	-3.792	-14	0.02465	K03263
	PiniT21_TRINITY_DN6990_c0_g1_i1	Mitochondrial protein import protein MAS5	-3.790	-14	0.02808	K09503
	PiniA27_R60830257991155905348619	40s ribosomal protein S17	-3.775	-14	0.02758	K02962
	PiniA21_R77098179731498821807202	60S ribosomal protein L8	-3.767	-14	0.02545	K02936
	PiniT23N_TRINITY_DN17749_c0_g1_i2	40S ribosomal protein S8	-3.763	-14	0.01052	K02995
	PiniA25_R64916201375318655579466 3	NA	-3.726	-14	0.01385	0
	PiniT27G_TRINITY_GG_34648_c0_g1_i2	calmodulin-like protein	-3.721	-14	0.00472	K13448
	PiniA29_R56940956912142723731419	NA	-3.714	-14	0.0209	0
	PiniA21_R77093757141354653557244	40s ribosomal protein s13	-3.712	-14	0.04322	K02953
	PiniT21_TRINITY_DN5819_c0_g1_i1	60S ribosomal protein L34	-3.685	-14	0.00742	K02915
	PiniT31G_TRINITY_GG_27806_c2_g1_i1	gibberellin 20 oxidase	-3.667	-13	0.00139	0
	PiniT21_TRINITY_DN25304_c0_g1_i3	40s ribosomal protein	-3.659	-13	0.01784	K02947
	PiniA21_R76604961917103046124655 81	FAD binding domain containing protein, expressed	-3.647	-13	0.01293	0
	PiniA21_R77567841562731321598810	rab gdp-dissociation inhibitor	-3.632	-13	0.04718	K17255
	PiniT23N_TRINITY_DN20642_c0_g1_i1	40S ribosomal protein S20	-3.627	-13	0.01576	K02969
	PiniT21N_TRINITY_DN15509_c0_g1_i2	elongation factor 1 gamma domain-containing protein	-3.627	-13	0.02858	K03233
	PiniA65_R144485572395891624129	NA	-3.619	-13	0.0081	0
	PiniT23N_TRINITY_DN17582_c0_g1_i1	40S ribosomal protein S5	-3.613	-13	0.02326	K02989
	PiniT23_TRINITY_DN31772_c0_g1_i1	Nucleolar protein	-3.598	-13	0.04407	K14564
	PiniA21_R78269771020288087087931	arp2 3 complex	-3.563	-13	0.04302	K17260

	PiniT25G_TRINITY_GG_43270_c0_g1_i1	germin-like protein	-3.559	-13	0.00463	0
	PiniA43_R3522242120675656712255 23	glutathione s-transferase	-3.539	-13	0.00149	K00799
	PiniT29G_TRINITY_GG_39129_c0_g1_i2	glyoxalase family	-3.539	-13	0.01682	0
	PiniT27N_TRINITY_DN32352_c0_g1_i2	zinc finger AN1 domain-containing stress-associated protein	-3.522	-12	0.01293	0
	PiniT21_TRINITY_DN24621_c0_g1_i1	Elongation factor	-3.509	-12	0.02579	K03232

HOST: CCTDscr vs CTDscr

UP

label	ID	annotation	log2FoldChange	actualFC	padj	KO
T_97	PiniA75_R885439183562016789061	1-aminocyclopropane-1-carboxylate synthase	2.40	6	0.0101617	K20772
T_96	PiniT27G_TRINITY_GG_4397_c0_g1_i5	chitinase	3.72	14	0.0143102	K20547
T_81	PiniT29N_TRINITY_DN35957_c0_g1_i9	reductase	3.57	13	0.0480644	K09753
T_80	PiniT21_TRINITY_DN29988_c1_g3_i16	reductase	3.79	14	0.0022784	K09753
T_68	PiniT31N_TRINITY_DN22323_c0_g1_i2	peroxidase	2.73	7	0.0428045	K00430
T_50	PiniA51_R261120512341337672394266	phosphatase 2C	3.26	11	0.0004107	K14497
T_41	PiniA29_R570890426182354792514658	respiratory burst oxidase	2.33	5	1.014E-06	K13447
T_16	PiniT23N_TRINITY_DN21702_c0_g1_i2	biotin carboxyl carrier protein of acetyl-CoA carboxylase	2.24	5	0.0030463	K02160
T_123	PiniT25G_TRINITY_GG_3639_c0_g1_i2	alcohol dehydrogenase	2.59	7	0.0055506	K18857
T_117	PiniT31N_TRINITY_DN33223_c0_g2_i2	starch branching enzyme	3.83	15	0.00186	K00700

T_107	PiniT29G_TRINITY_GG_51728_c3_g1_i8	glutathione peroxidase	2.22	5	0.0029436	K00432
	PiniA31_R54587091691260221124612	cytochrome P450	38.67	1496	1.159E-16	2
	PiniA21_J774650748568104308011	Isochorismatase family	32.17	1035	8.039E-10	
	PiniT23_TRINITY_DN31897_c1_g4_i1	resistance protein	25.14	632	8.536E-06	
	PiniA27_R6155962933430625311160	benzyl alcohol O-benzoyltransferase-like	10.31	106	0.0093744	K19861
	PiniT27N_TRINITY_DN25916_c0_g1_i2	Jacalin	8.72	76	3.83E-27	
	PiniT21_TRINITY_DN23497_c0_g1_i1	Non-LTR retroelement reverse transcriptase	8.60	74	0.0423194	
	PiniT31N_TRINITY_DN27123_c0_g1_i2	histone h2a	7.70	59	0.0029944	K11251
	PiniA41_J379171163545482462954	Protein PLANT CADMIUM RESISTANCE	7.45	56	0.0161293	
	PiniA41_R39749732389214652097382	zeta-chain (TCR) associated protein kinase	6.92	48	0.0005426	
	PiniT23_TRINITY_DN33381_c0_g3_i1	Inherit from euNOG: Retrotransposon protein	6.89	47	1.095E-05	
	PiniA71_R110891144650182636997	cytochrome b-c1 complex subunit	6.40	41	0.0004328	K00419
	PiniT21G_TRINITY_GG_6474_c1_g1_i1	Domain of unknown function (DUF1929)	5.94	35	0.0022749	K20929
	PiniT25_TRINITY_DN38354_c0_g1_i3	protein UNUSUAL FLORAL	5.87	34	0.0119536	
	PiniT21_TRINITY_DN11669_c0_g1_i1	SNF1-related protein kinase regulatory subunit	5.77	33	0.0125552	
	PiniA31_J548882568165713484522	0	5.72	33	0.0423747	

	PiniT21_TRINITY_DN17645_c0_g1_i1	B3 domain-containing protein	5.53	31	0.0016996	
	PiniT29N_TRINITY_DN37071_c2_g1_i1	UPF0481 protein	5.34	29	5.818E-06	
	PiniT25N_TRINITY_DN20564_c0_g1_i3	bidirectional sugar transporter	5.20	27	0.0163247	K15382
	PiniA75_R99209365510358220490	NA	5.14	26	0.0001799	
	PiniA71_R1200320840403546596	NA	5.08	26	0.0141217	
	PiniA55_R223342380645352902247	early light-induced protein	5.04	25	2.898E-05	
	PiniA27_R61512021023379924643841	NA	4.91	24	0.012747	
	PiniA71_R1079970110172737785646	Nuclear transcription factor Y subunit	4.74	22	1.871E-10	K08066
	PiniT21N_TRINITY_DN21901_c1_g3_i3	NA	4.68	22	1.795E-05	
	PiniT21N_TRINITY_DN22604_c0_g2_i1	response regulator	4.66	22	0.0004453	K14491
	PiniA43_S356923810658792518834	Retrotransposon protein	4.58	21	0.0110447	
	PiniT29_TRINITY_DN34133_c1_g1_i5	benzyl alcohol O-benzoyltransferase-like	4.50	20	0.0001822	K19861
	PiniT31G_TRINITY_GG_53077_c0_g1_i3	myb-like DNA-binding domain containing protein	4.48	20	5.662E-07	K09422
	PiniT21G_TRINITY_GG_30935_c0_g1_i1	phosphate-induced protein 1 conserved region domain containing protein, expressed	4.45	20	0.031619	
	PiniT21_TRINITY_DN26779_c2_g1_i2	Phosphoglycerate mutase	4.38	19	0.0003733	K15633
	PiniT27_TRINITY_DN33558_c1_g1_i4	0	4.38	19	0.0007406	

	PiniT23_TRINITY_DN32341_c3_g2_i4	cytochrome P450	4.11	17	0.0077386	K20562
	PiniA27_R61634281530590711685899	BAHD acyltransferase	4.01	16	1.863E-05	
	PiniA35_S49799411108406584642484	Myblike DNAbinding domain containing protein	3.94	16	0.0104062	K09422
	PiniT25N_TRINITY_DN26996_c1_g1_i3	NA	3.92	15	0.0134366	
	PiniT21G_TRINITY_GG_8187_c0_g1_i1	0	3.82	15	0.0005935	
	PiniT21N_TRINITY_DN22083_c0_g1_i10	O-methyltransferase	3.81	15	0.0027397	
	PiniA29_S5749409805157731685338	NA	3.80	14	0.0006162	
	PiniT25N_TRINITY_DN32333_c0_g1_i3	transcription elongation regulator	3.80	14	0.0429912	K12824
	PiniT29N_TRINITY_DN29155_c0_g2_i3	Universal stress protein	3.79	14	8.263E-06	
	PiniT29_TRINITY_DN38267_c1_g1_i1	thaumatin-like protein	3.74	14	0.000125	
	PiniT27N_TRINITY_DN31892_c1_g1_i5	heavy metal-associated domain containing protein, expressed	3.70	14	0.0006414	
	PiniT25_TRINITY_DN35883_c0_g1_i3	Calcium-binding peroxygenase involved in the degradation of storage lipid in oil bodies. May be involved in the interaction between oil bodies and vacuoles during seed germination and in the oxylipin signaling pathways and plant defense responses. Can catalyze sulfoxidation of thiobenzamide, hydroxylation of aniline	3.66	13	0.0016391	K17991
	PiniT27G_TRINITY_GG_14714_c2_g1_i1	ACT domain	3.54	13	0.0114989	

	PiniT23G_TRINITY_GG_21083_c0_g1_i1	Protein of unknown function (DUF1399)	3.52	12	4.08E-05	
	PiniT23N_TRINITY_DN25065_c0_g2_i6	CAP10	3.50	12	1.849E-05	
	PiniT31G_TRINITY_GG_18474_c0_g1_i4	Ulp1 protease family, C-terminal catalytic domain	3.49	12	0.0284282	K13464
	PiniA55_R23838055153494432364	Auxin responsive protein	3.45	12	0.0229654	K14488
	PiniA51_R259969419232429681993263	myb-like DNA-binding domain containing protein	3.43	12	0.0017278	K09422
	PiniA75_S991671138830398796859	Plant-specific domain TIGR01615 family protein	3.41	12	0.0058922	
	PiniA49_R3036415170595371068329	Plant synaptotagmin	3.40	12	0.0008963	
	PiniT29G_TRINITY_GG_7106_c0_g1_i1	Protein of unknown function (DUF679)	3.39	12	0.0077501	
	PiniT21_TRINITY_DN28463_c0_g1_i1	Inherit from NOG: Serine-rich	3.35	11	7.815E-06	
	PiniT27G_TRINITY_GG_34241_c0_g1_i2	Isoflavone reductase	3.35	11	0.0003475	
	PiniA55_J231482968774451162755	auxin-induced protein	3.31	11	0.0056407	K14488
	PiniT31_TRINITY_DN42546_c0_g1_i4	heavy metal-associated domain containing protein, expressed	3.30	11	6.818E-05	
	PiniT31N_TRINITY_DN35806_c0_g1_i14	Protein of unknown function (DUF1264)	3.29	11	0.0320821	
	PiniT29_TRINITY_DN42813_c1_g1_i15	NA	3.19	10	0.00152	
	PiniT31N_TRINITY_DN29890_c1_g1_i30	rop guanine nucleotide exchange factor	3.17	10	0.0160533	
	PiniT31N_TRINITY_DN35449_c0_g1_i2	NA	3.13	10	0.0002163	

	PiniT29G_TRINITY_GG_37013_c0_g1_i12	NA	3.13	10	1.693E-09	
	PiniA23_R709142742121280281174266	DNA mismatch repair	3.10	10	0.0067622	
	PiniT31N_TRINITY_DN37217_c1_g1_i1	acid-thiol ligase activity	3.09	10	0.0293764	
	PiniA31_R554047886092161535620	0	3.08	9	0.001779	
	PiniA25_R6804340205810743435553	0	3.08	9	0.0191033	
	PiniA71_R1091844141057110837263	Phospholipase A1-Igamma3	3.07	9	0.0486412	
	PiniA75_R90885089321421753187	THN	3.05	9	0.0018049	
	PiniA21_R774137512641218705269765	lob domain-containing protein	3.05	9	0.0331465	
	PiniA75_R8639472900309190773511	Plant lipoxygenase may be involved in a number of diverse aspects of plant physiology including growth and development, pest resistance, and senescence or responses to wounding (By similarity)	3.02	9	0.0187211	K15718
	PiniT21G_TRINITY_GG_15705_c0_g1_i1	Protein of unknown function (DUF679)	3.01	9	0.0493807	
	PiniA31_R5343349201027882550212O9	Transcription factor	3.00	9	5.403E-07	K09422
	PiniT29G_TRINITY_GG_45138_c1_g1_i1	peroxidase	3.00	9	0.0118299	K00430
	PiniA65_R16169731182181831420508	phosphate-induced protein 1 conserved region domain containing protein, expressed	2.99	9	6.985E-05	

	PiniT23N_TRINITY_DN25329_c0_g1_i6	Late embryogenesis abundant protein	2.96	9	0.0490268	
	PiniT27G_TRINITY_GG_16750_c0_g1_i2	C2 domain	2.95	9	0.0361261	
	PiniA33_R5269878120872571104839	0	2.93	9	0.028456	
	PiniT21_TRINITY_DN26471_c1_g2_i5	Transcription factor	2.90	8	0.0151255	
	PiniT29_TRINITY_DN42271_c0_g2_i1	exocyst complex component	2.90	8	0.0027315	K07195
	PiniA61_R1846673178616947991892	Phospholipase A1-Igamma3	2.90	8	0.001235	
	PiniT23N_TRINITY_DN24787_c0_g1_i4	cysteine-rich repeat secretory protein	2.90	8	0.0088985	
	PiniT25G_TRINITY_GG_17631_c0_g1_i1	chitinase	2.89	8	0.0065232	K01183
	PiniT23N_TRINITY_DN25329_c0_g1_i4	Late embryogenesis abundant protein	2.88	8	0.0033751	
	PiniA31_R55932461794122123571366	0	2.88	8	0.0214079	
	PiniT21_TRINITY_DN27669_c0_g1_i1	Auxin-repressed 12.5 kDa	2.88	8	0.0002478	
	PiniT23G_TRINITY_GG_44341_c0_g1_i1	UDP-glucoronosyl and UDP-glucosyl transferase domain containing protein, expressed	2.87	8	0.0360207	
	PiniA61_R1899091100139098792408	RING-H2 finger protein	2.87	8	0.0115723	K19040

DOWN						
label	**ID**	**annotation**	**log2FoldChange**	**actualFC**	**padj**	**KO**
T_95	PiniA31_R54284093258735253943602	copper-transporting ATPase	-4.10	-17	3.378E-07	K17686
T_94	PiniT31_TRINITY_DN39392_c0_g6_i2	geranylgeranyl pyrophosphate synthase	-2.29	-5	0.0397946	K13789
T_93	PiniA45_R34114711317151372700393	geranylgeranyl pyrophosphate synthase	-5.79	-33	0.0073764	K13789
T_90	PiniA43_S37907711604179612881297	flavonoid	-3.93	-15	0.0011932	K05280
T_9	PiniT23_TRINITY_DN30873_c1_g1_i4	glyceraldehyde-3-phosphate dehydrogenase	-2.73	-7	0.0002637	K05298
T_8	PiniA75_R958809134330011856035	Fructose-1,6-bisphosphatase	-3.17	-10	0.0251897	K03841
T_73	PiniA65_R14469511858123235511414	beta-glucosidase	-2.46	-6	0.0213184	K05350
T_72	PiniT23G_TRINITY_GG_38573_c0_g1_i1	beta-glucosidase	-4.81	-23	3.21E-05	K01188
T_7	PiniT21_TRINITY_DN28997_c0_g1_i7	GDSL esterase lipase	-2.19	-5	0.0176578	
T_69	PiniA21_R76526651311337126410345 86	Caffeoyl-coa o-methyltransferase	-2.73	-7	0.0025484	K00588
T_6	PiniA65_R148646291350171638114	Chlorophyll A-B binding protein	-4.75	-23	0.0138204	K08913
T_58	PiniT23_TRINITY_DN29986_c0_g1_i9	Xyloglucan endotransglucosylase hydrolase protein	-2.61	-7	0.0034225	K14504
T_5	PiniA55_R2246644967379371502837	Chlorophyll A-B binding protein	-2.89	-8	0.0422266	K08912
T_46	PiniA51_R27752171848192062043855	auxin-responsive protein	-3.41	-12	0.0029735	K14484
T_4	PiniA33_R5020254486235250750828	ferredoxin	-3.71	-14	0.0207504	
T_39	PiniA47_R31864421877247241067754	3-ketoacyl-coa synthase	-3.05	-9	0.0177929	K15397
T_38	PiniT21G_TRINITY_GG_42507_c0_g1_i1	enhanced disease susceptibility_t2		6	0.0066479	
T_32	PiniA35_J4690863748420311965897	NA	-2.55	-6	5.26E-09	

T_23	PiniT29_TRINITY_DN38261_c0_g1_i3	Haloacid dehalogenase-like hydrolase family protein	-2.17	-5	1.316E-10	
T_22	PiniA31_R53220451185399701353878	carbonic anhydrase	-5.56	-31	0.0341958	K01673
T_20	PiniA49_S30918941419182742617748	myristoyl-acyl carrier protein thioesterase	-3.92	-15	0.0194169	K10781
T_19	PiniA75_R906834140835193180693	myristoyl-acyl carrier protein thioesterase	-4.78	-23	7.555E-07	K10781
T_122	PiniA47_R31336441841265281129772	fatty acyl-CoA reductase	-4.34	-19	0.0032136	K13356
T_121	PiniA33_S51465322679652082693376	Hydrolyzes glycerol-phospholipids at the terminal phosphodiesteric bond (By similarity)	-4.37	-19	1.821E-06	K01115
T_109	PiniA71_R116835510819453172273	ribonucleoside-diphosphate reductase small	-2.91	-8	0.0361497	K10808
T_108	PiniA75_R888968287171873825850	Provides the precursors necessary for DNA synthesis. Catalyzes the biosynthesis of deoxyribonucleotides from the corresponding ribonucleotides (By similarity)	-2.85	-8	0.000728	K10807
T_106	PiniA51_S27583217221583911425340	glutathione s-transferase	-2.28	-5	1.373E-08	K00799
T_101	PiniT25G_TRINITY_GG_43132_c0_g1_i3	Glutathione S-transferase	-3.94	-16	0.0121586	K00799
	PiniA31_J54712651699214701002491	Cytochrome p450	-9.16	-84	1.173E-05	K20623
	PiniT25N_TRINITY_DN25348_c1_g1_i2	expressed protein	-8.98	-81	0.0007888	
	PiniA65_J1495745563133381356759	Tetraspanin family	-8.41	-71	0.0003092	
	PiniA39_J4297204225089644946096	peptide nitrate transporter	-7.87	-62	1.237E-07	
	PiniT25N_TRINITY_DN30094_c1_g2_i1	oxidoreductase, 2OG-Fe(II) oxygenase family protein	-7.84	-62	0.0038521	
	PiniA65_R14998951670238481429440	aspartic proteinase	-7.73	-60	2.068E-05	
	PiniA31_R559031193268301692129	resistance protein	-7.73	-60	0.0065673	

	PiniT29N_TRINITY_DN31029_c3_g1_i16	peroxidase	-7.54	-57	1.802E-05	K00430
	PiniA41_R38398042362464173625217	Lipase (class 3)	-7.48	-56	0.0009421	
	PiniT25_TRINITY_DN33543_c0_g4_i2	Retrotransposon protein	-7.37	-54	0.0393139	
	PiniA45_R342787268489782119716	C2 domain	-7.23	-52	3.307E-05	
	PiniA37_S4661949104963724109507	aspartic proteinase	-7.23	-52	0.0041663	
	PiniA23_R714858318672731332267 76	pectinesterase	-7.02	-49	8.003E-05	
	PiniA71_S117673058536364708645	0	-6.80	-46	4.421E-06	
	PiniT29_TRINITY_DN38097_c1_g1_i2	Histone H1	-6.66	-44	0.0001663	K11275
	PiniT21N_TRINITY_DN23423_c0_g2_i1	Fusaric acid resistance protein family	-6.63	-44	0.0001685	
	PiniT23N_TRINITY_DN25408_c0_g1_i7	subtilisin-like protease-like	-6.61	-44	0.0002681	
	PiniA21_R7835747936228495457704	Aluminum-activated malate transporter	-6.60	-44	0.0275739	
	PiniT21N_TRINITY_DN23146_c3_g2_i1	laccase-17-like	-6.59	-43	0.0004092	K05909
	PiniA55_J22808481501155861480706	Polygalacturonase	-6.53	-43	0.0050773	
	PiniT23_TRINITY_DN29577_c1_g1_i8	Gibberellin regulated protein	-6.53	-43	0.0024778	
	PiniT25_TRINITY_DN31604_c0_g1_i2	Caleosin related protein	-6.43	-41	1.935E-05	K17991
	PiniA65_R1604715106813707433484	peroxidase	-6.41	-41	2.538E-05	K00430
	PiniT21G_TRINITY_GG_15920_c0_g1_i1	cysteine-rich repeat secretory protein	-6.37	-41	0.0004453	
	PiniT29_TRINITY_DN38097_c1_g1_i4	Histone H1	-6.29	-40	0.0004449	K11275
	PiniT23N_TRINITY_DN24810_c2_g1_i3	serine threonine-protein kinase	-6.28	-39	1.122E-05	

	PiniA43_S35758979458044589352	Cysteine-rich receptor-like protein kinase	-6.26	-39	0.0025133	
	PiniA39_J4215820120633871842567	transcription	-6.24	-39	0.0073141	K09422
	PiniA43_S357768853097303608498	Protease inhibitor seed storage lipid transfer protein	-6.23	-39	0.0146309	
	PiniT25G_TRINITY_GG_20573_c0_g1_i1	0	-6.14	-38	5.893E-11	
	PiniT31G_TRINITY_GG_33953_c0_g1_i1	bidirectional sugar transporter	-6.10	-37	0.0012606	K15382
	PiniA37_R4663712987132952811044	DNA-binding protein ESCAROLA-like	-6.08	-37	0.0039013	
	PiniA65_S2711623931280	serine threonine-protein kinase	-6.05	-37	0.0470381	
	PiniA37_J436350045541902961652	Inherit from NOG: in maintaining the cortical microtubules organization essential for anisotropic cell growth	-6.03	-36	0.0052306	K18635
	PiniA23_R71563402092310902457289	Retrotransposon protein	-6.03	-36	0.0144648	
	PiniA31_R546940714773551130217 52	Inherit from KOG: stem-loop binding protein	-5.98	-36	0.0004983	K18710
	PiniA75_S18356110429052	Haloacid dehalogenase-like hydrolase family protein	-5.97	-36	0.0138497	K07025
	PiniT21N_TRINITY_DN20897_c1_g5_i5	0	-5.97	-36	0.0035469	
	PiniT23N_TRINITY_DN26212_c0_g1_i1	pectinesterase	-5.94	-35	7.122E-05	K01051
	PiniA51_R26319421341152486636408	peroxidase	-5.81	-34	1.222E-10	K00430
	PiniA47_J31640621581301641187335	fasciclin-like arabinogalactan protein	-5.78	-33	0.0141198	
	PiniA21_S78867401595143077646104	glycosyl hydrolase family 10 protein	-5.73	-33	0.0040696	
	PiniA71_R11594956315797460186	Basic blue protein	-5.72	-33	0.0141622	
	PiniT31_TRINITY_DN37844_c0_g1_i5	0	-5.67	-32	0.0016391	

	PiniT21_TRINITY_DN29577_c2_g2_i2	Plant non-specific lipid-transfer proteins transfer phospholipids as well as galactolipids across membranes. May play a role in wax or cutin deposition in the cell walls of expanding epidermal cells and certain secretory tissues (By similarity)	-5.63	-32	0.001	
	PiniA21_S77694521437131824006084	NA	-5.55	-31	0.0094766	
	PiniA21_S780158119499	denticleless protein homolog	-5.51	-30	0.0059326	K11790
	PiniA71_S110062966915102221498	heavy metal-associated domain containing protein, expressed	-5.44	-30	0.002447	
	PiniT25_TRINITY_DN26443_c0_g2_i2	Dirigent-like protein	-5.44	-30	0.0023108	
	PiniT21G_TRINITY_GG_30646_c0_g1_i1	N-acetyltransferase B complex (NatB) non catalytic subunit	-5.44	-30	0.0001387	K05909
	PiniA21_J77885721444137264241623	patatin group A-3-like	-5.44	-30	0.0015786	
	PiniA61_R189009771731371024533	NA	-5.44	-30	0.0064007	
	PiniA51_S28559411029485082265674	Xyloglucan endotransglucosylase hydrolase protein	-5.44	-30	0.0044465	K08235
	PiniT27_TRINITY_DN4865_c0_g1_i1	LRR_TYP	-5.42	-29	0.0346345	
	PiniT27G_TRINITY_GG_5484_c0_g1_i2	Protein of unknown function (DUF679)	-5.37	-29	0.0031847	
	PiniT25N_TRINITY_DN27608_c1_g1_i7	peroxidase	-5.36	-29	3.184E-10	K00430
	PiniA29_S5682050158747448390969	NA	-5.36	-29	0.0050995	
	PiniA39_R43628558028878521047	isoprenylated plant protein	-5.32	-28	0.0187395	
	PiniA31_S549523481638263312842	resistance protein	-5.30	-28	0.0142956	
	PiniA75_R915425129719974392693	peroxidase	-5.29	-28	0.0004328	K00430
	PiniT23N_TRINITY_DN24396_c0_g2_i7	glutathione s-transferase	-5.27	-28	3.503E-05	K00799

	PiniA35_R4747274250790807497607	sulfate transporter	-5.26	-28	5.077E-09	K17471
	PiniA21_R7718215916969843253862	Protease inhibitor seed storage lipid transfer protein (LTP) family protein	-5.25	-28	1.304E-05	
	PiniT27N_TRINITY_DN32015_c1_g2_i1	thaumatin-like protein	-5.24	-27	0.0119502	
	PiniT25G_TRINITY_GG_19762_c0_g1_i2	peptide transporter PTR3-A-like	-5.23	-27	2.836E-05	
	PiniT21G_TRINITY_GG_20586_c0_g1_i1	GDSL esterase lipase	-5.19	-27	0.0006995	
	PiniA75_R9347984962316529793	Chaperone protein dnaJ 8	-5.19	-27	0.0003622	
	PiniT23G_TRINITY_GG_55605_c0_g1_i1	protein CHUP1, chloroplastic-like	-5.17	-27	0.0320821	
	PiniA47_S31949691281267871577510	caffeic acid	-5.16	-27	0.0102937	
	PiniT25N_TRINITY_DN36309_c1_g1_i1	0	-5.13	-26	5.561E-06	

Table A1.3.

HOST: CTDsap vs CTMock						
Annotated	**biological process**	**Significant**	**Expected**	**rank**	**elim**	**classic**
GO:0010200	**response to chitin**	66	30	12	0.001989	4.26E−06
GO:0019752	**fatty acid metabolic process**	302	123	28	0.001061	6.32E-06
GO:0005975	**carbohydrate metabolic process**	152	66	69	0.001695	0.000573
GO:0055114	**obsolete oxidation−reduction process**	291	121	60	0.003797	0.001989

GO:0006520	**cellular amino acid metabolic process**	122	51	56	0.014409	0.000312
GO:0009755	hormone-mediated signaling pathway	349	158	46	0.023504	0.00991
GO:0032787	monocarboxylic acid metabolic process	176	73	80	0.024966	0.009225
GO:0031334	positive regulation of protein-containing complex assembly	12	3	5	0.042157	0.000129
GO:1901605	alpha-amino acid metabolic process	84	34	38	0.044111	0.001403
GO:0034622	cellular protein-containing complex assembly	78	32	36	0.044949	0.007861

HOST: CTDscr vs CTMock						
Annotated	**biological process**	**Significant**	**Expected**	**rank**	**elim**	**classic**
GO:0042254	**ribosome biogenesis**	70	36	38.14	0.000843	0.000109
GO:0006629	**lipid metabolic process**	262	152	142.75	0.000896	0.000373
GO:0016482	**cytosolic transport**	89	43	55.03	0.003486	0.000358
GO:0010200	**response to chitin**	146	75	79.55	0.003805	9.16E-05
GO:0051130	**positive regulation of cellular component organization**	79	46	17.43	0.004167	1.34E-07
GO:0016072	**rRNA metabolic process**	46	22	25.06	0.012083	0.003364
GO:1901607	alpha-amino acid biosynthetic process	65	35	35.41	0.009867	0.001257
GO:0006091	generation of precursor metabolites and energy	94	41	51.21	0.011479	0.001223

GO:0007034	vacuolar transport	19	7	10.35	0.013834	0.001932
GO:0032787	monocarboxylic acid metabolic process	200	100	108.97	0.014793	0.006195
GO:0071496	cellular response to external stimulus	87	37	47.4	0.015373	0.002531
GO:0006605	protein targeting	59	30	32.15	0.01686	0.011257
GO:0050832	defense response to fungus	112	49	61.02	0.017081	0.000336
GO:0006364	rRNA processing	45	22	24.52	0.017449	0.004936
GO:1901264	carbohydrate derivative transport	22	7	11.99	0.019758	0.000488
GO:0034470	ncRNA processing	58	28	31.6	0.021955	0.007303
GO:0072594	establishment of protein localization to organelle	53	27	28.88	0.022422	0.006882
GO:0006163	purine nucleotide metabolic process	154	63	83.9	0.022771	6.93E-06
GO:0044282	small molecule catabolic process	208	91	113.32	0.024604	4.09E-06

HOST: CTDsap vs CTDscr

Annotated	biological process	Significant	Expected	rank	elim	classic
GO:0006259	**DNA metabolic process**	119	40	36.15	0.000296	2.39E-08
GO:0010087	**phloem or xylem histogenesis**	47	11	8.67	0.000034	1.32E-07
GO:0032508	**DNA duplex unwinding**	12	2	39.8	0.006985	6.35E-05

GO:0006306	**DNA methylation**	33	9	10.03	0.012055	5.47E-05
GO:0010588	**cotyledon vascular tissue pattern formation**	34	9	10.33	0.023614	2.68E-06
GO:0010305	**leaf vascular tissue pattern formation**	40	12	13.67	0.038511	4.49E-05
GO:0006807	nitrogen compound metabolic process	948	296	288.01	0.003993	0.000941
GO:0006629	lipid metabolic process	139	40	42.23	0.038874	7.55E-05
GO:0016049	cell growth	61	15	18.53	0.040968	0.002122
GO:0009753	response to jasmonic acid	72	17	21.87	0.044901	0.035868
GO:0051239	regulation of multicellular organismal process	74	18	22.48	0.046194	0.037167

HOST: CCTDscr vs CTDscr						
Annotated	**biological process**	**Significant**	**Expected**	**rank**	**elim**	**classic**
GO:0006635	**fatty acid beta-oxidation**	10	1	24.32	0.034582	0.000524
GO:1901607	**alpha-amino acid biosynthetic process**	46	15	41.87	0.019654	0.002196
GO:0016071	**mRNA metabolic process**	32	10	29.91	0.024317	0.000918
GO:0010588	**cotyledon vascular tissue pattern formation**	70	44	32.9	0.027395	0.0005
GO:0051649	**establishment of localization in cell**	85	32	31.78	0.035156	0.003916

GO:0034613	cellular protein localization	61	23	22.81	0.036276	0.003106
GO:0015833	peptide transport	70	25	26.17	0.037967	0.003778
GO:0032787	fatty acid biosynthetic process	137	46	51.22	0.041522	0.006079
GO:0002252	jasmonic acid mediated signaling pathway	28	6	10.47	0.042772	0.005206
GO:0005975	carbohydrate metabolic process	119	47	44.49	0.044421	0.005155
GO:1901575	lipid catabolic process	225	89	84.12	0.045568	0.000984
GO:0015031	protein transport	62	22	23.18	0.046087	0.004253
GO:0045184	establishment of protein localization	62	22	23.18	0.046087	0.004253

PATHOGEN: CTDsap vs CTDscr

Annotated	biological process	Significant	Expected	rank	elim	classic
GO:0098813	**nuclear chromosome segregation**	34	7	7	0.013335	0.006525
GO:0031321	**ascospore-type prospore assembly**	26	14	46	0.019201	0.008243
GO:0016579	**protein deubiquitination**	31	9	1	0.032257	0.006998
GO:0019751	**polyol metabolic process**	17	5	19	0.038714	0.005448
GO:0006950	**response to stress**	291	81	86	0.045677	0.000728
GO:0071704	glutamine metabolic process	987	321	314	0.047424	0.058511

GO:1903046	meiotic cell cycle process	84	27	27	0.049866	0.07566

PATHOGEN: CCTDscr vs CTDscr						
Annotated	**biological process**	**Significant**	**Expected**	**rank**	**elim**	**classic**
GO:0046034	**ATP metabolic process**	93	41	36	0.0020751	0.00307
GO:0009063	**cellular amino acid catabolic process**	28	16	62	0.0031827	0.002902
GO:1901606	**alpha-amino acid catabolic process**	17	12	378	0.0048043	0.000744
GO:0022900	**electron transport chain**	16	11	19	0.0086826	0.001769
GO:0044271	**respiratory electron transport chain**	15	11	136	0.0098356	7.60E-04
GO:0051656	establishment of organelle localization	44	7	13	0.0104994	0.0017428
GO:0065003	protein-containing complex assembly	165	44	51	0.013462	0.0007145
GO:0006725	cellular aromatic compound metabolic process	455	134	139	0.0322162	0.0032625
GO:0046483	tetrapyrrole biosynthetic process	461	138	141	0.0407642	0.0037072
GO:0006412	translational elongation	171	43	52	0.0410456	1.19E-07
GO:0090304	nucleic acid metabolic process	267	82	82	0.0443922	0.0019443

APPENDIX A2
TERPENOIDS ARE INVOLVED IN EXPRESSION OF SYSTEMIC INDUCED RESISTANCE IN AUSTRIAN PINE

Data analysis

All recorded data for a sample j was represented by its corresponding column vector of X: $s_j = \left(x_{1,j}, x_{2,j}, \ldots . x_{p,j}\right)^T$, and the records for a given terpenoid compound I was represented by the corresponding transposed row vector of X: $c_i = \left(x_{i,1}, x_{i,2}, \ldots . x_{i,q}\right)^T$, and then the data was normalized by scaling to the z-score and to quartiles.

NMDS:

NMDS is a rank-based approach which produces ordination based on distance or pairwise dissimilarity matrix between objects in a low-dimensional space. The *metaMDS* function estimated dissimilarity measures for the $q_i \times q_{j,k}$ matrix of all pairwise distances using our specified Bray-Curtis distance algorithm $d_{j,k} = \frac{\sum |x_{i,j} - x_{i,k}|}{\sum (x_{i,j} + x_{i,k})}$, where $x_{i,j}$ refers to the quantity in column (i) for the pair of rows in comparison (j, k). The goodness of fit of the ordination and appropriate number of dimensions that best represent the matrix was estimated through multiple iterations of non-metric fit $R^2 = 1 - S^2$, where S is the Kruskal Stress value defined as $S = \sqrt{\frac{\sum_{j,k}(d_{j,k} - \widehat{d_{j,k}})^2}{\sum_{j,k} d_{j,k}^2}}$ between ordinated distance $d_{j,k}$ and predicted regression distance $\widehat{d_{j,k}}$. The optimal stress for the given matrix was graphed using the Shepherd's diagram that displays linear fit based on the squared correlation between goodness of fit of values and ordination distances.

HCA:

HCA is a bottom-to-top classification approach that produces separate clusters by grouping conjoint subsets of similar data, estimated using the distance vector $d_{j,k} = \left|\left|s_k - s_j\right|\right|^n$ between a pair of terpenoid compounds, s_j and s_k for a total of n sampled trees.

SOM:

In this analysis sample vectors s_j were mapped on a two-dimensional grid plane M of $x \times y$ neurons ($M_{x,y}$), also referred to as units. Each unit was then associated with a node that corresponds to the average of all data mapped under the specific node. Then, all nodes of the input layer were connected to corresponding nodes of the output layer using weight vectors, $w_{x,y} \in Q^p$. The unsupervised training algorithm simultaneously selected and adjusted random groups of feature vectors and projected the underlying structure on a two-dimensional space. Finally, SOM mapped the most closely located feature vectors to the closest output nodes of the feature map. The training algorithm was built using in the *kohonen* package, and summarized below.

1. Z-score normalization ($N_Z \in Q^{p \times q}$) of the raw terpenoid and other volatile compounds data
2. Randomization of feature vectors ($w_{x,y} \in Q^p$)
3. Through iterations of training cycle for all sample vectors s_j: (t_1, t_2, t_3,…. t_{max})
    a. Random selection of a normalized vector s_j.
    b. Winning node ($M_{x,y}$) identification based on closest distance between weight vector $w_{x,y}$ and sample vector:

$$\min\left(\left|\left|s_j - w_{x,y}\right|\right|^2\right) \forall M_{j,k} \in M$$

    c. Adjustment of the weight vector $w_{x,y}$:

$$w_{x,y}(t+1) = w_{x,y}(t) + \tau(t)[s_j - w_{x,y}]$$

    d. Estimation of the linear decline of training rate (τ) with respect to initial training rate $\alpha \in [0 \ldots 1]$ for t_{max}:

$$\tau(t) = \alpha \cdot \left(1 - \frac{t-1}{t_{max}}\right)$$

e. Adjustment of weight vectors of the neighboring nodes ($M_{x+\Delta x,y+\Delta y}$) for maintaining topology in p-dimensional input space:

$$w_{x+\Delta x,y+\Delta y}(t+1) = w_{x+\Delta x,y+\Delta y}t + \tau(t) \cdot \eta(r,t)[s_j - w_{x+\Delta x,y+\Delta y}(t)]$$

f. Using the Euclidean distance $r = \sqrt{\Delta x^2 + \Delta y^2}$ of the output nodes $M_{x,y}$ and $M_{x+\Delta x,y+\Delta y}$, v as the initial training radius, and $\sigma(t) = \tau(t) \cdot v \cdot \frac{1}{2} \cdot r$ as the training cycle dependent training radius, a gaussian function ($\eta(r,t)$ is determined as:

$$\eta(r,t) = e^{-\frac{1}{2}\left(\frac{r}{\sigma(t)}\right)}$$

g. A decision is made for training continuation based on the Euclidean distance between the winning node to its neighboring node, where increasing distance means smaller influence of the training on the corresponding feature vector. The training was stopped where the lowest distance was calculated twice, and the resultant training rate was reported suitable for the given data matrix.

Following the conclusion of training, a U-matrix was generated to determine structures generated from the resultant feature map in the form of colored nodes, where yellow nodes contained the maximum number of objects (terpenoid data) that were most closely related to each other, and red nodes contained least number of closely related objects. A mapping plot was further generated to represent the number of objects mapped to each node, and a Fanning plot was generated to identify the best representation of respective induction treatments on each node.

Spearman's Correlation:

. The correlations are based on non-metric monotonic relationships between two variables via ranks r_s, which is defined as $r_s = 1 - \frac{6\sum d_i^2}{n(n^2-1)}$, where d_i is the difference between the ranks of the two variables for total of n sampled trees. Following HCA of quartile-scaled data, the various terpenoid clusters formed by respective induction treatment types were also subjected to correlation with lesion sizes.

pre-challenge from the induction point

ID	Induction	Challenge	a-pinene	camphene	b-pinene	3-carene	myrcene	limonene	terpinolene	bornyl acetate	aterpineol	borneol	bphell	caryophyllene	germD	benzealdehyde	dodecanol	n-dodecyl_acrylate
1-C	Dsap	12h	960.71	17.54	38.61	0.1	12.98	68.11	2.05	11.05	0.1	0.1	10.48	3.76	35.42	0.1	3.42	23.35
2-C	Dsap	12h	154.71	2.61	10.42	0.1	2.4	23.95	0.1	2.51	0.1	0.1	4.01	3.11	0.1	0.1	5.11	23.25
7-C	Dsap	12h	673.46	13.39	39.93	0.1	10.32	79.73	0.1	7.62	0.1	0.1	8.97	18.06	31.2	0.1	1.47	2.09
19-C	Dsap	12h	363.16	6.95	15.16	0.1	5.68	35.79	1.26	2.63	0.1	0.1	4.21	19.05	64.42	0.1	4.53	2.32
10-C	Dsap	12h	287.64	5.84	15.08	0.1	4.08	20.11	0.1	6.11	0.1	0.1	3.53	17.39	21.33	0.1	0.1	2.85
11-C	Dsap	12h	517.37	11.48	56.29	0.1	8.68	58.08	0.1	12.57	0.1	0.1	10.58	9.08	67.17	0.1	2.4	12.38
3-B	Mock	12h	530.76	9.72	23.55	0.1	12.73	113.93	1.3	3.81	0.1	0.1	79.36	11.42	0.1	4.61	21.64	68.04
6-B	Mock	12h	420.72	11.71	27.03	0.1	22.52	341.44	0.1	25.68	0.1	0.1	0.1	163.96	204.05	0.1	34.23	42.79
12-B	Mock	12h	969.34	19.74	53.61	2.1	13.03	66.13	1.1	14.63	0.1	0.1	12.22	64.83	92.69	0.1	3.01	40.18
17-B	Mock	12h	206.52	51.66	133.54	0.1	25.16	117.18	2.07	2.07	8.8	2.48	30.43	4.45	21.84	1.76	5.8	1.97
38-B	Mock	12h	388.71	7.16	20.97	0.1	4.64	30.24	0.1	4.54	0.1	0.1	4.44	2.72	5.14	0.1	1.51	1.31

50-B	Mock	12h	359.83	6.55	14.85	0.1	4.37	27.73	0.1	4.8	0.1	0.1	0.1	26.86	0.1	0.1	3.71	371.4
5-A	NIC	12h	519.01	8.35	100.1	0.1	6.04	76.66	0.1	2.82	2.72	0.1	7.24	42.76	19.72	0.1	2.11	166.1
8-A	NIC	12h	120.31	35.95	38.78	0.1	8.81	60.06	0.1	4.4	25.47	7.13	9.75	18.13	2.52	0.1	3.35	14.88
16-A	NIC	12h	127.21	37.55	41.5	0.1	9.19	62.75	1.38	5.24	18.68	5.04	9.68	15.81	20.85	0.1	1.88	31.23
40-A	NIC	12h	432.55	6.91	22.98	0.1	4.57	29.57	0.1	2.77	0.1	0.1	3.94	7.02	19.15	0.1	6.38	23.09
54-A	NIC	12h	645.83	11.59	140.85	0.1	11.99	80.49	1.32	5.89	2.85	0.1	14.94	3.05	33.74	0.1	1.63	30.08
53-A	NIC	12h	123.43	22.65	181.12	0.1	27.23	111.78	1.83	19.34	0.1	0.1	30.43	19.68	5.72	372.54	544.16	710.07
9-C	Dsap	72h	251.39	4.37	19.72	2.03	2.77	12.15	0.1	2.88	0.1	0.1	2.88	0.1	0.1	2.88	4.26	1.07
27-C	Dsap	72h	230.43	4.35	10.22	0.1	2.5	20.65	0.1	0.1	0.1	0.1	3.37	2.93	5	2.61	3.8	2.93
36-C	Dsap	72h	881.54	15.77	33.33	0.1	10.9	59.49	1.92	14.49	0.1	0.1	12.18	43.08	211.67	549.74	797.82	915.9
39-C	Dsap	72h	230.65	4.98	13.03	0.1	9.2	104.6	0.1	4.98	0.1	0.1	5.56	38.89	19.35	706.51	958.43	1155.94
51-C	Dsap	72h	111.78	2.44	47.19	0.1	1.7	7.7	0.1	0.1	0.1	0.1	4.59	7.41	4.74	317.78	472.74	574.74
45-C	Dsap	72h	139.9	0.1	65.87	0.1	0.1	21.88	0.1	0.1	0.1	0.1	6.49	0.1	0.1	964.9	1321.88	1664.42

15-B	Mock	72h	236.69	3.63	21.88	0.1	2.62	39.92	0.1	3.13	2.82	0.1	3.23	14.82	11.69	1.41	2.42	0.1
18-B	Mock	72h	147.31	2.88	9.81	0.1	1.73	10.38	0.1	0.1	0.1	0.1	0.1	4.81	8.08	0.1	4.62	2.88
24-B	Mock	72h	58.13	1.33	25.49	0.1	1.21	8.74	0.1	2.31	0.1	0.1	0.1	5.22	10.19	2.91	6.55	1.21
32-B	Mock	72h	523	9.7	53.27	1.05	14.56	104.54	1.69	14.24	0.1	0.1	13.71	47.15	29.11	2.43	5.38	0.1
34-B	Mock	72h	357.16	21.57	39.51	0.1	17.75	202.65	1.86	17.06	0.1	0.1	12.65	5	0.1	2.75	1.37	5.1
52-B	Mock	72h	231.07	0.1	0.1	0.1	0.1	0.1	0.1	0.1	0.1	0.1	0.1	0.1	0.1	0.1	0.1	0.1
14-A	NIC	72h	189.77	0.1	8.93	0.1	0.1	26.79	0.1	0.1	0.1	0.1	4.71	0.1	13.8	2.6	0.1	0.1
25-A	NIC	72h	744.15	12.3	37.6	0.1	8.67	51.11	1.31	8.17	0.1	0.1	10.79	34.07	202.02	0.1	3.02	0.1
33-A	NIC	72h	501.38	8.89	45.85	1.88	4.84	46.05	0.1	4.94	0.1	0.1	5.14	2.77	5.43	2.57	1.09	0.1
35-A	NIC	72h	209.32	4.1	7.99	0.1	2.97	25.61	0.1	4	0.1	0.1	2.87	0.1	36.07	464.96	613.83	747.75
41-A	NIC	72h	192.59	4.05	9.72	0.1	3.82	20.6	0.1	1.62	0.1	0.1	3.7	0.1	13.43	648.03	1197.92	1393.75
47-A	NIC	72h	84.01	0.1	7.61	0.1	0.1	5.84	0.1	0.1	0.1	0.1	0.1	0.1	0.1	1159.14	1661.68	1912.94
21-C	Dsap	10day	290.78	5.21	43.29	0.1	3.51	5.91	0.1	0.1	0.1	0.1	4.71	0.1	0.1	0.1	1.5	32.97

20-C	Dsap	10day	509.45	9.32	23.36	0.1	10.24	110.5	0.1	3.94	0.1	0.1	9.32	19.03	10.76	466.4	974.15	1202.1
4-C	Dsap	10day	436.01	8.45	22.85	0.1	6.37	26.59	0.1	9	0.1	0.1	6.37	0.1	0.1	631.86	964.4	1142.94
28-C	Dsap	10day	1945.17	33.55	100.91	0.1	43.73	427.94	5.35	15.27	0.1	0.1	167.36	62.27	110.7	431.33	591.78	715.54
42-C	Dsap	10day	681.32	13.76	63.9	0.1	8.85	41.99	1.69	7.72	0.1	0.1	9.41	62.92	52.53	569.94	911.8	1053.93
43-C	Dsap	10day	3188.38	57.52	724.89	0.1	57.3	330.31	11.28	49.67	0.1	0.1	78.32	230.86	217.81	687.61	1103.1	1197.12
22-B	Mock	10day	288.66	5.18	151.4	0.1	4.86	29.48	0.1	3.13	0.1	0.1	12.74	7.02	15.33	416.63	603.56	695.36
23_B	Mock	10day	379.15	7.37	59.65	0.1	6.54	47.41	0.1	5.19	0.1	0.1	6.22	20.64	5.08	533.71	719.09	831.64
29-B	Mock	10day	243.29	5.06	18.35	0.1	3.42	9.87	0.1	6.84	0.1	0.1	4.43	8.61	19.24	460.76	654.94	865.06
30_B	Mock	10day	340.05	8.12	34.29	0.1	6.54	35.6	0.1	7.07	0.1	0.1	14.92	7.33	41.49	586.13	916.1	1025.79
37-B	Mock	10day	172.83	3.51	8.78	0.1	0.1	6.44	0.1	0.1	0.1	0.1	2.58	17.68	9.48	691.1	1064.17	1543.68
49-B	Mock	10day	5453.09	100	163.51	0.1	19.28	261.34	7.94	10.82	118.14	44.43	24.85	63.81	31.44	394.54	609.48	715.77
26-A	NIC	10day	452.57	7.92	20.1	0.1	6.34	42.48	0.1	0.1	0.1	0.1	7.23	2.48	17.62	318.12	429.41	527.62
13-A	NIC	10day	692.91	14.17	36.48	0.1	10.89	41.86	0.1	21.26	0.1	0.1	15.49	4.59	5.38	660.37	996.59	1154.99

31-A	NIC	10day	158.52	3.14	6.28	0.1	2.24	20.07	0.1	0.1	0.1	0.1	2.69	37.44	8.3	366.26	532.51	604.48
44-A	NIC	10day	640.84	17.56	44.08	0.1	58.4	1016.03	4.96	69.08	0.1	0.1	771.76	20.23	47.52	566.41	825.57	1019.27
46-A	NIC	10day	748.27	13.46	61.48	0.1	16.79	230.74	2.47	14.81	0.1	0.1	13.7	5.06	12.59	505.68	750.12	808.15
48-A	NIC	10day	660.15	12.1	34.11	0.1	7.7	29.71	0.1	9.05	0.1	0.1	7.58	16.87	25.06	568.22	863.45	1037.65

pre-challenge from the challenge point

ID	Induction	Challenge	a-pinene	camphene	b-pinene	3-carene	myrcene	limonene	terpinolene	bornyl acetate	aterpineol	borneol	bphell	caryophyllene	germD	benzealdehyde	dodecanol	n-dodecyl_acrylate
1-C	Dsap	12h	1230.43	4.35	10.22	0.1	2.5	20.65	0.1	0.1	0.1	0.1	3.37	2.93	5	2.61	3.8	32.93
2-C	Dsap	12h	311.78	2.44	47.19	0.1	7.75	7.7	0.1	8.17	0.1	0.1	4.59	7.41	4.74	317.78	472.74	574.74
7-C	Dsap	12h	939.9	12.87	65.87	0.1	5.1	21.88	0.1	0.1	0.1	0.1	6.49	0.1	20.02	964.9	321.88	1664.42
19-C	Dsap	12h	654.71	2.61	10.42	0.1	2.8	23.95	0.1	2.51	0.1	0.1	4.01	3.11	0.1	648.03	5.11	23.25
10-C	Dsap	12h	363.16	6.95	15.16	0.1	5.68	35.79	1.26	2.63	0.1	0.1	4.21	19.05	64.42	752.04	214.53	43.24
11-C	Dsap	12h	887.64	5.84	15.08	0.1	4.08	20.11	0.1	6.11	0.1	0.1	3.53	17.39	21.33	1159.14	347.97	28.52

3-B	Mock	12h	236.69	3.63	21.88	0.1	2.62	39.92	0.1	3.13	2.82	0.1	3.23	14.82	11.69	1.41	112.42	0.1
6-B	Mock	12h	147.31	2.88	9.81	0.1	1.73	10.38	0.1	0.1	0.1	0.1	0.1	4.81	8.08	0.1	234.62	2.88
12-B	Mock	12h	58.13	1.33	25.49	0.1	1.21	8.74	0.1	2.31	0.1	0.1	0.1	5.22	10.19	2.91	116.55	1.21
17-B	Mock	12h	523	9.7	53.27	1.05	2.4	54.54	1.69	4.24	0.1	0.1	13.71	47.15	29.11	2.43	195.38	0.1
38-B	Mock	12h	257.16	2.57	39.51	0.1	14.56	82.65	1.86	17.06	0.1	0.1	12.65	5	15.78	2.75	1.37	5.1
50-B	Mock	12h	0.1	0.1	0.1	0.1	0.1	0.1	0.1	0.1	0.1	0.1	0.1	0.1	0.1	0.1	398.67	0.1
5-A	NIC	12h	189.77	1.7	38.93	0.1	0.1	26.79	0.1	3.66	0.1	0.1	4.71	0.1	13.8	2.6	0.1	0.1
8-A	NIC	12h	244.15	12.3	37.6	0.1	8.67	51.11	1.31	1.93	0.1	0.1	10.79	34.07	0.1	133.28	233.02	0.1
16-A	NIC	12h	101.38	8.89	45.85	1.88	4.84	46.05	0.1	4.94	0.1	0.1	5.14	2.77	5.43	2.57	171.09	0.1
40-A	NIC	12h	209.32	5.7	7.99	0.1	2.97	25.61	0.1	4	0.1	0.1	2.87	0.1	36.07	464.96	213.83	0.1
54-A	NIC	12h	192.59	4.05	9.72	0.1	3.82	20.6	0.1	1.62	0.1	0.1	3.7	0.1	13.43	293.98	397.82	0.1
53-A	NIC	12h	84.01	0.1	7.61	0.1	0.1	5.84	0.1	0.1	0.1	0.1	0.1	0.1	0.1	172.48	258.43	0.1
9-C	Dsap	72h	517.37	31.48	56.29	0.1	22.52	58.08	0.1	12.57	0.1	0.1	10.58	9.08	67.17	631.86	342.4	12.38

27-C	Dsap	72h	673.46	13.39	39.93	0.1	10.32	179.73	0.1	7.62	0.1	0.1	8.97	18.06	131.2	569.94	1.47	1053.93
36-C	Dsap	72h	960.71	27.54	138.61	0.1	12.98	168.11	2.05	11.05	0.1	0.1	10.48	42.76	35.42	466.4	573.42	1142.94
39-C	Dsap	72h	251.39	4.37	19.72	2.03	25.16	212.15	0.1	2.88	0.1	0.1	79.36	62.92	78.45	732.88	4.26	1202.1
51-C	Dsap	72h	881.54	15.77	33.33	0.1	10.9	159.49	1.92	14.49	0.1	0.1	12.18	43.08	211.67	549.74	1197.92	1393.75
45-C	Dsap	72h	230.65	34.98	13.03	0.1	26.7	104.6	0.1	4.98	0.1	0.1	5.56	38.89	19.35	706.51	1661.68	1912.94
15-B	Mock	72h	530.76	9.72	23.55	0.1	12.73	113.93	1.3	3.81	0.1	0.1	2.88	11.42	0.1	4.61	221.64	68.04
18-B	Mock	72h	420.72	11.71	27.03	0.1	7.4	341.44	0.1	25.68	0.1	0.1	0.1	163.96	204.05	0.1	234.23	42.79
24-B	Mock	72h	969.34	19.74	53.61	2.1	13.03	66.13	1.1	14.63	0.1	0.1	12.22	64.83	92.69	0.1	313.01	40.18
32-B	Mock	72h	506.52	11.66	13.54	0.1	2.77	117.18	2.07	2.07	8.8	2.48	30.43	4.45	21.84	1.76	250.8	1.97
34-B	Mock	72h	388.71	7.16	20.97	0.1	4.64	30.24	0.1	4.54	0.1	0.1	4.44	2.72	5.14	0.1	191.51	1.31
52-B	Mock	72h	359.83	6.55	14.85	0.1	4.37	27.73	0.1	4.8	0.1	0.1	0.1	26.86	0.1	0.1	231.71	371.4
14-A	NIC	72h	219.01	6.35	30.1	0.1	4.04	76.66	0.1	2.82	2.72	0.1	3.24	3.76	19.72	0.1	2.11	166.1
25-A	NIC	72h	209.45	9.32	23.36	0.1	4.24	10.5	0.1	1.94	0.1	0.1	9.32	9.03	10.76	232.92	374.15	1.07

33-A	NIC	72h	181.32	1.76	23.9	0.1	3.85	11.99	1.69	1.72	0.1	0.1	4.41	11.29	12.53	77.11	111.8	2.09
35-A	NIC	72h	236.01	8.45	22.85	0.1	6.37	26.59	0.1	7.1	0.1	0.1	6.37	7.1	11.76	132.7	264.4	23.35
41-A	NIC	72h	132.55	6.91	32.98	0.1	4.57	29.57	0.1	2.77	0.1	0.1	3.94	7.02	10.15	342.12	216.38	23.09
47-A	NIC	72h	145.83	1.59	40.85	0.1	1.99	20.49	1.32	2.89	2.85	0.1	4.94	3.05	33.74	195.21	301.63	30.08
21-C	Dsap	10day	1274.21	37.55	41.5	0.1	9.19	262.75	11.38	5.24	18.68	5.04	9.68	15.81	20.85	0.1	1231.88	1154.99
20-C	Dsap	10day	890.78	5.21	43.29	0.1	13.51	5.91	0.1	0.1	0.1	0.1	771.76	0.1	0.1	0.1	1.5	1019.27
4-C	Dsap	10day	1230.43	22.65	181.12	0.1	27.23	111.78	1.83	19.34	0.1	0.1	30.43	19.68	5.72	372.54	544.16	710.07
28-C	Dsap	10day	1945.17	33.55	100.91	0.1	43.73	427.94	5.35	15.27	0.1	0.1	167.36	62.27	110.7	431.33	591.78	808.15
42-C	Dsap	10day	1200.31	35.95	38.78	0.1	18.81	60.06	0.1	4.4	25.47	7.13	9.75	18.13	2.52	0.1	1356.35	1037.65
43-C	Dsap	10day	3188.38	57.52	724.89	0.1	57.3	330.31	11.28	49.67	0.1	0.1	78.32	230.86	217.81	687.61	1103.1	1197.12
22-B	Mock	10day	288.66	5.18	151.4	0.1	4.86	29.48	0.1	3.13	0.1	0.1	12.74	7.02	15.33	416.63	603.56	695.36
23_B	Mock	10day	379.15	7.37	59.65	0.1	6.54	47.41	0.1	5.19	0.1	0.1	6.22	20.64	5.08	533.71	719.09	831.64

29-B	Mock	10day	243.29	5.06	18.35	0.1	23.42	9.87	0.1	6.84	0.1	0.1	4.43	8.61	19.24	460.76	654.94	865.06
30_B	Mock	10day	340.05	8.12	34.29	0.1	6.54	35.6	0.1	7.07	0.1	0.1	14.92	7.33	41.49	586.13	916.1	1025.79
37-B	Mock	10day	172.83	3.51	8.78	0.1	0.1	6.44	0.1	0.1	0.1	0.1	2.58	17.68	9.48	691.1	1064.17	1543.68
49-B	Mock	10day	545 3.09	100	163.51	0.1	19.28	261.34	7.94	10.82	118.14	44.43	24.85	63.81	31.44	394.54	609.48	715.77
26-A	NIC	10day	152.57	5.92	20.1	0.1	6.34	42.48	0.1	0.1	0.1	0.1	7.23	2.48	17.62	118.12	229.41	127.62
13-A	NIC	10day	292.91	4.17	26.48	0.1	4.89	41.86	0.1	2.26	0.1	0.1	5.49	4.59	5.38	160.37	296.59	31.23
31-A	NIC	10day	158.52	3.14	6.28	0.1	2.24	20.07	0.1	0.1	0.1	0.1	2.69	7.44	8.3	166.26	232.51	34.48
44-A	NIC	10day	140.84	7.56	44.08	0.1	8.4	16.03	0.96	3.08	0.1	0.1	4.71	10.23	27.52	166.41	225.57	32.97
46-A	NIC	10day	248.27	3.46	61.48	0.1	3.79	30.74	2.47	4.81	0.1	0.1	13.7	5.06	12.59	205.68	175.12	29.53
48-A	NIC	10day	160.15	12.1	34.11	0.1	2.7	29.71	0.1	9.05	0.1	0.1	7.58	6.87	25.06	278.22	163.45	14.88

APPENDIX A3
PHYTOHORMONE CROSSTALK MEDIATES SYSTEMIC INDUCED RESISTANCE IN AUSTRIAN PINE

Identification and quantification of phytohormones

The chosen UPLC-QqQ-MS/MS platform allows for enhanced resolution of mass traces for accurate identification of compounds, although with tradeoffs to sensitivity, i.e, the lowest response of mass traces that can be accurately measured in the analyte. This is indicated by variation in recoveries of targeted compounds in analyte, likely due to low ion resolution in MS1 transition during multiple reaction monitoring (MRM) based ionization and acquisition. We optimized this by tuning our instrument to MS1 resolution of 11.6/14.8, and MS2 resolution of 12.1/15.0. Solvent matrix effects were minimal upon using acetonitrile acidified with formic acid as the non-polar buffer solvent for column separation instead of acidified methanol, as the former is an aprotic solvent modifier suited for enhanced chromatographic selectivity (Hopkins, 2019). We confirmed the compound identities in our analyte based on comparable chromatographic responses of standard solutions with the corresponding responses of known concentrations of respective compounds spiked into the analyte (Pinasseau et al., 2016). Analyte extracts from tree species, specifically woody samples, are associated with high matrix effects on the response recovery of various phytohormone compounds; ion suppression for GA7, SA and ABA (–43, –22 and –19%, respectively), and ion enhancement for GA4, JA, brassinosteroids and zeatin (+25%), in MS/MS systems (Delatorre et al., 2017). It is likely that we could not detect significant responses in SA and GA compounds in our phloem analytes, possibly due to matrix-induced suppression of SA, methyl salicylate, GA3 and GA4. However, the optimum recoveries of ABA, JA, MeJA, JA-Ileu, and IAA were not affected by any matrix effects, and these compounds could be accurately identified. However, this could be a possible reason why we could not detect any significant response for some of the other targeted phytohormone compounds in our analytes. Nevertheless, our results confirm that the analytical recoveries of rare phytohormone compounds

and their derivatives can be accurately identified and quantified in Austrian pine phloem using the UPLC-QqQ-MS/MS pipeline.

Chromatography Today, March, 24–26. https://www.chromatographytoday.com/article/help-desk/63/advanced-chromatography-technologies/the-role-of-methanol-and-acetonitrile-as-organic-modifiers-in-reversed-phase-liquid-chromatography/2507

Pinasseau, L., Verbaere, A., Roques, M., Meudec, E., Vallverdú-Queralt, A., Terrier, N., Boulet, J.-C., Cheynier, V., & Sommerer, N. (2016). A Fast and Robust UHPLC-MRM-MS Method to Characterize and Quantify Grape Skin Tannins after Chemical Depolymerization. In *Molecules* (Vol. 21, Issue 10). https://doi.org/10.3390/molecules21101409

Delatorre, C., Rodríguez, A., Rodríguez, L., Majada, J. P., Ordás, R. J., & Feito, I. (2017). Hormonal profiling: Development of a simple method to extract and quantify phytohormones in complex matrices by UHPLC–MS/MS. *Journal of Chromatography B*, *1040*, 239–249. https://doi.org/https://doi.org/10.1016/j.jchromb.2016.11.007